THE EFFECT OF CHANGES IN PORE FLUID GEOCHEMISTRY ON THE ELASTIC-PLASTIC BEHAVIOUR OF LAKE AGASSIZ CLAY

By:

ALEXANDER G. MAN

A Thesis
Submitted to the Faculty of Graduate Studies
In Partial Fulfillment of the Requirements for the Degree of
DOCTOR OF PHILOSOPHY

Department of Civil Engineering
University of Manitoba
Winnipeg, Manitoba

December 2005

THE UNIVERSITY OF MANITOBA

FACULTY OF GRADUATE STUDIES

*****

COPYRIGHT PERMISSION

The Effect of Changes in Pore Fluid Geochemistry on the Elastic-Plastic Behaviour of Lake Agassiz Clay

BY

Alexander Man

A Thesis/Practicum submitted to the Faculty of Graduate Studies of The University of Manitoba in partial fulfillment of the requirement of the degree

Of

Doctor of Philosophy

Dedication

This thesis is dedicated to my father, the late Dr. S.C. Man (who was never late).

Abstract

Fresh water retention dykes at Seven Sisters Generating Station have experienced instabilities on an irregular basis since they were heightened in the late 1940's. Previous investigations compared three locations at the site; one section of dyke that had experienced previous instability; a second section that had remained stable; and a third, background location, that had not experienced dyke loading. Laboratory results on clay specimens from the stable and unstable sections showed greater brittleness and anisotropy at the unstable section. Slope stability modelling indicated that the stable and unstable sections both had safety factors greater than unity if post-peak strengths were used. Both were close to unity if residual strengths were used.

Differences in stress-strain behaviour and the time dependent nature of the problem suggested that the forebay water was leaching naturally occurring cementation from the foundation clay and subsequently changing its behaviour. This project compared the pore fluid geochemistry of samples from the unstable, stable and background sections. Both sections beneath the dyke had noticeably lower electrolyte concentrations, particularly components of gypsum, than the background section.

To examine a hypothesis that changes in pore fluid geochemistry, due to leaching of the forebay water, reduces cementation bonds in the high-plastic foundation clay, a laboratory testing program was undertaken to isolate the effects of pore fluid geochemistry on the elastic-plastic behaviour of Lake Agassiz clay. Yield loci were obtained for the natural clay from the background and unstable locations and a number of clays reconstituted with different pore fluid geochemistry. Geochemical conditions

examined included batches of clay reconstituted with deionized (DI) water, gypsum rich water, water acidified with sulphuric acid, sodium chloride brine and two batches that were washed with DI water (one and six pore volumes).

The results of the test program showed that yielding was influenced by the presence or absence of gypsum cementation. The size of the yield locus was reduced when pore fluid concentrations of calcium and sulphate were lowered to conditions that would result in the dissolution of gypsum. Loss of gypsum cementation reduced the amount of strain required for strain-softening from peak to post-peak and the development of a shear plane. Elevated pore fluid electrolyte concentrations increased the normally consolidated peak strength, post-peak strength and residual strength. The yield locus for artificially-weathered clay was smaller in p',q-space than that for the un-weathered soil, but its general shape was similar.

Using the laboratory yield locus, stress-deformation modelling indicated that the upper foundation clay yielded during the initial construction and raising of the dykes. Reducing the size of the yield locus by leaching would increase the amount of yielding beneath the dykes. Induced excess pore water pressures due to time-dependent yielding would be sufficient to cause a condition of instability of the Seven Sisters dykes.

Acknowledgements

I would like to thank my advisor, Dr. James Graham, for all of his support, advice, and encouragement throughout this project. He made the experience challenging, yet very enjoyable. Just the way life should be! I have especially enjoyed our weekly meetings. Having the opportunity to spend so much time with someone that has as much experience and insight as Dr. Graham was priceless.

I would also like to thank the members of my Advisory Committee: Dr. Marolo Alfaro, Dr. James Blatz, and Dr. Tee Boon Goh for their input and guidance. Special thanks go to James, who was the spark that ignited the interest in coming back to graduate school.

Financial support for my project was provided by NSERC, a University of Manitoba Graduate Fellowship, and Manitoba Hydro. Thanks go to Denis Dubois at Manitoba Hydro for arranging the field program.

A number of people working in the laboratory deserve acknowledgement. First of all, the Civil Engineering Technologists who helped with my research program including Kerry Lynch, 'Tai' Piamsalee, and Judy Tingley. I had a great time working with all of the graduate students in the Geotechnical Laboratory. Thanks again to Greg Siemens and Tim Krahn for taking all those readings!

Last but not least, I would like to thank all of my family, especially my wife Sara and kids, Rebecca and Nathan. Thank you for your love and support!

Table of Contents

List of Figures

List of Tables

List of Appendices

1.0 Introduction

1.1 Problem Statement

Failure of clay dam cores, embankments and natural slopes due to particle dispersion or other mechanisms believed to be related to changes in pore fluid chemistry have been reported in Australia, Canada and the United States (Sherard et al., 1972; Mitchell, 1993; Garinger et al., 2001, 2002, 2004). In the worst of these cases, the failures have resulted in uncontrolled releases of reservoir water. In the best of these cases, the failures were detected early enough to implement effective but costly remedial measures. This research was initiated to address some ongoing slope instabilities in freshwater retention dykes at a site in southern Manitoba that have experienced changes in pore fluid geochemistry.

The site is located at the Seven Sisters Generating Station, which is owned and operated by Manitoba Hydro. The extensive dyke system for the station was initially constructed in 1929 and the heights and lengths were increased in the late 1940's (Peterson et al., 1957). Since the dykes were raised, 13 instabilities have occurred on an irregular basis on the dry side of the dykes. Most of the instabilities involved subsidence of the dry side that was accompanied by crest settlement and cracking near the wet side shoulder. In some cases, bulging was observed at the toe (Rivard and Lu, 1978). In other cases, no bulging was observed. The instabilities appear to have occurred at random locations along the length of the dykes, despite conditions that would result in similar safety factors. Researchers and engineers who have worked on these dykes include Peterson et al. (1957), Casagrande (1959), Bjerrum (1969), and Liu and Dubois (1996). It should be noted that none of the instabilities at the site have

resulted in an uncontrolled release of reservoir water. Manitoba Hydro has been proactive in preventing further instabilities and has constructed supporting berms behind the dykes at various locations.

Studies conducted by Garinger et al. (2001, 2002 and 2004) and Man et al. (2003a,b) examined the stability of the dykes on the basis of laboratory testing of the highly plastic clay foundation soil. Specimens were tested from a section that had experienced instability in 1994 (SS-036), a second section that has remained stable (SS-040), and a 'background' location that had not been subjected to loading or seepage due to the construction of the dyke (SS-042). Based on triaxial testing and chemical analysis of extruded pore fluid, the authors postulated that physicochemical effects were influencing soil behaviour and the foundation clay probably contained cementation bonding that could be removed by leaching. The resulting quasi-stable microstructure could then be easily taken to failure by shear straining.

1.1.1 Foundation Soil Conditions

Figure 1.1 shows a cross-section through the dyke. The dykes consist of a clay core beneath a rip-rap shell. Their average height is approximately 7.0 m, the width of the crest is approximately 4.3 m, and the total length is about 12.8 km. The clay fill material extends to a depth of approximately 8 m below the crest and overlies highly plastic foundation clay deposited by Lake Agassiz. Bedrock was encountered at 13.11 m below crest level at the unstable section, at 12.75 m below crest level at the stable section and >9.8 m below ground level at the background section. At various depths above the bedrock, the foundation clay becomes silty with lower plasticity.

Hydrometer tests on the foundation soil showed very high clay-size fractions ranging from 95% to 99% in the foundation clay. Clay minerals account for between 67% and 81% of the total composition of Lake Agassiz clay. The clay size fraction in Glacial Lake Agassiz clay from Winnipeg consists of approximately 75% montmorillonite, 10% illite, 10% kaolinite and 5% quartz (Loh and Holt, 1974; Baracos, 1977). The remaining soil fraction consists primarily of silt-sized particles composed of limestone and dolomite (Baracos and Graham, 1980). The foundation clay contains localized nodules or accretions of white precipitate material that has been identified elsewhere in the Lake Agassiz clays as gypsum (Baracos 1977).

Atterberg limits performed on the foundation soil from Seven Sisters resulted in liquid limits ranging from 100 to 120% and plastic limits from 30 to 45% at the unstable section. At the stable and background sections, liquid limits ranged from 80 to 117% and plastic limits from 20 to 35%. A summary of soil classification data for the foundation clay is provided in Table 1.1.

1.1.2 Triaxial Behaviour

Specimens were obtained from the highly plastic foundation soil at the unstable, stable and background sections for isotropically consolidated undrained (CIŪ) triaxial tests. The testing was done in part by Garinger (2002) and in part by the author. These tests are widely used in practice to develop appropriate strength properties for engineering problems. Four to six specimens of the high-plastic foundation clay were tested from each section. All specimens were taken from elevations of 267.7 m to 265.5 m. Table

1.2 provides a summary of triaxial behaviour, including peak, post-peak and residual friction angles, and strain-softening rates.

Figure 1.2 shows typical stress-strain results from CIŪ triaxial tests on the background, stable and unstable sections at an effective confining stress of 200 kPa. The tests indicate strain-softening stress-strain behaviour, with peak strengths being reached at 1 to 3% strain. The background specimen is much more ductile (less brittle) than the other two specimens in both its shear behaviour and pore water pressure response. Table 1.2 and Figure 1.2 show that softening of specimens from the unstable section is steeper and more marked than at the stable and background sections.

Figures 1.3, 1.4 and 1.5 show deviator stress, $q = (\sigma_1 - \sigma_3)$ versus mean effective stress, $p' = (\sigma'_1 + \sigma'_3)/3$ for the background, stable and unstable sections, respectively. As observed in Figure 1.2, the specimens were clearly strain-softening, supporting the suggestion that the clay is cemented. This is supported by the early sections of some of the stress paths in Figure 1.3 where cementation bonds appeared to delay the initiation of shear generated pore water pressures. 'Post-peak shearing resistance was taken at about 2% to 4% axial strain, shown as the open circles in the figures. These resistances can be taken to be close to the 'normally consolidated' or critical state resistances. Lines connecting these 'post-peak' points on the plots of deviator stress *versus.* mean effective stress in Figures 1.3, 1.4 and 1.5 produce values of ϕ'_{nc} (with $c' = 0$) of approximately 13° in the foundation clay of the unstable section, 14° at the stable section and 13° at the background section (Table 1.2). In terms of what is normally seen in clays, these are very low values of ϕ'_{nc}. They correspond to rather poorly defined 'post-

peak plateaus' in the q *versus,* ε_1 diagrams that represent a limited period of constant shearing resistance before other mechanisms begin to operate.

Following the post-peak plateaus, some tests showed a further reduction in deviator stress with additional axial strain and the development of well-defined failure planes. When failure planes developed, they first appeared quite early in the tests, between 1% and 6% axial strain. After the tests ended, the failure planes were separated and examined. They were shiny and slickensided. The lowest shearing resistance in the tests has been interpreted as residual strength, even though it is unusual to reach residual conditions in triaxial tests. Connecting the lowest deviator stresses in the q versus p' plots in Figures 1.3, 1.4 and 1.5, and assuming no cohesion, the residual friction angle ϕ'_r was found to be 10° for the unstable section and 11° for the stable and background sections. These values correspond quite well with 'residual' results from direct shear tests (Garinger, 2002).

The slopes of the early stages of the q-p′ plots in Figures 1.3, 1.4 and 1.5 indicate anisotropic elasticity with a greater elastic stiffness in the horizontal direction (Graham and Houlsby, 1983). A greater degree of anisotropy, as indicated by a larger angle between the stress path and the constant-p′ direction, was observed for the unstable section (Figure 1.5) compared with the other sections (Figures 1.3 and 1.4). The greater anisotropy implies that for the same stress state, clay at the unstable section can generate higher excess pore water pressures during shearing than the stable section. This is illustrated in the lower diagram of Figure 1.2, which shows changes in pore water pressure versus axial strain. At early stages in the tests, the specimens from

the background section (Figure 1.3) and the stable section (Figure 1.4) followed similar $\Delta p'/\Delta q$ ratios. Unexpectedly, at later times in the tests, the stress paths bent towards $\Delta p'/\Delta q$ ratios similar to the unstable section (Figure 1.5). Further testing is required to determine the cause of this observation. Table 1.3 shows values of $\Delta p'/\Delta q$ in the linear sections of these graphs.

1.1.3 Slope Stability Modelling

Garinger (2002) reported results of slope stability modelling at the site. Modelling was conducted using computer software created by Geo-Slope International Ltd. SLOPE/W was used to determine the factor of safety at the stable and unstable dyke sections using, firstly, a Morgenstern-Price generalized limit equilibrium solution with constant interslice force inclination (Spencer solution). Water pressures were taken from steady state seepage analysis using SEEP/W. A second analysis that combined SEEP/W, SIGMA/W, and SLOPE/W was conducted using the stresses obtained in the stress-deformation analysis. The objective of these analyses was to evaluate the safety factors at the unstable and stable sections.

The two methods of stability analyses were each performed using two sets of material properties. The results are summarized in Table 1.4. Cases 1a and 1b used 'post-peak' (that is, 'normally consolidated', 'critical state' or 'undrained strength at large strains' - USALS) friction angles in the upper foundation clay. A small cohesion of 5 kPa was also included to account for the curvature of strength envelopes for smectitic clays. ('Normally consolidated', 'post-peak', 'USALS', and 'critical state' are all numerically similar, though each has a slightly different conceptual framework.) Cases 2a and 2b

used residual strength parameters $c_r' = 5$ kPa and $\phi_r' = 9°$ for the upper foundation clay in both sections. These values were based on the results of direct shear testing conducted by Garinger (2000). Cases 1a and 2a in Table 1.4 used the Morgenstern-Price solution with interslice force inclination θ = constant, while Cases 1b and 2b imported stress distributions from SIGMA/W. The ϕ^b parameter, describing the increase in shearing resistance with soil suction in the shell, was assumed to be 12° for the dyke material. (A sensitivity analysis showed that uncertainties in the selection of ϕ^b had little effect on the safety factor in these calculations for $7° \leq \phi^b \leq 25°$). The dyke and the lower foundation clay at both sections were modelled by 'peak' strength parameters $c' = 20$ kPa, $\phi' = 23°$ and $c' = 20$ kPa, $\phi' = 24°$, respectively. Figures 1.6 and 1.7 show typical results for critical slip surfaces, phreatic surfaces, and safety factors for Case 2b at the unstable section and the stable section, respectively.

The results in Table 1.4 indicate that the Generalized Limit Equilibrium method using the Morgenstern-Price solution and the solutions using stress distributions imported from a finite element stress-deformation analysis produce very similar results in this problem. Cases 1a and 1b both used 'post-peak' strengths in the upper foundation clay. The results show safety factors of around 1.15 at the previously unstable section and 1.22 at the currently stable section. The conclusion is that if post-peak strengths were operating, both sections should be stable if pore water pressures are based on steady state flow. Cases 2a and 2b again produce generally similar results, though in this case, results for both sections are close to 1.00. They suggest that if residual strengths were operating, both sections would fail.

Clearly the analyses summarized in Table 1.4 are not by themselves sufficient to identify the conditions under which one section of the Seven Sisters dyke became unstable while the other section remained stable. Some other mechanism must be operating that can influence the rate at which strengths deteriorate from post-peak to residual. With the levels of safety factor associated with post-peak strengths (Cases 1a and 1b), it is likely that creep shear straining occurred over time since construction and that more creep straining took place at the unstable section than at the stable section. The foundation clay at the site is markedly strain-softening (Figure 1.2). The stress-deformation analysis mentioned earlier showed that heightening of the dykes in the late 1940s could cause sufficient shear straining over time to take the clay from peak to post-peak strength, and indeed to residual strength (Garinger et al., 2004).

1.1.4 Analysis of Pore Fluid Chemistry

In searching for this alternate mechanism, Garinger et al. (2004) proposed that forebay water leaching beneath the dykes was depleting cementation bonds in the foundation clay. Geochemical characterization of the site was conducted with guidance from the author to examine this hypothesis. Specimens for pore fluid analysis were obtained from the highly plastic foundation soil at the unstable, stable and background sections. At each section, four specimens of pore fluid were extracted for analysis, the first being approximately 0.5 to 1 m below the top of the foundation clay layer. The other three specimens were then taken from between 1.5 to 2.5 m below the top of the foundation layer.

Pore fluid samples were obtained by extruding saturated paste samples through a 0.45 micron filter. The pore fluid specimens were analyzed for major ions including sodium Na^+, calcium Ca^{2+}, magnesium Mg^{2+}, chloride Cl^-, sulphate SO_4^{2-} and bicarbonate HCO_3^-. Electrical conductivity (EC) and pH were also measured.

The dissolved metals were analyzed by flame atomic absorption spectrophotometry (APHA 3111:B, 1998). Anions including chloride and sulphate were analyzed by ferricyanide and methylthymol blue colourimetry, respectively (APHA 4500-Cl:E and APHA 4500-SO4:F, 1998). Bicarbonate was measured by titration with 0.01N HCl (HA 2320:B, 1998). Electrical conductivity was determined using a conductivity cell (APHA 2510:B, 1998) and pH was determined electrometrically (APHA 4500-H:B, 1998).

Table 1.5 presents results of the pore fluid testing, while Figures 1.8 to 1.10 show graphs of selected parameters (Ca^{2+}, SO_4^{2-} and Na^+/Ca^{2+}) versus elevation at each of the three sections, respectively. The results reveal significant changes in pore fluid chemistry beneath the dykes compared to the background section. They suggest three possible mechanisms that may be responsible for the observed instabilities. These include: (1) lower electrolyte concentrations beneath the dykes, (2) lower electrolyte valence beneath the dykes and (3) loss of gypsum ($CaSO_4 \cdot 2H_2O$) cementation with time. Such changes can affect compressibility, strength, and hydraulic conductivity of the clay (Barbour and Yang, 1993).

The results indicated significantly lower total electrolyte concentrations beneath the dyke relative to the background location and noticeably lower concentrations near the surface

than at depth. The most significant trends were the notably lower concentrations of calcium, magnesium and sulphate beneath the dykes relative to the background location. The concentrations of these ions beneath the dykes were consistently lower than at the background location throughout the entire depth of testing. The difference was especially evident at elevations below 267 m. Worth noting are the broadly similar concentrations of the various ions at the stable and unstable sections. (The unstable section generally had concentrations slightly lower than the stable section, but both were significantly lower than the background section.) This is obviously a concern since it implies that conditions at the stable section may be approaching those at the unstable section.

With the exception of bicarbonate, all of the major ions were observed to increase in concentration with depth at each section. This is likely the result of downward leaching before construction of the dykes (downward gradients have been measured at the site), followed by horizontal leaching after construction of the dykes and filling of the reservoir. From normal seepage considerations, a greater number of pore volumes can be expected to have passed through the upper parts of the foundation soil, close to the dykes.

The reductions of calcium and magnesium concentrations shown in Table 1.5 increase the monovalent to divalent cation ratio (Figure 1.10). That is, the overall valence of the electrolytes in the pore fluid decreases. This is indicated by both the Na/Ca ratio and the sodium adsorption ratio (SAR) presented in Table 1.5. The entire unstable profile shows Na/Ca ratios greater than the background range. The Na/Ca ratios at the stable section are generally less than at the unstable section. However, the ratios for the upper three

samples from the stable section were greater than comparable values for the background location.

The lower concentrations of calcium and sulphate in the pore fluid in the foundation clay beneath the dyke suggests loss of gypsum ($CaSO_4 \cdot 2H_2O$) beneath the dykes with time. Table 1.5 presents saturation index (SI) values for gypsum ($K_{sp\ gypsum} = 10^{-4.6}$ at 25°C) and Figure 1.11 shows calculated values of ion activity product (IAP) for gypsum *versus* elevation for each section. Under-saturated conditions are noted throughout the entire unstable and stable sections with respect to gypsum. In contrast, the background section is under-saturated near the top of the clay foundation but shifts to gypsum-saturated conditions with depth. The forebay water is under-saturated with respect to gypsum and can therefore remove gypsum from the foundation soil by dissolution.

Only small differences in concentration were observed for sodium, chloride and bicarbonate between the three locations. The similarities in bicarbonate concentration suggests that carbonate leaching, and therefore loss of carbonate cementation, was probably not a factor. This was confirmed by saturation indices calculated by the author for calcite.

1.1.5 Discussion of Problem

When post-peak strengths were used in the stability analyses, the solutions indicate that the unstable and stable sections show factors of safety greater than unity (Garinger et al., 2002). When residual strengths were used, both sections show factors of safety less

than unity. Therefore, other processes had to be examined to allow instability to be modelled and the location of future instabilities identified.

The brittle and possibly cemented structure observed in the triaxial tests (Figures 1.2 to 1.5) and the results of the pore fluid chemical analyses (Table 1.5 and Figures 1.8 to 1.11) suggest that the pore fluid chemistry in the highly plastic clay may have been altered due to slow seepage of the water from the forebay through the foundation soil in a normal response to differences in hydraulic potential across the dyke. The rates at which this seepage takes place will be affected by irregular sand or silt partings that are seen in lacustrine clays and may therefore influence the rates at which individual dyke sections move towards failure.

The concentrations of calcium and sulphate measured at the background section indicate that the pore fluid was strongly supersaturated with respect to gypsum. With supersaturated conditions away from the dykes, gypsum precipitation would be expected, as was observed in the field at the background location, and would result in cementation of the soil. The differences in chemistry suggest a reduction in gypsum cementation beneath the dykes. This is reflected in the electrolyte concentration data, where significantly lower concentrations were measured in the pore water samples extracted from beneath the dyke. Gypsum is soluble in water and can be readily leached as relatively fresh reservoir water flows through the dyke foundation. The forebay water is under saturated with respect to gypsum (Figure 1.11) and therefore has the capacity to dissolve gypsum.

Three factors related to geochemical changes could therefore be contributing to the instability of the dykes. (More detailed background to the following section will be given in Chapter 2. This section is included to show the general thought processes that led to the author's project.) According to diffuse double layer (DDL) theory, lower electrolyte concentrations and valence can increase the DDL thickness. This translates into increased interparticle repulsion ($|R-A|$), increasing water content, and a decrease in interparticle contact stress (σ^*) for a constant effective stress (where $\sigma^*+|R-A|=\sigma'$). These changes can affect shear strength in two ways. First, the decrease in σ^* will result in a loss of shear strength represented by $\sigma^*\tan\phi'^*$, where ϕ'^* is the frictional component of shear strength contributed by true interparticle contacts. Second, the increase in $|R-A|$ causes a decrease in ϕ', since the plasticity index increases (Ho, 1985; Hawkins and McDonald, 1992; and Barbour and Yang, 1993). These mechanisms are believed to be the cause of clay dam core dispersion in the United States and Australia (Mitchell, 1993).

Finally, the loss of cementation bonding can also be expected to increase the brittleness and decrease the undrained shear strength of the soil (Figure 1.2). Removal of gypsum cementation by leaching can create a more brittle soil similar to what is indicated by Figure 1.2. Garinger et al. (2004) suggested that generally, the cementation at Seven Sisters maintains a quasi-stable soil structure that reflects the depositional conditions. Upon straining of the soil, whether due to heightening or to slow creep straining, the quasi-stable structure can be destroyed, causing the observed strain-softening behaviour.

Specimens from beneath the dykes were clearly strain-softening in a way that clay from the background section was not (Figures 1.2 to 1.5). Usually, strain-softening suggests an overconsolidated, cemented, or 'structured' material. The morphology of the site is such that there has never been historical deposition that was followed by erosion. Any apparent preconsolidation pressures will therefore be due to desiccation effects, former changes in ground water level at times of drier climate in the period since deposition, creep associated with aging, or some form of cementation. Maximum shearing resistance came at relatively small axial strains, often in the range 1 to 4%. The friction angles were similar between the three tested sections. However, the foundation clay in the unstable section generally softened more quickly with strain than the clay from the stable and background sections. There were also differences in the rates at which straining generated pore water pressures. The brittle, strain-softening behaviour has been seen in some other test programs on Lake Agassiz clay (Baracos, 1977; Graham et al.,1983).

Removal of gypsum cementation by leaching beneath the dykes can create a soil with the brittle responses shown in Figure 1.2 for the stable and unstable sections. It seems likely that the original cementation in the background clay (Figure 1.11) can maintain a quasi-stable soil structure that reflects the depositional conditions. This initial structure may consist of some flocculated edge to face contacts with interposed cementation bonds (Baracos, 1977). Alternatively, the cementation may be between aggregates consisting largely of face-to-face interactions using models identified by Yong et al. (1992). Upon straining of the soil, the quasi-stable structure will be destroyed, causing the observed strain-softening behaviour. The laboratory and finite element analyses both showed that dyke loading could produce the small deformations needed to strain

the soil past 'peak' to 'post-peak' resistance. If cementation at the interparticle contacts is lost, the soil structure will more readily yield and the soil will display a higher degree of strain-softening.

An additional feature should also be considered. The q versus p' plots (Figures 1.3, 1.4 and 1.5) show that the upper foundation clay beneath the dyke has remarkably linear behaviour until quite close to failure, with the soil from the unstable section being more anisotropic than the stable section. The greater anisotropy of the material at the unstable section produces larger pore water pressures as the material moves towards shear failure (Figure 1.2), and therefore lower undrained shear strengths for a given consolidation pressure. Under undrained conditions, the more brittle, more anisotropic leached soil, with higher strain-softening rates will fail earlier than less brittle, less anisotropic material.

1.1.6 Summary of Problem Statement

Changes in pore fluid chemistry have been correlated to embankment and natural slope stability problems in Australia, Canada and the United States. In the case study being examined here, the dyke instabilities at Seven Sisters appear to be related to changes in pore fluid geochemistry in the Glacial Lake Agassiz clay foundation soil. The observed changes in pore fluid chemistry include decreased total electrolyte concentrations, elevated Na/Ca ratios and conditions that would result in gypsum dissolution beneath the dyke. These geochemical changes can result in increased DDL thickness and the loss of cementation bonding. The evidence presented suggests a causal relationship

between chemistry changes and soil behaviour but the relationship had not been proven prior to this study.

The studies of the stable and previously unstable dykes showed that both would be stable if post-peak strengths were operative; but they would both be unstable if residual strengths were operative. Two significant questions remain. Firstly, what processes permit reduction of strengths from post-peak to residual values in sections that have not yet become unstable? Secondly, what processes allow stable dykes to become unstable on an irregular basis? The first issue is one of strength and the second is one of time.

The questions are important as the awareness of dam and slope safety increases in the general public and among professionals responsible for dams and slopes. In the past, the general practice was to construct dams to be safe immediately following construction. Following completion, the weight of the embankments generally leads to increasing strength of the foundation soils. As a result, long-term stability has been assumed if the structures were stable for the first few years of operation. This does not always appear to be the case, as some dykes such as those at Seven Sisters have become unstable even though conventional analysis predicts them to be stable. At Seven Sisters, the foundation clay is laminated, fissured, expansive and is subject to seepage of fresh water. It appears possible that under these conditions, the foundation clay may weaken with time and dykes that were predicted to be stable may become unstable.

In order to prove the relationship between pore fluid chemistry and soil behaviour, and to better understand and model the site, further testing was required to isolate the effects of geochemistry on Lake Agassiz clay in terms of elastic-plastic behaviour (that is, chemo-elastoplasticity).

Developing the program of study to examine the hypothesis was based on the earlier studies by Garinger et al. (2004) and some initial pore fluid chemistry studies by the author. This earlier work led to the understanding that at Seven Sisters, groundwater leaching resulted in changes in soil properties and behaviour sufficient to cause the observed dyke instabilities. The resulting chemical changes were responsible for the change in elastic-plastic behaviour of the soil. The timing of this change is controlled by the rate of seepage beneath the dykes.

1.2 Hypothesis

The hypothesis that was examined in this research project is that changes in pore fluid geochemistry due to leaching with fresh water results in reduction of naturally occurring cementation bonds in Lake Agassiz clay. This subsequently influences the extent of elastic behaviour as represented, for example, by the yield locus, and in the strain-softening behaviour of the high-plastic clay. Potential mechanisms responsible for the measured changes in soil properties and behaviour include the dissolution of cementation bonds and changes in DDL thickness due to changes in electrolyte concentrations and/or changes in the monovalent to divalent cation (Na/Ca) ratio. Cementation likely influences the elastic behaviour and yielding, whereas DDL

interactions might dominate plastic behaviour once failure deformations begin to occur along a shear plane.

1.3 Objectives and Methodology of Research

This thesis document confirms the relationship between pore fluid chemistry and elastic-plastic soil behaviour. The project examines the hypothesis that leaching by relatively fresh groundwater has weakened cementation bonds, lowered pore fluid electrolyte concentrations, increased the Na/Ca ratio and produced changes in soil properties and behaviour such anisotropy, brittleness and yield loci.

The objectives of the research are as follows:

- to isolate the effects of pore fluid chemistry on elastic plastic behaviour of Lake Agassiz clay using reconstituted soil to eliminate field variability,
- to establish a chemo-elastoplastic model for selected inorganic parameters in reconstituted Lake Agassiz clay,
- for the Seven Sisters case study, to determine the mechanical behaviour of the soil before and after leaching in order to demonstrate that leaching can in fact produce the anisotropy and brittleness shown in the specimens tested by Garinger (2002), and;
- to update the slope stability model for the Seven Sisters case study originally developed by Garinger (2002).

The methodology for reaching these objectives includes conducting a literature review to assess what is known regarding the effect of pore fluid chemistry on soil properties and behaviour, the problems associated with the leaching of clays, and the field of chemo-

elastoplastic constitutive models. Building on existing knowledge, a laboratory and modelling program was established to address the hypothesis.

1.4 Organization of Thesis

The organization of this thesis is as follows. Following this introductory chapter, Chapter 2 reviews the literature relevant to this research. The chapter begins with a review of the components and structure of natural clays, followed by a discussion of the physico-chemical interactions of the components and how the interactions of the components affect soil properties and behaviour in response to changing pore fluid chemistry. The prior understanding of the elastoplasticity of Glacial Lake Agassiz clay and of chemo-elastoplastic models are then discussed and areas requiring further experimental data are identified.

Chapter 3 presents the field sampling, soil characterization and laboratory testing programs undertaken by the author. Preparation of reconstituted specimens and geotechnical and geochemical testing procedures are then described.

The results of the geochemical analysis and geotechnical testing programs are presented in Chapter 4. Initial physical and chemical properties of the natural and reconstituted specimens are tabulated. Yielding, critical state and end-of-test stress states and specific volume data for each of the examined physical and chemical conditions are tabulated and yield loci presented. This section includes the remaining elastic plastic parameters such as the elastic moduli, flow rule and hardening law for the tested soils.

Chapter 5 provides an analysis and discussion of the laboratory data. Comparison of stress-strain behaviour and yield loci are presented for each of the physical and chemical conditions in the program. The results are used to establish a preliminary chemo-elastoplastic model for Lake Agassiz clays.

Using the information gained in Chapter 5, modelling of the Seven Sisters site is re-visited. Chapter 6 presents the results of the modelling. A synthesis and discussion of the laboratory testing and modelling programs is provided in Chapter 7.

Finally, Chapter 8 presents the conclusions of the research program and provides suggestions for further research.

2.0 Literature Review

The properties and behaviour of high-plastic clay can vary widely with changes in environmental conditions. The variations can be of major importance in geotechnical and geoenvironmental engineering applications. Changing pore fluid chemistry is one of the environmental conditions that can occur within the lifetime of many engineering projects, and it is well known that pore fluid chemistry influences clay soil properties and behaviour including strength, compressibility and hydraulic conductivity. The effects have been observed, for example, in clay barriers for brine containment and natural clay slopes in Canada, and in the dispersion of dam cores in Australia and the United States. Recently, preliminary studies of the Seven Sisters site in southern Manitoba have revealed a correlation between pore fluid chemistry and soil behaviour. However, the literature lacks experimental data regarding the effect of pore fluid chemistry on the yielding characteristics of high-plastic clay, a subject that will here be called chemo-elastoplasticity.

Plastic clays with a high content of smectite minerals are frequently used in geotechnical and geoenvironmental applications for their low hydraulic conductivity and contaminant attenuation properties. These properties make them suitable for barrier materials for controlling groundwater flow and containing contaminants. The geotechnical properties and behaviour of such clay soils are controlled by mineralogy, interparticle forces, soil structure and the physicochemical interactions between adjacent clay particles (Barbour and Yang, 1993). Changes in pore fluid geochemistry can influence the physicochemical interactions between the clay particles and subsequently influence the overall geotechnical behaviour of the soil. Each of these contributing factors must be

understood in order to consider the influence of changing pore fluid chemistry on soil properties and behaviour.

Several examples of applications where changes in pore fluid chemistry can be a factor are listed below:

- clay barriers for containment cells and lagoons, landfill liners and isolation of hazardous and nuclear wastes;
- embankments, dam cores and natural slopes that are susceptible to leaching and/or infiltration of water with different chemistry than the water in which the clay was initially deposited, for example, clay cores and foundations of water retention and tailings dykes; and
- contamination by organic liquids and in situ containment of contaminated sites.

Depending on the specific application, different changes in pore fluid chemistry can be expected and each may have different effects on soil properties and behaviour. These changes need to be considered to ensure continued acceptable long-term performance of the original design.

In order to help understand the effect of pore fluid chemistry on soil properties and behaviour, a review of clay mineralogy, soil structure, cementing minerals, and the physicochemical interactions between soil water, clay particles and pore fluid electrolytes is provided in the early sections of this chapter. This is followed by a review of recent work on chemo-elastoplastic models available in the literature and the current understanding of elastic-plastic behaviour in Lake Agassiz clay at the beginning of this project.

2.1 Clay Mineralogy

The term 'clay' can be used to refer to (1) a size fraction of soil having an effective diameter less than 2 μm; or (2) it can be used to refer to a particular type of mineral. The clay size fraction is usually dominated by clay minerals, mostly various forms of alumino-silicates with a sheet-like structure. In addition, the clay-size fraction often contains non-clay minerals consisting of small particles derived from physical weathering products such as quartz, carbonates and sulphates. In this discussion, we are concerned with clay minerals. The clay minerals are of interest because their mineralogy is responsible for their behavioural dependence on environmental conditions such as pore fluid chemistry. The characteristics of clays are a result of their small grain size, their platy particle shape, their high surface area and net negative surface charge. Table 2.1 provides a summary of the principal characteristics of clay minerals.

Clay minerals are secondary minerals formed by the chemical weathering of parent minerals such as feldspars (Faure, 1991). They are layered alumino-silicates (i.e. phyllosilicates) consisting of various arrangements of silica tetrahedral sheets and aluminum octahedral sheets. The basic silica tetrahedral and aluminum octahedral structural units are shown in Figure 2.1 (Mitchell, 1993). The silica tetrahedral unit consists of silica tetrahedra linked in a sheet pattern which are in the order of 10 Å thick. Each tetrahedron shares three of its bottom oxygen atoms. The aluminum octahedral unit consists of aluminum surrounded by six hydroxyl groups (OH^-) arranged to form an octahedron.

The silica tetrahedral and aluminum octahedral units can be arranged in various patterns and linked together by different types of bonds. Primary or inter-atomic bonds occur between atoms to form molecules. For example, a silica sheet and an alumina sheet can share a layer of oxygen between them. These bonds are relatively strong and are not easily broken by conventional engineering works (Mitchell, 1993). Secondary bonds occur between atoms of two separate molecules and are relatively weak. Examples of secondary bonds include Van der Waals forces and hydrogen bonds. Van der Waals forces are bonds attributed to electrical or electromagnetic attraction between a system of molecules caused by fluctuating dipoles. Hydrogen bonds result from the force of attraction between positive and negative dipoles, where the positive dipole consists of a hydrogen atom (Mitchell, 1993). Figure 2.2 (Mitchell, 1993) shows the various combinations of silica tetrahedral and aluminum octahedral units that comprise the various clay minerals. The most commonly encountered clay minerals in engineering practice and research include kaolinite, illite and montmorillonite (which is one of the smectite group).

Kaolinite consists of repeating layers of silica and alumina sheets, that is, they are 1:1 clay minerals. Bonding between the silica and alumina sheets is through a shared layer of oxygen atoms. A single kaolinite particle may include over 100 stacks of the basic units. Adjacent basic units are held together by hydrogen bonding between hydroxyls from the alumina sheet on one face and oxygen atoms from the silica sheet on the opposite face (Yong et al, 1992). The hydrogen bonds are relatively strong, which prevents hydration between layers. As such, kaolinite has a relatively low plasticity, relatively low surface area (10-20 m^2/g), low swelling potential and is a relatively poor adsorbent.

The basic structure of illite consists of an alumina octahedral sheet sandwiched between two silica tetrahedral sheets. Adjacent basic units are linked to other units by relatively strong bonding via non-exchangeable potassium ions. Potassium ions are the right size to fit in hexagonal 'holes' in the silica sheets. Soils containing illite have properties between that of low activity (defined as the ratio of plasticity index to the percentage of clay size particles in the soil) kaolinite and high activity, such as montmorillonite.

Smectite clays, of which montmorillonite is perhaps the most common example, are also 2:1 clay minerals in which each basic unit consists of an aluminum octahedral sheet sandwiched between two silica tetrahedral sheets. A layer of water and exchangeable ions is located between two basic montmorillonite clay particles. The bond between two adjacent clay particles is relatively weak and can change thickness with changing water content and pore fluid chemistry. The ease of adsorption of additional water between layers results in the highly plastic and expansive behaviour of montmorillonite (Craig, 1992; McBride, 1994). This, combined with a high specific surface area and cation exchange capacity (CEC), makes montmorillonite a good material for use in liners and barriers.

Silicon and aluminium within the silica tetrahedra and aluminium octahedra, respectively, can be partially replaced by other elements of similar size in a process known as isomorphous substitution. Isomorphous substitution of silicon or aluminium by atoms of lower valency (but similar atomic radius) results in a net negative charge on the clay particle surface. Common substitutions include aluminium for silicon in the tetrahedral

sheets and magnesium, iron or lithium for aluminium in the octahedral sheets (Mitchell, 1993). In montmorillonite, for example, one magnesium atom substitutes for every six aluminium atoms which results in the following formula:

$$(Al_{5/3}, Mg_{1/3})Si_4O_{10}(OH)_2. \qquad [2.1]$$

This results in a net one-third negative charge per 367 gram molecular weight (i.e. 0.333/367 = 91 meq/100 g). This high surface charge combined with the high surface area of montmorillonite (up to 800 m^2/g), produces highly active surfaces, which are important with respect to water, electrolyte and contaminant interaction (Mitchell, 1993; Yong et al, 1992).

Isomorphous substitution results in a fixed surface charge and accounts for the majority of the charge in 2:1 clay minerals. In contrast, isomorphous substitution contributes a minor portion of surface charge for 1:1 clay minerals such as kaolinite, which has a surface charge that depends on pH. The surface charge of kaolinite arises from unsatisfied valence charges at the edges of particles. At the edges of platey clay particles, hydroxyl groups within the alumina sheets are exposed and can dissociate. These amphoteric or variable charge surfaces are similar to hydrous oxide surfaces with surface charges that depend on pH. When pH is high (that is the H^+ concentration is low), protons dissociate from the hydroxyl groups, resulting in an increased net negative surface charge. On the other hand, when pH is low (that is the H^+ concentration is high), the hydroxyl groups will incorporate more protons, which can result in a positive surface

charge. At some pH, known as the point of zero charge (p_{zc}), the surface charge will be balanced (Stumm, 1992; Yong et al, 1992).

2.2 Soil Water

The properties of water and the interactions between water and solid soil particles are important to the overall chemical and physical behaviour of clay soils. A water molecule contains eight outer shell electrons arranged in pairs that form an overall tetrahedral pattern (Mitchell, 1993). This arrangement results in a separation between the positive and negative atomic charge centres of the molecule, thus resulting in a strong dipole. Since water molecules are polar, they are attracted to charged clay surfaces, forming a layer of 'adsorbed' water. Hydrogen bonds form between the negatively charged mineral surface and the net positive end (the hydrogen atom) of water molecules (Mitchell, 1993). Alternate mechanisms of water adsorption by clay surfaces, including ion hydration, attraction by osmosis and dipole attraction are described by Mitchell (1993). The strength of the bond to the surface depends on the magnitude of the negative surface charge (that is, charge density) and decreases with distance from the surface, up to a distance where the water is governed by purely gravitational forces (Craig, 1992; Mitchell, 2000). The polar nature of water also makes water molecules attracted to each other and to ions (charged atoms or molecules) in solution. These attractions lead respectively to hydrogen bonding between adjacent water molecules and to ion hydration.

Electrochemical interactions between clay minerals and water result in water being present in several forms in clay soils (Stepkowska, 1990). Smectite clay particles often

group into 'peds' or 'aggregates' with small spaces (nano-pores) between the particles and larger spaces (micro-pores) around and between the peds. (The pore size distribution is therefore bi-modal (Yong et al., 1993)). Adsorbed water is located between clay platelets and surrounding the aggregates of platelets. Under normal conditions, this water does not flow. This water is strongly attached over one to four molecular layers of water (~1 nm or up to approximately 20 Å) between platelets and up to seven molecular layers of water from an external surface of a cluster of clay platelets (Sposito, 1984; Loret et al., 2001). Adsorbed water either in or around aggregates of clay particles has properties different from that of bulk water (Low, 1979). Structural water in the form of hydroxyl groups is part of the structural lattice of clay and cannot be removed at temperatures less than 350°C (Hueckel, 1992).

Water that is able to flow under ordinary hydraulic gradients (at room temperature) is contained by micropores and macropores. The presence of adsorbed water extending into micropores reduces the size of 'pore throat' openings that are available for the flow of free water. That is, the hydraulic conductivity of clay varies with the thickness of the layer of adsorbed water. Macro-pores are larger than the micropores and consist of fractures and fissures.

2.3 Cementation in Clay Soils

Cementation in clays is believed to contribute to brittle, strain-softening stress-strain behaviour, increases in strength, increases in sensitivity, and apparent preconsolidation pressures. Common cementing agents in natural soils include carbonates, sulphates, hydrous and anhydrous iron and aluminium oxides, manganese oxides, silicates and

organic matter (Moum, et al 1971; McKyes et al, 1974; Yong et al, 1979; Quigley, 1980; Torrance, 1983; Mitchell, 1993; Corrigan et al, 2001). A list of several naturally occurring cementing minerals and their solubility products are listed in Table 2.2.

Following deposition of the clay, cementing minerals may precipitate on soil particles and at interparticle contacts. This can contribute to the peak strength of clay by helping to lock the soil into a metastable structure and may control yielding behaviour. This effect has been attributed to the presence of cementing agents at concentrations as low as 1%, where precipitation of the minerals at interparticle contacts result in a "spot welding" effect (Berry and Torrance, 1998). If cementation is lost due to leaching, the soil becomes more brittle, since strength is rapidly lost after the bonds holding the structure together are weakened. The mechanism and rate of cementing mineral dissolution is related to mineral solubility (Table 2.2). Dissolution of relatively less soluble minerals tends to be controlled by surface reactions whereas the dissolution of relatively soluble minerals, such as gypsum, is controlled by transport processes (Appelo and Postma, 1996). The effects of leaching are discussed further in Section 2.6.

Boone and Lutenegger (1997) examined calcite and dolomite content with depth, geographic location, and geologic origin and indicated the impact on engineering behaviour. Carbonates were found to be the main cementing agents in soils around the world. Cementation generally increases the undisturbed (intact) strength. However, when remoulded or disturbed, the soil is prone to collapse and rearrangement of the particles, which can often lead to a rapid decrease in the strength of the soil. The study indicated that carbonate leaching due to seepage might be an important mechanism in reducing shear strengths and creating slope instability. The authors suggested that the

degree of cementation caused by carbonate minerals could depend on interrelationships between the preconsolidation pressure, mineralogy, rate of deposition, and the particle size distribution. Routine testing for carbonate content was suggested as an index parameter of soil mineralogy and engineering behaviour.

Gypsum ($CaSO_4 \cdot 2H_2O$) has been identified as a potential cementing mineral in clays and tills of the Canadian prairies (Van Stempvoort, 1994). Sulphate (SO_4^{2-}) is commonly the dominant anion in shallow glacial sediments, the source of which is the oxidation of sedimentary sulphur (S) in the upper 10 to 15 m weathered zone. The form of the original sedimentary sulphur is a combination of pyrite and organic sulphur (Van Stempvoort, 1994). The source of the calcium consists of carbonate parent material. Following the production of sulphate by weathering in shallow deposits, it can precipitate with calcium as gypsum, be transported laterally or downward by groundwater flow. Under anaerobic conditions, the sulphate can be reduced back to sulphide.

The status of a potential cementing mineral can be evaluated if its solubility is known. For example, the equilibrium reaction for gypsum is:

$$CaSO_4 \cdot 2H_2O(s) \leftrightarrow Ca^{2+} + SO_4^{2-} + H_2O. \qquad [2.2]$$

Using the Law of Mass Action, the ion activity product (IAP) for equation [2.2] is defined as:

$$[Ca^{2+}][SO_4^{2-}] = IAP \qquad [2.3]$$

where $[Ca^{2+}]$ and $[SO_4^{2-}]$ are the activities of calcium and sulphate in solution, respectively (Faure, 1991). The IAP can then be compared to the solubility product constant (K_{sp}) using the saturation index, SI to estimate whether the pore fluid is under-saturated, at equilibrium, or super-saturated with respect to gypsum:

$$SI = \log(IAP/K_{sp}). \qquad [2.4]$$

SI values of zero indicate the system is at equilibrium. Positive SI values indicate super-saturated conditions in which mineral precipitation can be expected. Negative SI values indicate under-saturated conditions when mineral dissolution can be expected.

It should be noted that the solubility of the mineral in question can be influenced by other factors such as temperature and ionic strength. For example, the solubility of gypsum increases significantly for sodium chloride concentrations ranging from 0 mg/L to 100 mg/L (Freeze and Cherry, 1979). Gypsum solubility reaches a peak at approximately 125 mg/L of sodium chloride and then decreases with further increases in ionic strength.

The balance between equilibrium, dissolution and precipitation of a cementing mineral can be affected by leaching, contamination by acids, inorganics or organic compounds and biological decomposition of organic contaminants or natural organic matter (Faure, 1991; Fleming et al, 1999; Hutchison et al, 1992; Rowe, 2002). For example,

heterotrophic bacteria utilize organic compounds as both an energy source and a carbon source for cell maintenance and reproduction (Weidemeier et al, 1995). Energy is released by microbially mediated oxidation-reduction (redox) reactions, involving the transfer of electrons from the organic compound (electron donor) being oxidized to an electron acceptor. Initially, biodegradation will proceed by aerobic respiration where oxygen is used as the electron acceptor and is reduced to water. Once the available oxygen is depleted, aerobic metabolism is over-taken by anaerobic metabolism and alternate electron acceptors are employed. Alternate electron acceptors, in order of preference (based on energy released) include nitrate, manganese, ferric iron, sulphate and carbon dioxide (Wiedemeier et al, 1995). The metabolic by-products of these reactions are responsible for changes in pore fluid chemistry.

Consistent throughout the biological reactions is the production of carbon dioxide gas (Domenico and Schwartz, 1990; Weidemeier et al, 1995; Rowe, 2002). Therefore, these biological reactions are coupled with the chemistry of the carbonate minerals. Carbon dioxide dissolves into pore water forming carbonic acid ($H_2CO_3^*$, where $H_2CO_3^* = CO_2(aq) + H_2CO_3$) which dissociates to release protons, the bicarbonate ion (HCO_3^-) and the carbonate ion (CO_3^{2-}) in the following series of reactions:

$$CO_2(g) + H_2O \leftrightarrow H_2CO_3^* \quad [2.5]$$

$$H_2CO_3^* \leftrightarrow HCO_3^- + H^- \quad [2.6]$$

$$HCO_3^- \leftrightarrow CO_3^{2-} + H^- \quad [2.7]$$

For a pH in the range of 6.35 to 10.33, the dominant species will be the bicarbonate ion. If the partial pressure of carbon dioxide increases due to continued biodegradation of organics, an increase in H_2CO_3* concentration will occur, with a corresponding decrease in pH of the pore water. The decrease in pH is subsequently buffered by the presence of carbonate minerals in the soil. The system will experience an increase in solubility and dissolution of calcium and magnesium from calcite ($CaCO_3$) and dolomite ($MgCO_3$) in the soil, respectively. According to Le Châtelier's principle, increases in H_2CO_3* concentration causes a shift to the right in the following equation (Faure, 1991; Lessard and Mitchell, 1985):

$$CaCO_3 + H_2CO_3^* \leftrightarrow Ca^{2+} + 2HCO_3^- \qquad [2.8]$$

This reaction brings Ca^{2+} into solution, increases electrolyte concentration, decreases the monovalent/divalent cation ratio and increases alkalinity of the pore fluid. If the soil is then subject to leaching, the dissolved calcium can be removed from the system. This shifts the equilibrium of cementing agents such as calcite and gypsum towards dissolution.

In contrast, the anaerobic environment produced by bacterial decomposition of organics favours the reduction of other ionic species in the soil and may contribute to precipitation of different cementing agents (Lessard and Mitchell, 1985). Ferric (iron III, Fe^{3+}) oxides are reduced to soluble ferrous (iron II, Fe^{2+}) oxides in the iron-reduction process and sulphate is reduced to hydrogen sulphide by sulphate-reducing bacteria (SRB) in the

sulphate reduction process. These products result in the formation of insoluble iron oxide and iron sulphide minerals which may contribute to the amount of cementation bonding:

$Fe^{2+} + H_2S \rightarrow$ black amorphous FeS $\rightarrow$ slowly crystallizes $\rightarrow FeS_2$ (pyrite). [2.9]

Based on the preceding paragraphs, there are a number of naturally occurring materials that can contribute to the cementation of clay soils and their tendency to form or dissolve can change due to common mass transport and geochemical processes.

2.4 Physicochemistry of Clay Soils

The effects of environmental loadings on clays, including changes in chemistry and temperature, have been handled classically using diffuse double layer theory (Yong et al, 1992). The theory is generally considered applicable to natural and reconstituted soils containing polar pore fluids when the micropore spaces around aggregates of clay particles are sufficiently large. The pore space between aggregates of clay platelets in densely compacted clays, such as bentonite-based buffer materials used for nuclear waste disposal, appear to be too small for diffuse double layers to develop (Hueckel, 1992; Yong, 1992; Karnland, 1997; Dixon et al, 2002). The following section provides an overview of diffuse double layer theory.

2.4.1 Clay-Water-Electrolyte System

Negatively charged clay surfaces attract cations and repel anions dissolved in the pore fluid. The combination of the charged clay surface and the distributed charge in the liquid phase is known as the diffuse double layer (DDL). The DDL model was originally proposed independently by Gouy in 1910 and Chapman in 1913, and later modified by Stern in 1924. The theory developed by Gouy and Chapman assumed that the ions within the resulting distributed electrical charge consisted of point charges. This assumption results in an over-estimate of computed concentrations next to the charged clay surface. Stern modified the theory, recognizing that the ions have a finite size that controls the maximum concentration of ions at the clay surface (Mitchell, 1993). Although it is perceived as an incomplete model (Yong et al., 1992), DDL theory assists in understanding the effects of soil-groundwater and soil-waste interactions on geotechnical properties, ion exchange and contaminant transport. Figure 2.3 (Yong et al., 1992) illustrates the basis of the DDL model.

The differential equation used for computing the ion concentrations and the corresponding distribution of electrical potential in the DDL is obtained by combining the Poisson equation with the Boltzmann equation (Mitchell, 2000; Yong et al, 1992).

The Poisson equation allows computation of the electrical potential as a function of distance from the charged surface of a single clay particle:

$$\frac{d^2\Psi}{dx^2} = \frac{-4\pi\rho}{D}$$

[2.10]

where Ψ is electrical potential (in volts) at a point within the DDL and is defined as the work required to move a positive unit charge from infinity to a given point in the electrical field of the DDL, x is the distance from the surface (in m), ρ is the charge density (in Cm^{-3}) at a point in the DDL and D is the dielectric constant (unitless) of the pore fluid. The dielectric constant is the ratio of electrical permittivity (ε in $C^2J^{-1}m^{-1}$) of the pore fluid to the electrical permittivity of a vacuum (ε_0 = 8.8542 x 10^{-12} $C^2J^{-1}m^{-1}$) and reflects how easily a molecule of the pore fluid medium can be polarized and oriented in an electrical field relative to a vacuum.

Charge density is the charge per unit volume resulting from the sum of the contribution of charge from all species in solution:

$$\rho = \sum n_i z_i e$$

[2.11]

where e is the charge of an electron (1.602 x 10^{-19} coulomb), z_i is the valence of the i^{th} ion species and n_i is the concentration of the i^{th} ion species. The concentration, n_i, at a given point in the DDL is given by the Boltzmann equation:

$$n_i = n_{io} \exp\left(\frac{-z_i e\Psi}{kT}\right) \qquad [2.12]$$

where n_{io} is the reference ion concentration in the bulk pore fluid (i.e. beyond the influence of the DDL), k is the Boltzmann constant (1.38 x 10^{-23} JK^{-1} = the gas constant per molecule, that is R/N where N = Avogadro's number, R = the gas constant), and T is temperature (in K) . Substituting Equation [2.12] into Equation [2.11] gives:

$$\rho = \sum_i n_{i0} z_i e \exp\left(\frac{-z_i e\Psi}{kT}\right) \qquad [2.13]$$

which is known as the Boltzmann distribution for electrical charge as a function of distance from the mineral surface. Finally, substituting Equation [2.13] into Equation [2.10] combines the Poisson equation with the Boltzmann distribution:

$$\frac{d^2\Psi}{dx^2} = \frac{-4\pi}{D} \sum n_i z_i e \exp\left(\frac{-z_i e\Psi}{kT}\right) \qquad [2.14]$$

which is known as the Poisson-Boltzmann equation (Yong et al, 1992; Mitchell, 2000). This equation provides the relationships between ionic distribution and electrical potential within the pore fluid of the diffuse layer with respect to distance from the clay particle. The general configurations of these relationships are shown in Figures 2.4 and

2.5 (Mitchell, 1992), respectively. Integrating the Poisson-Boltzmann equation from the charged mineral surface to a point in the pore fluid where electrical charge is balanced provides an estimate of the thickness of the DDL:

$$\frac{1}{K} = \sqrt{\frac{D\kappa T}{8\pi n_i z_i^2 e^2}} \qquad [2.15]$$

where $1/K$ is the distance from the charged surface to a point in the pore fluid where the bulk pore fluid chemistry is reached and cationic charge is balance by anions (Mitchell, 2000; Yong et al, 1992). Equation [2.15] shows the effect of changing pore fluid chemistry, specifically concentration and valence of dissolved solutes and dielectric constant and temperature of the pore fluid, on the thickness of the DDL.

2.4.2 Factors Influencing Diffuse Double Layer Thickness

Based on Equation [2.15], as electrolyte concentration or valence increases, the thickness of the DDL decreases. The effect of increasing ion concentration is illustrated in Figure 2.6. In this case, more cations in the pore fluid balance the negative surface charge more effectively and the background pore fluid chemistry will be reached at a closer distance from the particle surface.

Similarly, cations with a higher valence will also balance the negative surface charge more effectively than ions with lower valency and produce a decrease in the thickness of the DDL. The effect of increased valence is shown in Figure 2.7. It is well established (Mitchell, 1993) that multivalent cations are preferentially adsorbed on clay mineral

surfaces. Relatively low concentrations of multivalent cations can therefore influence DDL thickness. The relative concentration of monovalent cations to divalent cations is often expressed as a monovalent to divalent cation ratio (for example Na/Ca) or sodium adsorption ratio (SAR). The SAR is used to represent the relative concentrations of monovalent sodium to the divalent cations calcium and magnesium that are in the adsorbed complex. It is given by:

$$SAR = \left[\frac{Na^{+}}{\left[(Ca^{2+} + Mg^{2+})/2 \right]^{1/2}} \right] \qquad [2.16]$$

with units of $(meq/L)^{1/2}$. The proportion of sodium in the adsorbed layer is an important factor influencing the structural status of a soil (Mitchell, 1993). It indicates the susceptibility of a soil structure to breakdown due to clay particle dispersion.

According to Equation [2.15], increases in the dielectric constant and temperature will increase the thickness of the DDL. This is the case for the dielectric constant, where for example the DDL thickness will decrease if water (D=80 at 20°C) is replaced by an organic liquid with D<10. However, increasing temperature decreases the dielectric constant and the net effect on the thickness of the DDL will depend on clay mineralogy (AECL, 1997). The overall effect of changes on temperature on the product of $D\,T$ and DDL thickness is generally small (Mitchell, 1993), but may produce some unexpected mechanical effects (Graham and Lingnau, 1995).

Although pH is not one of the variables in Equation [2.15], it can influence DDL thickness by directly affecting the surface charge of the particle. As mentioned earlier, hydroxyl groups on exposed surfaces and edges of alumina octahedra can dissociate. Higher pH (that is, basic conditions with low H^+ concentration) will cause protons to dissociate from the hydroxyl groups leaving a greater net negative charge on the particle surface. The higher surface charge will increase the DDL thickness by attracting more cations to the particle surface (Yong et al, 1992).

DDL theory is useful in the development and evaluation of remediation and/or containment options for contaminated sites. The presence of organic non-aqueous phase liquids (NAPL), such as fuel hydrocarbons and chlorinated solvents in soil will directly change the thickness of the DDL and will lead to biogeochemical reactions that also influence the DDL thickness. Organic contaminants directly affect the DDL by changing the dielectric constant of the pore fluid. The dielectric constants of organic liquids (<10) are much lower than that of water (80.1), meaning that the non-polar organic molecules will not readily align in an electric field relative to water. Movement of bulk hydrocarbons between particles forces water and ions out, and may insulate the repulsive forces between two particles. Alternatively, the organic molecules may not align with the electrical field of clay particles, thus suppressing the size of the double layer.

2.4.3 Diffuse Double Layer Interactions and Contribution to Effective Stress

The practical importance of potential fields around a single particle is that changes in DDL thickness resulting from changes in pore fluid chemistry produce changes in interparticle repulsion between two adjacent particles. This will lead to changes in soil strength, compressibility and hydraulic conductivity, and thus changes in response of the soil to applied loading.

Depending on geological and environmental conditions, there are three kinds of interparticle contacts found in clay soils. These are (1) edge-to-edge contacts, (2) edge-to-face contacts and (3) face-to-face contacts. These contacts contribute to σ' in Terzaghi's (1925) effective stress principle $\sigma = \sigma' + u$, where σ is total stress, σ' is effective stress and u is pore water pressure. The difference in nature of these contacts allows σ' to be separated. The edge-to-edge and edge-to-face contacts contribute to σ' directly as true interparticle contacts. When two clay particles face one another (Figure 2.8), a repulsive stress (R) (expressed as force per unit area, or unit force) will result due to electrostatic repulsion of cations from overlapping DDLs (Figure 2.9). More extensive DDLs will result in higher repulsive stresses for a given particle spacing. DDL thickness, and in consequence R, are therefore sensitive to changes in pore fluid chemistry. Concurrently, smaller attractive stress (A) will exist between the particles due to London-Van der Waals forces. These attractive stresses are due to universal forces of attraction caused by fluctuating dipoles and are insensitive to changes in pore fluid chemistry (Mitchell, 1993). In general, repulsion is the dominant stress. The resultant of

these two long-range stresses has been termed the net long-range repulsive unit force (or stress) $|R-A|$ (Lambe, 1960).

It is frequently understood that 'effective stress' comes only from the integration of edge-to-edge and edge-to-face contacts. In fact, Terzaghi explicitly included effects like those that arise from the $|R-A|$ unit force. Extension of the commonly understood effective stress concept are needed for situations where the soil has a significant physicochemical component that influences its behaviour. The net long-range repulsive stress will contribute to the total effective stress where a portion of the effective stress is carried by true physical contacts between soil particles and the remainder is carried by $|R-A|$. This can be written as:

$$\{\sigma'\} = \{\sigma^*\} + \{|R-A|\} \qquad [2.17]$$

where σ^* is the stress transferred between true physical contacts between soil particles, including friction and cementation bonds (Graham et al, 1989, 1992).

Repulsion, which is largely controlled by pore fluid chemistry, can play a dominant role in controlling volume change and shear strength of active clay soils (Barbour and Yang, 1993; Mitchell, 1993). If the pore fluid chemistry changes in such a way that the DDL becomes more extensive, repulsive stresses will increase. This will lead to swelling of expansive clays under constant loading or increased swelling pressure if restrained at constant volume. Under undrained conditions with constant total stress and pore water

pressure, it leads to a decrease in the physical contact stress σ^*. It can also lead to dispersion of suspensions and possible increases in hydraulic conductivity of dam cores, for example. On the contrary, if changes in pore fluid chemistry result in thinner DDL conditions, expansive clays will consolidate in a process called chemo- or osmotic consolidation under drained conditions. For undrained conditions with constant total stress and pore water pressure, σ^* will increase. Flocculation of suspensions may be observed, accompanied by increases in hydraulic conductivity.

As shown earlier, models based on DDL theory can calculate electrical potential between two face-to-face clay particles under some specified physicochemical conditions. The corresponding repulsive force can then be computed from the electrical potential. Limitations can be expected since the theory considers just two particles in a polar pore fluid. As a result, the theory provides good quantitative agreement only for the case of smectites with dilute pore fluids and a face-to-face fabric. For example, the measured swelling pressures of montmorillonite with high pore fluid concentrations are significantly higher than those predicted by DDL theory (Guimaraes et al., 2001). Other models have been developed such as DVLO (Derjaguin, Verwey, Landau, Overbeek) theory to address the limitations of DDL theory (Komine and Ogata, 1995; Yong et al, 1992). Despite its limitations, DDL theory provides a useful, accessible qualitative reference for the evaluation of the effects of electrolyte concentration, valence, dielectric constant and temperature on the behaviour of clays.

2.5 Soil Structure

As mentioned in Section 2.2, individual clay particles are generally grouped into aggregates in natural soils. The arrangement of particles within a single aggregate can be described as microfabric, and the arrangement of a number of aggregates can be described as macrofabric. For natural smectitic clays, the microfabric is dominated by clusters of 5 to 15 face-to-face platelets of individual clay particles separated by nanopores in the order of 10 to 20 Å thick (Loret et al, 2001). These pores contain in the order of several (1-4) water molecules with different density and viscosity than that of free water in larger pores. This water cannot flow easily, even when subjected to high hydraulic gradients. In contrast, micropores around and between the aggregates are in the order of 1 μm in size and contain water that can flow under ordinary hydraulic gradients. Other larger features such as cracks, fissures, laminations and root holes contribute to macroporosity of natural clays (Low, 1979; Mitchell, 2000).

In contrast, densely compacted clays such as the bentonite-based compacted buffer materials used for nuclear waste disposal contain aggregates of individual clay particles on the order of 1000 platelets thick (Loret, 2001). All of the pores are of the order of 6 to 50 Å which is believed to be too small for diffuse double layers to develop (Dixon et al, 2002; Hueckel, 1992; Karnland, 1997; Yong, 1992).

In less compacted applications, (for example bentonite slurry trenches and cut-off walls) individual particles within a clay suspension can be arranged in a variety of ways as shown in Figure 2.10. Examples of clay particle arrangement within a single aggregate of natural clay are shown in Figure 2.11. Interactions between the aggregates provide

the ultimate control of strength, compressibility and hydraulic conductivity in natural clays (Barbour and Yang, 1993).

In natural clays with well developed diffuse double layers, pore fluid chemistry influences the inter-relationship of the aggregates by influencing the net $|R-A|$ stresses. Interaction between aggregates changes as the DDL changes. As a result, the amount of friction between aggregates, the soil hydraulic conductivity and the compressibility of the soil skeleton will also change. If the repulsive forces are small or do not exist (that is the DDLs are thin), the particles can approach one another. Aggregates will then tend to contract towards adjacent aggregates and increase friction within the soil. There will also be a tendency to consolidation and decreased permeability if sufficient confining pressure is present. In contrast, DDL shrinkage can result in large increases in hydraulic conductivity due to cracking, if confining stresses are insufficient to close these features. If repulsive forces are dominant (extensive DDLs), the aggregates will tend to separate and/or disperse, reducing inter-aggregate friction and potentially leading to swelling and permeability decreases. This discussion can also be extended to include shear planes with predominantly face to face particle orientation. Here, it is expected that the net $|R-A|$ stresses will influence friction along the shear plane and control residual strength.

2.6 Leaching and Dispersion of Clay

Groundwater seeping through clay barriers, embankments, dam cores, and natural slopes can change pore fluid chemistry, result in the dissolution of cementation bonds at interparticle contacts, and erode dispersive clays (Mitchell, 1993). Leaching of an originally salt-rich pore fluid by relatively fresh groundwater lowers electrolyte concentrations and typically increases the monovalent/divalent cation ratio (that is, it

lowers the valence of the pore fluid). As shown in the previous section, increases in the monovalent/divalent cation ratio and decreases in total ion concentration both result in expansion of the diffuse double layer (DDL) and increased interparticle repulsion (R). This can increase soil volume or swelling pressure and decrease shear strength. If a sufficient increase occurs in R, a dispersive clay may result. Dispersive clays are defined by spontaneous detachment of clay particles from each other, after which, they essentially become suspended in water (Sherard et al, 1972). This potentially serious effect has resulted in the formation of erosion channels and tunnels in clay structures. It has resulted in the catastrophic failure of a number of well-constructed dams, embankments and slopes composed of smectite clays through the development of piping channels and internal erosion.

The susceptibility of a clay to leaching and subsequent changes in behaviour begins with the conditions under which the soil was formed. During soil deposition, pore fluid chemistry may have been different from its present conditions. For example, the soil may have been deposited under brackish or salt-water conditions as in the case of the marine clays of Scandinavia or the estuarine clays of the St. Lawrence Lowlands (Quigley, 1980). These clays appear to be rarely smectitic and are mostly illites or chlorite-illite mixtures. Under these conditions the soil particles are deposited with a flocculated, largely edge-to-face structure. After deposition, cementing agents such as calcite ($CaCO_3$) and gypsum ($CaSO_4 \cdot 2H_2O$) may precipitate on soil particles and at interparticle contacts if supersaturated conditions exist. Following isostatic uplift or a eustatic drop in sea level, the clay is removed from the high ion concentration environment of its deposition in seawater and is subject to leaching by relatively fresh water. Freshwater leaching can occur as a result of artesian (upwards) seepage of

groundwater, percolation of precipitation through natural slopes, or seepage through engineered embankments. The leaching process can occur by advection or diffusion out of clay as freshwater flows through more permeable features such as fractures and fissures or silt and sand lenses (Torrance, 1974). If cementation is lost due to leaching, the soil may become more brittle in terms of shear resistence since strength is rapidly lost after the bonds holding the structure together are weakened.

Leaching, and its resulting changes in pore fluid chemistry and degree of cementation, affect what is known as the 'sensitivity of clay soils. The sensitivity of a soil refers to the ratio of its undisturbed undrained strength to its remoulded undrained strength at the same water content (Terzaghi, 1944). This ratio will range from 2 to 16 for mildly sensitive to highly sensitive clays and from 16 to over 100 for 'quick' clays that turn into a viscous fluid upon remoulding (Craig, 1992; Mitchell, 1993). If a sensitive soil undergoes straining, its quasi-stable existing structure may collapse. This can result in up to a 50% reduction in undisturbed strength and the potential for a quick clay to form (Kazi and Moum, 1973). Leaching is a concern for both natural and engineered slopes and embankments where changes in pore fluid chemistry may affect their stability.

Changes in soil properties and behaviour as a result of leaching have been observed by a number of researchers. Leaching tests performed on natural Norwegian marine clays resulted in decreased strength and increased sensitivity from approximately 8 to 200 as salt concentration was reduced from approximately 15 g/L to 2 g/L (Bjerrum and Rosenqvist, 1956). The leaching hypothesis was confirmed using reconstituted Åsrum clays consolidated in salt water with a concentration of 35 g/L. Sensitivity was found to increase from 5 to 110 in the leached specimens.

Similar effects on sensitivity are observed in clays containing significantly less salt content, with the controlling factor being attributed to the monovalent/divalent cation ratio. Champlain Sea (Leda) clay in eastern Canada generally contains less than 1 g/L salt content with a maximum of approximately 2 g/L. Sensitivity of this soil was found to increase from less than 20 to approximately 900 as the monovalent cation concentration increased from 75% (the approximate value for sea-water) to 95% of the cation concentration after leaching. Biological decomposition of organic matter was proposed as the cause of the dissolution of divalent cations (Lessard and Mitchell, 1985). As discussed in Section 2.3, carbon dioxide produced during biodegradation reacts with pore water to form carbonic acid. Carbonic acid subsequently dissolves carbonates in the soil (reducing the amount of cementation) and increases the alkalinity of the pore fluid. With the divalent cations from carbonates mobile in the pore fluid, they become susceptible to removal by leaching. An increase in the monovalent/divalent cation ratio, which increases repulsive forces and DLL thickness, was considered a requirement for the formation of 'quick' Champlain Sea clay (Eden and Crawford, 1957; Penner, 1963).

2.7 Chemo-Elastoplasticity of Clays

Traditionally, modelling the constitutive behaviour of clays has handled strength, compressibility, saturation/groundwater flow, heat conduction and mass transport separately. However, clay structures used for containment of any liquid or waste material requires a coupled approach. Combined stability and deformation computations will be increasingly needed as geotechnical engineers move toward an increased emphasis on limit states design. The mechanical performance of a clay structure or

barrier depends both on the initial and the incremental effective stresses, which are simply expressed as the difference between total stresses and measured pore water pressures. The net repulsive component of the effective stresses (Equation 2.17) depend on temperature and physicochemical interactions. Meanwhile, pore water pressures depend on hydraulic conductivity, which is a function of volumetric strain and is controlled by the DDL behaviour. Physicochemical interactions depend on pore fluid chemistry, which can induce volume strain (Quigley and Fernandez, 1991; Hueckel, 1992).

Elastic-plastic constitutive models are commonly used to describe the behaviour of clays. The basis of elastic-plastic soil mechanics is that stresses and strains are comprised of two parts that include an elastic component and a plastic component. The transition between purely elastic behaviour and the onset of plastic deformation is known as yielding. Prior to the onset of plastic straining, a region in stress-strain space exists where straining is essentially elastic. Within this region, all strains are considered to be elastic and recoverable. The elastic region is bounded by a yield surface or yield locus. When the stress state of a soil is taken to the yield surface, total strain will consist of both elastic and non-recoverable plastic deformation.

Elastic-plastic models have five primary requirements including definition of (1) a yield locus, (2) elastic parameters, (3) a flow rule, (4) a hardening law and (5) a strength law or failure criterion. The ultimate goal of a chemo-elastoplastic model is to define soil behaviour in terms of elastic-plastic soil mechanics in relation to geochemical changes.

Research on the effect of pore fluid chemistry on soil properties and behaviour began with compatibility testing of clay barriers with various contaminants associated with, for example, landfill leachate, brine wastes, hydrocarbons and nuclear waste. The primary objective of this initial work was to quantify changes in hydraulic conductivity. The research led to a number of important observations that appeared to be consistent with DDL theory. Addition of various chemicals to clay barrier materials in flexible wall permeameters revealed increases in hydraulic conductivity ranging from 0 to 5 orders of magnitude, increases that obviously have serious implications with respect to performance. Examples include Budhu, 1991; Dragun, 1988; Dragun, 1991; Fernandez and Quigley, 1985; Graham et al, 2001; Kashir and Yanful, 2001; and Middleton and Cherry, 1994. The increases in hydraulic conductivity have been attributed to DDL shrinkage (caused by decreased dielectric constant, increased electrolyte concentration or increases in valence) that leads to volume change of the clay aggregates and increased porosity, resulting in more free water within a micropore. It was quickly recognized that the magnitude of the change in hydraulic conductivity depended on confining pressure and hence, effective stresses in the specimen (Figure 2.12, Barbour and Yang, 1993).

Studies on the effects of highly concentrated salt brines on the volume straining of natural clays from Western Canada led to the concept of osmotic consolidation (Barbour and Fredlund, 1989). Large decreases in specific volume have been measured as a result of brine permeation. The high electrolyte concentrations associated with the brines depress DDLs. This in turn increases interparticle stresses (σ^*) and allows tighter particle spacing. This effect is displayed in Figure 2.13 (Mesri and Olson, 1971; Barbour and Fredlund, 1989), which shows consolidation

curves for a number of specimens prepared with different electrolyte concentrations in their pore fluid. Figure 2.14 (Barbour and Yang, 1993) shows osmotic consolidation of a specimen as it is permeated with brine at constant total stress. The steep drop in the curve as it is permeated with brine suggests yielding despite no changes in the applied stress. It is apparent that the change in chemistry has changed the soil structure, which in turn may cause changes in hydraulic conductivity. The degree to which physicochemical changes affect hydraulic conductivity and volume change depend on the initial structure of the soil and the confining stress (Barbour and Yang, 1993; Guimaraes et al, 2001).

Research on chemo-mechanical models is recent, fairly restricted and depends on validation from a limited database. Experimental work on chemo-elastoplastic models is small. A common goal of the chemo-mechanical models is to relate soil strength to chemistry of the pore fluid. They require a series of assumptions for the ways in which elasticity, yielding, plastic hardening, a flow rule, and a failure criterion vary with the chemistry of the pore fluid. A number of researchers have developed relationships between ionic concentration and soil strength through triaxial testing (Barbour and Yang, 1993; Di Maio and Fenelli, 1994; Di Maio and Onorati, 1999; Ho, 1985; Hueckel, 1997; Loret et al 2001; Olson, 1974; Torrance, 1999). Increases in shear strength with increasing electrolyte concentration and valence have been attributed to decreases in the net long-range electrostatic repulsive stress due to decreased DDL thickness. Well developed DDLs would be expected to reduce friction between adjacent clay particles, especially when they are in a face to face orientation such as along a shear plane. As the net long range repulsive stress decreases, the proportion of effective stress carried by true interparticle contacts increases if external loading is available to force the

particles together. The shearing resistance at inter-aggregate contacts therefore increases. This has been shown to increase the friction angle ϕ' by approximately 3.5 degrees in Regina clay (Figure 2.15, Barbour and Yang, 1993) and also both the normally consolidated and over-consolidated strength envelopes (Ho, 1985; Barbour and Yang, 1993) (Figure 2.16).

Chemo-mechanical models have evolved towards true chemo-elastoplastic (CEP) models by considering chemistry, stress states and volume states together, in an elastic-plastic framework. The models have typically combined independent strength and compressibility data available in the literature for comparison. Hueckel (1992) extended a previously proposed thermo-elastoplastic model for clay to include the effects of chemistry (Figure 2.17, Hueckel, 2001). The models proposed by Hueckel assume isotropic elasticity independent of concentration, elliptical yield loci, plastic hardening independent of concentration, $\phi' = \phi'(c)$, and associated flow. The equations for the model use microscopic and molecular mechanics to describe behaviour of fluid within nanopores. The model handles the strain produced by the interaction of temperature, stress and chemical loads by including the total accumulated mass transfer of adsorbed water by these processes as a single variable Ω, defined as the time integral over the mass transfer rate:

$$\Omega = \int \dot{\mu}(\dot{T}, \dot{D}, \dot{c_i}) dt \qquad [2.18]$$

where $\dot{\mu}$ is the mass transfer rate (per unit volume) from the solid to liquid phase, T is temperature D is the dielectric constant and c_i is the ionic concentration. The elastic volumetric strain component of the model is defined as follows:

$$\varepsilon_v^e = \frac{1}{\kappa(\Omega)}\sigma' - \alpha(\sigma')\Delta T + \beta\Delta D + \gamma\Delta c_i + \ldots \qquad [2.19]$$

where $\kappa(\Omega)$ is the elastic bulk modulus (dependent on the total accumulated mass transfer), σ' is effective stress and α, β and γ are the cubic thermal expansion coefficient, the flocculation coefficient (dielectric constant effects) and the osmotic consolidation coefficient (concentration effects), respectively. These parameters describe the reversible volumetric strain component of each mechanism. Graham (2003) has spoken of the difficulties of calibrating the large number of coupled parameters in this type of modelling.

Plastic straining of specimens that were initially within their elastic region of behaviour has been observed by increasing temperature (Campanella and Mitchell, 1968; Baldi et al, 1987; and Hueckel and Baldi, 1990); with increasing ionic concentration or valence (Olson and Mesri, 1970; Barbour and Fredlund, 1989) or decreasing dielectric constant (Fernandez and Quigley, 1991). This behaviour has been attributed to a reduction in adsorbed water, which results in some of the previously adsorbed water becoming mobile, thus allowing non-recoverable reduction in specific volume. Based on these studies, chemical softening (that is, reduction of the region of elastic behaviour) can occur. Hueckel (1992) used an elliptical modified Cam-Clay yield surface with a strain hardening law to describe yielding and plastic hardening under chemical or thermal loading:

$$f = \left(\frac{2p'}{p'_c(\Omega,\varepsilon_v^{pl})} - 1\right)^2 + \left(\frac{2q}{M(\Omega)p'_c(\Omega,\varepsilon_v^{pl})}\right)^2 = 0 \qquad [2.20]$$

where p' is the mean effective stress, p'_c is the apparent isotropic preconsolidation pressure, ε_v^{pl} is the plastic volumetric strain, q is the deviator stress and $M(\Omega)$ is the slope of the critical state line as a function of soil chemistry. Using the theory discussed earlier, shrinking of the elastic region and a corresponding reduction of p'_c is expected with increasing ionic strength, increasing valence, increasing temperature and decreasing dielectric constant.

Chemo-mechanical models based on Cam-Clay have been applied to the results of only a few laboratory testing programs. Hueckel (1997) applied his model to the results of oedometer tests under assumed K_o stress state conducted by Fernandez and Quigley (1985, 1991). The experiments were conducted using miscible organic contaminants including dioxane and ethanol. Decrease in volume was observed with the permeation of these fluids through clay specimens that were installed in an oedometer. The mechanism of chemo-plastic consolidation was associated with the simultaneous occurrence of chemical softening, shrinking of the yield surface and plastic strain hardening which compensates for the shrinking. Using several simplifying assumptions, the model developed by Hueckel (1997) was able to quantitatively evaluate the chemically induced strains and softening created by the reduction in dielectric constant by flow through the laboratory specimens. Figure 2.18 (Hueckel, 1997) provides an example of calculated values for a chemical softening function compared to experimental data. The difference between the modelled and experimental results at lower concentrations was attributed to neglecting the variation of the plastic modulus with concentration. The need for further testing on a broader range of conditions was identified.

Also starting with Cam-Clay, Loret et al. (2001) developed a CEP model for homoionic expansive (Na-montmorillonite) clays. The model was established within a three-dimensional framework that included p',q-space and p',volume-space. One-dimensional chemo-mechanical loading results of Di Maio and Fenelli (1997), which involved tests using distilled pore water and NaCl-saturated pore water, were combined with drained and undrained triaxial results of Di Maio and Onorati (1999). These experiments were used to calibrate their coupled chemo-mechanical model. Constant isothermal conditions, chemical equilibrium, and uniformity of chemical fields within the specimens were assumed in both the testing and the modelling. The model was able to reproduce both qualitatively and quantitatively the experimental results observed during chemical and combined chemo-mechanical loading. Figure 2.19 (Loret et al., 2001) compares the experimental results to the model simulations. The figure shows chemically induced consolidation with an increase in salinity of the pore fluid under a constant applied stress. Their work was also successful in simulating triaxial test results on reconstituted Bisacia clay with distilled and 1M NaCl solution. These results are shown on Figure 2.20. Gajo et al. (2000) subsequently extended this work for heteroionic expansive clays in a step towards the evaluation of natural clays. The authors identified the lack of experimental data that examines the reduction of electrolyte concentration.

Guimaraes et al. (2001) developed a chemo-mechanical constitutive model based on a 'double structure' conceptual model used for unsaturated clays that distinguishes between behaviour at the microstructural and macrostructural levels. Physicochemical effects control the microstructural level and the macrostructural level consists of particle aggregates and macropores whose behaviour can be described by conventional models.

The model assumes that the microstructural behaviour is not influenced by the macrostructure but changes in the microstructure can cause plastic deformations in the macrostructure. The model was able to reproduce the vertical strain and volume change results observed for a number of oedometer experiments. Figure 2.21 (Guimaraes et al., 2001) provides an example of the modelled results compared to experimental measurements. The model was not able to simulate the reduction of electrolyte concentration after one exposure cycle. Further experimental work will help advance their work, particularly concerning the reversibility (or lack thereof) of chemical changes.

These earlier studies of chemo-elastoplasticity focused on microscopic interactions between clay, water and chemicals and, independently, the resulting effects on permeability, volume change and strength. The subsequent chemo-elastoplastic models were primarily based on microscopic and molecular mechanics and extended to macroscopic models. These models were initially compared to earlier experimental work, mostly done by others. More recently the models have been compared to triaxial test results combined with independent volume change data. Further experimental work on macroscopic elastic-plastic behaviour of clay, including volume measurement, in relation to chemistry is required to advance the field of research.

2.8 Elastoplasticity of Lake Agassiz clay

Some of the best-known early work on the elastic-plastic behaviour of natural clays was conducted on Lake Agassiz clay (Graham et al, 1983; Graham and Houlsby, 1983; Graham and Li, 1984; Graham et al, 1988). However, the work was restricted to

saturated specimens tested with constant temperature and constant chemistry. The data are some of the most comprehensive data published and considered all the necessary elements of an elastic-plastic model. Lake Agassiz clay was shown to behave as an elastic-plastic material with many of the fundamental features of critical state soil mechanics. However, its behaviour was found to differ from some of the traditional Cam-Clay assumptions that were developed through testing reconstituted materials. For example, natural clays are commonly anisotropic due to their mode of deposition. This is reflected by anisotropic elasticity and asymmetrical yield loci. (The classic Cam-Clay model assumes isotropic elasticity and symmetric yield loci.)

Yield loci for Lake Agassiz clay from four different depths at a site in Winnipeg are shown in p',q-space, p',V-space and V,q-space in Figure 2.22, where V is specific volume, the volume occupied by a unit volume of mineral particles. The same data were also normalized by dividing the yield stresses by the one-dimensional preconsolidation pressure, representing the stress history of the specimens. This reduces the four yield envelopes into a single envelope for ease of comparison to other data (Figure 2.23). In contrast to Cam-Clay, the p',q plots show that the yield loci for natural soil is not elliptical and the hooked p',V plots revealed that the elastic wall is not vertical for natural soil. The data presented in Figures 2.22 and 2.23 can be constructed into a three-dimensional state boundary surface as shown in Figure 2.24. It is notable that the state boundary surface is approximately symmetrical about the p',V-plane.

Reconstituted Lake Agassiz clay made with distilled, deionized water from the same location displayed similar stress-strain behaviour, strengths and yielding as found in the natural specimens (Graham and Li, 1985). The geometric shape of the yield loci was

therefore not attributed to geological ageing or weathering. However, differences were observed when examined in p',V –space, the normal consolidation lines (NCLs) and critical state lines (CSLs) of the reconstituted specimens plotted at lower specific volumes than the natural clay (Figure 2.25).

2.9 Summary of Literature Review and Justification of Research

The preceding sections show clearly that pore fluid chemistry influences clay strength, compressibility and hydraulic conductivity. Links have been established experimentally, but separately between chemistry and hydraulic conductivity, chemistry and volume change, and chemistry and strength. The literature provides general support for the hypothesis of the project, but does not provide direct answers that permit understanding of the behaviour of the dykes at Seven Sisters.

General theoretical models and mathematical formulations that would be required to examine problems such as the Seven Sisters case study in an elastic-plastic framework have been established by others. However, there is a lack of experimental data from tests that examine the yielding characteristics of clay under varying conditions of pore fluid geochemistry. Further, the established chemo-elastoplastic models assume isotropic elasticity and elliptical yield loci. These assumptions may not apply to natural or cemented clays. There is a lack of triaxial test data with good geochemical characterization and careful attention to monitoring volume changes which would be required for a complete description within an elastic-plastic framework. No such testing program has ever been reported in the literature. Doing so for the Seven Sisters clay will be the main contribution of this research to the study of chemo-elastoplasticity. This

justifies the program outlined in the following chapter, which examines the effect of differing pore fluid chemistry on the yielding behaviour of Lake Agassiz clay.

The earlier (constant chemistry) work on Lake Agassiz clay, combined with knowledge of its mineralogy and in situ pore fluid chemistry (Garinger et al., 2004) suggests that Lake Agassiz clay exhibits elastic-plastic behaviour which may be influenced by chemistry in two different ways.

1) Precipitation or dissolution of cementing agents has the potential to influence yielding, brittleness and strain-softening behaviour.
2) Physicochemical interactions (DDL thickness) have the potential to dominate post yield behaviour and shearing resistance whenever particle orientation becomes face to face, for example along a shear plane.

The study reported in the following chapters improves the understanding of clay foundations such as those found at the Seven Sisters site, and of clay barriers where changes in pore fluid geochemistry threaten soil performance. The resulting chemo-elastoplastic model will be used to modify the stress-deformation and slope stability models established by Garinger et al. (2004). The results of the research may provide insight to other similar situations where dykes, flood control structures and bridge approach embankments are constructed on expansive plastic clays.

3.0 Materials and Methods

The previous chapter showed that high-plastic clays are susceptible to changes in pore fluid chemistry and that a number of problems related to chemical changes have occurred throughout the world. It was also shown that Lake Agassiz clays behave as an elastic-plastic material. This chapter describes the methodology used to link these two topic areas and examine the effects of pore fluid chemistry on the elastic-plastic behaviour of Lake Agassiz clay.

3.1 Design of Experimental Program

Section 1.3 outlined the objectives of the experimental program, the first of which was to isolate the effects of pore fluid chemistry on elastic-plastic behaviour of Lake Agassiz clay. This was addressed by making a number of blocks of reconstituted soil, each with different pore fluid geochemical conditions but with the same stress history and similar initial water contents and specific volumes. Using reconstituted soils served to eliminate the natural variability in the field, and the effects of sampling disturbance. It also ensured a uniform distribution of geochemical conditions within each block of soil.

The geochemical conditions included in this study were developed in blocks of soil prepared with (1) deionized water used for the control tests; (2) gypsum-rich water to simulate background conditions at Seven Sisters; (3) acidic water (H_2SO_4) to reduce the effects of carbonate cementation, if any; (4) salt water to increase electrolyte concentration, decrease valence and increase the solubility of gypsum; and (5) washed soil (with two degrees of washing) to simulate the unstable section at the Seven Sisters

site by lowering electrolyte concentrations and reducing the concentration of potential cementing agents.

The degree of washing required to obtain conditions similar to the Seven Sisters unstable section was guided by geochemical modelling using the United States Geological Survey (USGS) PHREEQCi code. The code can calculate the distribution of aqueous species (speciation) coupled with one-dimensional transport and cation exchange reactions. The speciation calculations use the chemical analysis of a water to calculate the distribution of aqueous species. The model was set up to simulate the flow of reservoir water through the background Seven Sisters soil under the influence of advection and dispersion. It was used to estimate the geochemical evolution of the soil beneath the dykes and to compare the geochemical data for the background, stable and unstable locations. Chapter 6 provides details of the model development, assumptions and input parameters.

The results of the PHREEQCi simulation showed a breakthrough curve for the major ions of concern including calcium, sulphate and sodium (Figure 3.1). The figure indicates that the reservoir water is capable of leaching these ions from the background soil. The loss of sulphate is especially marked, with approximately 60% removal after only one pore volume has passed through the soil and approximately 90% after two pore volumes have passed through the soil. This is consistent with the information in Table 2.2, which indicates that the dissolution rate of sulphate is controlled by transport rather than reaction kinetics (Appelo and Postma, 1996). Comparing the measured concentrations of sulphate at the stable and unstable sections to the modelled sulphate leaching curve (Figure 3.1) suggests that just under one pore volume of forebay water

had passed through the stable section and just over one pore volume had passed through the unstable section. Based on the results of the geochemical modelling exercise, three points along the modelled sulphate leaching curve were targeted for preparing the blocks of reconstituted soil. These included (1) a block of soil with chemistry similar to the chemistry of the background soil (gypsum-rich block); (2) a block of soil that had been washed by one pore volume of deionized (DI) water; and (3) a block of soil that had been washed by more than two pore volume of DI water. More detailed information will be presented in this chapter about how these samples were prepared.

An important objective of the experimental program was to determine the mechanical behaviour of the natural background soil before and after leaching in the laboratory. The tests would hopefully demonstrate that leaching can produce the anisotropy and brittleness shown in the natural specimens tested by Garinger (2002). Specimens of the background Seven Sisters soil were built into flexible wall permeameters for permeation with reservoir water following ASTM D 5084. At the time of writing, after approximately one year of permeation, less than one pore volume has passed through the majority of the specimens. They are therefore not ready for testing at the time this thesis is being prepared. Permeation is continuing with a view to future testing as part of a follow-up research program.

In order to determine yield loci and strength envelopes for the reconstituted, natural background and unstable soils, each soil type was subjected to a series of tests. These included undrained triaxial tests with pore water pressure measurement, drained triaxial stress paths along a number of different stress paths, and 1D compression (oedometer

tests). (A sufficient number of natural specimens from the background and unstable sections were available for characterization of their respective yield loci.) Details of the testing program follow.

3.2 Field Sampling and Soil Characterization Program

The reconstituted blocks and undisturbed samples of natural background clay were obtained from a specially excavated test pit adjacent to Manitoba Hydro borehole SS-042 at Seven Sisters. The test pit was located in an area unaffected by the flow of reservoir water beneath the dykes. The soil profile had been previously characterized geochemically by Garinger (2002). The test pit was excavated with a small backhoe to a depth of 4 m below grade. This depth equates to an elevation of 266 m, which corresponded to the general elevation of interest beneath the dykes. The soil profile was logged in detail and the deposit characterized approximately using a pocket penetrometer and torvane for indexing purposes.

Grab samples were collected at various locations throughout the profile for soil chemical analysis and general laboratory characterization. The samples for chemical analysis were packed into glass jars with Teflon lined lids (supplied by the commercial laboratory) and stored in an ice chilled cooler. These samples were shipped to Philip Analytical Services Corp. (PASC) in Mississauga, ON within 24 hours of sample collection for chemical analysis. The remaining grab samples were placed in plastic Ziploc bags and transported back to the University of Manitoba Geotechnical Laboratory for geotechnical indexing, including natural water contents, liquid and plastic limits and particle size analysis.

Shelby tube samples were obtained at the base of the excavation at depths of 2.9 m to 3.4 m, 3.5 m to 4.0 m and 4.0 m to 4.5 m below grade using the bucket of the backhoe to carefully push the tubes into 'undisturbed' soil at the base of the excavation. The Shelby tubes were left in the base of the excavation for approximately 15 minutes before they were carefully rotated and recovered using a chain attached to the bucket of the backhoe. The tube samples were sealed in the field with plastic end caps and carefully transported back to the laboratory where they were sealed with wax and stored in a walk-in refrigerator prior to extruding and testing.

Bulk samples were obtained from the 3.5 to 4.0 m depth interval for the preparation of the reconstituted soils. The soil was placed in plastic-lined Rubbermaid containers and transported back to the laboratory. Attempts were also made to collect undisturbed block samples using the Domaschuk block sampler at the same depth. However, the backhoe was not able to advance the sampler without rocking it and this resulted in significant sample disturbance. The Domaschuk sampler was considered unusable when used with the backhoe.

In the laboratory, soil samples from selected depths of the test pit were tested for grain size distribution by hydrometer following ASTM Method D 422-63 (ASTM, 2000a), water content following ASTM Method D 2216 (ASTM, 2000b) and Atterberg limits following ASTM Method D 4318-98 (ASTM, 2000c). These methods were also used to characterize the reconstituted soils described below.

Hydraulic conductivity was determined for the natural background (3.5 to 4.0 m) and reconstituted specimens in flexible wall permeameters following ASTM Method D 5084-90 (ASTM, 2000d). Specimens were 51 mm diameter by 100 mm long. Following saturation with 100 kPa backpressure, the specimens were permeated under an upward gradient of 77, being careful to maintain the entire specimen within the region of elastic stress-deformation behaviour. During permeation, the pore water pressures were 50 kPa and 125 kPa at the top and bottom of the specimens respectively, and the cell pressure was 175 kPa.

3.3 Preparation of Reconstituted Soil Blocks

The bulk soil samples obtained from depths of 3.5 to 4.0 m from the background section test pit were oven-dried, pulverized into a powder and thoroughly mixed. For each type of selected soil chemistry, the pore fluid of choice and dry soil was weighed into a 29.2 cm diameter by 55.9 cm long cylindrical mixing chamber (Figure 3.2) at water contents approximately 1.8 times the liquid limit of the clay, which in this case was approximately 100%. The slurries were mixed vigorously for a minimum of five 30 minute periods and held under a vacuum to remove air over a minimum two day period.

The slurries were then gently poured into a one-dimensional consolidation cylinder fitted with a lever-loading system and top and bottom drainage (Figure 3.3). This was used to compress the slurry and produce samples that could be prepared for triaxial or oedometer testing. The cylinder consisted of a 254 mm diameter steel pipe with a removable bottom plate and piston style top cap. The bottom plate and top cap both had porous stones connected to the drainage leads. The slurries were separated from the porous stones by

fibre glass filter discs. The filter discs contained no carbon in order to reduce the growth of bacteria that could restrict drainage. The one-dimensional consolidation apparatus and details of its operation were described in detail by Li (1983).

The slurries were incrementally loaded with pressures of 25, 36, 50, 90, 129 and 225 kPa. Each loading was held for the same period of time for each block of soil (one day for the earlier load increments up to two weeks for the later increments) with the final load being held for a longer period of 42 days to permit full consolidation with some creep or 'aging'. (Burland, 1990).

After the final loading was complete, the last litre of effluent recovered from the consolidation cylinder was sampled for chemical analysis, the cylinder was removed from the load frame and the bottom plate was removed. The cylinder was then inverted and placed in an extrusion frame with a hydraulic piston that forced out the block of clay by pushing on the top cap (Figure 3.4).

Immediately after extrusion, the top 3.5 to 4 cm of the block was removed with a cutting wire guided by the edge of the extrusion frame. This slab was used for the preparation of oedometer specimens. The rest of the block was carefully divided into 14 sections of sufficient size to make 50 mm diameter by 100 mm long triaxial specimens. All specimens were triple wrapped in plastic food wrap, taped and sealed in Ziploc bags. The wrapped specimens were stored in a walk-in refrigerator (approximately 10°C) to await testing.

Seven blocks (approximately 30 cm diameter by 18 cm tall) of reconstituted clay were prepared with pore fluid conditions that included deionized (DI) water, gypsum rich water (two blocks), acidified deionized water, salt water and two batches of clay that were washed with 1.1 and 6.5 pore volumes of DI water before consolidation. Details of the preparation of samples with the various pore fluid conditions are as follows:

- **Deionized (DI) Water** – The clay block prepared with deionized water was created to be the control block of soil. Specimens made from this block were labelled AMR3.
- **Gypsum Rich Water** – This pore water was prepared by dissolving 2g/L of laboratory grade gypsum in deionized water prior to mixing with the dry soil. At this concentration, which is close to the solubility of gypsum, some precipitate was noted at the base of the container and the solution was assumed to be saturated with respect to gypsum. Two blocks of soil containing this pore fluid were made to produce enough specimens to examine the effects of freeze-thaw cycles on cementation. Specimens made from these blocks were labelled AMR1 and AMR2.
- **Sulphuric Acid (H_2SO_4)** – This clay was prepared initially with deionized water and then sulphuric acid was added incrementally to the slurry. The acid was added as 24 N sulphuric acid in approximately 20 mL doses until the characteristic carbon dioxide off-gassing had substantially decreased (indicating the destruction of the majority of the existing carbonate minerals). The slurry was monitored for pH after each dose of acid. Each addition of acid initially reduced the pH of the slurry below 4.5. This was subsequently buffered to a pH close to 7 after approximately 24 hours. The final concentration of sulphuric acid added to the slurry was 132 meq/L. Specimens made from this block were labelled AMR4.

- **Sodium Chloride (NaCl) Salt Water** – The salt water was prepared by adding 50 g/L of laboratory grade sodium chloride to deionized water before mixing with the dry soil. Specimens made from this block were labelled AMR6.

- **Washed** – The blocks of washed clay were prepared by passing deionized water through the slurries in a 39 L slow mixing chamber (Figure 3.5). Water contents of the slurries were maintained at approximately 1.8 to 2.0 times the liquid limit. The mixing chamber was designed for upward flow and fitted with motorized mixing blades. Porous stones covered with filter cloth were sealed at the top and bottom of the chamber. On a daily basis, approximately 2 to 4 L of water passed through the chamber over an eight hour period, during which the mixing motor was on. Flow was stopped and the mixing motor was turned off overnight to prevent over-loading of the mixing motor. Washing continued the following day. Electrical conductivity (EC) and pH of the effluent was monitored regularly to determine appropriate times to collect effluent samples for chemical analysis. Two batches of clay were washed using the chamber, one subjected to an equivalent of 1.1 pore volumes (PV) of water (AMR5) and one subjected to an equivalent to 6.5 pore volumes of water (AMR7). The equivalent pore volumes were calculated based on the final porosity of the soil. Channelling was suspected during the preparation of the AMR5 batch. As a result, the mixing blades were extended for the preparation of the AMR7 batch. As it was not possible to verify perfect contact between the slurry and the wash water, the actual number of effective pore volumes is likely less than the volumes indicated above. The pore volumes are therefore considered approximate.

3.4 Geochemical Analysis Program

3.4.1 Soil Chemical Analysis

Clay samples from the natural background location, the unstable section and all of the reconstituted specimens were submitted to PASC in Mississauga, ON for chemical characterization. Four samples were submitted from the Seven Sisters background location test pit (SS-042-TP1) and one additional sample was submitted from the unstable section from a depth of 10.7 m below grade which here represents the upper foundation clay. In addition, a sample of Winnipeg clay (from 6.1 m below grade at the University of Manitoba to the southwest of the Frank Kennedy Centre) was submitted for analysis to allow for comparison between this study and the work conducted by Graham, el al. (1983) and Graham and Li (1985). Duplicate samples of the natural samples were submitted on separate occasions for quality assurance/quality control (QA/QC).

The soil samples were analyzed for metals following acid extraction, major anions, sodium adsorption ratio (SAR), EC, cation exchange capacity (CEC) and pH. The metals were analyzed by inductively coupled plasma (ICP) spectrophotometry following USEPA Method No. 6010. Anions, bromide and orthophosphate were analyzed by ion chromatography following USEPA method No. 300.0/Standard Methods (1985) No. 429.0. SAR was calculated after determination of cations by ICP AES (aqueous extraction using a 1:2 soil to water ratio) following McKeague Methods of Soil Analysis No. 3.23/3.26. EC and pH were determined from the extract of a saturated paste following McKeague Methods of Soil Analysis No. 3.21/4.13. CEC was determined by displacement with sodium, replacement with ammonium and subsequent analysis of sodium by ICP AES following McKeague Method of Soil Analysis No. 3.34.

3.4.2 Pore Fluid Analysis

Samples of pore fluid were obtained from the natural background, stable and unstable locations at Seven Sisters by extruding saturated paste samples through a 0.45 micron filter. As described in Section 3.3, the last litre of pore fluid extruded from the 1D consolidation apparatus was sampled and submitted for chemical analysis. The pore fluid samples from the natural background, stable and unstable sections were analyzed at the Soil Science Laboratories at the University of Manitoba as part of the work presented by Garinger et al. (2004). Chemical analyses of the pore fluid from the reconstituted soil was conducted by Philip Analytical Services Corp. (PASC) in Mississauga, ON using the same analytical methods. These are outlined in the following paragraphs.

Chemical analysis of the pore fluid included the major ions (Na, K, Mg, Ca, Fe, Cl, SO_4, HCO_3, and CO_3), electrical conductivity (EC), pH and alkalinity. The metals were analyzed by flame atomic absorption spectrophotometry (APHA Method 3111:B, 1998). Anions including chloride and sulphate were analyzed by ferricyanide and methylthymol blue colorimetry, respectively (APHA Method 4500-Cl:E and APHA Method 4500-SO4:F, 1998). Bicarbonate was measured by titration with 0.01N HCl (APHA Method 2320:B, 1998). EC was determined using a conductivity cell (APHA Method 2510:B, 1998) and pH was determined electrometrically (APHA Method 4500-H:B, 1998).

3.5 Geotechnical Testing Program

Yield loci and strength envelopes for each soil type were determined by conducting stress controlled and strain controlled triaxial tests and oedometer tests. Strain controlled triaxial tests included isotropically consolidated, undrained tests with pore

water pressure measurement (CIŪ tests) and isotropically consolidated, drained tests (CID tests). Stress controlled triaxial tests included isotropic consolidation, lateral expansion with q/p′ = -3/2, constant p′, q/p′ = 1.25 and K_0 consolidation. The program completed triaxial tests on 56 specimens and oedometer tests on 16 specimens. The triaxial tests were performed on 51 mm diameter by 100 mm long specimens. Duplicates of a number of tests with the same soil type were performed to gain confidence with the repeatability of the results and their interpretation. Table 3.1 provides a summary of the laboratory testing program. Details of the testing procedures for each type of test are provided below.

3.5.1 Isotropic Consolidation and Strain Controlled Undrained Triaxial Tests

The CIŪ tests were conducted in accordance with ASTM D 4767 and standardized operating procedures developed at the University of Manitoba Geotechnical Laboratory. A photograph of the testing equipment is provided in Figure 3.6. Specimens from each of the various blocks of clay were tested at isotropic consolidation pressures lower than and higher than the pressure at which the blocks of clay were initially prepared. These will be referred to as 'overconsolidated' and 'normally consolidated' specimens, respectively. Overconsolidated specimens were tested at an isotropic effective stress of 100 kPa, which resulted in overconsolidation ratios ranging from 1.1 to 2.5, depending which block was being used. Normally consolidated specimens were incrementally loaded, with drainage leads open, to a final isotropic effective stress of 350 kPa. Incremental loading allowed for the determination of the isotropic consolidation yield stress and isotropic normal consolidation line (Iso NCL) for each soil type. At the end of

isotropic consolidation (defined by a volume strain of less than 0.1% over a 24 hour period), all specimens under went a 'B test' to check the saturation level in the entire test installation, including the specimen, filter stones, cell base, pressure transducer blocks and pressure lines. When $B = \Delta u/\Delta p$ was greater than or equal to 98%, the specimens were acceptable for undrained shearing using an axial strain rate of 15%/day.

Specimens of the natural background clay, clay from the unstable section, and reconstituted, gypsum-rich clay were subjected to high pressure isotropic consolidation to confirm the position of the Iso NCL and obtain the intrinsic compression line (ICL) defined by Burland (1990). Figure 3.7 shows the apparatus used for these tests, which was capable of pressures up to 4 MPa. The specimens were incrementally loaded to a maximum isotropic effective stress of approximately 3.6 MPa. After the final loading, the specimens were unloaded to 500 kPa to produce over consolidated specimens, and allowed swell. The specimens were then quickly removed, weighed, re-trimmed to obtain water content samples and rebuilt into the strain controlled loading frame for undrained shearing at an effective stress of 500 kPa. Re-trimming was required to reshape the specimens into uniform cylinders. The specimens generally had an 'hour glass' shape after the isotropic consolidation phase.

3.5.2 Isotropic Consolidation and Strain Controlled Drained Triaxial Testing

The CID tests were conducted generally in accordance with ASTM D 4767 except that drainage was allowed during the shearing phase of the test. The CID tests used the same testing equipment as the CIŪ tests (Figure 3.6). All the CID tests were conducted

on overconsolidated specimens, starting at an effective isotropic consolidation pressure of 100 kPa. Drained shearing was conducted using an axial strain rate of 1%/day. Volume change measurements were taken regularly throughout the tests.

3.5.3 Stress Controlled Drained Triaxial Stress Path Testing

As mentioned earlier, the program of drained, stress controlled tests, included stress paths with q/p′ = -3/2, constant p′ and q/p′ = 1.25. The tests used the equipment shown in Figure 3.8. The tests were conducted to supplement the yielding information obtained by the strain controlled tests. All the stress controlled tests started at p′ = 100 kPa and the q/p′ = -3/2 and q/p′ = 1.25/1 tests were started at p′ = 100 kPa, q = 0. Each specimen was loaded incrementally past its yield stress until failure was observed. Load increments for all of the stress controlled tests were calculated using the following equation:

$$\sigma'_1 = \sigma'_3 \left(1 - \frac{a}{A}\right) + \frac{W_0 + P}{A} \qquad [3.1]$$

where a is the cross-sectional area of the piston in the triaxial cell, A is the instantaneous sample cross-sectional area = Volume/Height (assuming, as is common, that the specimen remains cylindrical), W_0 is the dead load contribution from the top half of the specimen, upper half of membranes and O-rings, top cap, piston, load balls and weight hanger, and P is the extra loading on the hanger. Noonan (1980) provides a detailed description of the load increment procedures.

Some K_0 consolidation tests were conducted to supplement the oedometer data and examine the assumption of $K_0 = 0.78$ for the Seven Sisters clay. The test procedures involved consolidation under a series of loads with $\sigma_3' = 0.78\sigma_1'$. The specimens were incrementally loaded along the $K_0 = 0.78$ line in p',q-space, past the yield stress, to a final loading with p' = 350 kPa. After completion of the final loading, the specimen was prepared for undrained shear starting from the same stress state on the K_0 line as the end-of-consolidation state. (These tests have been labelled CAŪ tests). At the end of the final increment of consolidation, the piston of the cell was locked in place and the weight hanger removed. The former load on the piston was then replaced by the strain controlled compression frame before the piston lock was removed. The specimens were then back pressured in 50 kPa increments to a final back pressure of 200 kPa for a minimum of 24 hours. A minimum B = 98% was again required before shearing was commenced. During each back pressuring increment, the cell pressure and the load on the piston was adjusted to maintain the specimen on the $K_0 = 0.78$ line.

3.5.4 Oedometer Testing

Oedometer tests were conducted on soil from the natural background location and the unstable section, as well as on all of the reconstituted blocks of clay. The testing procedures were in general accordance with ASTM method D 2435 (ASTM, 2000f). All specimens were tested in a 63.5 mm diameter by 19 mm tall cutting ring. Before loading began, specimens were trimmed so their heights were 1.3 mm less than the height of the cutting ring. This was done in case swelling occurred after the addition of water. Deionized water was added to the surrounding sleeve approximately ten minutes after

the initial loading was applied. A load increment ratio (LIR) of 1.8 was utilized between successive increments. Increments were added to a maximum loading of approximately 3.2 MPa. This loading took the specimens well past their preconsolidation pressures and produced a well-defined normal consolidation line. Each load increment was applied for approximately 24 hours.

4.0 Results

4.1 Soil Characterization

Samples of clay were obtained from the same elevations (Elevation 266.5 to 266.0 m) at the background section and the foundation clay beneath the dykes. The samples were used for testing in both their natural state and for the preparation of reconstituted specimens. The samples consisted of greyish-brown firm clay with traces of silt. The clay was laminated and fissured. The laminations were horizontal, approximately 1 to 2 mm thick and defined by alternating colours of brown and darker greyish-brown. Both vertical and sub-horizontal fissures (cross-cutting the horizontal laminations) were observed. The spacing between fissures was approximately 30 cm. White pockets of gypsum were observed along some of the vertical fissures. Figure 4.1 is a photograph of the clay showing a gypsum pocket.

Table 4.1 provides a summary of general geotechnical properties of the clay utilized in the geochemical and geotechnical testing programs. Water content, bulk density, unit weight, specific volume and porosity values are the average of the initial properties measured on triaxial and oedometer specimens. The initial properties of all of the reconstituted clays were similar. Of these clays, water content ranged from 57% to 63%, bulk density ranged from 1.636 to 1.692 Mg/m^3, specific volume ranged from 2.554 to 2.743 and porosity ranged from 61% to 64%. The natural background clay was slightly drier, but had a density similar to that of the reconstituted clays (which were consolidated using a vertical pressure of 225 kPa). The natural clay from the unstable section was drier still and had the highest density of all of the tested clays suggesting that dyke loading had caused additional consolidation of the foundation clay.

The hydraulic conductivity (measured in the labaoratory) of all of the reconstituted clays was similar with an average value of 7×10^{-11} ms^{-1}. This indicated that under the same stress state during 1D consolidation, the changes in pore fluid chemistry did not significantly change the hydraulic conductivity of the reconstituted material over the range of concentrations examined. The hydraulic conductivity of the natural clays was slightly lower than the reconstituted clays (4×10^{-11} ms^{-1} and 3×10^{-11} ms^{-1} for the background location and the unstable section, respectively).

With the exception of the clay reconstituted with NaCl brine, all of the clays had a plastic limit in the order of 28% and a liquid limit ranging from 103 to 114%. The plastic limit of the NaCl clay was slightly higher at 39% and the liquid limit was significantly lower at 79%. This reduction in plasticity index is consistent with that observed for other Canadian clays and clay tills exposed to elevated concentrations of NaCl (Barbour, 1990).

Grain size distribution of the natural background, stable and unstable sections was presented in Chapter 1 (Table 1.1). All of the tested soil had clay fractions approaching 100% with trace amounts of silt.

The similar soil characteristics, particularly water content, specific volume and hydraulic conductivity, between all of the tested clays suggest similar initial microstructures. Achieving similar initial conditions was important from the standpoint of isolating the effect of pore fluid chemistry on the subsequent geotechnical behaviour of the clays.

4.2 Geochemical Analysis

4.2.1 Soil Chemical Analysis

Table 4.2 shows the results of the soil chemical analyses. The clay made with DI water was considered the baseline control sample for the purpose of comparison with the other batches of clay. This soil represents average conditions at the background section as it was a well homogenized composite sample of the stock soil used to prepare the various blocks of clay. In general, the sample from the background section, which was a discrete sample from the field sampling program, was in agreement with the results for the clay made with DI water. The parameters that displayed the most significant differences between the various batches included calcium, sodium, chloride, sulphate, sodium adsorption ratio (SAR) and cation exchange capacity (CEC).

As expected, the gypsum-rich clay contained elevated calcium and sulphate concentrations relative to the control made with DI water. A portion of the added calcium ions appeared to be adsorbed onto the clay particles. Calcium is one of the most strongly adsorbed cations, and once adsorbed, other common cations have limited ability to replace the calcium (Faure, 1991).

The addition of H_2SO_4 increased the sulphate concentration relative to the control clay made with DI water. When acid was added to the wet soil, significant carbon dioxide off-gassing was observed. This indicated the loss of carbonates which may have contributed to cementation within the clay. The calcium concentration was generally the same for the

clays made with both H_2SO_4 and DI water. However, the overall calcium cementation may have shifted from carbonate-based to sulphate-based cementation in the block prepared with H_2SO_4. That is, any calcium carbonate cementation that was destroyed by the addition of acid may have re-precipitated as gypsum. Sulphuric acid was selected to simulate the potential effects of acid mine drainage on clay barriers and potentially eliminate any carbonate cementation. However, if the contribution of calcite cementation is to be completely isolated, a different acid, such as hydrochloric acid, would be required.

As expected, the clay reconstituted with salt water contained elevated concentrations of sodium and chloride relative to the control clay made with DI water. The high concentration of sodium in the pore fluid increased the sodium adsorption ratio by two orders of magnitude. The total concentrations of calcium and sulphate were relatively low in the NaCl clay compared to the control clay made with DI water. This may be due to sodium chloride increasing the solubility of gypsum. With more gypsum in solution during 1D consolidation, more calcium and sulphate would be lost as pore water was expelled.

The clay that was washed with approximately six pore volumes (6 PV) of DI water contained lower concentrations of calcium, sodium and sulphate relative to the control clay made with DI water. The greatest change was observed for sulphate, which dropped from 7,970 mg/kg in the control clay made with DI water to 980 mg/kg in the clay washed with six pore volumes of DI water, indicating the overall loss of gypsum. One anomaly to note was the observed increase in chloride in the clay washed with six pore volumes of DI water (31 mg/kg relative to 12 mg/kg). This was unexpected since DI water was used to wash the soil and the soil was not exposed to any other sources of chloride.

As mentioned earlier, the discrete sample of natural clay from the background location displayed chemistry that was generally consistent with the control clay made with DI water. The exception was the sodium concentration which was elevated in the natural background specimen (455 mg/kg) relative to the control made with DI water (280 mg/kg). The reason for the difference is unknown and may be the result of field variability.

Comparing the soil chemistry of the natural clay from the unstable section to that of the natural clay from the background location, the unstable section contained relatively less calcium and sulphate, and relatively more sodium and chloride (Table 4.2). The relative depletion was approximately 3,000 mg/kg for calcium and approximately 7,000 mg/kg for sulphate. These differences are comparable to the differences achieved between the reconstituted clay that was washed with six pore volumes of DI water and the control clay made with DI water. This indicates that the comparison between the behaviour of these reconstituted clays closely models the geochemical changes observed at the site without any differences due to field variability or stress history.

The Winnipeg clay sample was analysed to allow comparison between this program and earlier work characterizing the elastic-plastic behaviour of Winnipeg clay conducted by Graham et al. (1983) and Graham and Li (1985). Notable differences between the Seven Sisters clay and Winnipeg clay included relatively elevated calcium, sodium and chloride concentrations (approximately 5,500 mg/kg, 625 mg/kg and 450 mg/kg, respectively) in the Winnipeg clay sample. These results translated to a higher SAR than the Seven Sisters clay. Of particular interest, Winnipeg clay contained notably lower sulphate

concentrations, with approximately 6,700 mg/kg less sulphate than the Seven Sisters clay. Despite this, Graham et al. (1983) reported marked yielding behaviour indicative of cementation. Further, gypsum precipitate and gypsum rosette (selenite) crystals are regularly observed in Winnipeg clay.

4.2.2 Analysis of Pore Fluid Chemistry

Table 4.3 presents the results of the chemical analyses conducted on the pore fluid. As for the soil chemical analysis program, the clay made with DI water was considered the baseline control sample for the purpose of comparisons between the various batches of clay. It should be noted that the results of chemical analysis on the pore fluid should not be confused with the soil chemistry analysis. The results of the soil analyses are considered total concentrations that will consist of mineral concentrations in both the soil and pore fluid. The pore fluid results represent concentrations only in the liquid phase. While similar trends can be expected below the saturation point of a given mineral, at concentrations greater than saturation there will be less of an observed difference, even though total concentrations may be quite different. This is evident when comparing the chemistry of the pore fluid from the gypsum-rich clay and that of the clay made with DI water. For example, both clay types are saturated with respect to gypsum (that is, gypsum will precipitate given the geochemical conditions), as will be discussed below. As such, the pore fluid concentrations are similar, despite differences that were noted in the total soil concentrations discussed above. The major importance of the pore fluid chemical analyses was to determine saturation states of various potential cementing minerals. This will be further discussed in Section 4.2.3.

There were several notable differences in pore fluid chemistry between the clay made with acidified water compared to the control made with DI water. Firstly, as expected, the addition of sulphuric acid (H_2SO_4) increased the sulphate concentration and dissolved metal concentrations including potassium, magnesium and manganese. Secondly, it was mentioned earlier that off-gassing due to the dissolution of carbonates was observed. This appeared to cause an increase in bicarbonate and total alkalinity as the acid was buffered. At the end of consolidation, the soil appeared to be 'over-buffered' with a final pH of 8.4. Finally, the overall effect of acidification was an increase in electrolyte concentration as reflected by increases in electrical conductivity (EC) and ionic strength of the pore fluid.

As observed in the total soil chemistry, the clay made with salt water contained elevated concentrations of sodium and chloride relative to the control made with DI water. Increased dissolved concentrations of calcium, potassium, magnesium, manganese and sulphate were also observed relative to the control made with DI water. These changes resulted in relatively high electrical conductivity and ionic strength compared to the control made with DI water. Calcium and sulphate concentrations in the pore fluid of the clay made with salt water were present at concentrations greater than the pore fluid from the control made with DI water. This reflects an increase in gypsum solubility by the presence of elevated concentrations of NaCl (Freeze and Cherry, 1979).

Both of the washed clays displayed relatively lower sulphate concentrations, EC and ionic strength in their pore fluids compared to the control made with DI water. After approximately six pore volumes of washing, marked decreases in calcium and sulphate concentrations were noted. The calcium concentration dropped from 548 mg/L to 96 mg/L (83% reduction) and the sulphate concentration dropped from 2,690 mg/L to 224 mg/L

(92% reduction) in the clay washed with six pore volumes of DI water, compared to the control clay made with DI water. This same trend and similar amounts of relative depletion was observed between the natural clay from the unstable section compared to the clay from the background location. The calcium concentration dropped from 680 mg/L to 172 mg/L (75% reduction) and the sulphate concentration dropped from 3,660 mg/L to 972 mg/L (73% reduction) in the unstable section clay compared to the background section clay. This further supports the ability of the reconstituted clays to model the geochemical changes observed at the Seven Sisters site.

Figure 4.2 compares the measured sulphate concentrations in the pore fluid of selected reconstituted and natural clays to the PHREEQ leaching simulation results. In developing the geochemical model, the pore fluid chemistry of the background location was utilized for the initial conditions in the soil. The chemistry of the forebay water (Table 4.3) was specified as the permeating fluid. The PHREEQ simulation was briefly discussed in Section 3.1 and further details regarding the geochemical modelling will be provided in Chapter 6. In Figure 4.2, the measured sulphate concentrations were plotted on the simulated leaching curve and the corresponding number of pore volumes was determined for qualitative comparison. The pore fluid chemistry of the gypsum-rich clay plots at the upper end of the leaching curve, near the sulphate concentration measured in the pore fluid of the clay from the background location. As such, the clay reconstituted with gypsum-rich water is comparable to the natural background location. These clays were considered representative of initial conditions that have not been influenced by the chemistry of the forebay water. The clay washed with one pore volume of DI water plots slightly above the one pore volume point on the simulated leaching curve. This is in agreement with the channelling that was suspected though the slurry during that

experiment. The sulphate concentration measured in the pore fluid of the clay from the unstable section plots just below the simulated one pore volume concentration. Finally, the washed 6PV clay plots at the bottom of the leaching curve and approaches steady state leached conditions.

4.2.3 Saturation Indices of Cementing Minerals

Section 2.3 introduced the concept of calculating mineral saturation indices (SI) to determine whether a mineral is at equilibrium; in a state of dissolution; or super-saturated and in a state of precipitation. As mentioned in Section 3.1, speciation calculations can be completed using a geochemical model such as PHREEQ knowing the chemical composition of a sample of water. Table 4.4 presents the saturation index (SI) values for a number of potential cementing minerals that were determined using PHREEQ. The negative SI values indicate that the mineral is in a state of dissolution, that is any contribution to cementation by that mineral would be reduced. The positive SI values indicate that the mineral is in a saturated state and precipitating. Saturation index values near zero indicate that the mineral is near equilibrium with its solid phase.

The results in Table 4.4 indicate gypsum is at equilibrium, or slightly over-saturated, in the clays reconstituted with gypsum-rich water, DI water, acidified (H_2SO_4) water, and NaCl brine, as well as the natural clay from the background location. The reconstituted clay that was washed with one pore volume of DI water was at equilibrium, or slightly under-saturated with respect to gypsum. Gypsum was in a state of dissolution in the reconstituted clay washed with six pore volumes of DI water and the natural clay from the unstable section. The pore fluids of all of the clays were over-saturated with respect to

calcite, aragonite and dolomite, and all were under-saturated with respect to anhydrite. Based on these results, gypsum displayed a trend supporting its importance at the site. The forebay water was under-saturated with respect to all of the listed minerals, indicating that it has the capacity to cause dissolution of these minerals.

4.2.4 Summary of Geochemical Analyses

Based on the results of the geochemical analyses and speciation calculations, the following summarizes the geochemical differences between each type of clay relative to the control clay made with DI water.

- **Gypsum Rich** – These batches of clay (AMR1 and AMR2) contained slightly elevated gypsum relative to the control made with DI water. Electrolyte concentrations in theses samples were similar to those measured in the discreet sample from the background location. Gypsum was near equilibrium (slightly over-saturated) indicating the presence of gypsum in the solid phase.
- **H_2SO_4** – This clay (AMR4) contained relatively less carbonate minerals. Re-precipitation of calcium as gypsum may have off-set some of the carbonate loss.
- **NaCl** – This clay (AMR6) had an elevated ionic strength and increased SAR. The high concentration of NaCl increased the solubility of gypsum and therefore reduced the amount of gypsum in the solid phase.
- **Washed 1PV** – This clay (AMR5) had slightly less gypsum than the control clay made with DI water. Gypsum was near equilibrium (slightly under-saturated).

- **Washed 6PV** – This clay (AMR6) had lower ionic strength and significantly less gypsum than the DI water control. Gypsum was in a state of dissolution indicating the reduction of cementation due to gypsum in this clay.
- **Natural Background** – This clay was gypsum saturated with similar chemistry as the control clay made with DI water, but with natural aging and soil structure.
- **Natural Unstable** – This clay had lower ionic strength and significantly less gypsum than the DI water control and the natural background clay. Gypsum was in a state of dissolution indicating the reduction of cementation due to gypsum in this clay.

4.3 Geotechnical Testing

The CD attached to this thesis contains the results of the geotechnical testing program outlined in Table 3.1. Single folders for each test contain Excel files with raw data, spreadsheet calculations and plots. Each folder was named after the specimen data it contains. The prefix of the specimen names correspond to the clay type and the suffix after the dash indicate the test type, either triaxial (T) or oedometer (O), and the test number. For example, AMR1-T10 represents triaxial test number ten, which was conducted on gypsum rich (AMR1) clay. Specimen names starting with SS indicate natural Seven Sisters clay. The SS is followed by the depth from which the sample was taken and then the test number. Each folder also contains any photographs of the corresponding specimen. A guide to the contents of the CD is provided in Appendix A. The guide contains a specimen log that indicates the type of clay used for each test and the type of test that was conducted on each specimen. The guide can be used to quickly find the appropriate folder on the CD for a specific test.

The following sections provide examples of typical test results for each type of test that was performed. Interpretation of the yield stress for each type of test is discussed. Defining the yield point was not always trivial. Early in the testing program it was recognized that for most tests, it was possible to define a range of stresses over which yielding occurred. This led to the definition of an inner and outer yield locus. Inner and outer yield loci have been identified by other researchers including Graham and Au (1985) and Jardine et al. (2004). In Section 4.3.6, the yielding results for each type of clay are combined and presented in p',q-space and log p',V-space to define the respective yield loci. Section 4.3.7 presents a summary of elastic-plastic parameters obtained from the results.

4.3.1 Isotropic Consolidation

Isotropic consolidation to stresses higher than the respective yield points were conducted on 12 specimens including AMR1-T11, AMR2-T15, AMR2-T16 (gypsum rich), AMR1-T50 (freeze/thaw gypsum rich), AMR3-T17 (DI water), AMR4-T24 (H_2SO_4), AMR6-T43 (NaCl), AMR7-T54 (Washed 6PV), SS3.8D-T18, SS3.9E-T33 (Natural Background) and SS11.9U-T31, SS10.7U-T44 (Natural Unstable).

Figure 4.3 shows some typical isotropic consolidation results for a gypsum rich specimen (AMR2-T16). The upper plot shows the log p',V data for isotropic consolidation to 350 kPa and the lower plot shows the same data plotted on a linear scale. Yielding was interpreted as the intersection of the two lines in each case. Consistent yield point results were obtained from both types of plots. In this case, yield was interpreted at p' = 130 kPa.

Figure 4.4 shows isotropic consolidation results for a gypsum rich specimen (AMR2-T15) tested in the high pressure cell (Figure 3.7). The specimen was compressed to a maximum effective stress of 3,363 kPa. Yield was interpreted at p′ = 127 kPa which is consistent with the results for the same clay type using the low pressure apparatus.

4.3.2 Strain-Controlled Undrained Triaxial Testing

Isotropically consolidated and undrained triaxial tests (CIŪ tests) were conducted on thirty specimens as listed in Table 3.1 and Appendix A. This includes the tests listed in section 4.3.1, which underwent undrained shearing after completion of the isotropic consolidation portion of the test. These tests were conducted using the triaxial testing equipment for strain controlled tests. This chapter concentrates on presenting the test results. They will be discussed more fully in Chapter 5.

Figures 4.5 and 4.6 show some examples of typical CIŪ test results. The results are for gypsum rich specimen AMR1-T47 which was isotropically consolidated to an effective stress of 100 kPa (That is, over-consolidated. The isotropic preconsolidation pressure for this clay was 135 kPa). Figure 4.5 presents deviator stress and change in pore pressure against axial strain in the upper and lower plots, respectively. Yield was interpreted at the intersections of the straight lines shown in the figure. The inner yield point was identified between the early linear portion of the curve and the non-linear portion. The change in pore water pressure versus axial strain plot indicates decreasing pore water pressures following yield (dilative behaviour) up to the end of the strain-softening portion of the curve. It is postulated that the decrease in pore pressure is a

response to dilation of the soil that was formed during consolidation at a higher stress state than the CIŪ test. During 1D consolidation of the gypsum rich clay, cementation would have locked the soil structure at its highest effective stress. If these bonds are broken at a lower effective stress, the (expansive) soil will tend to dilate as indicated by the drop in pore pressure.

The second straight line portion of the stress-strain curve was interpreted as plastic behaviour where cementation bonds are presumably being broken and destructuring with non-recoverable straining occurring. After continued straining, sufficient cementation bond destruction and particle alignment occurs to allow the formation of a shear plane and strain-softening. The strain-softening position on the stress-strain curves corresponded to visual evidence of the formation of a distinct shear plane. After the end of testing, all of the shear planes were observed to be shiny and slicken-sided.

Figure 4.6 shows the principal effective stress ratio against axial strain in the upper plot and deviator stress against mean effective stress in the lower plot for the same test as shown in Figure 4.5. As for the other parameters plotted against axial strain, yielding was interpreted as the intersection between the two straight lines. In p',q-space, yielding corresponded to the peak value for the test shown. In some tests, peak was reached after yielding during the second straight line portion of the stress-strain curve prior to shear plane development.

4.3.3 Strain Controlled Drained Triaxial Testing

Strain controlled, drained triaxial tests (CID tests) were conducted on 11 specimens including AMR1-T10, AMR2-T14 (gypsum rich), AMR1-T49 (freeze/thaw gypsum rich), AMR3-T35 (DI water), AMR4-T22 (H_2SO_4), AMR6-T41 (NaCl), AMR5-T38 (washed 1PV), AMR7-T52, AMR7-T55 (Washed 6PV), SS3.6D-T19 (Natural Background) and SS10.7U-T20 (Natural Unstable).

Figures 4.7 and 4.8 show some examples of typical CID test results. The results are for gypsum rich specimen AMR1-T10 which was isotropically consolidated to an effective stress of 100 kPa (over-consolidated). Figure 4.7 presents deviator stress and volume strain against axial strain in the upper and lower plots, respectively. Figure 4.8 presents the principal effective stress ratio versus axial strain and deviator stress versus mean effective stress in the upper and lower plots, respectively.

Three straight line portions of the stress-strain curve (Figure 4.7) were commonly identified in the CID test results. These included an initial stiff portion of the curve, followed by an intermediate section with less slope, before an almost flat section that was interpreted to be equivalent to the flat plastic section of the CIŪ test results. True yielding (defined in this program as 'outer' yield) was interpreted at the intersection of the intermediate and upper straight lines. This was based on good correlation with other plots such as the volume strain versus axial strain and principal effective stress ratio versus axial strain plots. The three plots indicate yielding at an axial strain of approximately 4%. The intersection between the early, stiff portion of the curve and the

intermediate portion was interpreted in this program as an inner yield point, which occurred at approximately 1% axial strain.

Table 4.5 presents the interpreted yield point based on five different plots for the data presented in Figures 4.7 and 4.8 (specimen AMR1-T10). Plots examined include maximum principal effective stress versus axial strain, mean effective stress versus volume strain, deviator stress versus axial strain, principal effective stress ratio versus axial strain and volume strain versus axial strain. The results indicate that the interpretation of yield is consistent regardless of plot type and not an artefact of how the data are plotted.

Two independent triaxial cells, data acquisition and constant rate of strain presses were used during the testing program. One of the cells was newer and had a smoother piston bearing. In order to confirm the data produced by each machine was comparable with the other, two independent tests were conducted on the same clay. Figure 4.9 shows the stress-strain results for two specimens of the washed 6PV clay conducted using the two sets of triaxial testing apparatus. The upper plot shows data produced by the older apparatus and the lower plot was the data produced by the newer apparatus with the smoother piston. While the data produced by the newer equipment contained less 'noise', the two tests produced very similar results.

4.3.4 Stress Controlled Drained Triaxial Stress Path Testing

Several drained triaxial stress paths were examined under incremental stress controlled conditions. Constant p′ tests following p′ = 100 kPa were conducted on each type of

clay. Two tests following the K_0 consolidation line (with K_0 = 0.78) were conducted for comparison with the oedometer tests. These tests were followed by undrained shearing (CAŪ tests). Finally, several supplemental defined stress paths were conducted to further define the shape of the gypsum rich yield locus. These included stress paths following q/p' ratios of -1.5 and 1.25.

4.3.4.1 Constant p' Tests

As listed on Table 3.1, constant p' tests were conducted on nine specimens including AMR2-T21, AMR2-T23, AMR2-T29 (gypsum rich), AMR3-T56 (DI water), AMR4-T26 (H_2SO_4), AMR6-T40 (NaCl), AMR7-T53 (Washed 6PV), SS3.5D-T32 (Natural Background) and SS10.7U-T34 (Natural Unstable).

Figure 4.10 shows an example of typical results obtained from the constant p' tests. The results presented are for gypsum rich specimen AMR2-T29. For stress paths to the left of the apex of the yield locus, it is common to take the end of test rupture point as the yield point. However, the stress-strain results were notably bi-linear before rupture occurred. The intersection of the two lines was interpreted as an inner yield point and the rupture point was interpreted as an outer yield point. No significant volume change was measured for any of the constant p' tests. As such, the data analysis was limited to plotting deviator stress versus axial strain for the constant p' tests.

4.3.4.2 K_0 Consolidation Tests

K_0 consolidation tests were conducted on two specimens including AMR2-T30 (gypsum rich) and SS3.9D-T36 (Natural Background). The results for the gypsum rich specimen AMR2-T30 are shown in Figure 4.11. This figure presents deviator stress and volume strain against axial strain in the upper and lower plots, respectively. The data in both plots was notably bi-linear with yielding being interpreted as the intersection of the two lines. Good agreement of yield interpretation was observed between both plots.

4.3.4.3 Other Defined Stress Path Tests

Lateral expansion stress path tests following q/p′ = -1.5 were conducted on two gypsum rich specimens including AMR2-T37 and AMR2-T39. Figure 4.12 shows the results for specimen AMR2-T37. As for the constant p′ tests, the end of test rupture point was interpreted as yielding for these tests. Again, inner yield points were evident from the bilinear nature before rupture. The intersection of the two lines was interpreted as an inner yield point and the rupture point was interpreted as an outer yield point. A small amount of negative volume change (expansion) was measured in these tests. However, this only occurred near the end of the tests and insufficient resolution was achieved for plotting volume change results. As such, the data analysis was limited to plotting deviator stress versus axial strain for the lateral expansion tests.

Defined stress path tests following q/p′ = 1.25 were conducted on two specimens including AMR2-T42 (gypsum rich) and SS3.5E-T46 (Natural Background). Figure 4.13 presents the results for the gypsum rich specimen AMR2-T42. This figure presents deviator stress and volume strain against axial strain in the upper and lower plots,

respectively. The data in both plots were notably bi-linear with yielding being interpreted as the intersection of the two lines. Good agreement of yield interpretation was observed for both plots.

4.3.5 Oedometer Testing

Oedometer tests were conducted on the following 16 specimens: AMR1-O4, AMR1-O5, AMR1-O6, AMR2-O7, AMR1-O14 (gypsum rich), AMR3-O8, AMR3-O13 (DI water), AMR4-O11 (H_2SO_4), AMR6-O15 (NaCl), AMR5-O12 (washed 1PV), AMR7-O16 (Washed 6PV), SS3.7D-O9 (Natural Background) and SS10.7U-O10 (Natural Unstable).

Figures 4.14 and 4.15 present the combined oedometer results of selected specimens. Figure 4.14 provides the vertical effective stress versus specific volume results and Figure 4.15 show the results of the same tests in terms of change in specific volume ΔV versus vertical effective stress. The upper plots include the results of the reconstituted specimens and the lower plots include the results of the natural specimens, with the gypsum rich results for comparison. Table 4.6 provides a summary of the oedometer results.

Little difference was observed between the gypsum rich, DI water, NaCl and H_2SO_4 reconstituted specimens. The specific volumes of the washed 6PV specimen were slightly higher than the other reconstituted specimens, but the curve shape and yield point were similar to that of the others. This is evident in Figure 4.15.

The natural background and reconstituted (gypsum rich) specimens both had very similar initial specific volumes. The initial specific volume of the unstable section was relatively low, further suggesting that the foundation clay beneath the dykes had experienced some plastic hardening. The preconsolidation pressures of the natural specimens were not as clearly defined as the reconstituted specimens possibly because of soil fabric or some weathering-induced macrostructure. The lower plots of Figure 4.14 and 4.15 show that the effects of aging increase the preconsolidation pressure, yet the slopes of the pre and post-yield curves were similar.

4.3.6 Yield Loci

The results of the triaxial and oedometer testing program described above were interpreted in terms of elastic-plastic soil mechanics as described in Section 2.7. The first task in developing an elastic-plastic model is to determine the yield locus. Yield loci and representative stress paths for the clays reconstituted with gypsum rich water, DI water, H_2SO_4, NaCl brine, and the reconstituted clay washed with six pore volumes of DI water, as well as natural clay from the background location and unstable section are presented on Figures 4.16 to 4.22, respectively. The upper diagrams show the yield loci in p',q-space and the lower diagrams show the yield loci in log p',V-space.

As discussed in the earlier sections of this chapter, the CIŪ, CID and incrementally loaded tests showed evidence of an early (or inner) yield which has been interpreted as a transition between primarily linear elastic behaviour to non-linear behaviour before true yielding and the onset of plastic hardening (defined in this program as outer yield). True elasticity between the inner and outer yield points has not been examined. (Similar

'inner' yield loci have been identified by other researchers, for example Jardine et al. (2004), but not for soft, plastic clays.) For reference, both the inner and outer yield points of the tests used to construct these diagrams are included in Table 4.7. The inner and outer yield loci were visually fitted to these points.

The most extensive testing was conducted on the clay reconstituted with gypsum-rich water (Figure 4.16), with replicate tests conducted for a number of stress paths. This provided confidence in the amount of variability in the definition of the yield loci and its overall shape. The yield locus for this clay was then considered the baseline for comparison with the other clays. A lesser number of tests was conducted on the other clays in order for more geochemical conditions to be examined as part of this research program.

The q,p'-plot in Figure 4.16 shows examples of the stress paths utilized for yield loci characterization. For clarity, not all of the tests have been shown, but all of the yield points have been included. The data plotting along the p' axis is from isotropic consolidation tests. Specimens following this stress path do not fail as the stress path does not intersect the failure envelope. They do yield, however. As such, these specimens were sheared using undrained strain controlled conditions following sufficient straining to define the yield point. Specimen AMR1-T11 is an example of the data obtained from isotropic consolidation tests followed by undrained shearing.

Similar to the isotropic consolidation tests, the specimens following the K_0 consolidation line yield but do not fail. Specimen AMR2-T30 (Figure 4.16) illustrates the K_0

consolidation stress path. Following sufficient definition of the yield stresses for a given specimen, the specimen was sheared using undrained strain controlled conditions from the final stress state on the K_0 consolidation line (CAŪ).

Specimen AMR2-T42 in Figure 4.16 is an example of the q/p′ = 1.25 stress path. Specimens following this stress path will yield, and then with further stressing move to failure. This stress path was followed using incremental stress controlled tests. These tests are simple to conduct and provide good definition of the yield point. However, strain-softening could not be observed.

An example of the q/p′ = 3 stress path is illustrated by Specimen AMR1-T10 in Figure 4.16. This stress path was followed by conducting CID tests. The q/p′ = 3 stress path could be followed using strain controlled conditions since the cell pressure remains constant for this stress path. This provides the advantage of being able to define the yield point and observe failure and strain-softening. For these reasons, the CID test was one of the most diagnostic tests of the program.

Specimen AMR2-T29 in Figure 4.16 shows the constant p′ stress path (that is Δp′=0). Tests conducted to identify yield stresses are usually performed under drained conditions. However, very little volume change was observed during these tests. Therefore, the results of strain controlled undrained (CIŪ) tests starting at the same initial isotropic consolidation pressure as the constant p′ tests were considered in the definition of the yield loci. The cluster of yield points along this stress path are a combination of results from constant p′ and CIŪ tests.

A lateral expansion stress path was followed for two specimens using a q/p'=-1.5 ratio. Specimen AMR2-T37 in Figure 4.16 provides an example of this stress path. For specimens that yield on the left side of the yield locus peak, the plastic strain increment vector includes a negative (expansive) plastic volumetric strain component. As the specimen strain softens, water content therefore increases producing a less stiff, weaker specimen. This is consistent with the observation of swelling in these specimens measured after removal of these specimens.

All of the yield loci shown in Figures 4.16 to 4.22 displayed anisotropic characteristics. The assumption of isotropic elasticity used in Cam-clay modelling results in elliptical yield loci that, when traced into p',V-space appear as straight lines. In contrast, yield loci in p'q-space for all of the soils tested in this program were not elliptical and the elastic walls were inclined. The inclination of the elastic walls produces 'hook' shaped traces in p',V-space. Yielding along the isotropic consolidation lines occurred at lower mean effective stresses than for the K_0 stress path (and the q/p' = 1.25 stress path where tested). This resulted in barrel-shaped yield loci in p',q-space, indicating some degree of elastic anisotropy (Graham and Houlsby, 1983).

The lower plots in Figures 4.16 to 4.22 show the yield loci in log p',V-space. The anisotropy noted in the p',q plots translated to hooked traces with inclined elastic walls in log p',V-space. Also shown are the isotropic normal consolidation lines (Iso-NCL), 1D normal consolidation lines (1D NCL) and critical state lines (CSL). With the exception of the yield locus for the NaCl clay, the Iso-NCLs plotted above the 1D-NCLs, which in turn

plotted above the CSLs. The 1D-NCL and Iso-NCL were reversed in the case of the NaCl clay yield locus. With the available data, it was generally appropriate to show the range within the 1D-NCL and Iso-NCL plotted.

The yield loci can be normalized with respect to various parameters to permit comparison with the natural specimens from different depths. Normalization also permits comparison with testing programs conducted by others. Common normalization parameters include the preconsolidation pressure (σ_{zc}'), isotropic preconsolidation pressure (p_c') and the equivalent mean effective pressure (p_e'). The equivalent mean effective pressure is the mean effective pressure on the isotropic normal consolidation line corresponding to the current specific volume of the specimen. Table 4.7 presents the yielding data and values of the normalization parameters for each specimen used for characterization of the yield loci.

Figure 4.23 presents the outer yield data normalized with respect to the measured 1D preconsolidation pressure. For clarity, the stress paths have been omitted. The upper plot shows the results for the reconstituted specimens. The larger yield locus in the figure consists of the best visual fit to the gypsum rich specimens and the smaller yield locus is the best visual fit to the specimens reconstituted from the clay washed by six pore volumes of DI water. The remaining reconstituted specimens were not significantly different than the gypsum rich specimens in p',q-space. The results indicate that lowering ionic strength and the removal of gypsum shrinks the yield locus. Chapter 5 provides a further discussion regarding the effects of pore fluid chemistry on the yield locus.

The lower plot of Figure 4.23 shows the results of the natural clay from Seven Sisters compared to the reconstituted gypsum rich specimens. Both the background and unstable sections reduced to approximately the same yield locus with an apex at approximately $q/\sigma'_{zc} = 0.45$. In contrast the yield locus for the clay reconstituted with gypsum rich water was significantly larger, peaking at almost $q/\sigma'_{zc} = 0.8$. Both yield loci converged at both ends with lower values of q/σ'_{zc}.

For the reconstituted specimens, the applied 1D consolidation pressure is known and can also be used for normalization instead of the measured preconsolidation pressure. The 1D consolidation pressure was corrected by an amount (25 kPa) calculated from the stress system in the consolidation cell to account for side-wall friction in the apparatus. This reduced the consolidation pressure to 200 kPa. Figure 4.24 shows the yield data normalized with respect to the 1D preconsolidation pressure. This normalization procedure resulted in greater separation of the specimens reconstituted from the clay washed with six pore volumes relative to the other reconstituted specimens. Tighter grouping was also achieved.

Figure 4.25 presents the yield data normalized with respect to p_c' determined from the isotropic consolidation tests. The results were similar to that of the yield loci normalized with respect to the preconsolidation pressure. However, there was slightly less separation between the gypsum rich and washed clay yield loci. As expected, the two yield loci converged along the lower right-hand side as they approached $p'/p'_c = 0$.

A greater degree of scatter was observed when the yield data were normalized with respect to p_e' (Figure 4.26). A similar amount of scatter was observed by Oswell (1991) for sand-bentonite buffer material and Li (1983) for Winnipeg Clay. However, the best visual fit yield loci show generally similar trends as the other normalized plots. The upper plot shows separation of the gypsum rich and washed clay yield loci. The best visual fit to the natural specimens was less obvious. It was also shifted to the left compared to the yield locus for the reconstituted gypsum rich clay.

Based on the above, normalizing with respect to the measured 1D and isotropic preconsolidation pressures was considered the most appropriate method for comparing the different types of clays. Following this conclusion, the normalized inner yield loci in p',q-space (Figure 4.27) and the outer yield loci in p',V-space were established (Figure 4.28). The complete yield loci in p',q',V-space are presented in Figures 4.29 to 4.32, inclusive. The first two of these figures are the yield loci normalized with respect to the 1D preconsolidation pressure for the reconstituted and natural clays, respectively. The last two of these figures are the yield loci normalized with respect to the measured isotropic preconsolidation pressure (p'_c). The curves were developed visually in all cases. Once a curve was developed, it was mapped between p',q-space and p',V-space normailized with respect to σ'_{zc} and p'_c. The process was repeated until the best visual fits were obtained for both plots. Inner and outer yield loci are shown in p',q-space, but for clarity the inner yield loci have been omitted in p',V-space. The inner yield loci were the same general shape as the outer yield loci, only plotting slightly higher in p',V-space.

4.3.7 Elastic-Plastic Parameters

Elastic-plastic parameters were obtained from the triaxial tests described earlier in this chapter. Of these, the yield loci were presented in the previous section. The remaining components of the elastic-plastic model, which consist of the elastic parameters (isotropic and anisotropic), flow rule, hardening law and failure criterion, will be developed in this section. Tables 4.8 to 4.11 provide a summary of the elastic-plastic parameters. Details of the data and procedures used to obtain the elastic-plastic parameters are discussed in the following paragraphs.

4.3.7.1 Elastic Parameters

The isotropic elastic parameters presented on Table 4.8 were established from pre-yield stress-strain behaviour. Hooke's Law is commonly used to describe linear isotropic elastic behaviour, with Young's Modulus (E) relating stress and strain. Young's Modulus was determined from linear sections of the principal effective stress and axial strain data of the drained triaxial test (CID) results.

Changes in shape that occur as a specimen is stressed are described by Poisson's ratio (ν), which relates radial strain to axial strain. Poison's ratio was also calculated from the pre-yield data of the CID tests, knowing void ratio and corresponding axial strain ($\nu = 0.5(1\text{-}e/\varepsilon_1)$).

Two isotropic elastic parameters commonly used in soil mechanics include the bulk modulus (K) and shear modulus (G). Table 4.8 shows values of K and G interpreted

directly from the test data. The bulk and shear moduli relate changes in volume and shear strain to the mean effective stress and deviator stress, respectively. The bulk moduli were determined from the pre-yield change in specific volume as a function of mean effective stress data from the isotropic consolidation tests. The shear modulus was determined from the deviator stress versus axial strain curves of the drained triaxial test (CID) results. In linear isotropic elasticity, these parameters are uncoupled with the following matrix notation:

$$\begin{bmatrix} p' \\ q \end{bmatrix} = \begin{bmatrix} K & - \\ - & 3G \end{bmatrix} \begin{bmatrix} \varepsilon_v \\ \varepsilon_s \end{bmatrix} \qquad [4.1]$$

The elastic parameters described above apply to isotropic soils. However, soils usually display anisotropic behaviour. Graham and Houlsby (1983), compared the predictions of isotropic and anisotropic elastic parameters for Lake Agassiz clay. Their study indicated that the elastic moduli were stress path dependent and that a better prediction of elastic behaviour could be achieved by assuming anisotropic elasticity. Graham and Houlsby (1983), modified Equation [4.1] to account for shear strains caused by changes in mean effective stress and volume strains caused by changes in the deviator stress. This was achieved by including a cross anisotropic modulus (J) as follows:

$$\begin{bmatrix} p' \\ q \end{bmatrix} = \begin{bmatrix} K & J \\ J & 3G \end{bmatrix} \begin{bmatrix} \varepsilon_v \\ \varepsilon_s \end{bmatrix} \qquad [4.2]$$

The anisotropic elastic parameters for this program were determined using the techniques developed by Graham and Houlsby (1983). A single triaxial test is not sufficient to solve for the elastic constants in Equation 4.2 since there are two equations and three unknowns. In order to solve Equation 4.2, a minimum of two drained triaxial tests with different q/p' ratios are required. Two triaxial tests provide four equations with three unknowns, giving a redundancy of equations. By using a least squares regression method it is possible to solve Equation 4.2 for a number of tests by minimizing the errors.

The procedure for determining the anisotropic elastic moduli was as follows. The changes in p', q, ε_v and ε_s in the elastic region were found for each test. Slopes were obtained at a point in the test approximately half way between the start of the test and the yield point in terms of q. To simplify the calculations, the K, J and 3G constants in Equation 4.2 are replaced by C_1, C_2 and C_3, respectively, where $C_1=3G/(3KG-J^2)$, $C_2=-J/(3KG-J^2)$ and $C_3=K/(3KG-J^2)$. The sum of the errors is:

$$\sum_{tests}\left\{\left(C_1\delta p'+C_2\delta q-\delta\varepsilon_v\right)^2+\left(C_2\delta p'+C_3\delta q-\delta\varepsilon_s\right)^2\right\} \qquad [4.3]$$

Equation 4.3 is then differentiated with respect to C_1, C_2 and C_3 and set to zero to minimize the error, giving:

$$\frac{\delta(error)}{\delta C_1}=\sum 2\left(C_1\delta p'+C_2\delta q-\delta\varepsilon_v\right)\delta p'=0 \qquad [4.4]$$

$$\frac{\delta(error)}{\delta C_2} = \sum \{2(C_1\delta p' + C_2\delta q - \delta\varepsilon_v)\delta q + 2(C_2\delta p' + C_3\delta q - \delta\varepsilon_s)\delta p'\} = 0 \qquad [4.5]$$

$$\frac{\delta(error)}{\delta C_3} = \sum 2(C_2\delta p' + C_3\delta q - \delta\varepsilon_s)\delta q = 0 \qquad [4.6]$$

Data from the triaxial tests were substituted into Equations 4.4 to 4.6 which were then solved for K, G and J. The available data included results from the CID and constant p' tests for all of the clays tested in this program. The exceptions were the reconstituted gypsum clay and the natural Seven Sisters background section clay which was tested more thoroughly.

Table 4.9 provides a summary of the anisotropic elastic parameters. Similar results were obtained for the natural clay from the Seven Sisters background location compared to the values obtained by Graham and Houlsby (1983) for Winnipeg clay. The coupling modulus for these clays was negative, indicating that the soil is stiffer horizontally than vertically. This is consistent with the observation of laminations within both of these clays. Applying stress parallel to the lamination planes would likely result in greater resistance than applying stress perpendicular to laminations. In the case of applying stress parallel to the lamination planes, more compressible laminations would compress to a larger degree than in the case of applying stress perpendicular to the laminations. In contrast, the reconstituted clays generally showed similar stiffness in both directions. This reflects the lack of macro-structure in the reconstituted soils.

Better agreement with the work conducted by Graham and Houlsby (1983) on Winnipeg clay was obtained for the clays that had more than two tests available for the least squares regression calculation and in particular the natural clay from the background location at Seven Sisters. This provided some degree of confidence with the moduli determined for the clay reconstituted with gypsum-rich water and the natural clay from the background section. Several anomalies were noted for the clays that only had two triaxial tests available for the calculation. For example, very high values of K and J were obtained for the clay reconstituted with DI water. These values should be viewed with caution until further testing is completed.

Two factors placed limitations on the confidence in determining accurate anisotropic elastic moduli. First was the limited number of tests with suitable data for most of the material tested (that is, at least two tests are required). This precluded the luxury of removing data that did not agree well with the predicted volume and shear strains. Other researchers have removed sporadic test results based on comparing the predicted strains to measured values (Oswell, 1991). Second was the apparent effect of friction in the piston bearings on incremental stress controlled tests. The elastic moduli were very sensitive to slight changes in the input data and the results were not as consistent as the isotropic elastic moduli determined using strain controlled testing. This appears to be due to varying amounts of friction in the piston depending on its point in travel through the bearing. On an individual basis, the tests provided good yielding data, but the elastic moduli need to be confirmed. Further testing is recommended using constant rate of stress testing (for example, using a Bishop and Wesley cell with GDS controllers) or repeating the incremental stress controlled tests with a rotating piston to eliminate friction.

4.3.7.2 Flow Rule

The flow rule relates the plastic volumetric and shear strain components (ε_v^p, ε_s^p) to the stress state at yield (p'_y, q_y). It describes the relative proportion of plastic shear strain to plastic volume strain. The flow rule is determined by examining the direction of the plastic strain increment vectors after yielding. If the plastic strain increment vectors are plotted in $\varepsilon_s^p, \varepsilon_v^p$-space, a curve could be established such that each vector was normal to the curve. This curve is called the plastic potential. When the plastic potential is different from the yield surface, the flow rule is termed non-associated. When the plastic strain increment vectors are perpendicular to the yield surface, that is the plastic potential and the yield surface are the same, the flow rule is termed associated. For the general case, non-associated flow applies. However, it is common to assume associated flow in order to define the plastic potential and yield surface with a single function and therefore simplify numerical analyses.

Plastic strains were separated from elastic strains graphically using plots of p′ versus ε_v and q versus ε_s. Figure 4.33 shows the separation of elastic and plastic strains. A constant stress increment of 0.1 p_c' in the direction of the stress path was used to determine the plastic strain components. For any single test, the appropriate component of the same increment was applied to both of the stress-strain plots. The plastic strains were measured directly from the graphs at the separation of the elastic and plastic portions of the stress-strain plots over the selected stress increment as shown on Figure 4.33.

This procedure proved to be difficult for any of the tests to the left of the yield locus apex. That is, the constant p' and lateral expansion tests. For these tests, rupture was taken as the outer yield point and the transition to true plastic behaviour. The difficulty arose from the rate at which rupture would occur after yield. Often, rupture would occur immediately after a load increment, with no opportunity to obtain any readings during plastic deformation. This is a drawback of incremental stress controlled tests and was noted earlier by Graham et al. (1983) for the Winnipeg Clay. For these tests, plastic strain increment vectors were obtained using the last load increment before rupture. Although this is not an ideal procedure for determining plastic strain increment vectors, it was the only option available for the available data. The results should be viewed as qualitative and will certainly be low with respect to magnitude of volume strains.

The plastic strain increment vectors are defined by the $\varepsilon_s^p / \varepsilon_v^p$ ratios. When these vectors are plotted at the yield stress of each test in p',q-space the flow rule can be determined. Figure 4.34 shows the plastic strain increment vectors in relation to the yield loci in p'/p'_c, q/p'_c-space. The natural and reconstituted specimens have been separated. Based on this figure, non-associated flow generally applies. The exception to this is perhaps the lateral expansion test and some of the CID tests conducted on the reconstituted specimens

Examination of Figure 4.34 reveals that the direction of plastic strain increment vector deviation from the normal to the yield loci is systematic. At the front of the yield loci, where the curve approaches $p'/p'_c = 1.0$, the deviation is counter-clockwise from the normal. On the left hand side of the CID stress path data, the deviation is generally clockwise from the

normal. This observation is consistent with the results obtained by Graham et al (1983) using Winnipeg clay and Oswell (1991) using sand-bentonite buffer material.

4.3.7.3 Hardening Law

The hardening law describes how much the yield surface will expand or contract in response to a stress increment. It is obtained by performing consolidation tests at increasing isotropic stresses beyond the yield point. For isotropic hardening, the yield locus is assumed to change size but maintain the same shape. The hardening law can be written as follows:

$$\varepsilon_v^p = \frac{\lambda - \kappa}{V} \ln(p') \qquad [4.3]$$

where κ and λ are slopes of the unload/reload and normal consolidation loading lines in V,ln (p') –space, respectively. The κ term represents pure elastic volume strain and the λ term represents total volume strain. Therefore, the difference between the two terms is the plastic volume strain.

Straight lines were fitted to the pre- and post-yield sections of the isotropic consolidation curves (See Figures 4.3 and 4.4), which is one of the assumptions of Cam-clay models. The values of κ were determined from the pre-yield change in specific volume as a function of mean effective stress. Values of λ were determined from the post-yield

change in specific volume as a function of mean effective stress. Table 4.10 provides a summary of the results.

4.3.7.4 Failure Criterion

The Mohr-Coulomb failure criterion is commonly used in elastic-plastic soil mechanics. The criterion requires two material parameters that represent the cohesion and frictional resistance of the material. The failure criterion was determined from the 'rupture' or 'large strain' end-of-test data. At this point in the test, cohesion along the failure plane was considered destroyed and the failure criterion was represented by the slope of the critical state line passing through the origin.

Table 4.11 presents the critical state parameter, M_{cs}, and its corresponding effective stress friction angle (Φ'_{cs}) for each of the tested clays (Note: $\sin \Phi'_{cs} = 3M_{cs}/(6+M_{cs})$). With the exception of the clay reconstituted with gypsum-rich water, the natural clay from the background location and unstable section, limited numbers of tests on normally consolidated specimens were available. In these cases, M_{cs} was determined from the CIŪ tests that were normally consolidated to 350 kPa then sheared undrained. Also included in Table 4.11 are the residual strength parameters M_r and Φ'_r. These parameters were determined from end-of-test data where well defined failure planes developed. Only small differences were noted in Φ'_{cs} and Φ'_r. This is not surprising since they are controlled by the mineralogy of the clay after all cementation has been destroyed. The similar values of Φ'_{cs} suggest small to negligible differences in DDL thickness. If DDL thicknesses were significantly different, the Φ'_{cs} values would also be expected to be different.

5.0 Discussion of Test Results

The results of the laboratory testing program described in Chapter 4 revealed interesting changes in strength, strain-softening and yielding behaviour in response to changes in pore fluid geochemistry. This chapter provides further discussion on these changes. The first section looks at the effect of pore fluid geochemistry on strength and strain-softening behaviour. This section shows that the presence of gypsum in the saturated state controls overconsolidated peak strength, while normally consolidated peak strength is influenced by DDL effects. The discussion then looks at how the presence and amount of gypsum influences strain-softening behaviour. This is followed by a brief discussion of the effect of pore fluid chemistry on strain-softening behaviour.

The second section of this chapter discusses the effect of pore fluid chemistry on yielding. The discussion expands on the inner and outer yield loci defined in Chapter 4. The mechanisms controlling the yield loci are discussed. The information discussed in this chapter provides a basis for establishing a state boundary surface as a function of chemistry. This information is presented in the third section of this chapter as part of a chemo-elastoplastic model for the reconstituted clay.

The fourth section of this chapter explores the differences between natural and reconstituted clays with similar pore fluid chemistry. The pore fluid chemistry of the clay reconstituted with gypsum-rich water was designed to be similar to that of the natural clay from the background location. This provided the opportunity to compare a natural soil to a reconstituted soil with closely similar chemistry.

Any differences between the natural and reconstituted clays could be expected to be the result of weathering, aging or differences in fabric and macrostructure due to deposition and genesis (for example, fractures, fissures and laminations) that occurs in natural specimens. To test this, a freezing-thawing experiment was conducted on the reconstituted soil, to determine if any of the observed differences could be reproduced in the laboratory. The fifth and last section of this chapter presents the results of the freezing-thawing experiment.

5.1 Effect of Pore Fluid Geochemistry on Strength and Strain-Softening Behaviour

Peak strength envelopes were constructed for each of the reconstituted clays. Figure 5.1 shows an example. The envelopes consisted of three straight line segments. The first segment followed the left hand side of the yield loci at a q:p' ratio of approximately 2 x M_{cs}. The second segment represented the overconsolidated range, with a slope approximately tangent to the apex of the yield loci. The last segment represented the normally consolidated peak strength.

Figure 5.2 compares the peak strength envelopes for the different chemistries. Increased ionic strength (that is, increased electrolyte concentration) resulted in an increase in normally consolidated peak strength. This trend was observed for the clay reconstituted with brine (ionic strength = 1.2 mol/kg) and to some degree for the clay reconstituted with acidified water (ionic strength = 9.2×10^{-2} mol/kg), compared to the clay reconstituted with gypsum-rich and DI water (both with ionic strength ~7×10^{-2} mol/kg). Increasing ionic strength by the addition of NaCl or acid did not affect peak strength

unless the clays were normally consolidated. The clays reconstituted with gypsum-rich water, DI water, acidic water and brine all had the same overconsolidated peak strength. This suggested that something else was responsible for the overconsolidated peak strength.

The answer to this appears to lie in the saturation state of gypsum. (The saturation states of the other potential cementing minerals such as calcite, aragonite and dolomite remained generally consistent and in a state of saturation. Further, the geochemical modelling, which is presented in Chapter 6, revealed that the concentration of gypsum was two orders of magnitude greater than the next most abundant potential cementing mineral, in this case calcite.) Both the clay reconstituted with gypsum-rich water and the clay reconstituted with DI water was saturated with respect to gypsum (Table 4.4). In other words, both of these clays contained solid phase gypsum capable of contributing to cementation bonding. No difference in peak strength was observed between these two soils despite there being less gypsum in the clay reconstituted with DI water (Tables 4.2 and 4.3). The clay reconstituted with DI water contained 25% less sulphate (based on soil chemical analysis) than the clay reconstituted with gypsum rich water. For the range of gypsum concentrations examined here, the amount of gypsum did not change the peak strength.

In contrast, the clay washed with six pore volumes of DI water was under saturated with respect to gypsum (as indicated by a negative saturation index for gypsum in Table 4.4). This means that gypsum was in a state of dissolution and any gypsum cementation would be reduced. This clay contained 91% less sulphate than the clay reconstituted with gypsum-rich water. Compared to the others, less gypsum in the solid phase (which

would be capable of contributing to cementation) was present in this washed clay. As shown in Figure 5.3, the clay washed with six pore volumes of DI water had a lower peak strength in the overconsolidated range than the other reconstituted clays. All of the other clays were saturated with respect to gypsum. As long as gypsum was in a state of saturation, the overconsolidated peak strengths were the same. After gypsum was brought to a state of dissolution, overconsolidated peak strength was reduced.

The observed differences between normally consolidated peak strengths and overconsolidated peak strengths in Figure 5.2 suggest that different mechanisms control soil behaviour in these two regions of stress-strain behaviour. Overconsolidated peak strengths appear to be controlled by the presence of cementation, whereas normally consolidated peak strengths appear to be influenced by DDL effects. In the normally consolidated range, the original cemented soil structure is destroyed by the shear straining preceding failure. Destructuring brings particles into a tighter arrangement with closer face-to-face particle contact, especially along a shear plane. This forces the interaction of neighbouring DDLs. If the DDLs are significantly thinner, such as for the clay reconstituted with brine, adjacent particles will be forced closer together and increased friction will result as particles slide past one another. This was reflected by the higher critical state strength and residual strength determined for the clay reconstituted with brine relative to the other reconstituted clays (Table 4.11). The critical state strengths and residual strengths of all but the clay reconstituted with brine were very similar, indicating that the differences in chemistry between these did not result in significant DDL changes.

Differences due to chemistry were also observed in the pre-failure undrained triaxial stress paths, particularly below the overconsolidated strength envelopes. The lower diagram of Figure 5.3 shows p′,q stress paths from the CIŪ tests conducted on the reconstituted clays. The stress paths of the clays that were saturated with respect to gypsum (that is, all but the washed clay) initially followed close to a 'drained' q:p′ stress path of slope 3:1 even though the tests were undrained. It appears that the presence of cementation prevented the build-up of pore pressures for a short period of shearing in the test (up to between 0.3% and 0.6% axial strain). As the test continued, pore pressures began to increase and the stress path bent slightly to the left and became vertical. In contrast, this behaviour was not observed in the specimen of washed clay. The stress path of this specimen was almost vertical, with a slight lean in the opposite direction to the early parts of the other tests. The removal of gypsum cementation appeared to reduce the ability of the clay to delay the onset of pore pressure build-up.

The discussion, so far, has been concerned with peak strengths and undrained elastic behaviour as a function of chemistry. In the overconsolidated range, the presence of gypsum in the saturated state appeared to be more important than the actual amount of gypsum. In contrast, strain-softening behaviour (that is, post-yield, plastic behaviour prior to reaching critical state) is influenced by both the presence and amount of gypsum. Figure 5.4 compares stress-strain results from the CID tests conducted on the clays reconstituted with gypsum-rich water and DI water; and reconstituted clays washed with one and six pore volumes of DI water. The clays reconstituted with gypsum-rich and DI water both had the same peak strength and were both saturated with respect to gypsum. However, the clay reconstituted with DI water contained 25% less sulphate than the gypsum rich clay. Figure 5.4 suggests that the presence of less gypsum

cementation in the clay made with DI water required less strain to form a shear plane. The gypsum-rich clay required over 12% axial strain for the formation of a shear plane. Approximately 8% axial strain was required to form a shear plane in both the clay reconstituted with DI water and the reconstituted clay washed with one pore volume of DI water.

In terms of peak strength and strain-softening behaviour, the reconstituted clay washed with one pore volume of DI water behaved very similarly to the clay reconstituted with DI water. The pore fluid analysis of the clay washed with one pore volume of DI water indicated that it was slightly under-saturated with respect to gypsum and contained slightly less sulphate than the clay reconstituted with DI water. The clay washed with one pore volume of DI water appears to be at the transition point between gypsum-saturated conditions at which no changes in yielding or peak strength are observed and under-saturated conditions with respect to gypsum, that lead to lower yield points and peak strength.

The reconstituted clay washed with six pore volumes of DI water had the lowest peak and critical state strengths of the specimens shown on Figure 5.4. A shear plane developed in this specimen at approximately 7.5% axial strain, but the specimen did not fully strain soften to critical state until approximately 13.5%. It is speculated that stress relief from the drop at 7.5% and the increased bulging observed in this specimen delayed complete strain-softening. (This trend was also noted for the CIŪ tests shown in Figure 5.3.) However, it is clear that this amount of washing resulted in a weaker material.

Other chemical factors besides the amount of gypsum also influenced post yield, plastic behaviour. Figure 5.5 compares the stress-strain results from CID tests conducted on the clays reconstituted with gypsum-rich water, acidic water, brine and the clay washed with six pore volumes of DI water. Again, similar peak strengths were reached by the clays that were saturated with respect to gypsum. The clay reconstituted with brine required significant strain for the development of a shear plane. Although no additional potential cementing minerals were added, this clay required almost as much strain to form a shear plane as the clay reconstituted with gypsum-rich water. Three percent more axial strain was required to develop a shear plane in this clay compared to the clay reconstituted with DI water (Figure 5.4). Increased inter-particle friction from thinner DDLs appeared to increase the amount of strain required for the development of a shear plane. (As will be discussed in Section 5.2, the end-of-test specific volumes of the clay reconstituted with brine were lower than the control clay made with DI water.)

5.2 Effect of Pore Fluid Geochemistry on Yielding

Figures 4.29 and 4.31 compare the yield loci of the reconstituted clays. In these figures, the yield stresses p'_y,q_y have been normalized with respect to the 1D and isotropic preconsolidation pressure p'_c, respectively. In normalized p',q-space, these figures indicate that all of the reconstituted soils that were saturated with respect to gypsum have the same inner and outer yield loci. This included the clays reconstituted with gypsum-rich water, DI water, acidic water and brine. This is consistent with the similar overconsolidated peak strengths noted for these clays.

In contrast, the yield loci of the reconstituted clay washed with six pore volumes of DI water was smaller than those of the reconstituted clays that were saturated with respect to gypsum. Washing in the laboratory primarily removed sulphate, leaving gypsum in an under-saturated state. The removal of gypsum reduced both the inner and outer yield loci and increased the spacing between them. That is, a greater effect was observed on the inner yield locus. This implies that inner yield loci are controlled by cementation and the outer yield loci are more a function of clay mineralogy and structure. It is believed that this is the first time this distinction has been made.

The same trend was noted in the natural clays. The inner yield locus of the clay from the unstable section was smaller than the inner yield locus of the clay from the background location. (Recall that the unstable section was under-saturated with respect to gypsum while the background location was over-saturated with respect to gypsum.) This was so, even though clay at the unstable location had experienced decreases in specific volume as indicated by its position in the normalized p',V plots of Figures 4.30 and 4.32. Lower specific volumes are associated with plastic hardening and plastic hardening normally implies expansion of the elastic region. Even though clay from the unstable location had undergone plastic hardening, initial yielding began earlier than in clay from the background location. In the normalized p',q-space in Figures 4.30 and 4.32, the outer bounds of the yield loci were very similar for both of the natural clays. In fact, they were identical in p'/p'_c,q/p'_c-space. This suggests that the outer yield locus is dominated by mineralogy and interlocking or friction between clay particles (fabric) rather than geochemistry (for the concentrations examined).

To illustrate these different mechanisms of shearing resistance and when they are mobilized, the following paragraphs track the progression of one of the triaxial tests. Figure 5.6 tracks the progress of a CID test (AMR1-T10) as the specimen is stressed through the inner and outer yield loci, into plastic behaviour and finally to the development of a shear plane. From the start of the test (point a) to the inner yield (point b), the soil behaviour is linear, presumably with intact cementation bonds. The cementation helps to hold the initial meta-stable structure or fabric of the clay. This portion of the stress strain curve is characterized by relatively stiff, linear-elastic behaviour. The inner yield point was identified in this study as the transition to less stiff, non-linear behaviour before true yielding and the onset of plastic hardening.

Between the inner and outer yield points (points b and c) in Figure 5.6, cementation bonds at interparticle contacts begin to break. Clay mineralogy and particle interlocking begin to dominate the clay's resistance to shear. The presence of less cementation causes the inner yield point to be reached at smaller strains than more strongly cemented clay and increases the distance between the inner and outer yield points. Up to the outer yield point, plastic volume straining has not yet been initiated. The outer yield represents the onset of plastic deformation. This point was defined by clear yield points using multiple plots of the test data (Table 4.5).

After point (c) in Figure 5.6, cementation bonds continue breaking and particle re-arrangement or destructuring begins. The amount of cementation in the clay and the position of the stress path relative to the yield loci affect the distance between points (c) and (d). The presence of more cementation increases the strain required for the formation of a shear plane at point (d). More cementation provides greater resistance to

destructuring. From point (c) to point (d), destructuring continues and particles are increasingly forced into a tighter face-to-face arrangement. Now DDL effects begin to influence behaviour. Thinner DDLs, as for the clay reconstituted with brine, have lower repulsive forces, thus increasing the amount of true inter-particle contacts. Friction between particles will be higher, resulting in increased peak strength and greater distances between the outer yield point and the formation of a shear plane (point d).

At point (d) in Figure 5.6, sufficient particle alignment exists for the formation of a shear plane and strain-softening occurs. All of the cementation bonds along the shear plane are broken at this point in the test. Point (e) represents the interpreted post-peak or critical state point of the test. Beyond this point, particles in the shear plane slide past one another in a face-to-face orientation and a slickensided surface is developed. At this point, clay mineralogy and factors influencing DDL thickness control the soil behaviour.

The above paragraphs of this section have focused on soil behaviour in p′,q-space. The following paragraphs of this section look at the results in p′,V-space. All of the yield loci for the reconstituted specimens had similar shapes in p′,q and p′,V-space (Figures 4.29 and 4.31). However, there were two notable differences in p′,V-space. The clay reconstituted with brine plotted at lower specific volumes than the clay reconstituted with gypsum-rich water. The reconstituted clay washed with six pore volumes of DI water plotted at higher specific volumes than the clay reconstituted with gypsum-rich water. In other words, the washed clay potentially had a more open structure at the time of yielding and the clay reconstituted with brine had a tighter structure at the time of yielding. The differences appear to originate from the differences in chemistry affecting

how tightly the clays consolidated from a slurry. The differences can be explained using DDL theory.

The specimens of reconstituted clay washed with six pore volumes of DI water had a higher average specific volume. Washing lowered the ionic strength of this soil compared to the other reconstituted clays. Lower electrolyte concentrations allow thicker DDLs to develop for a given pressure. Thicker DDLs in turn result in increased R-A. Therefore, as a slurry of particles with relatively thick DDLs is compressed, the final specific volume will be higher for the same total stress. However, the similarity between the critical state strength envelopes suggests similar DDL thicknesses. As such, the initial microstructure was likely similar.

The opposite occurs for the specimens reconstituted with brine. In this case, the increased electrolyte concentration depresses the thickness of the DDLs relative to the other reconstituted clays. Thinner DDLs result in decreased R-A for a given pressure, and this allows adjacent particles to get closer to each other. Therefore, as a slurry of particles with relatively thin DDLs is compressed, the final specific volume will be lower for the same total stress.

The shape of the outer yield locus (for example in the lower p',V diagram of Figure 4.31) for the specimens reconstituted with brine suggests this clay was more anisotropic than the other reconstituted soils. This indicates that as the clay reconstituted with brine is stressed in shear towards yield, a greater amount of volume change occurs. This is consistent with DDL theory as discussed above. The higher ionic strength of the clay

made with brine depresses the DDLs and results in lower repulsive forces between particles. Therefore as the structure collapses at yield, the particles are forced closer together than in the other clays.

The results of the CID tests appear to agree with this observation (lower diagram of Figure 5.5). The clay reconstituted with brine required almost as much strain to form a shear plane as the clay reconstituted with gypsum rich water (even though additional gypsum was not added to the clay made with brine). Increased inter-particle friction from thinner DDLs appeared to increase normally consolidated peak strength (Figure 5.2) and increase the amount of strain required for the development of a shear plane (Figure 5.5).

Figure 5.7 compares the position and slope of the normal consolidation lines (NCLs) of the reconstituted clays. The same data used to construct the yield loci in Figures 4.29 and 4.31 was used for this figure, except that the data were not normalized. The lower diagram show the data in p',V-space. The NCLs were parallel and therefore had similar λ-values (Table 4.10). This agrees with similar C_c values determined from the oedometer results for the reconstituted clays (Table 4.6). The relative positions of the NCLs of the reconstituted clays are consistent with the geochemical influences on specific volume outlined earlier. The NCL of the washed clay plotted above the NCLs of the other clays and the clay reconstituted with brine plotted below the NCLs of the other clays.

Similar to what Graham et al. (1983) observed for Winnipeg clay, the isotropic-NCL plotted above the 1D-NCL in p',V-space for the specimens reconstituted with gypsum-rich water

but the separation was much less than would be associated with the elliptical yield loci and straight κ-lines of Cam-Clay. A limited number of tests were available for constructing the isotropic and 1D-NCLs for clay reconstituted with brine and reconstituted clay washed with six pore volumes of DI water. As such, the NCLs for these clays were presented as single lines.

5.3 Chemo-Elastoplastic Model

Chapters 4 and 5 provide sufficient information to develop a chemo-elastoplastic (CEP) model for the reconstituted clay. Components that must be considered in the characterization of an elastic-plastic model include definition of (1) a yield locus, (2) elastic parameters, (3) a flow rule, (4) a hardening law and (5) a strength law or failure criterion. The goal of the CEP model is to quantify changes in these components as a function of chemistry. The selected geochemical parameter was sulphate concentration as it (1) is a primary constituent of gypsum (which appeared to be the most abundant potential cementing mineral), (2) it showed the most differentiation between the clays of interest, and (3) can be easily measured. The following paragraphs describe the variation of the elastic-plastic model components with sulphate concentration in the order listed above. The section ends with the description of a strain-softening model to supplement the CEP model.

Starting with the yield locus, Section 5.2 stated that the presence of gypsum in the saturated state controls the size of the yield locus in p',q-space. Specimens that were saturated with respect to gypsum shared the same inner and outer yield loci in p',q-space even though the pore fluids were otherwise different. Based on the similar yield

loci observed for the clays reconstituted with gypsum-rich and DI water, it appears that the mere presence of gypsum in the saturated state controlled the maximum size of the yield loci. When gypsum was washed from the soil and brought to an under-saturated state, the inner and outer yield loci were reduced and had larger separation.

Two tests conducted on the reconstituted clay that was washed with one pore volume of DI water were used to further refine the model. At the time the laboratory testing program was being conducted, the importance of the test results from this type of clay was not understood. Its chemistry was similar to the clay reconstituted with DI water and at first glance, so was its behaviour. After further examination of the test results, however, it was found to be at equilibrium or slightly under-saturated with respect to gypsum and it yielded at smaller strains than the clays that were saturated with respect to gypsum. This provided the opportunity to interpolate a fourth set of yield loci at a different sulphate concentration. Figures 5.8 and 5.9 show respectively the outer and inner yield loci for clay reconstituted with gypsum-rich water and the clay washed with six pore volumes of DI water. Also shown on these diagrams are a limited number (three) inner and outer yield points for the clay washed with one pore volume of DI water. Using these plots, an intermediate set of yield loci could be drawn with a similar shape between the better-defined yield loci for clay that was saturated with respect to gypsum and clay that was under-saturated with respect to gypsum.

Figure 5.10 combines the yielding results for the same clay with four different concentrations of sulphate into a state boundary surface for the chemo-elastoplastic model. The figure shows that with lower sulphate concentrations sufficient to create an under-saturated state with respect to gypsum, the yield loci are reduced and the

separation between the inner and outer yield loci increases. No significant change was observed between the gypsum saturated clay reconstituted with gypsum-rich water and similar clay reconstituted with DI water. This is believed to be the first time it has been possible to construct a chemistry-controlled state boundary surface of this nature.

Section 4.3.7.1 and Table 4.8 presented elastic parameters for the reconstituted clays. These data are isotropic elastic parameters. As discussed in Chapter 4, further characterization will be required to evaluate the anisotropic elastic parameters with confidence. Figure 5.11 shows the variation in E, K, and G with sulphate concentration. In all cases, the elastic parameters increased with increasing sulphate concentration.

Section 4.3.7.2 presented the available information used to determine the flow rule. Figure 4.34 indicated that non-associated flow generally applies. However, further testing is required for better definition. It is common to assume associated flow in order to define the plastic potential and yield surface with a single function and therefore simplify numerical analyses (Graham et al., 1983).

The parameters describing the hardening law (Cam-Clay parameters κ and λ) were discussed in Section 4.3.7.3 and the results were summarized on Table 4.10. Pre-yield behaviour appeared to be influenced by chemistry. The Cam-Clay parameter κ increased from approximately 0.05 for the gypsum-rich clay (sulphate concentration = 2,810 mg/L), to 0.07 for the clay made with DI water, and finally to 0.085 for the clay washed with six pore volumes of DI water. This says that more volumetric straining occurs with decreasing sulphate concentration. This trend is consistent with the trend noted for

the elastic parameters in 5.11. No clear trend was observed with respect to λ. Changes in chemistry did not appear to have a significant effect on λ for the clays considered in this CEP model. This might have been expected, knowing that these clays had the same normally consolidated strength envelopes.

The failure criterion defined by M_{cs}, as described in Section 4.3.7.4, was not influenced by sulphate concentration. All of the clays considered in this model had M_{cs} values close to 0.5. This is consistent with these clays having similar normally consolidated peak strengths as discussed in Section 5.1 and in the previous paragraph.

The dependency of strain-softening behaviour on chemistry discussed in Section 5.1 can be used to supplement the above CEP model. Recall that the clay reconstituted with DI water strain softened sooner than the clay reconstituted with gypsum rich water. Despite the same yield locus, the presence of more gypsum delayed strain-softening. This implies another dimension to the chemo-elastoplastic model.

Also recall that the behaviour of the reconstituted clay washed with one pore volume of DI water was very similar to the clay reconstituted with DI water in drained shearing. Both had similar peak strengths and both strain-softened at approximately the same amount of shear strain. Both of these clays had similar overall chemistry, but the reconstituted clay washed with one pore volume had 17% less sulphate in the pore fluid and was slightly under-saturated with respect to gypsum. The transition to different yielding and strain-softening behaviour therefore occurred beyond this geochemical condition. That is, more than one pore volume was required before significant changes

in strain-softening behaviour could be expected. However, changes in yielding were observed at this sulphate concentration. Stress-strain and yielding behaviour are therefore not entirely coincident with changes in sulphate concentration.

Figure 5.4 can be used to describe a strain-softening model as a function of chemistry. This diagram (for a common consolidation pressure of 100 kPa) indicates that yielding occurs at approximately q = 120 kPa if the clay is saturated with respect to gypsum and at q = 100 kPa if the clay is under-saturated with respect to gypsum. Yielding occurs at approximately 2.5% axial strain regardless of chemistry (outer yield). The maximum peak strength of the reconstituted clay is approximately q = 150 kPa. This peak strength is constant for gypsum-saturated conditions. Peak strength lowers to approximately q = 120 kPa for under-saturated conditions with respect to gypsum. For gypsum saturated conditions, an increase in sulphate concentration from approximately 2,200 mg/L to 2,800 mg/L increases the amount of strain required for strain-softening to occur from approximately 9% axial strain to 13% axial strain.

5.4 Comparison of Reconstituted and Natural Clay

The objective of the testing conducted on reconstituted soils with different pore fluid chemistry was to provide insight regarding the changes in behaviour observed at the Seven Sisters site between the unstable, stable and background locations. As discussed in Chapter 1, Garinger el al. (2004) initially examined these three locations. The current study built upon the work by Garinger and his colleagues by defining the yield loci for the background section, unstable section and reconstituted soils. The reconstituted clays were designed have similar chemistry (and by implication,

cementation) as the background location and unstable location at the Seven Sisters site. This provided an opportunity to compare a natural soil to a reconstituted soil with closely similar chemistry and, knowing the effects of gypsum leaching on yielding, to comment on the observed changes in behaviour at the Seven Sisters unstable section. The following discussion compares the three soils.

Comparing the results for the three natural clays from the site at Seven Sisters indicated that for a given laboratory preconsolidation pressure, the peak strength of the foundation clay at both locations beneath the dyke were similar, but higher than the background location (Figure 1.2). This suggests that some plastic hardening had occurred in the foundation clay beneath the dyke. That is, loading from the dyke had exceeded the preconsolidation pressure in at least some of the foundation clay. However, at large strains, closely similar critical state strength envelopes were determined for all three of the locations (Figures 1.3, 1.4 and 1.5). Figure 5.12 shows p',q plots for the reconstituted clay. These can be compared with corresponding plots in Figures 1.3, 1.4 and 1.5 for the natural clay. The critical state strength envelope for this material was generally the same as the clay from the three field locations with M_{cs} = 0.51 (Table 4.11).

The slopes of the q-p' plots in Figures 1.3, 1.4 and 1.5 indicate anisotropic elasticity with greater elastic stiffness in the horizontal direction (Graham and Houlsby, 1983). The degree of anisotropy is indicated by the slope $\Delta p'/\Delta q$. Compared with the other locations, a greater degree of anisotropy is seen in specimens from the unstable location. The greater anisotropy implies that for the same stress state, clay at the unstable location can generate higher excess pore water pressures during shearing than

similar clay from the stable location. It will therefore fail at lower undrained shear strength than clay from the stable or background locations. This is illustrated in Figure 1.2, which shows changes in pore water pressure versus axial strain.

Figure 5.13 shows the stress-strain data from CID tests conducted by the author on the background location, unstable location and the clays reconstituted with DI and gypsum rich water. The isotropic consolidation pressure was 100 kPa in all cases. Peak strength and strain-softening behaviour showed the same trends between the background and unstable locations that were noted in the CIŪ tests results (Figure 1.2). That is, the unstable section had higher peak strength and was more brittle than the background section. Strain-softening was observed in all four specimens, but it occurred at different axial strains. Significantly more strain was required to develop a shear plane in the reconstituted clay than either of the natural clays. Shear planes developed at 2.7%, 4.7%, 8.6% and 12.8% for the background location, unstable location, clay reconstituted with DI water and the clay reconstituted with gypsum rich water, respectively. The chemistry of the clay reconstituted with DI water and the background sections were very similar (Table 4.2 and 4.3), yet the background section strain softened earlier. Some other mechanism besides chemistry, such as existing planes of weakness, soil fabric, macrostructure or fissures must be responsible for the difference in behaviour (Barbour, 1990).

Figures 4.30 and 4.32 compare the yield loci of the clay reconstituted with gypsum-rich water and the natural background and unstable sections. In these figures, the yield stresses p'_y, q_y have been normalized with respect to the 1D and isotropic

preconsolidation pressure p'_c, respectively. The normalized yield locus of the reconstituted soil was significantly larger and had a different shape than the corresponding loci for the natural clays. The reconstituted soil remained elastic under higher shear stresses than the natural clays and converged with the yield loci of the natural clays at both low p′ and high p′. The yield loci of the natural clays displayed shapes similar to that of Lake Agassiz clay from the Winnipeg Area (Graham et al., 1983). As with the strain-softening behaviour seen above, since the chemistry of the reconstituted clay and the background section were similar, the difference in yielding must be due to something besides chemistry.

The traces of the yield loci in p′,V-space in the lower diagrams of Figures 4.30 and 4.32 suggest that anisotropy increases in moving from the reconstituted clay, to the natural background clay, to the natural clay from the unstable location. This is indicated by the how much the elastic wall 'leans' toward lower specific volumes. The hooked shape of the reconstituted soil spanned a narrow band. (If it was completely isotropic, the band would reduce to a straight line in p′,V-space.) The natural specimens from the background location had a more open hook shape than the reconstituted soil, indicating that the elastic wall leaned more to lower specific volumes and therefore has greater anisotropy. The natural unstable location produced specimens with the most open hook shape indicating the largest degree of anisotropy of the three soils. This is consistent with the results shown earlier in Figures 1.3, 1.4 and 1.5 from undrained CIŪ tests on specimens from the background, stable and unstable locations, respectively.

The lower diagram in Figure 5.14 shows the same data as Figures 4.30 and 4.32, only now they are in non-normalized space. This allows comparison of the positions of the

normal consolidation lines (NCLs). The slopes of the isotropic and 1D NCLs were similar for a given clay, but differed between the reconstituted, natural background location and natural unstable section. The slope of the NCLs for the reconstituted soil was the steepest (highest value of $\lambda = 0.32$), followed by the clay from the background location ($\lambda = 0.18$) then the clay from the unstable section ($\lambda = 0.16$). The difference between the natural and reconstituted clays is likely the result of aging in the field and differences in fabric.

5.5 Effect of Freezing and Thawing Cycles on Yielding

Earlier sections showed that the presence of gypsum cementation affects yielding, specifically the inner yielding at which linear behaviour gives way to non-linear behaviour. However, two observations have not been explained. The reconstituted clay yielded at larger strains and developed shear planes at larger strains than the natural clay even though the chemistry was the same. These observations lead to a hypothesis that weathering induces weaknesses that result in a smaller yield locus. The hypothesis was examined by subjecting several specimens of clay reconstituted with gypsum-rich water to freezing-thawing cycles.

Three specimens that had been cyclically frozen and then thawed were tested for comparison with specimens of the same reconstituted clay that had not been frozen. The program included CIŪ, CID and isotropic consolidation to 350 kPa followed by undrained shear. The specimens were prepared by subjecting clay reconstituted with gypsum rich water to six freezing-thawing cycles. Each freezing-thawing cycle consisted of placing the specimens wrapped in plastic wrap into a freezer for 24 hours at a

temperature of -10°C and following this by a 24 hour period at room temperature. The freezing was from all surfaces of the cylindrical specimens. An initial test showed that the macro-structure of the clay after six freezing-thawing cycles was significantly different from that of unfrozen soil. The frozen-thawed clay had a blocky structure and a high water content at the surface of the specimen. This made it impossible to touch the specimen without destroying it. Successful tests could only be obtained by installing specimens into the triaxial apparatus while they were still frozen.

The final thaw cycle was completed in the triaxial cell and resulting volume changes were monitored. As soon as the specimens began to thaw, water was expelled. In contrast, little or no water expulsion occurred in unfrozen specimens at the same pressure. The freezing-thawing cycles brought water from the core of the specimen to its surface. As such, consolidation (compression) took place in the centre of the specimen during the freeze-thaw cycles. When the water was expelled during thawing, the outer portions of the specimen consolidated. The average water content of the specimens was reduced by 12% after thawing at an isotropic consolidation pressure of 100 kPa.

Figure 5.15 presents the results of a CID test conducted on unfrozen clay reconstituted with gypsum-rich water compared to the same clay subjected to six freeze-thaw cycles. The isotropic consolidation pressure was 100 kPa. The freezing-thawing cycles reduced the amount of strain required to develop a shear plane. The unfrozen clay strain-softened at 12.8% axial strain. In comparison, the clay subjected to freezing-thawing cycles strain softened at 8% axial strain. Further, the clay subjected to freeze-thaw cycles had a much less defined 'plastic plateau' than any of the other reconstituted

clays. This is consistent with the earlier comparison of the results from reconstituted soil and natural soil discussed in Section 5.4. The blocky structure produced by freezing-thawing appears to lower the ability of the soil to carry shear stress at intermediate strains.

The results of CIŪ tests provided further and more dramatic evidence of the decrease in shearing resistance. Figure 5.16 compares the results of the CIŪ tests on unfrozen and frozen-thawed specimens of reconstituted gypsum-rich clay. Freezing and thawing reduced both the peak strength and yield stress of the reconstituted clay. Similar to the CID tests in Figure 5.15, the stress-strain curve of the specimen subjected to freeze-thaw did not flatten after reaching peak and it developed a shear plane at smaller strains than its unfrozen counterpart. In p',q-space (lower diagram in Figure 5.16), the unfrozen soil initially followed close to a drained q:p' stress path of 3:1. As discussed in Section 5.1, it appeared that the presence of cementation prevented the build-up of pore pressures for a short period of time in the test. As the test continued, pore pressures began to increase and the stress path bent slightly to the left and then became vertical. The frozen-thawed specimen followed a different stress path with a more negative slope $\Delta p'/\Delta q$. The change in slope indicates a considerable increase in anisotropy higher stiffness in the horizontal than the vertical direction. In this case, pore water pressures began to increase immediately after shear stress began to be applied. Freeze-thaw cycles appeared to reduce the ability of any cementation in the clay to delay the onset of pore pressure build-up. The p',q behaviour of the frozen-thawed specimen is much more like the natural specimens than the unfrozen specimens.

Figure 5.17 compares the yield points from the frozen-thawed specimens to the yield locus shown earlier for the unfrozen reconstituted clay with the same pore fluid chemistry. The p',q plot indicates that freezing-thawing reduces the size of the inner and outer yield loci. The reduction in size was despite the decrease in specific volume shown in the log p',V diagram shown in the lower part of the figure. Such a decrease in specific volume would normally be associated with a larger yield locus in p',q-space and an expansion of the elastic region. In other words, the frozen-thawed clay lost water but did not harden.

6.0 Modelling the Seven Sisters Site

The hypothesis for the project on the Seven Sisters dykes was that seepage of forebay water through the foundation clay leached naturally occurring cementation minerals from the clay and subsequently changed its elastic-plastic behaviour. The laboratory testing program supported the hypothesis by showing that the reduction of gypsum cementation (1) reduced peak strength, (2) changed the stress-strain behaviour and (3) reduced the size of the yield locus. Measured geochemical differences between the foundation clay beneath the dykes and the background clay were consistent with observed differences in soil behaviour.

This information leads to a conceptual model for the site that says seepage beneath the dykes is bringing gypsum into a state of dissolution. The leaching reduces cementation bonding and allows removal of the associated ions. Mass removal would likely be dominated by advection along horizontal silt and fine sand partings. Removal of ions associated with gypsum at the surfaces of the preferential flow paths would set up concentration gradients and result in diffusion of calcium and sulphate from the clay matrix into the preferential flow paths. The geochemical changes result in mechanical changes, after approximately one pore volume of flow, that are sufficient to result in instability of the embankments.

The next step in the project was to examine this conceptual model and build this new understanding into the numerical modelling that was initiated by Garinger (2002).

The conceptual model, suggests that there are a number of processes that influence the foundation performance at Seven Sisters. These include groundwater movement, geochemical reactions and subsequent geomechanical changes. Mitchell (1993) provides a detailed list of coupled processes that can occur in clay soils (Table 6.1). We know these processes are coupled and several of them are likely active at the Seven Sisters site. Individually, these processes can be quite complex. When the processes are coupled, the complexity of the problem increases. Current modelling techniques and software for the most part are not capable of handling these processes concurrently. They must be decoupled and handled separately (Barbour and Krahn, 2004). Some solutions (thermo-hygro-mechanical, or THM, models) are available, but calibration of the required constitutive models is unclear. Useable chemo-hydo-mechanical (CHM) models are not available.

The approach used in this study was to reduce the problem into a number of separate models, each designed to be used sequentially to guide the subsequent model. The state of knowledge about the site is not at the point of being able to allow predictive modelling of slope instability. As such, the purpose of the modelling was to help understand the important mechanisms involved in the problem (Krahn, 2003). Following paragraphs outline the overall modelling approach, the software employed and the purpose of each step.

As mentioned in Chapters 3 and 4, the U.S. Geological Survey (USGS) PHREEQCi software for geochemical modelling was used to model the geochemistry of the foundation clay and its interaction with the forebay water. The purpose of this step was

to determine the amount of forebay water required to bring any of the potential cementing minerals into a state of dissolution within the foundation clay.

The next step was to take the information from the geochemical modelling and use it to identify zones beneath the dykes that have experienced sufficient mass transport for the dissolution reaction to occur. Groundwater flow and mass transport modelling was conducted using finite element programs SEEP/W and CTRAN/W developed by GeoSlope International Ltd. The models were used to identify the position of the advective front in relation to the geochemical modelling results. The combined purpose of the seepage and mass transport modelling was to examine possible scenarios that could have resulted in the observed geochemical changes beneath the dyke relative to background soil conditions. This was undertaken by conducting a sensitivity analysis of various hydraulic conditions.

The initial goal was to use the results of the mass transport model to guide the stress-deformation analysis by identifying where in the foundation clay changes may have occurred in the yield loci. However, as presented in the following sections, these models were treated as independent sensitivity analyses. The stress-deformation analysis was conducted using SIGMA/W, which is also a finite element program developed by GeoSlope International Ltd. Pore water pressures were obtained from steady-state seepage analysis using SEEP/W and directly input into the stress-deformation analysis. The purpose of the stress-deformation modelling was to incorporate a Modified Cam-Clay model for the upper foundation clay and examine potential yielding beneath the dykes. The size of the yield locus was varied to simulate a reduction due to chemical

changes. The calculated amounts of straining were used to justify reduction of strength of the upper foundation clay from peak, to post-peak, and then residual strength.

As mentioned, sequential seepage, stress-deformation and slope stability modelling was used to determine the factor of safety of the dykes. In order to remove the assumptions for interslice forces in the slope stability analysis, sequentially-coupled stress-deformation and seepage analysis were used as precursors to determining the factor of safety using the slope stability software. Slope stability modelling was done using SLOPE/W, another product created by GeoSlope International Ltd. A range of stress-deformation model results were input into the slope stability model to examine their effect on the factor of safety.

Each of the modelling packages mentioned above, must be used properly with the appropriate input parameters and boundary conditions. What can seem to be an insignificant error in setting up a model may lead to misleading results. It is also important to recognize the limitations of the software and the available data. The following sections provide a brief description of each software package, a discussion of any software or data limitations and the input parameters and boundary conditions used to set up each model. This is followed by the results obtained from the modelling packages.

6.1 Geochemical Modelling

Knowing the equilibrium solubility constant (K_{sp}) for a single mineral, it is a simple task to calculate the equilibrium distribution of dissolved species originating from that mineral in

contact with water (Section 2.3). However, when considering a number of minerals and their activity coefficients, the calculation becomes complex. In this case, the equilibrium equations for all of the species and their complexes being considered must be solved simultaneously. Geochemical modelling programs can be used to quickly determine the simultaneous solution of the equations for all of the species present.

The PHREEQCi program was used to model the Seven Sisters problem. PHREEQ is a geochemical modelling program that was originally developed by Parkhurst and Appelo (1990) for the USGS. The interactive version was later developed by Charlton and Parkurst (2002). PHREEQ stands for pH (PH), redox (RE), equilibrium (EQ). The C stands for the language the program was written in and the i stands for the interactive version. The code is capable of calculating the distribution of aqueous species (speciation) coupled with one-dimensional transport. The speciation calculations use the chemical analysis of a water sample to calculate the distribution of aqueous species. The most useful results of the speciation calculations are the saturation indices (SI) for various minerals. The saturation indices indicate whether a given mineral is in a saturated state (mineral precipitation), a state of dissolution, or at equilibrium (Section 2.3).

The obvious advantage of using a geochemical model for the Seven Sisters problem is the ability of such models to simulate chemical interaction of the original pore fluid beneath the dykes with the forebay water. PHREEQ's ability to handle chemical reactions is superior to that available with more complex coupled flow and transport models that can handle 2D and 3D problems. The main disadvantage of current geochemical modelling programs is that only 1D transport can be modelled. Therefore, PHREEQ was used to compare the progress of the dissolution reactions for several potential cementing minerals present in

the clay to the position of the advective front in 1D. The results could then be used in combination with a mass transport model (CTRAN/W) capable of handling the geometry of the Seven Sisters problem.

Given the strengths and limitations of the geochemical modelling software, the objective of the geochemical model was to estimate the number of pore volumes of forebay water that would be required to bring any of the potential cementing minerals into a state of dissolution.

6.1.1 Input Parameters and Boundary Conditions

Table 6.2 shows a summary of input parameters for the geochemical model. The geochemical model was set up to simulate the flow of forebay water through a 20 m long (horizontal) column of the upper foundation clay below the centre of the dyke. The column was discretized into 10 cells. The groundwater velocity was indirectly input into the software by specifying the residence time in each cell. Residence time steps were calculated using a head drop of 3.5 m over the length of the column, a porosity of 60% and a range of values of hydraulic conductivity from $2x10^{-9}$ m/s to $2x10^{-7}$ m/s. In order to simulate the passing of 10 pore volumes of forebay water through the column, 100 shifts (time steps) were specified. The boundary conditions at each end of the column were specified as flux boundaries.

Dispersivity (α) values were assumed and subjected to a sensitivity analysis. Simulations were run with no dispersion ($\alpha = 0$), $\alpha = 2$ m, $\alpha = 10$ m and $\alpha = 20$ m (Walton, 1988). The

diffusion coefficient was also assumed and set at a value of 2×10^{-10} m^2/s (Fetter, 1999) for all cases except the run that excluded diffusion and mechanical dispersion.

The initial geochemical conditions in the column were obtained from the results of the geochemical analyses conducted on pore fluid samples from the background location. The chemistry of the forebay water was specified as the permeating fluid. The geochemical data for the initial conditions and the permeating fluid are listed in Table 4.3.

6.1.2 Geochemical Modelling Results

The geochemical modelling was completed early in this program of study and used to guide the experimental design (Chapter 3). Results of the geochemical modelling were presented in Figure 3.1. This figure shows the removal of sulphate, calcium and sodium as the column is permeated with forebay water. Figure 4.2 shows the same modelling results compared to the sulphate concentrations of each of the tested clays. These figures indicate a significant drop (approximately 60% removal) in sulphate concentration after only one pore volume of forebay water has passed through the column. The geochemistry of the natural unstable location plots close to the one pore volume mark on the modelled curve.

Figure 6.1 shows the saturation indices for a number of potential cementing minerals as 10 pore volumes are passed through the column. The curves indicate that potential cementing minerals include calcite, aragonite, dolomite and gypsum. These minerals shift to a state of dissolution after approximately 0.5 to 1.5 pore volumes of forebay water are passed through the column. Although gypsum was the first to shift to a state

of dissolution, it was identified as the major contributor to cementation in the Seven Sisters clay based on having the highest total concentrations by over two orders of magnitude. (In terms of molality, approximately 2.5 orders of magnitude more $CaSO_4$ was present in the soil than $CaCO_3$.) Further, the soil profile was saturated with respect to calcite at the stable, unstable and background sections of the Seven Sisters site (Figure 1.12). In contrast, the clay beneath the dykes was under-saturated with respect to gypsum, while the background section was super-saturated with respect to gypsum (Figure 1.11). Gypsum was the only mineral that displayed a flip from super-saturated conditions in the background soil, to under-saturated conditions beneath the dykes.

Figure 6.2 compares the individual saturation indices for each of the tested clays to the modelled results for gypsum. The clay from the background location and the clay reconstituted with gypsum rich water both plotted on the super-saturated portion of the curve. The reconstituted clay that was washed with one pore volume of DI water plotted just below equilibrium. Both the clay from the unstable section and the reconstituted clay that was washed with six pore volumes of DI water plotted on the under-saturated portion of the curve, at approximately 1.3 and 2.2 pore volumes, respectively. As will be discussed in Section 6.2, the passing of one pore volume of forebay water beneath the dykes is conceivable. The observation that the reconstituted clay that was washed with six pore volumes of DI water plotted at 2.2 pore volumes suggests incomplete contact in the mixing/leaching chamber.

The number of pore volumes at which gypsum passes from a state of super-saturation to dissolution depends on the dispersivity of the soil. Since the dispersion characteristics of the site were unknown, a sensitivity analysis was conducted by varying the value of

the dispersivity coefficient (α). The lower diagram of Figure 6.2 shows the results of the sensitivity analysis. The analysis indicates that gypsum in the foundation clays would be in a state of dissolution after approximately 0.5 to 1 pore volume of reservoir water had passed through the clay. The laboratory testing program showed that mechanical differences occurred shortly after an equivalent of approximately one pore volume of water was passed through the soil. Also, the gypsum saturation index for the unstable section plots at approximately one pore volume on the modelled curve.

Based on this information, the one pore volume point was selected as a representative point at which leaching produces geochemical changes sufficient to reduce the yield locus. Selecting this point also produces some conveniences for the 2D mass transport model. The 2D mass transport model only has to identify the position of the advective front with less importance placed on the dispersion coefficient.

The results were not sensitive to the amount of residence time in each cell. This indicates that the dissolution kinetics are 'instantaneous' relative to the groundwater velocity. Therefore, hydraulic conductivity was not a factor in this analysis. This is consistent with Table 2.2, which indicates that the dissolution rate of sulphate minerals is controlled by transport (Appelo and Postma, 1996).

6.2 Seepage and Mass Transport Modelling

The purpose of the seepage and mass transport modelling was to investigate where in the foundation clay the constitutive behaviour might have changed due to the loss of gypsum cementation. Based on the results of the geochemical modelling, this requires the model

to identify where approximately one pore volume of forebay water has passed through the foundation clay.

The SEEP/W and CTRAN/W programs were used to model seepage and mass transport at the Seven Sisters site. SEEP/W uses the finite element method to solve the partial differential equation that describes groundwater flow. The partial differential equation is based on Darcy's Law:

$$q = -K\frac{\partial h}{\partial l} \qquad [6.1]$$

where q is specific discharge, K is hydraulic conductivity, h is total head and l is distance. Darcy's Law applies to groundwater flow through saturated and unsaturated soils with appropriate values of hydraulic conductivity depending on the degree of saturation.

The two dimensional form of the governing partial differential equation describing groundwater flow is as follows:

$$\frac{\partial}{\partial x}\left(K_x\frac{\partial h}{\partial x}\right)+\frac{\partial}{\partial y}\left(K_y\frac{\partial h}{\partial y}\right)+Q=\frac{\partial \Theta}{\partial t} \qquad [6.2]$$

In this equation, K_x is hydraulic conductivity in the horizontal (x) direction, K_y is hydraulic conductivity in the vertical (y) direction, Q is the applied boundary flux, Θ is the volumetric

water content and t is time (Krahn, 2004a). The first two terms describe the flow through an element of soil in the x and y directions, respectively. The equation says that the amount of flow into or out of an element of soil at a given time is equal to the change in volumetric water content. For steady state flow, there is no change in volumetric water content with time and the right hand side of Equation 6.2 becomes zero.

The groundwater velocity field calculated by SEEP/W is taken as input by CTRAN/W to solve the advection-dispersion equation using the finite element method. The one dimensional form of the governing partial differential equation (for an element of length ∂x) describing mass transport is as follows:

$$\frac{\partial C}{\partial t} = D\frac{\partial^2 C}{\partial x^2} - v\frac{\partial C}{\partial x} \qquad [6.3]$$

where C is concentration, t is time, D is the dispersion coefficient and v is the average linear velocity (Krahn, 2004b). The dispersion coefficient combines the processes of mechanical dispersion with molecular diffusion which both serve to move mass ahead of the advective front and into adjacent flow tubes. Mechanical dispersion is defined by the dispersivity of the porous media multiplied by the average linear velocity. The sum of mechanical dispersion and the molecular diffusion coefficient, D*, is the hydrodynamic coefficient of dispersion, D, with units of L^2/T. Since adsorption and decay were not being considered for the Seven Sisters problem, their terms have not been included in Equation 6.3.

SEEP/W and CTRAN/W are suitable programs for modelling seepage and mass transport beneath an earth fill dam, respectively. Limitations in modelling such problems arise primarily from the lack of field data rather than the ability of the software to handle the relevant processes. For example, data for hydraulic conductivity, which is perhaps the most important parameter in seepage and mass transport modelling, are often limited. The solution to a mass transport problem is only as good as the input data and will be inherently non-unique. Engineering judgement is required to make appropriate assumptions regarding un-characterized parameters and to scrutinize the subsequent output.

Other data limitations that make modelling the Seven Sisters site difficult include the lack of spatial and temporal chemistry data. Limited spatial information precludes the evaluation of natural heterogeneity versus the anomalies that have been caused by the groundwater and chemistry conditions at the site. The lack of temporal data precludes model calibration and the dispersion characteristics are unknown. As for the geochemical modelling presented earlier, values for similar materials available in the literature had to be used. Changes in dispersion will change concentrations in front of and behind the advective front, but it will not change its position. This is an additional convenience of the dissolution reaction being complete at the advective front, where an accurate dispersivity estimate becomes less important.

CTRAN/W does not handle geochemical changes as well as a geochemical modelling program such as PHREEQCi. However, the geochemical modelling indicated that only the position of the advective front is required from a 2D mass transport model. That is, the objective of the seepage and mass transport modelling was to identify the soil

through which approximately one pore volume of forebay water pass over the past 70 years. CTRAN/W is well suited to do this. The laboratory testing program indicated that reductions in the yield locus could be expected after one pore volume of forebay water had passed through the foundation clay. It was anticipated that results of the mass transport analysis could potentially provide insight for setting up the stress-deformation model.

6.2.1 Input Parameters and Boundary Conditions

Garinger (2002) established a steady state seepage model for the site. The geometry of the problem was determined from construction drawings of the dyke and the results of material testing that identified the various zones of dyke and foundation materials (Garinger, 2002; Chapter 1). The model was calibrated to historical vibrating wire piezometer data from instruments located near each section by adjusting infiltration through the crest of the embankment. Hydraulic parameters were obtained from the results of flexible wall hydraulic conductivity tests on intact specimens from intact Shelby tube samples. Table 6.3 presents a summary of parameters selected for the seepage and mass transport models.

The hydraulic conductivity testing undertaken by Garinger (2002) was done over a range of pressures and was also conducted with flow perpendicular to the horizontal laminations and parallel with the laminations. Only small variations in hydraulic conductivity were observed in the vertical and horizontal hydraulic conductivity of the foundation over a range of pressures representative of in situ conditions beneath the dykes. For the unstable section, the hydraulic conductivity was slightly higher in the

horizontal direction (that is, parallel with the laminations) than in the vertical direction with an average K_y/K_x ratio of 0.5. For the stable section, the hydraulic conductivity was slightly higher in the vertical direction than in the horizontal direction, with an average K_y/K_x ratio of 1.6. The base model created by Garinger utilized a K_y/K_x ratio of 1.0. Garinger (2002) noted that the effect of the K_y/K_x ratio on the factor of safety was small in terms of any differences in pore water pressures. The test results suggest there has been more seepage, and therefore more leaching at the unstable section than at the stable section.

Saturated hydraulic conductivities were used for all materials in the model except for the dyke fill material. To account for unsaturated conditions within the upper portions of the dykes, an unsaturated conductivity function obtained from SoilVision Systems Ltd. was input into the model. The function is provided in Figure 6.3.

Input requirements for the mass transport model included groundwater velocities within the domain, and dispersivities of the various materials in the model. Groundwater velocities calculated by the seepage model were used as input for the mass transport model. An assumed dispersivity of 10 m was used for the various soil types in the model. Since the dissolution reaction for gypsum can be considered instantaneous upon arrival of the advective front, the effects of sorption and decay were not required in the model.

For the seepage model, the boundary condition on the forebay side of the dykes was set with a hydraulic head of 274.25 m. This value was based on historical records and remains relatively constant. The boundary condition on the dry side of the dykes was

set with a hydraulic head of 270 m, which coincides with the elevation of the ground surface and a sand drain at the toe of the embankment. The boundary conditions were applied to the clay core rather than the rip-rap shell. The shell was not considered relevant to the seepage and mass transport models due to its much higher hydraulic conductivity which would not significantly affect flow and pore water pressure distribution.

The mass transport model considered a constant concentration source along the forebay side of the dykes. Knowing the results of the geochemical model, the purpose of the mass transport model was only to identify the position of the advective front of the forebay water (that is, $C/C_0 = 0.5$). It is at this point that one pore volume of forebay water has passed through an element of the foundation clay and gypsum is brought to a state of dissolution. The upstream boundary condition was set at $C/C_0 = 1.0 \times 100\%$, representing 100% forebay water. The initial conditions within the domain were $C/C_0 = 0$.

6.2.2 Seepage and Mass Transport Modelling Results

Using the same homogeneous hydraulic parameters and boundary conditions as Garinger (2002), the initial transport simulation indicated that the advective front would have only penetrated on the order of 1 m into the dyke and foundation after approximately 70 years (Figure 6.4). This suggests that either the bulk hydraulic conductivity of the formation used in the model was incorrect or there is natural variability in gypsum concentrations in the upper foundation clay. Assuming that the observed differences in chemistry were the result of leaching, the advective front must

have passed beneath the dyke. On the other hand, the observed differences in gypsum distribution may be due to field scale heterogeneities and groundwater flow did not cause the observed differences between the geochemistry at the background section relative to the geochemistry beneath the dykes. Both scenarios are possible and they both may contribute. There is insufficient data to distinguish these issues except for some unpublished geophysical survey results. Geophysical surveying of the dykes using electromagnetic techniques (EM-31) suggested that there is in fact an anomaly with low electrical conductivity associated with the dykes (J. Hayles, Pers. Comm., 2002). This implies that the presence of the dykes caused the anomaly rather than natural variability. Further (3D) characterization of geochemical conditions at the site is required at both the dykes and in background areas to determine the natural variability of gypsum distribution and to better define any anomalies beneath the dyke.

The amount of seepage that passes beneath the dykes is controlled by hydraulic conductivity. The base model utilized the results of hydraulic conductivity test on laboratory specimens. These may not reflect the in situ hydraulic conductivity of the formation which, due to fractures, fissures, sand and silt partings, may be up to several order of magnitudes higher than what is measured in the laboratory. Research conducted on the hydraulic conductivity of Lake Agassiz clays near the Seven Sisters site (Day, 1977; Pach, 1994) indicated that the bulk field scale hydraulic conductivity is on the order of two to three orders of magnitude higher than what is typically measured in the laboratory on the same clay. Both vertical fissures and horizontal silt and fine sand partings have been observed at the site. Therefore the in situ hydraulic conductivity is therefore likely higher than what was measured in laboratory specimens.

Given the discrepancy between laboratory and field hydraulic conductivities, the best option, given the available information, was to evaluate a number of scenarios that may help explain the observed geochemical differences at the site. This was undertaken by conducting a sensitivity analysis on hydraulic conductivity of the foundation clay and the dyke fill material. Hydraulic conductivity was increased up to 3.5 orders of magnitude to be consistent with the research comparing laboratory tests on small intact laboratory specimens to field tests by Day (1977) and Pach (1994). Anisotropy and the effects of any high permeability zones such as fine sand and silt lenses were also considered. The following summarizes the findings of the analysis. All mass transport simulations were for a 70 year life span.

Figures 6.5 and 6.6 show the effects of increasing hydraulic conductivity of the foundation clays by 3 and 3.5 orders of magnitude, respectively, from the base model. These results indicate that if the hydraulic conductivity is increased by 3.5 orders of magnitude, the advective front only reaches as far as the centre line of the dyke after approximately 70 years. Even if the hydraulic conductivity of homogeneous, intact foundation clay was three orders of magnitude higher than what is measured in the laboratory, the advective front would not have reached the dry side of the dykes where the instabilities were observed.

Figures 6.7, 6.8 and 6.9 show the effects of anisotropy K_x/K_y on mass transport. In these simulations, the horizontal hydraulic conductivity was not allowed to be greater than 3.5 orders of magnitude greater than the values determined by laboratory testing. As expected, lowering the hydraulic conductivity in the vertical direction resulted in a narrower plume of forebay water. Lower vertical hydraulic conductivities reduced

vertical penetration and ultimately reduced lateral migration of the advective front. These cases were therefore not critical compared to the isotropic simulations.

Figure 6.10 shows the effects of increasing the hydraulic conductivity of the dyke fill material and the foundation clay by 3.5 orders of magnitude. As expected, the result of increasing the hydraulic conductivity of the dyke was to concentrate flow through the dyke with less flow through the foundation materials. Increasing anisotropy of the dyke and fill materials slightly increased the amount of flow through the foundation (Figure 6.11). However, neither of these scenarios appear to be responsible for the changes in chemistry at the centre line of the dykes.

The final case evaluated the effects of a preferential flow path beneath the dyke. In this case, advective mass transport will dominate in the layer with higher conductivity and diffusion will dominate in the layer with lower conductivity. This was modelled by including a 0.1 m thick more pervious seam through the upper foundation with a hydraulic conductivity of $1x10^{-5}$ m/s (This conductivity can be considered to represent a silty or clayey sand layer). Although a seam this thick may not be representative of field conditions, it is conceivable that 100 sand laminations that are 1 mm thick exist in the foundation clay. (Modelling the 0.1 m seam was at the limits of the available computing power due to the fine mesh that was required.) The results of this simulation are shown in Figure 6.12. The results show that flow is concentrated through the seam as it passes beneath the dyke and the advective front passes though all of the overlying foundation material on the dry side of the dyke.

The seepage and mass transport analysis suggest that preferential horizontal flow paths are responsible for allowing sufficient groundwater flow to pass beneath the dykes to account for the observed geochemical conditions beneath the dykes. These preferential flow paths could include horizontal laminations of higher permeability material, interconnected vertical fractures or fissures (both of these features have been observed in the field), and high hydraulic conductivity zones at the till-bedrock interface.

6.3 Stress and Deformation Modelling

The SIGMA/W program was used to model stress and deformation of the Seven Sister's problem. SIGMA/W is a finite element based program designed to perform stress and deformation analysis of earth structures such as embankments in two dimensions. For a two-dimensional plane strain problem, there are three basic strain components to be solved for. These include:

$$\varepsilon_x = \frac{\partial u}{\partial x} \qquad [6.4]$$

$$\varepsilon_y = \frac{\partial v}{\partial y} \qquad [6.5]$$

$$\gamma_{xy} = \frac{\partial u}{\partial y} + \frac{\partial v}{\partial x} \qquad [6.6]$$

where ε_x is longitudinal strain in the x-direction, ε_y is longitudinal strain in the y-direction, γ_{xy} is shear strain in the x,y plane and u and v are the displacement components in the x and y-directions, respectively.

The fundamental constitutive relationship used in the formulation of SIGMA/W that relates stresses and strains is a linear elastic model:

$$\{\sigma\} = [E]\{\varepsilon\} \qquad [6.7]$$

where the stress tensor, σ, is related to the strain tensor, ε, by a matrix, E, representing the stiffness of the material. For an isotropic linearly elastic material, the input parameters include Young's Modulus and Poisson's ratio, ν. If this constitutive model is chosen, the E, ν parameters are incorporated into the stress-strain relationship as follows:

$$\begin{Bmatrix} \sigma_x \\ \sigma_y \\ \sigma_z \\ \tau_{xy} \end{Bmatrix} = \frac{E}{(1+\nu)(1-2\nu)} \begin{bmatrix} 1-\nu & 0 & 0 & 0 \\ 0 & 1-\nu & 0 & 0 \\ 0 & 0 & 1-\nu & 0 \\ 0 & 0 & 0 & \frac{1-2\nu}{2} \end{bmatrix} \begin{Bmatrix} \varepsilon_x \\ \varepsilon_y \\ \varepsilon_z \\ \gamma_{xy} \end{Bmatrix} \qquad [6.8]$$

where σ_x, σ_y and σ_z are stresses in the x, y and z directions and τ_{xy} is the shear stress in the x-y plane (Krahn, 2004c).

Provided the linear isotropic elastic model is a reasonable assumption for a given project, Equation 6.8 can be used to calculate in situ stress in the soil prior to any engineering work. These results are then input as initial conditions for the stress-deformation model that simulates the applied loading. SIGMA/W allows the use of other constitutive relationships to modify the stress-strain relationship for the loading phase of a given problem. In previous stress-deformation modelling of the Seven Sisters site, Garinger (2002) employed (1) elastic, (2) elastic perfectly-plastic and (3) strain-softening constitutive models to define the upper foundation clay.

Since yielding and the effect of reduction in the size of the yield locus were of interest in this study, the Modified Cam-Clay model was employed to define the upper foundation clay. The Modified Cam-Clay model is considered a critical state model as well as an elastic, plastic-hardening model. The elastic and plastic hardening behaviour is defined by the slope of the isotropic unload-reload line, κ, and the slope of the isotropic normal consolidation line, λ, respectively. The vertical position of the κ,and λ lines on the volume axis is specified by, Γ, the specific volume of the critical state line when p' is 1.0 (Krahn, 2004c).

SIGMA/W establishes a yield locus for a given element by taking the in situ stresses, p'_0, q_0, for that element and positioning a Modified Cam-Clay ellipse around p'_0, q_0. (This assumes isotropic elasticity and elliptical yield loci. It is recognized that these assumptions differ from the laboratory results described in Chapters 4 and 5). The user specifies the OCR, K_0 (via ν) and M. This allows the maximum pressure experienced by a given element to be calculated using:

$\sigma'_{xmax} = \sigma'_{y0} \times K_0 \times OCR$ [6.8]

and

$\sigma'_{ymax} = \sigma'_{y0} \times OCR$ [6.9]

From σ'_{xmax} and σ'_{ymax}, p'_{max} and q_{max} are determined, giving a point on the yield locus. The isotropic preconsolidation pressure is then computed using the following equation:

$$p'_c = \frac{1}{M^2 p'_{max}} \left(q_{max}^2 + M^2 p_{max}^2 \right) \quad [6.10]$$

Knowing p'_c, an ellipse is drawn starting at the origin with its apex at the point on the critical state line corresponding to $p'_c/2$.

Using the Modified Cam-Clay model limits the analysis in that the model can not directly handle the anisotropy that was observed in the yield loci determined from the laboratory program. Therefore, a range of elliptical yield loci that match various portions of actual yield loci have to be examined. In order to match the top of the yield locus determined in the laboratory, an artificially high M value was required. The implications of this are that the post-peak stress state in the model will be higher than what was actually measured in the laboratory. Further, SIGMA/W is formulated for small strain cases and not for post failure deformation. The model can be expected to underestimate strain-softening behaviour, especially in the cemented clays at Seven Sisters.

Despite these limitations, SIGMA/W in combination with SEEP/W is high-end state-of-practice software used to analyse seepage and stress-deformation problems similar to the Seven Sisters problem. In this study, the stress-deformation model was used for two purposes: (1) to examine strains and yielding in the foundation clay as the dykes were constructed using a range of yield loci, and (2) to evaluate stresses that could be imported into the slope stability model as an alternative to assuming an interslice inclination function.

6.3.1 Input Parameters and Boundary Conditions

Table 6.4 lists the input parameters used for the stress-deformation modelling. With the exception of the upper foundation clay, all of the model layers were assigned the same constitutive models and parameters as used by Garinger (2002), to allow comparison of the results from the two programs. Garinger (2002) modelled the rip-rap as a linear elastic material; the dyke fill as an elastic perfectly-plastic material; the upper foundation clay as a strain-softening material; and the lower foundation clay as an elastic perfectly-plastic material. The parameters for these models were based on the triaxial testing conducted by Garinger (2002) and an assumed Poisson's ratio. For this study, the upper foundation clay was divided into two layers. The upper 1 m of this unit was considered a crust layer and was defined using a strain-softening model with the same parameters that Garinger (2002) used to define the upper foundation clay. The remainder of the upper foundation clay was defined using the Modified Cam-Clay model.

The 'base case' parameters for the Modified Cam-Clay model used an OCR of 2.5. This was based on oedometer results for the background section compared to the in situ stresses. A value of M = 1.5 was selected by matching the height of the Modified Cam-Clay elliptical yield locus to the anisotropic yield locus that was measured in this research for the background section (Figure 4.30 and 4.32). The anisotropic yield locus was scaled using the same p'_c determined for the Modified Cam-Clay yield locus with an OCR of 2.5. Since a perfect match between the elliptical yield loci and the anisotropic yield loci determined from the laboratory program was not possible, the stress-deformation modelling exercise involved conducting a sensitivity analysis on the size of the yield locus for the upper foundation clay. The assumed yield loci for the modelling were varied from (1) normally consolidated conditions (OCR = 1); (2) an approximate match to the inner yield locus of the unstable section (OCR = 2.3 and M = 1.1); and (3) an ellipse slightly larger than the outer yield locus (OCR = 3 and M = 1.33).

The stress-deformation modelling was staged as follows. The in situ stresses were first established as initial conditions prior to construction of the dykes. Two stages were used to simulate the construction of the first set of dykes in 1929. This was followed by another two stages to simulate raising of the dykes between 1947 and 1949. The stress state at the end of the fourth stage was subsequently used as stress state conditions for the slope stability analysis.

Boundary conditions for the in situ model were specified as fixed along the bottom of the model. Along the two edge boundaries, boundary conditions permitted vertical displacements but no lateral displacements (rollers). For the subsequent models involving loading, the base and both side boundaries were specified as fixed.

6.3.2 Stress and Deformation Modelling Results

Figures 6.13 and 6.14 show the zones that yielded (shaded) in the stable and unstable sections models, respectively. The first two diagrams represent the construction of the first dyke at the site. The subsequent diagrams represent raising of the dykes in two increments. Note that some degree of yielding was identified for all four of the fill increments. These figures show that relatively more yielding occurred in the upper foundation clay at the unstable section. This is especially evident at the third fill step when the dykes were being raised. If the yield loci are reduced to simulate the effects of chemistry, increased areas of yielding are observed at both the stable and unstable sections (Figures 6.15 and 6.16).

The modelling results suggest that heightening of the dykes in the late 1940's produced localized maximum shear strains of the order of 10% directly beneath the centre line of the dyke at both sections. Average shear strains in the upper foundation clay ranged from approximately 2% to 10%. When these values are compared with the triaxial tests for the background section, it appears that heightening of the dykes could have easily produced enough shear straining to cause significant strain-softening in portions of the upper foundation clay. This result has been used by the author to justify selecting post-peak strengths, or even residual strengths in the slope stability modelling presented in the next section.

Figures 6.17 and 6.18 show the Modified Cam-Clay yield loci used in the modelling compared with the anisotropic yield loci determined from the laboratory testing program for the stable and unstable sections, respectively. Each figure includes plots for four

points along the failure surface (points 1 to 4, with point 1 being at the toe and point 4 being closest to the centre line of the dyke) and one beneath the centre line of the dyke (point 5). The anisotropic yield locus was scaled using the same p'_c used to draw the Modified Cam-Clay ellipse for the base case. Larger and smaller Modified Cam-Clay yield loci are also shown to provide a range of possible conditions in a sensitivity study. The expanded Modified Cam-Clay yield locus was selected as the outer bound of the anisotropic yield locus and the reduced Modified Cam-Clay yield locus was fitted to the anisotropic inner yield locus. Stress paths determined from the models using both Modified Cam-Clay and strain-softening constitutive models are shown for comparison. The plots show that the stress state at the toe of the embankments (point 1) remains in the elastic region for all of the construction stages at both sections. At point 2, which is the lowest point on the failure surface, the stable section generally remained within the elastic region while the unstable section was observed to plot closer to the outer yield locus. At points 3 and 4, both sections were observed to yield due to the construction of the initial dyke. However, yielding at the unstable section generally occurred at one stage earlier than the stable section. Yielding occurred immediately after construction of the first lift at the centre line of the dyke for both sections (point 5).

There are some important implications of the stress paths for the locations where yielding occurred (i.e. points 3, 4 and 5). The upper foundation material near these points yielded as the dyke was initially constructed (1929) and then raised (1947). The stress paths for these points indicate significant volumetric straining relative to shear straining. This indicates that excess pore water pressures would be generated in these areas, with settlement occurring as the excess pore water pressures dissipated. All of these points were located near the centre of the dyke, toward the dry side. This general

area coincides with the field observation of 'slumping' at the unstable section. It will be remembered that the owner reported a failure mechanism of slumping and settlement.

The stress paths shown in Figures 6.17 and 6.18 are for 'steady-state' drained conditions with no shear-generated excess pore water pressures. The ability to dissipate the excess pore water pressure depends on the relationship between plastic volumetric straining and hydraulic conductivity. If drainage is allowed, settlements will stop. If drainage is relatively inhibited, on-going settlements, shear straining, and perhaps a switch to undrained shearing can be expected. In this case, pore water pressures would increase faster than they could be dissipated. (This situation would be aggravated by significant strain-softening such as that seen in Figures 1.2 and 5.13.) The last two increments of construction, representing raising of the dykes, would have initially increased the pore water pressures at these points by at least an amount equivalent to the additional mean effective stress ($\Delta u = \Delta p$) if the loading was rapid enough that no drainage took place. This would reduce the factor of safety and will be examined in the following chapter as a separate scenario of the slope stability modelling. There are two conditions that would generate excess pore water pressures: (1) raising the dykes, since the upper foundation clay was normally consolidated after construction of the first dyke, and (2) reduction of the size of the yield locus associated with chemical changes therefore producing yielding in a larger portion of the upper foundation clay over the long term.

Good agreement was generally observed between the stress paths developed using Modified Cam-Clay (Figures 6.17 and 6.18) and the author's re-plotting of Garinger's (2004) strain-softening stress calculations. However, the stress paths produced by the

strain-softening model plotted slightly higher (produced more shear stress) than the Modified Cam-Clay model. This is due to strain-softening being handled better by the strain-softening model than the Modified Cam-Clay model. (Modified Cam-Clay is recognized as not being capable of handling strain-softening well.) However, the Modified Cam-Clay model provides a better representation of the yielding, which was significant in this project and was used to guide slope stability modelling shown in the following section.

Three significant outcomes from the stress-deformation modelling have implications for slope stability modelling. One, more yielding was observed at the unstable section than at the stable section. Two, reducing the size of the yield locus increases size of the yielded zone. These first two observations imply that chemistry, in addition to the usually considered conditions of the geometry of the problem and the properties of the soil layers, could be responsible for the instability at the unstable section. Three, yielding (either by short term construction loading or longer term chemically induced softening) likely generated excess pore water pressures through strain-softening that would have affected stability. The slope stability modelling presented in the following section further examines these outcomes.

6.4 Slope Stability Modelling

The purpose of the slope stability modelling was to investigate if changes in constitutive behaviour due to straining or chemical changes were sufficient to identify instability at the unstable section while the stable section remains stable. This was done by varying the size of the Modified Cam-Clay yield locus and by varying the strength of the upper

foundation clay. Secondly, the modelling investigated the potential effects of any yielding-induced excess pore water pressures on the factor of safety. (This latter mechanism will be explored in more detail in Chapter 7.)

The preceding section described modelling that was done using SIGMA/W to examine the stress states beneath the dyke and to identify areas that may have yielded in the upper foundation clay. However, the stress-deformation analysis could not determine the overall factor of safety of the dykes. To do this, a limit equilibrium analysis is required. SLOPE/W compares the maximum resisting shear strength to the global average mobilized shear resistance along a specified failure surface to determine a factor of safety. Although this is an effective method for determining the factor of safety, the position of the failure surface may not necessarily be correct. A series of potential failure surfaces needs to be examined to determine the failure surface with the lowest factor of safety.

To calculate the factor of safety SLOPE/W uses the General Limit Equilibrium method, (Bishop and Morgenstern, 1960) which is based on the statics of a series of vertical slices above the failure surface. The forces acting on a slice include the normal force, P, acting at the base of each slice which is determined by the summation of forces in the vertical direction, and the interslice normal force, E, which is determined by summation of forces in the horizontal direction for each slice. The factor of safety can be based on moment or horizontal force equilibrium. Without assuming the direction of the resultant interslice forces, the problem is indeterminate. The interslice force assumption can be handled in several ways including: (1) the 'Ordinary' method, which assumes the interslice forces are parallel to the base of the slice, (2) the Bishop method, which

considers normal forces between slices, but not shear forces, and (3) the Morgenstern-Price method, which uses an interslice force function. The Ordinary and Bishop methods only satisfy moment equilibrium while the Morgenstern-Price method satisfies both force and moment equilibrium (Graham, 1984).

The Geoslope suite of modelling programs allows an alternate method for determining the factor of safety (or stability factor), where stresses calculated by SIGMA/W are used to eliminate the need to assume the interslice forces. SIGMA/W determines the normal stress, σ_n, and shear stress mobilized, τ_m, at the base and centre of each slice using the following equations:

$$\sigma_n = \frac{\sigma_x + \sigma_y}{2} + \frac{\sigma_x - \sigma_y}{2}\cos 2\theta + \tau_{xy}\sin 2\theta \qquad [6.11]$$

$$\tau_m = \tau_{xy}\cos 2\theta - \frac{\sigma_x - \sigma_y}{2}\sin 2\theta \qquad [6.12]$$

where σ_x is the total stress in the x-direction at the centre of the slice base, σ_y is the total stress in the y-direction at the centre of the slice base, τ_{xy} is the shear stress at the centre of the slice base, and θ is the angle measured from the positive x-axis to the normal stress vector. The stability factor can then be calculated from the global average value of the ratio of the available maximum shear strength to the mobilized shearing resistance that is mobilized along the failure surface (Krahn, 2004d).

This method has several advantages over traditional limit equilibrium methods. The need for an interslice force assumption is eliminated; there are no iterative convergence problems since the approach is deterministic; the ground stresses are closer to the actual field conditions; and there is indirect consideration for stress concentrations and arching within the soil (Krahn, 2004d). However, care must still be taken to select an appropriate constitutive model and associated parameters in the stress-deformation analysis in SIGMA/W.

The modelling conducted by Garinger (2002) for the Seven Sisters site used both the Morgenstern-Price generalized limit equilibrium solution and the stresses generated from stress-deformation analysis. (It will be remembered that from Chapter 1, that Garinger's (2004) work could identify conditions under which the stable and unstable sections would both fail. It could not identify the conditions under which a previously stable section would unexpectedly fail.) Good agreement was achieved between the two methods of computing factors of safety. The purpose of the author's study was to evaluate the influence of yielding on slope stability. As such, only the method based on stresses determined by the stress-deformation modelling was used.

The objective of the slope stability analyses was to evaluate safety factors at the two sections of interest, with the upper foundation clay being defined using the Modified Cam-Clay model while varying the size of the yield locus. Next, the amount of straining modelled beneath the dykes justified varying the strengths of the upper foundation clay to post-peak or even residual strengths. This chapter uses pore water pressures obtained from steady-state (fully drained) seepage calculations. The next chapter will examine the effect of additional excess pore water pressures that would have been

produced following yielding and strain-softening, either by construction loading or chemically induced yielding.

6.4.1 Input Parameters

Consistent finite element meshes were used for the seepage, stress-deformation and slope stability modelling. Pore water pressures were imported from steady state SEEP/W analysis with a full reservoir (Forebay elevation 274.25 m). Stress states determined using a range of yield loci were imported into SLOPE/W to determine the factor of safety for each scenario. Circular failure surfaces were specified using a grid of rotational centre points and several tangent lines to define the radius of the failure surface. Separate studies performed by the author (Garinger et al, 2004) indicated only small differences between factors of safety calculated using circular and non-circular surfaces.

Table 6.5 summarizes the input parameters for the slope stability modelling. The factor of safety was determined for each case using both post-peak and residual strength in the upper foundation clay. Post-peak strengths of 14° and 13° were used for the stable and unstable sections, respectively. These values were determined from the triaxial testing conducted by Garinger (2002). A residual strength of 9° was used for both sections. This value was determined from direct shear testing conducted by Garinger (2002). A small cohesion of 5 kPa was included in both cases to provide an approximation to the curvature of the failure envelope in smectite clays. An additional scenario was examined that used two different strengths in the upper foundation clay:

residual strength where the stress-deformation analysis indicated yielding and post-peak strength in the remainder of the layer.

Parameters for the rip-rap shell were the same as those used by Rivard and Lu (1978) for the Seven Sisters site, with a $\Phi' = 35°$ and no cohesion. The strength parameter Φ^b, which defines the increase in shear strength with suction, was assumed to be 12° for the dyke material. A sensitivity analysis conducted by Garinger (2002) indicated that uncertainties in the definition of Φ^b had little effect on the factor of safety. The dyke and lower foundation materials were modelled using peak strength parameters similar to those used by Rivard and Lu (1978); $c' = 20$ kPa and $\Phi' = 23°$ for the dyke, and $c' = 20$ kPa and $\Phi' = 24°$ for the lower foundation clay.

6.4.2 Results of Analysis

Table 6.6 presents the results of the slope stability modelling using a range of yield loci in the upper foundation clay to evaluate the interslice force distributions. Figures 6.19 and 6.20 show the base case results for the stable and unstable sections, respectively. The results show factors of safety of approximately 1.19 at the stable section and 1.07 at the unstable section if post-peak strengths are used for the upper foundation clay. The conclusion is that if post-peak strengths were operating, both sections should be stable though the unstable section would be experiencing larger amounts of straining. If residual strengths are used for the upper foundation clay, the factors of safety for both sections are close to 1.00. This suggests that if residual strengths were operating, both sections would be unstable. These results are consistent with the results obtained by Garinger (2002).

Introducing the Modified Cam-Clay model into the problem further distinguished the unstable and stable sections. Incorporating the Modified Cam-Clay model for the definition of the upper foundation clay in the unstable section resulted in a lower factor of safety than was determined previously by Garinger (2002) (FS = 1.07). Garinger (2002) reported a factor of safety of 1.15 for the unstable section and 1.22 for the stable section while using post-peak strengths. These values were closely reproduced in this program by using a strain-softening model in the upper foundation clay (Table 6.6). The lower factor of safety obtained using the Modified Cam-Clay model implies that geometry and properties contribute to the differences between the stable and unstable sections. The upper foundation clay thickness was approximately 3.5 m at the stable section and approximately 5.0 m at the unstable section. The greater thickness of the upper foundation clay at the unstable section resulted in more settlement beneath the center-line of the dyke.

Changing the size of the yield locus in the SIGMA/W analysis (that feeds the stress state into the SLOPE/W model) did not change the slope stability modelling results. This is because only the stress state was passed between the two models and this only affects the interslice forces, which have a secondary effect on factor of safety in this application. The final stress state after the last fill increment is similar regardless of when the soil yielded. Therefore the model does not reflect the change in strength that yielding and plastic straining could have caused.

In an attempt to model areas in the upper foundation clay that may have experienced a reduction in strength due to construction-induced plastic straining, results from the stress-deformation modelling were used to identify areas where lower strengths could justifiably be assigned in the slope stability model. Recall that the stress-deformation analysis indicated that sufficient strains were induced in the upper foundation clay to mobilize post-peak or even residual strength in some areas. The areas that were shown to yield in the stress-deformation analysis are the most likely to have experienced this reduction in strength. The delineation of yielded areas could therefore be used to reduce the strength in those areas for the slope stability modelling. This approach was used to determine if this mechanism could have caused instability shortly after construction or after chemically induced yielding over the long term. Areas that where identified to have yielded in the stress-deformation analysis were assigned residual strength parameters and the remainder of the layer was assigned post-peak strength.

The results in Table 6.6 indicate that the stability factor is reduced closer to unity (1.07) for the stable section, but not to a condition of failure for this scenario. An example of these results is shown in Figure 6.21. In contrast, for the unstable section, the stability factor was reduced to below unity (0.94) indicating that if this was the mechanism of failure, the slope would likely have failed shortly after construction. This analysis was done with most of the foundation clay having post-peak strength and only the yielded areas in the cross-section being reduced to residual strength.

However, short term yielding caused by the dyke loading did not immediately cause instability at the unstable section. Failure at this section took place many years after construction. It appears that some other time-dependent factor was involved that would

promote the drop in strength from post-peak to residual in a larger portion of the upper foundation clay than what can be accounted for by yielding due to construction. Knowing that this section remained stable for approximately 45 years supports the hypothesis of softening through changes in geochemistry and that this controlled stability at the site over the long term.

Changing the size of the yield locus in SIGMA/W did not completely capture the potential effects of yielding (due to construction loading or chemical factors) on the stability of the embankments. This chapter has spoken about straining that could lower the available strengths from peak to residual, though such reductions might be larger than could reasonably be expected. Another mechanism, or rather two related mechanisms may be possible, and to the author's knowledge have not been examined before. Seepage beneath the dykes causes reduction of the size of the yield loci, but also, importantly, reduction in the strains needed to initiate these reductions (Figure 5.4). The reductions are very abrupt and occur with small strains (high values of the strain-softening rate (Table 1.2)). It is likely therefore that sudden localized destructuring would be accompanied by increases in pore water pressure. This could, as a 'worst case' produce a transition from the steady state (drained) pore water pressures used previously in this chapter, to higher (undrained) pore water pressures, and result in lower factors of safety. This possibility will be discussed in more detail in Chapter 7.

7.0 Synthesis and Discussion

Up to this point, this document has separately presented the results of the laboratory testing program and, using the resulting elastic-plastic model developed for the upper foundation clay at the Seven Sisters site, presented the results of a number of modelling scenarios aimed at exploring various mechanisms involved in the problem. The following section synthesises the results of both programs into a single picture for the site. The subsequent section discusses the strengths and weaknesses of the overall research program. This leads to a number of conclusions and recommendations for future research, which are presented in Chapter 8.

7.1 Testing and Modelling Programs

The laboratory testing program provided several important results for consideration in the modelling exercise. Namely, leaching of gypsum cementation was shown to reduce the size of the yield locus, reduce the amount of strain required for strain-softening to occur and develop a shear plane and lower peak strengths. The goal of the modelling was to incorporate this knowledge to advance the modelling of the site. Specifically, the Modified Cam-Clay constitutive model was incorporated, but adjusted in such a way that the effects of chemical changes in the foundation soil were included in an appropriate way.

Incorporation of this model provided a better definition of how the clay was behaving beneath the dykes. Evidence of yielding beneath the dykes was observed in the laboratory testing results as indicated by relatively lower specific volumes in the natural specimens (Figures 4.30 and 4.32). Based on the stress-deformation modelling, larger

areas of clay that had yielded due to loading from construction of the dykes were observed beneath the (2D) unstable section than beneath the stable section. This appears to be the result of the upper foundation clay being thicker at the unstable section. When the size of the yield locus was reduced to reflect the effects of leaching, the area of yielded clay beneath the dykes increased at both sections. The importance of this observation is that any chemically induced reductions in the size of the yield locus will promote yielding, straining and strain-softening to post-peak shearing resistance. With this insight, two competing mechanisms have been identified. Dyke loading resulted in yielding and plastic hardening of the upper foundation clay. This tended to strengthen the clay. Subsequently, geochemical changes caused additional yielding due to chemically-induced reductions in the yield locus. This tended to weaken the clay.

Both mechanisms of yielding can result in the generation of excess pore water pressures. In Chapter 6, stress paths plotted from results of the stress-deformation modeling results indicated the potential for significant volume strain in the areas beneath the dykes that were shown to yield. This was important because it shows the potential for the generation of excess pore water pressures if drainage could not take place sufficiently quickly. The difference between the two mechanisms is timing. Yielding due to dyke loading would produce excess pore water pressures as the dykes were constructed. Chemically induced yielding would occur at later times since this process requires leaching of cementation bonds. It is therefore time dependent.

Incorporation of the Modified Cam-Clay model for the upper foundation clay provided only a slight improvement to the slope stability modelling done previously for the site using steady state groundwater conditions. (Previous slope stability modelling focused

only on steady state groundwater conditions, Garinger et al. (2004).) It did however, further differentiate the unstable and stable locations with respect to factor of safety. The unstable section was found to be less stable than the stable section, with little capacity to resist failure (FS = 1.07). The difference was due primarily to geometry since the same Modified Cam-Clay parameters, which were based on results from laboratory testing of the background section, were used for both sections. Nevertheless, the overall results were broadly similar to the results obtained by Garinger (2002). When the post-peak strengths were used, both sections had a factor of safety greater than one, that is, they were both stable. When residual strengths were used, both sections had a factor of safety less than one, that is, they both failed.

The hypothesis proposed at the beginning of this thesis was that changes in chemistry could result in strength reduction. The laboratory program confirmed this hypothesis. A logical next step is to examine the effect of reducing the size of the yield locus on the factor of safety to simulate chemically induced softening. Before this was attempted, the results of the geochemical testing and modelling were combined with seepage and mass transport modelling to help determine where the reduction in the yield locus should be applied to the upper foundation clay.

Correlation of the laboratory program and geochemical modelling showed that if approximately one pore volume of forebay water had flowed through the upper foundation clay, the size of the yield locus would be reduced (Figure 4.2 combined with the information in Figures 4.29 to 4.32). This indicates that the yield locus in the modelling could be reduced where this amount of flow occurred. The goal of the seepage and mass transport modelling was to identify where in the foundation clay this

might be possible. The size of the yield locus could then be reduced accordingly in the stress-deformation model, and the effects incorporated into slope stability modelling. However, limited field data, particularly of measurements of field scale hydraulic conductivity, meant that this was only possible as a sensitivity analysis. More detailed in situ measurements of hydraulic conductivity at the site would be required to permit construction of a more formal model to describe the observed differences in geochemistry.

In the sensitivity analysis, the size of the yield locus in the stress-deformation model that fed the stress state to the stability model was reduced. This was done to test if such reductions would result in lower factors of safety. The results showed that in fact reducing the size of the yield locus increased the amount of yielding beneath the dykes, but did not significantly reduce the factor of safety. This reflects the inability of the modelling to handle both yielding and strain-softening at the same time. The Modified Cam-Clay model does not reflect some of the critical differences observed in strain-softening behaviour that were observed in the laboratory. Specifically, a soil rich in gypsum takes more strain to reach post-peak strength and ultimately residual strength (Figure 5.4). Less gypsum reduces the amount of strain required to cause strain-softening to post-peak or even residual strengths (and a condition of instability). The yield function in the SIGMA/W formulation of the Modified Cam-Clay model can be considered simply a 'flag' in this application. Under drained, steady-state conditions, the final stresses sent to SLOPE/W were similar regardless of when the clay yielded.

The conclusion thus far is that the modelling analyses described so far are not by themselves sufficient to identify conditions under which one section of the dyke became

unstable while the other section remained stable. Using steady state groundwater conditions, the only way to get the slopes to fail was to input residual strengths, which are usually associated with pre-existing failure. However, we know that the unstable section only failed for the first time after many years of successful operation, when it was apparently operating at a higher strength than residual. The stress-deformation modelling showed similar strains for both sections.

Lower sulphate concentrations were measured at the unstable section than the stable section. As a result of Figure 5.4, less strain would therefore have been required before strain-softening began. As the clay yielded and strain-softening began due to changes in chemistry, pore water pressures would be expected to increase, especially since destructuring took place rapidly. A reasonable limit to this behaviour would be to consider a sudden 'snap-through' from drained, steady-state behaviour to undrained behaviour. This was not captured by the previous modelling approach.

To further examine this issue, the effect of elevated pore water pressures (that is, undrained conditions) due to yielding on the factor of safety was examined while using post-peak strengths in the upper foundation clay. The objective here was to determine if there is a set of conditions that could result in failure of the dykes while post-peak strengths are operative. Recall that the modelling presented in Chapter 6 used steady-state (drained) pore water pressures. This was initially thought to be justified since the instability being modelled occurred approximately 45 years after the dykes were raised. However, as mentioned in the preceding paragraph, it is possible that yielding due to geochemical changes may have occurred over this period and resulted in excess pore water pressures, with 'snap-through' into undrained conditions. Piezometers were only

installed after many of the instabilities at the site had taken place. As such, no elevated pore water pressures associated with the destructuring of the upper foundation clay were recorded.

The ability of the upper foundation clay to dissipate excess pore water pressures will depend on the relationship between plastic volumetric straining (which may be influenced by geochemical changes) and hydraulic conductivity. If drainage exceeds the development of excess pore pressures, settlements will eventually stop and steady state groundwater conditions will be valid. If the excess pore water pressures cannot dissipate sufficiently rapidly, on-going settlements can be expected. This type of behaviour was observed at the New Liskeard embankment failure in Ontario (Folkes and Crooks, 1985) where a dynamic equilibrium between plastic straining and dissipation of the subsequent excess pore water pressures was observed. As implied earlier, if yielding due to construction loading was responsible for the elevated pore water pressures, problems would be expected in the short term, soon after the end of construction. In contrast, if geochemically induced yielding was responsible, longer term problems might be expected. This latter scenario would agree with the observation of settlement at the crest associated with the instabilities at the Seven Sisters dykes.

Consideration of undrained stability analysis will be done in two stages. The first deals with pore water pressures induced by raising the dykes in the 1940's. The second deals with the case where leaching reduces the size of the yield loci, and rapid strain-softening produces a change from 'steady-state' to 'strain-softened' behaviour. Dealing first with raising of the dykes, the change in mean effective stress, $\Delta p'$, due to dyke loading was used to estimate worst case pore pressures in the upper foundation clay. This amount is

represented by the component of the stress paths shown in Figures 6.17 and 6.18 in the p′ direction, for the last two fill increments, that is, raising of the dykes. It was assumed that $\Delta u = m\Delta p'$, with m ranging from 0.25 to 1.0 (values of m = 1.0 represent elastic isotropic response to undrained loading and is conservative in what is in reality an anisotropic clay). For these conditions, and using post-peak strengths, the factor of safety was close to or less than unity for both sections as long as m was 0.5 or greater (Table 7.1). At m = 0.25, the stable section had a factor of safety of 1.11 and the unstable section had a factor of safety closer to 1.0. These simulations were run using post-peak strengths, indicating that a reduction in strength from post-peak to residual was not needed as it was in the earlier simulations. Both sections can fail at post-peak strengths if yielding induces elevated pore water pressures. This applies to the short term, response immediately after construction.

Now consider the second category of undrained stability analysis, the effects of a sudden destructuring associated with chemical changes. Figure 7.1 follows the stress history of an element of soil beneath the dykes. The figure can be used to estimate the maximum possible excess pore water pressures that the upper foundation clay may have experienced. Using Modified Cam-Clay to characterize the behaviour of the upper foundation clay, the stress-deformation modelling showed that yielding occurred beneath the dykes after they were initially constructed in 1929. Therefore, plastic hardening of the foundation clay likely occurred at the site. This is supported by the lower specific volumes measured beneath the dyke relative to the background location. The initial response to loading is assumed to be elastic, isotropic and undrained for this discussion (a vertical line from the initial in situ stress to point A in Figure 7.1). Yielding would have been associated with excess pore water pressures that slowly dissipate with time (points

A to B in Figure 7.1). As the excess pore water pressure dissipates, the stress state moves away from critical states and the stability of the embankment increases. This form of solution is broadly equivalent to the commonly used approach in which $\Delta u = \overline{B}\,\Delta\sigma_v$. In Lake Agassiz clay, it has been common to take $\overline{B} = 1$.

Almost 20 years later, well after any of the initial excess pore water pressure would have dissipated, the dykes were raised to their current elevation. Once again, the stress-deformation modelling showed more yielding as the dykes were raised. As the dykes are raised, the initial stress path can again be approximated as vertical in Figure 7.1 if conditions are assumed to be elastic, isotropic and undrained (point C). As drainage occurs, the stress state moves to point D. Along this segment, straining occurs. After the final stages of construction, the element is then normally consolidated and positioned on the state boundary surface associated with the level of stress at that point beneath the dyke. The outer yield locus shown in Figure 7.1 represents the expanded elastic region with the original soil chemistry, cementation, and microstructure.

After raising the dykes, stability problems became evident on an irregular basis. Some of the instabilities occurred unexpectedly following durations up to approximately 50 years after the dykes were raised. This is well after any excess pore water pressures generated during construction would have dissipated.

The time dependency of the problem, along with the highly strain-softening behaviour of the upper foundation clay, led to the hypothesis that forebay water was leaching cementation bonds from the clay. The laboratory testing program showed that the

reduction of gypsum cementation reduced the size of the yield locus, and resulted in the formation of a shear plane at lower strains with lowered peak strength.

Stress-strain behaviour in terms of strain-softening will be influenced by chemistry. If there is sufficient cementation bonding, pore water pressures will dissipate before strain-softening occurs. The clay will reach steady state at point D and the slope remains stable. If there is insufficient cementation bonding, strain-softening to the critical state line might occur somewhere between points C and D. With excess pore water pressure, the slope becomes unstable in the short term. This balance will depend on how fast the clay can dissipate the excess pore water pressures. There is therefore a balance to be drawn between the rate at which forebay water is leaching through the foundation soil (and therefore reducing the yield loci) and the rate at which shear-generated pore water pressures can dissipate. Both mechanisms depend on the magnitude of the hydraulic conductivity.

If the slope remains stable in the short term, the element of soil will remain at point D over the long term unless something causes a reduction in the size of the yield locus. After approximately one pore volume of forebay water passes though the soil, any solid phase gypsum that may be contributing to cementation bonding is brought into a state of dissolution. (This reduces the size of the yield locus (Figure 4.30)). The yield locus shrinks as shown in Figure 7.1. That is, changes in chemistry are softening the clay that was in a normally consolidated state. Reduction of the yield locus results in straining as the soil adjusts to the change. The stress path drops towards the critical state line. If enough straining takes place, the clay strain softens to the critical state (post-peak) line (point E). With lower gypsum concentrations, this strain-softening occurs at smaller

strains (Figure 5.4). The stress deformation modelling showed strains in the order of 2% to 5%, with localized maximum strains up to 10% at the centre line of the dyke. The triaxial testing program showed that this amount of strain is sufficient to mobilize post-peak strengths in the upper foundation clay (Figures 5.3 and 5.4).

The amount of excess pore water pressure associated with the strain-softening to the critical state line can be calculated using Figure 7.1:

$$\Delta u = \frac{2}{3}(1 - M_{cs})p'_2 \qquad [7.1]$$

where p'_2 corresponds to the mean effective stress at which the strain-softening occurs, that is, along the path from point D to E in Figure 7.1. This calculation assumes that a yielding element of foundation clay softens under conditions where the vertical stress remains constant while total horizontal pressure increases, transferring horizontal pressure laterally to neighbouring elements.

Values of excess pore water pressure in the upper foundation clay calculated using Equation 7.1 were higher than the values used in the earlier modelling of construction generated pore water pressures (Table 7.1). The new modelling showed that excess pore water pressures produced during softening were sufficient to cause instability, even if post-peak strengths were used in the upper foundation clay.

The finding that softening-induced (destructured) elevated pore water pressures can bring the factor of safety of both sections to less than unity, even if post-peak strengths

are operative, links the modelling, laboratory testing and geochemical results. The modelling indicated that yielding occurred beneath the dykes. This can increase pore water pressures and mobilize post-peak strengths. The laboratory program showed that reduction in cementation can also induce yielding and reduce the amount of strain required to reach post-peak strengths. At later times, the geochemical changes observed beneath the dyke were sufficient to bring gypsum into an under-saturated state (Gypsum cementation was in a state of dissolution beneath the dykes). Upon strain-induced destructuring, the combination of elevated pore water pressures and mobilization of post-peak strengths results in a safety factor less than one. In this way, the modeling identifies a possible mechanism for the time-dependent, irregular failures at Seven Sisters.

7.2 Strengths and Weaknesses of Research Program

The primary contribution of this thesis to the literature has been the results of the laboratory testing program. The program was designed to investigate the hypothesis developed for the Seven Sisters site in south-eastern Manitoba. The hypothesis said that seepage of forebay water through the upper foundation clay was leaching naturally-occurring cementing minerals from the clay and subsequently changing its mechanical behaviour. To address this hypothesis, the laboratory program investigated the stress-strain and yielding behaviour of Glacial Lake Agassiz clay that was reconstituted with a series of different pore fluid geochemical conditions and in its natural state. The results were presented in both p',q-space and p',V-space. This type of work on the chemo-elastoplasticity of clay soils has not previously been presented in the available literature.

The testing program showed that pore fluid chemistry influences clay behaviour in two different ways. One, pore fluid chemistry influences the saturation state of potential cementing minerals that occur in natural clays. The presence of gypsum cementation influenced the size of the yield locus (Figures 4.29 to 4.32 and 5.10) and over-consolidated peak strength (Figure 5.2). Specimens saturated with respect to gypsum generally shared the same yield locus. When the specimens were under-saturated with respect to gypsum, the size of the yield locus was reduced. In terms of stress-strain behaviour, the presence and amount of gypsum cementation was important. Specimens that contained relatively more gypsum cementation required more straining before strain-softening and the development of a shear plane (Figure 5.4).

Two, diffuse double layer effects come into play after the initial soil structure and cementation is destroyed. Specimens with elevated pore fluid electrolyte concentrations had higher normally consolidated peak strengths (Figure 5.2) as well as critical state and residual strengths (Figures 5.3 to 5.5).

The laboratory program was therefore successful in addressing the hypothesis by demonstrating that the mechanical behaviour of Glacial Lake Agassiz clay can be influenced by pore fluid geochemistry. The work is highly original and provides a significant contribution to the field of chemo-elastoplasticity. Nowhere in the literature has the link between pore fluid geochemistry of potential cementing minerals and elastic-plastic soil mechanics been examined in such detail.

The modelling work was supplemental to the laboratory testing program and was not the main focus of the thesis. It was used to explore a number of scenarios, given the available information, and to link the laboratory work back to the original problem. The modelling that was conducted was considered as a series of 'simulations' of likely scenarios and not as formal 'predictions'. It was completed to examine a number of mechanisms that appear to be important at the site and in doing so, it has enhanced the understanding of the field project. Its principal contribution to the literature has been its ability to calculate for the first time the effects of chemistry-induced strain-softening on slope stability if destructuring causes a transformation from steady-state, drained conditions to undrained conditions.

Following paragraphs outline areas where more information is needed to better address the original problem and some of the weaknesses of the laboratory testing program.

The original research proposal included X-ray diffraction (XRD) and scanning electron microscope (SEM) work to quantify and potentially observe the potential cementation minerals. It was determined that the available XRD equipment at the University of Manitoba could not achieve the required detection limit to quantify the various cementation minerals of interest. At the time of writing this thesis, the SEM at the University of Manitoba was not functional.

Further site characterization of the Seven Sisters site would be required to advance the modelling work. Specifically, more spatial information with respect to geochemistry, in situ hydraulic conductivity and thickness of the upper foundation clay at both sections is

needed. The geochemical results could then be compared to the geophysical anomalies reported at the site. Information on possible high hydraulic conductivity zones would be particularly helpful. In situ hydraulic conductivity measurements could be used to enhance the seepage and mass transport modelling.

Freezing and thawing cycles had the same effect on yielding of reconstituted clays as did the reduction in gypsum cementation. At the Seven Sisters site, all of the clays have been subjected to weathering. The effects of weathering could be expected to be similar across the entire site. However, this has not been proven. In contrast, leaching of gypsum cementation will be influenced by irregular sand or silt partings and will be variable. Leaching is controlled by hydraulic conductivity and dispersion, both of which can be quite variable across a given site.

Natural, undisturbed specimens of the background and unstable locations at Seven Sisters were collected for comparison of their corresponding yield loci. Part of the original proposal was to leach some of the natural clay specimens from the background location with forebay water to model the site. Half of the natural background specimens were subjected to leaching with forebay water in flexible wall permeameters. Due to time limitations, this experiment was not completed in time for the writing of this thesis. After approximately one year of permeation, only 0.5 pore volumes had passes through the specimens. The experiment will be continued. A minimum of two pore volumes will be passed through each of the leached specimens. Triaxial tests will be conducted on the natural specimens and this will permit the construction of a yield locus for the clay before and after leaching.

Some minor improvements to the testing procedures and equipment could have enhanced the laboratory testing program. At the start of the program, the available triaxial equipment was not equipped for anisotropic consolidation. For consistency, isotropic consolidation was used throughout the program. A number of CAŪ tests indicated slightly different behaviour than the corresponding CIŪ tests, and this warrants further consideration.

The data used to calculate the anisotropic elastic parameters was limited. This was due to having a limited number of tests from each different soil chemistry (for reasons of program duration). This precluded being selective in the removal of any outliers. Measurement of axial strain during the isotropic consolidation test would have provided an additional test per soil condition, which would have greatly increased the confidence in the calculated values. Employing rotating pistons to eliminate friction would have also increased the confidence in the results. Further testing using constant rate of stress testing (for example, using a Bishop and Wesley cell with GDS controllers) would have strengthened the program by permitting a more detailed examination of other defined stress paths. This would have enhanced the definition of the yield loci and the anisotropic elastic parameters.

The value of the reconstituted batch of soil that was washed with one pore volume of DI water was not fully appreciated at the time of testing. At first glance, the geochemistry and mechanical behaviour appeared to be the same as the control batch prepared with DI water. After the testing program was completed, it was realized that the inner yield

locus of this material was smaller than the other clays that were saturated with respect to gypsum. This corresponded with lower sulphate concentrations. Only three tests were conducted on this batch of clay. Results from these tests were very useful in formulating the understanding of the project. More testing on this clay would have been valuable.

8.0 Conclusions and Suggestions for Future Research

8.1 Conclusions

The primary conclusions of the research program are as follows:

- Presence of gypsum influenced the size of the yield locus for Lake Agassiz clay in p',q-space. Specimens that were saturated with respect to gypsum shared the same general yield locus. The size of the yield locus was reduced when pore fluid concentrations of calcium and sulphate were lowered to conditions that would result in the dissolution of gypsum.
- The transition from linear to non-linear stress-strain behaviour (defined in this program as inner yield) is controlled by the presence and amount of gypsum. True yielding with the onset of plastic deformation (defined in this program as outer yield) is controlled by clay mineralogy and structure.
- Reductions in the amount of gypsum reduced the amount of strain required for strain-softening from peak to post-peak and the development of a shear plane.
- Elevated pore fluid electrolyte concentrations increased the normally consolidated peak strength, post-peak strength and residual strength.
- The natural clay strain-softened sooner and had a smaller and flatter normalized yield locus than the reconstituted clay with the same pore fluid chemistry. The differences in size and shape between the yield loci of the reconstituted and natural clays was attributed to differences in soil fabric and weathering induced macrostructure in the natural soil.

- Freezing and thawing cycles reduced the size of the yield locus in p',q-space, peak strength, the amount of strain required for strain-softening from peak strength to post-peak strength with the accompanying development of a shear plane.

Secondary conclusions of the research program are as follows:

- Using the yield locus determined for natural specimens from the background location at the Seven Sisters site, stress-deformation analysis indicated that the upper foundation clay yielded during the initial construction and raising of the dykes. Reduction of the size of the yield locus would increase the amount of yielding beneath the dykes. Chemically induced yielding would be expected to be time dependent, whereas yielding due to construction loading would be expected shortly after construction.
- Excess pore water pressures produced by strain-softening following chemistry induced reductions in yield loci would be sufficient to cause a condition of instability at the Seven Sisters site while post-peak strengths are operative.

8.2 Suggestions for Future Research

The following is a list of suggestions for future research:

- Complete the leaching experiment on natural clay and determine the yield locus of the leached material.
- Examine spatial variation in geochemistry and weathering of the upper foundation clay at the Seven Sisters site.

- Examine healing time of gypsum cementation by allowing different amounts of time between end of consolidation and shear.
- Examine true elasticity by conducting cyclic loading tests.
- Conduct scanning electron microscope analyses on the natural and reconstituted clays.
- Conduct X-ray diffraction analysis on the white precipitate observed in the fissures of the natural clay.
- Create a reconstituted clay acidified with HCl instead of H_2SO_4 to better isolate carbonate based cementation.
- Repeat several of the incremental stress-controlled tests using strain controlled GDS apparatus.
- Examine the difference between isotropic and anisotropic consolidation of triaxial specimens.
- Repeat the freezing and thawing experiment on the reconstituted clay that was washed with six pore volumes to try to distinguish the effects of chemistry versus the effects of freezing and thawing weathering.

9.0 References

AECL. 1997. The buffer/container experiment: results, synthesis, issues. Atomic Energy of Canada Limited Report, AECL-11746, COG-97-46-I, December 1997.

American Public Health Association (APHA). 1998. Standard methods for the examination of water and wastewater, 20th Edition. American Water Works Association and Water Environment Federation.

ASTM. 2000a. Standard test methods for particle size analysis of soils, Method D 422-63 (Reapproved 1998). American Society for Testing and Materials, Philadelphia, Pa.

ASTM. 2000b. Standard test methods for laboratory determination of water (moisture) content of soil and rock, Method D 2216. American Society for Testing and Materials, Philadelphia, Pa.

ASTM. 2000c. Standard test methods for liquid limit, plastic limit and plasticity index of soils, Method D 4318-98. American Society for Testing and Materials, Philadelphia, Pa.

ASTM. 2000d. Standard test methods for measurement of hydraulic conductivity of saturated porous materials using a flexible wall permeameter, Method D 5084-90. American Society for Testing and Materials, Philadelphia, Pa.

ASTM. 2000e. Standard test methods for consolidated undrained triaxial compression test for cohesive soils, Method D 4767-95. American Society for Testing and Materials, Philadelphia, Pa.

ASTM. 2000f. Standard test methods for one-dimensional consolidation properties of soils, Method D 2435-96. American Society for Testing and Materials, Philadelphia, Pa.

Appelo, C.A.J., and Postma, D. 1996. Geochemistry, groundwater and pollution. A.A. Balkema. Rotterdam.

Baldi, G., Borsetto, M., Hueckel, T., and Peano, A. 1987. Coupling of thermo-plastic and hydraulic effects in a clay repository: near field analysis. In Coupled processes associated with nuclear waste repositories. Edited by C.F. Tsang. Academic Press, Orlando, Fl., pp. 565-580.

Baracos, A. 1977. Compositional and structural anisotropy of Winnipeg soils – a study based on scanning electron microscope and X-ray diffraction analyses. Canadian Geotechnical Journal, **14**(1): 125-137.

Baracos, A. and Graham, J. 1980. Landslide problems in Winnipeg. Specialty Conference on Slope Stability Problems in Urban Areas. Canadian Geotechnical Society. Toronto, Ontario.

Barbour, S.L. 1990. The impact of sodium-chloride solutions on the geotechnical properties of clay soils, a review of clay-brine interaction. Geotechnical Engineering Group, Department of Civil Engineering, College of Engineering, University of Saskatchewan, Saskatoon, Saskatchewan.

Barbour, S.L. and Fredlund, D.G. 1989. Mechanisms of osmotic flow and volume change in clay soils. Canadian Geotechnical Journal, **26**: 551-562.

Barbour, S.L. and Krahn, J. 2004. Numerical modelling – prediction or process? Geotechnical News.

Barbour, S.L. and Yang, N. 1993. A review of the influence of clay-brine interactions on the geotechnical properties of Ca-montmorillonitic clayey soils from western Canada. Canadian Geotechnical Journal, **30**: 920-934.

Berry, R.W. and Torrance, J.K. 1998. Mineralogy, grain-size distribution and geotechnical behaviour of Champlain clay core samples, Quebec. The Canadian Mineralogist, Vol. 36. pp. 1625-1636.

Bishop, A.W. and Morgenstern, N.R. 1960. Stability coefficients for earth slopes. Geotechnique, Vol. 10, pp. 129-150.

Bjerrum, L. and Rosenqvist, I. Th. 1956. Some experiments with artificially sedimented clays. Geotechnique, Vol. 6, pp. 124-136.

Bjerrum, L. 1969. Discussion of main session 5, Stability of Natural Slopes and Embankment Foundations. In Proceedings of the 7th International Conference on Soil Mechanics and Foundation Engineering, Mexico City, Mexico, **3**, 377-414.

Boone, Storer J. and Lutenegger, Alan J. 1997. Carbonates and cementation of glacially derived cohesive soils in New York State and southern Ontario. Canadian Geotechnical Journal, **34**: 534-550.

Budhu, Muniram. 1991. The permeability of soils with organic fluids. Canadian Geotechnical Journal, **28**: 140-147.

Burland, J.B. 1990. On the compressibility and shear strength of natural clays. Géotechnique, **40**(3): 329-378.

Campanella, R.G., and Mitchell, J.K. 1968. Influence of temperature variations on soil behaviour. ASCE Journal of the Soil Mechanics and Foundations Division, 94(SM3): 709-734.

Casagrande, A. 1959. An unsolved problem of embankment stability on soft ground. In Proceedings of the 1st Pan-American Conference on Soil Mechanics, Mexico City, **2**, 721-746. publ. Sociedad Mexicana de Mecanica de Suelos, Mexico City, Mexico 1960.

Charlton, S.R., and D.L. Parkhurst. 2002. PHREEQCI: A graphical user interface to the geochemical model PHREEQC. U.S. Geological Survey Fact Sheet FS-031-02.

Corrigan, C.A., Jamieson, H.E., and Remenda, V.H. 2001. Fracture wall cements and coatings from two clayey till aquitards. Groundwater, Vol. 39, No. 5, pp. 786-794.

Craig, R.F. 1992. Soil Mechanics. Chapman & Hall. Boundary Row, London.

Day, J.M. 1977. Analysis of movement and hydrogeochemistry of groundwater in the fractured clay and till deposits of the Winnipeg area, Manitoba. Thesis presented to the University of Waterloo, in partial fulfillment of the requirements for the degree of Master of Science.

Di Maio, C., and Onorati, R. 1999. Prove di laboratorio: influenza di composizione del liquido di cella. Rendiconti del XX Convegno Nazionale di Geotecnica, Parma, 87-94.

Di Maio, C., and Fenelli, G.B. 1994. Residual strength of kaolin and bentonite: the influence of their constituent pore fluid. Géotechnique, **44**(4): 217-226.

Dixon, D.A., Chandler, N.A., and Baumgartner, P. 2002. The influence of groundwater salinity and interfaces on the performance of potential backfilling materials. 6th International Workshop on Design and Construction of Final Repositories "Backfilling in Radioactive Waste Disposal". Brussels.

Domaschuk, L. 1977. Soil block sampler. Canadian Geotechnical Journal, **14**: 262-265.

Domenico, P.A. and Schwartz, F.W. 1990. Physical and chemical hydrogeology. John Wiley & Sons, Inc. New York.

Dragun, J. 1988. The soil chemistry of hazardous materials. Hazardous Materials Control Research Institute. Greenbelt, Maryland.

Dragun, J., Mason, S.A., and Barkach, J. 1991. What do we really know about the fate of diesel fuel in soil systems? in Hydrocarbon Contaminated Soils, Volume I. Kostecki, P.T., and Calabrese, E.J. Eds. Lewis Publishers, Inc. Chelsea, Michigan.

Eden, W. J., and Crawford, C. B. 1957. Geotechnical properties of Leda clay in the Ottawa area. Proceedings of the Fourth International Conference on Soil Mechanics and Foundation Engineering. Vol. 1, pp. 22-27.

Faure, G. 1991. Principles and applications of inorganic geochemistry. Macmillan Publishing Company. New York.

Fetter, C.W. 1999. Contaminant Hydrogeology. 2nd Ed. Prentice-Hall, Inc.

Fernandez, F. and Quigley, R.M. 1985. Hydraulic conductivity of natural clays permeated with simple liquid hydrocarbons. Canadian Geotechnical Journal, **22**: 205-214.

Fernandez, F. and Quigley, R.M. 1991. Controlling the destructive effects of clay-organic liquid interactions by application of effective stresses. Canadian Geotechnical Journal, **28**: 388-398.

Fleming, I.R., Rowe, R.K., and Cullimore, D.R. 1999. Field observations of clogging in a landfill leachate collection system. Canadian Geotechnical Journal, **36**: 685-707.

Folkes, D.J. and Crooks, J.H.A. 1985. Effective stress paths and yielding in soft clays below embankments. Canadian Geotechnical Journal, **22**: 357-374.

Freeze, R.A., and Cherry, J.A. 1979. Groundwater. Prentice-Hall Inc. New Jersey.

Gajo, A., Loret, B., and Hueckel, T. 2000. Electro-chemo-mechanical couplings in saturated porous media: elastic-plastic behaviour of heteroionic expansive clays. International Journal of Solids and Structures.

Garinger, B. 2002. Instability of dykes at Seven Sisters Generating Station. M.Sc. Thesis, Department of Civil Engineering, University of Manitoba, Winnipeg.

Garinger, B., Alfaro, M., Graham, J. and Dubois, D. 2001. Stability of dykes at Seven Sisters Generating Station. 54th Canadian Geotechnical Conference, Calgary, Alberta, pp. 259-265.

Garinger, B., Man, A., Alfaro, M., Graham, J., Goh, T.B. and Dubois, D. 2002. Physicochemical investigation of the foundation at Seven Sisters dykes. 55th Canadian Geotechnical Conference, Niagra Falls, Ontario.

Garinger, B., Alfaro, M., Graham, J., Dubois, D., and Man, A. 2004. Instability of Dykes at Seven Sisters Generating Station. Canadian Geotechnical Journal, **41**: 959-971.

Graham, J. 1984. Methods of stability analysis. In 'Slope instability', Eds. D. Brunsden and D.B. Prior, pp. 171-216. Wiley-Interscience, New York.

Graham, J. and Au, V.C.S. 1985. Influence of freeze-thaw and softening effects on stress-strain behaviour of natural plastic clay at low stresses. Canadian Geotechnical Journal, **22**: 69-78.

Graham, J. and Houlsby, G.T. 1983. Anisotropic elasticity of a natural clay. Géotechnique, **33**(2): 165-180.

Graham, J., Noonan, M.L. and Lew, K.V. 1983. Yield states and stress-strain relationships in a natural plastic clay. Canadian Geotechnical Journal **20**: 502- 516.

Graham, J. and Li, E.C.C. 1985. Comparison of natural and remolded plastic clay. Journal of Geotechnical Engineering, Vol. 111, No. 7, pp. 865-880.

Graham, J., Crooks, J.H.A. and Lau, S.L.K. 1988. Yield envelopes: identification and geometric properties. Géotechnique, **38**(2): 125-134.

Lingnau, B.E., Graham, J. and Tanaka, N. 1995. Isothermal modeling of sand-bentonite mixtures at elevated temperatures. Canadian Geotechnical Journal, **32**: 78-88.

Graham, J., Oswell, J.M. and Gray, M.N. 1992. The effective stress concept in saturated sand-clay buffer. Canadian Geotechnical Journal, **29**(6): 1033-1043.

Graham, J., Saadat, F., Gray, M.N., Dixon, D.A., and Zhang, Q.Y. 1989. Strength and volume change behaviour of a sand-bentonite mixture. Canadian Geotechnical Journal, **26**: 292-305.

Graham, J., Yuen, K., Goh, T.B., Janzen, P. and Sivakumar, V. 2001. Hydraulic conductivity and pore fluid chemistry in artificially weathered plastic clay. Engineering Geology, 60(2001) 69-81.

Graham, J. 2003. R.M. Hardy Address: Soil parameters for numerical analysis of clays. Canadian Geotechnical Conference. Winnipeg, Manitoba.

Guimaraes, L., Sanchez, A. and Olivella. 2001. Chemo-mechanical modelling of expansive clays. 6th International Workshop on Key Issues on Waste Isolation Research. Paris.

Hawkins, A.B. and McDonald, C. 1992. Decalcification and residual shear strength reduction in Fuller's Earth Clay. Géotechnique, **42**(3): 453-464.

Ho, Y. A. 1985. The effects of brine contamination on the properties of soils. M.Sc. Thesis, Department of Civil Engineering, University of Saskatchewan, Saskatoon.

Hueckel, T., and Baldi, G. 1990. Thermoplasticity of saturated soils and shales: constitutive equations. ASCE Journal of Geotechnical Engineering, 116(GT12): 1765-1777.

Hueckel, T,A. 1992. Water-mineral interaction in hygromechanics of clays exposed to environmental loads: a mixture-theory approach. Canadian Geotechnical Journal, **29**: 1071-1086.

Hueckel, T,A. 1997. Chemo-plasticity of clays subjected to stress and flow of a single contaminant. International Journal for Numerical and Analytical Methods in Geomechanics. Vol. 21, pp 43-72.

Hutchison, I.P.G. and Ellison, R.D. 1992. Mine waste management. California Mining Association. Lewis Publishers Inc. Michigan.

Jardine, R.J., Gens, A., Hight, D.W. and Coop, M.R. 2004. Developments in understanding soil behaviour. Keynote Address, Advances in Geotechnical Engg. Proc. Skempton Memorial Conference. Telford, London UK, pp. 103-207.

Kashir, M. and Yanful, E.K. 2001. Hydraulic conductivity of bentonite permeated with acid mine drainage. Canadian Geotechnical Journal, **38**: 1034-1048.

Karnland, O. 1997. Bentonite swelling pressure in strong NaCl solutions. Correlation between model calculations and experimentally determined data. Technical report 97-31. Swedish Nuclear Fuel and Waste Management CO – SKB. Clay Technology, Lund, Sweden.

Kazi, A., and Moum, J. 1973. Effect of leaching on the fabric of normally consolidated marine clays. Proceedings of the International Symposium on Soil Structure. Gothenburg, Sweden. Pp.137-152.

Krahn, J. 2001. R.M. Hardy Address: The limits of limit equilibrium analysis. Canadian Geotechnical Journal 40, pp. 643-660.

Krahn, J. 2004a. Seepage modeling with SEEP/W, An engineering methodology. Geo-Slope International, Ltd.

Krahn, J. 2004b. Transport modeling with CTRAN/W, An engineering methodology. Geo-Slope International, Ltd.

Krahn, J. 2004c. Stress and deformation modeling with SIGMA/W, An engineering methodology. Geo-Slope International, Ltd.

Krahn, J. 2004d. Stability modeling with SLOPE/W, An engineering methodology. Geo-Slope International, Ltd.

Lambe, T.W. 1960. A mechanistic picture of shear strength in clay. Proceedings, ASCE Research Conference on the Shear Strength of Cohesive Soil, Boulder, CO. pp. 555-580.

Lessard, G. and Mitchell, J.K. 1985. The causes and effects of aging in quick clays. Canadian Geotechnical Journal, **22**: 335-346.

Li, E.C.C. 1983. A geotechnical study of remoulded Winnipeg clay, thesis presented to the University of Manitoba, in partial fulfillment of the requirements for the degree of Master of Science.

Liu, V.P.H. and Dubois, D.P. 1996. Seven Sisters Generating Station dykes risk analysis. In Proceedings of the 49th Canadian Geotechnical Conference, St. John's Newfoundland, pp. 351-360.

Loh, A.H., and Holt, R.T. 1974. Directional variation in undrained shear strength and fabric of Winnipeg upper brown clay. Canadian Geotechnical Journal, **11**: 430-437.

Loret, B., Hueckel, T. and Gajo, A. 2001. Chemo-mechanical coupling in saturated porous media: elastic-plastic behaviour of homoionic expansive clays. International Journal of Solids and Structures.

Low, P.F. 1979. Nature and properties of water in montmorillonite-water systems. Soil Science Society of America Journal, 43:651-658.

Man, A., Garinger, B., Alfaro, M., Graham, J., and Goh, T. B. 2003a. Effect of Pore Fluid Chemistry on the Triaxial Behaviour of a High-plastic Clay. Vancouver Geotechnical Society.

Man, A., Graham, J., Alfaro, M., and Goh, T. B. 2003b. Changes in Clay Behaviour Produced by Seepage Under a Water Retention Dyke. 56th Canadian Geotechnical Conference, Winnipeg.

McBride, M.B. 1994. Environmental Chemistry of Soils. Oxford University Press. New York, NY.

McKyes, E., Sethi, A., and Yong, R.N. 1974. Amorphous coatings on particles of sensitive clay soils. Clays and Clay Minerals, 22:427-433.

Mesri, G., and Olson, R.E. 1971. Consolidation characteristics of montmorillonite. Géotechnique, **21**: 341-352.

Middleton, T.A., and Cherry, J.A. 1994. Organic chemical effects on clay permeability. Engineering for Waste Isolation. CSCE Special Publication, Toronto, Ontario.

Mitchell, J.K. 1993. Fundamentals of soil behaviour. 2nd ed. John Wiley & Sons, Inc. New York.

Mitchell, J.K. 2000. Physicochemistry of soils for geoenvironmental engineering. In Geotechnical and geoenvironmental engineering handbook. Rowe, R.K. (Ed.). Kluwer Academic Publishers. Boston.

Moum, J., Loken, T., and Torrance, J.K. 1971. A geochemical investigation of the sensitivity of a normally consolidated clay from Drammen, Norway. Géotechnique, **21**: 329-340.

Noonan, M.L. 1980. Limit state studies in Winnipeg clays. Thesis presented to the University of Manitoba, in partial fulfillment of the requirements for the degree of Master of Science.

Olson, R.E. 1974. Shearing strength of kaolinite, illite and montmorillonite. ASCE Journal of the Geotechnical Engineering Division, 100(GT11): 1215-1229.

Pach, J.A. 1994. Hydraulic and solute transport characteristics of a fractured glacio-lacustrine clay, Winnipeg, Manitoba. Thesis presented to the University of Waterloo, in partial fulfillment of the requirements for the degree of Master of Science.

Parkhurst, D.L. and C.A.J. Appelo. 1999. User's guide to PHREEQ (version 2): A computer program for speciation, batch reaction, one-dimensional transport, and inverse geochemical calculations. U.S. Geological Survey Water Resources Investigations 99-4259.

Penner, E. 1963. Sensitivity in Leda clay. Nature, Vol. 197, No. 4865, pp. 347-348.

Peterson, R., Iverson, N.L. and Rivard, R.J. 1957. Studies of several dam failures on clay foundations. In Proceedings of the 4th International Conference on Soil Mechanics and Foundation Engineering, London, U.K., pp. 348-352.

Quigley, R.M. 1980. Geology, mineralogy, and geochemistry of Canadian soft soils: a geotechnical perspective. Canadian Geotechnical Journal, **17**:261-285.

Rivard, P.J. and Lu, Y. 1978. Shear strength of soft fissured clay. Canadian Geotechnical Journal, **15**, 382-390.

Rowe, R.K. 2002. Latest advances in the modelling of clogging of leachate collection systems. 2nd Canadian Specialty Conference on Computer Applications in Geotechnique. Winnipeg, Manitoba.

Sherard, J. L., Decker, R. S., and Ryker, N. L. 1972. Piping in earth dams of dispersive clay. Proceedings of the ASCE Specialty Conference on the Performancec of Earth and Earth-Supported Structures. Purdue University, pp. 589-626.

Sposito, G. 1984. The surface chemistry of soils. Oxford University Press. New York.

Stepkowska, E.T. 1990. Aspects of clay/electrolyte/water system with spatial reference to the geotechnical properties of clays. Engineering Geology, 28:249-268.

Stumm, W. 1992. Chemistry of the solid-water interface, processes at the mineral-water interface in natural systems. Wiley Interscience. New York.

Terzaghi, K. 1944. Ends and means in soil Mechanics. Engineering Journal of Canada. Vol. 27, pp.608.

Torrance, J.K. 1974. A laboratory investigation of the effect of leaching on the compressibility and shear strength of Norwegian marine clays. Géotechnique, **24**(2): 155-173.

Torrance, J.K. 1983. Towards a general model of quick clay development. Sedimentology, 30: 547-555.

Torrance, J.K. 1999. Physical, chemical and mineralogical influences on the rheology of remoulded low-activity sensitive marine clay. Applied Clay Science, 14(1999) 199-223.

University of Manitoba. Geotechnical group standard laboratory instructions for triaxial testing at the University of Manitoba.

Van Stempvoort, D.R., Hendry, M.J., Schoenau, J.J., and Krouse, H.R. 1994. Sources and dynamics of sulphur in weathered till, Western Glaciated Plains of North America. Chemical Geology, 111: 35-56.

Walton, W.C. 1988. Practical aspects of groundwater modelling: National Water Well Association, Worthington, Ohio.

Wiedemeier, T., Wilson, J.T., Kampbell, D.H., Miller, R.N., Hansen, J.E. 1995. Technical protocol for implementing intrinsic remediation with long-term monitoring for natural attenuation of fuel contamination dissolved in groundwater. Volume I. Air Force Center for Environmental Excellence. Technology Transfer Division. Brooks AFB. San Antonio, Texas.

Yong, R.N., Sethi, A., and La Rochelle, P. 1979. Significance of amorphous material relative to sensitivity in some Champlain clays. Canadian Geotechnical Journal, **16**: 511-520.

Yong, R.N., Mohamed, A.M.O. and Warkentin, B.P. 1992. Principles of contaminant transport in soils. Elsevier. Amsterdam.

TABLES

Table 1.1. Summary of classification information from Seven Sisters foundation clay.

Section	Unstable	Stable	Background
Borehole	SS-036	SS-040	SS-042
Depth to bedrock (m)	13.11	12.75	> 9.8
Liquid limit w_L (%)	99 - 119	80 - 112	100 - 118
Plastic limit w_P (%)	34 - 44	20 - 36	26 - 31
Water content w (%)	42-56	39 - 50	54 - 61
Clay fraction (%)	~ 100	~ 96*	~ 100

Note: - * decreasing to 72% in the lower, less plastic foundation clay

Table 1.2. Comparison of triaxial behaviour.

Section	Peak Strength	Post-peak Strength	Residual Strength	Strain-softening Rate (kPa/% Strain)
Background	15°	13°	11°	11
Stable	15°	14°	11°	14
Unstable	15°	13°	10°	51

Table 1.3. $-\Delta p'/\Delta q$ ratios.

Isotropic Consolidation Pressure (kPa)	Unstable	Stable	Background	
			Early	Late
100	0.38	-	0.17	-
200	0.53	0.31	0.26	-
400	0.50	0.27	0.34	0.56
450	0.43	0.38	-	-
500	-	-	0.31	0.50
550	0.45	0.25	-	-
Average	0.46	0.30	0.27	0.53

Table 1.4. Summary of slope stability analyses.

Analysis	Material Properties	Interslice Assumptions	Unstable Section	Stable Section
Case 1a	Post-peak	Morgenstern-Price	1.16	1.23
Case 1b	Post-peak	FEM (SIGMA/W)	1.15	1.21
Case 2a	Residual	Morgenstern-Price	0.97	0.98
Case 2b	Residual	FEM (SIGMA/W)	0.97	1.01

Table 1.5. Results of pore fluid chemical analysis.

Section	El. (m)	EC (µS/cm)	pH	Na (mg/L)	Mg (mg/L)	Ca (mg/L)	Cl (mg/L)	SO_4 (mg/L)	HCO_3 (mg/L)	Na/Ca	SAR $(meq/L)^{1/2}$	Gypsum SI
Unstable	267.7	772	8.1	62	71	30	6.4	243	130	1.80	1.41	-1.70
Unstable	266.7	1370	8.2	104	114	112	11.2	720	117	0.81	1.65	-0.86
Unstable	266.4	1340	8.2	102	108	113	10.3	708	104	0.78	1.65	-0.85
Unstable	266	1650	7.9	116	131	172	10.0	972	88	0.59	1.62	-0.61
Stable	267.8	546	8.2	26	58	28	3.0	153	113	0.81	0.65	-1.87
Stable	267	1190	8.1	58	115	97	6.3	609	95	0.52	0.94	-0.96
Stable	266.5	3520	8.1	148	159	164	14.3	2016	113	0.78	1.98	-0.46
Stable	266	1810	8.1	74	159	220	10.5	1122	92	0.29	0.93	-0.49
BKG	267.8	1460	8.0	64	160	125	1.4	870	85	0.44	0.89	-0.78
BKG	266.8	3950	7.8	108	505	554	3.0	3360	55	0.16	0.80	0.06
BKG	266.6	4160	7.7	116	533	680	6.0	3750	64	0.15	0.81	0.16
BKG	266.2	4150	8.6	116	505	680	6.2	3660	61	0.15	0.82	0.15

Notes:
- BKG = background section
- El. = elevation
- EC = electrical conductivity
- SAR = sodium adsorption ratio = $Na^{+}/[(Ca^{2+} + Mg^{2+})/2]^{1/2}$
- SI = $\log(IAP/ K_{sp})$

Table 2.1. Characteristics of common clay minerals (After Mitchell, 1993 and Yong et al, 1992).

Characteristic	Kaolinite	Illite	Smectite
Structure	1:1	2:1	2:1
Bonding	Strong H-bonds	Strong K-bonds	Very weak bonds
Basal spacing, nm	0.72	1.0	≥1.0
Source of charge	Broken edge bonds	Isomorphous substitution, Some broken edge bonds	Isomorphous substitution, Some broken edge bonds
Isomorphous substitution	Negligible	Al for Si	Mg for Al Al for Si Fe for Al
Charge characteristics	Mostly variable	Mostly fixed	Mostly fixed
Cation exchange capacity, eq kg^{-1}	0.03 – 0.15	0.1 – 0.4	0.8 – 1.5
Specific surface area, $m^2 g^{-1}$	10 – 20	65 – 100	Up to 800
Particle shape	Plates	Plates	Plates/films
Relative particle size	Large	Medium	Very small
Liquid limit, %	30 – 75	60 – 120	100 – 900
Plastic limit, %	25 – 40	35 – 60	50 – 100
Activity	< 0.5	0.5 – 1	1 – 7
Shrink/swell	Negligible	Low	Very high
Hydraulic conductivity, m s^{-1}	$10^{-7} – 10^{-9}$	$10^{-8} – 10^{-9}$	$10^{-9} – 10^{-11}$
Compression index	0.2 – 0.3	0.5 – 1.1	1.0 – 2.6
Shear strength, ϕ', degrees	24 – 30	17 – 26	5 - 17

Table 2.2. Common cementing minerals, their solubility and factors controlling dissolution rate (After Appelo and Postma, 1996; Faure, 1991).

Mineral Name	Chemical Formula	Solubility, K_{sp} (mol/L)	Dissolution Rate Control
Anhydrite	$CaSO_4$	$10^{-4.5} - 10^{-4.36}$	Transport
Gypsum	$CaSO_4 \cdot 2H_2O$	$10^{-4.6} - 10^{-4.58}$	Transport
Calcite	$CaCO_3$	$10^{-8.48} - 10^{-8.35}$	Surface reaction
Aragonite	$CaCO_3$	$10^{-8.34} - 10^{-8.22}$	Surface reaction
Dolomite	$CaMg(CO_3)_2$	$10^{-17.9} - 10^{-17.09}$	Surface reaction

Table 3.1 Summary of geotechnical testing program.

Soil Type	Isotropic Compression CIŪ	Oedometer	q/p' = Ko, CAŪ	q/p' = 1.25	CID	CIŪ	Constant p'	q/p' = -1.5
Reconstituted:								
Gypsum Rich	T11, 15, 16	O4, 5, 7, 14	T30	T42	T10, 14	T7-9,12,13, 47	T21,23,29	T37, 39
Freeze/Thaw	T50	--	--	--	T49	T48	--	--
DI Water	T17	O8, O13	--	--	T35	T27, 28	T56	--
H_2SO_4	T24	O11	--	--	T22	T25	T26	--
NaCl	T43	O15	--	--	T41	T45	T40	--
Washed 1PV	--	O12	--	--	T38	--	--	--
Washed 6PV	T54	O16	--	--	T52, 55	T51	T53	--
SS Natural:								
Background	T18, 33	O1-3, 9	T36	T46	T19	T1-6	T32	--
Unstable	T31, 44	O10	--	--	T20	BG	T34	--
Leached BKG	Leaching	Leaching	--	Leaching	Leaching	Leaching	Leaching	--

Notes:
- PV = pore volume
- SS = Seven Sisters natural foundation clay
- BG = Garinger, 2002 program
- Leached BKG clay project continuing, <1PV as of 2005.

Table 4.1. Summary of general geotechnical properties.

Soil Type	Water Content, w (%)	Bulk Density, ρ_b (Mg/m^3)	Unit Weight, γ_{sat} (kN/m^3)	Porosity, n (%)	Hydraulic Conductivity, K (ms^{-1})	Plastic Limit, w_P (%)	Liquid Limit, w_l (%)	Plasticity Index, I_p
Reconstituted:								
Gypsum Rich	60.1	1.656	16.2	62.5	$9.9x10^{-11}$	33.2	103.2	70.0
DI Water	57.4	1.679	16.4	61.4	$6.5x10^{-11}$	33.3	94.2	60.9
H_2SO_4	57.2	1.692	16.6	61.0	$6.3x10^{-11}$	32.8	101.7	68.9
NaCl	57.5	1.682	16.5	61.0	$8.9x10^{-11}$	39.3	78.8	39.5
Washed 1PV	57.0	1.676	16.5	61.0	$7.3x10^{-11}$	31.1	99.1	68.0
Washed 6PV	63.2	1.636	16.0	64.0	$9.8x10^{-11}$	33.2	104.9	71.7
SS Natural:								
Background	55.7	1.671	16.5	60.6	$4.1x10^{-11}$	27.8	113.6	85.8
Unstable	50.0	1.715	16.9	58.3	$2.9x10^{-11}$*	43.4**	111.7**	68.3

Notes: - All reconstituted clays consolidated to a final pressure of 225 kPa
- Average properties from triaxial tests.
- * = Garinger, 2002 program Seven Sisters unstable section foundation clay Sample 4 from El. 265.3 m to 264.6 m.
- ** = Garinger, 2002 program Seven Sisters unstable section foundation clay Sample 1 from El. 265.9 m to 265.3 m.

Table 4.2. Soil chemistry results.

	Reconstituted Clay					Natural Clay		
Parameter	Gypsum Rich	DI Water	H_2SO_4	NaCl	Washed 6PV	SS BKG	SS Unstable	Winnipeg Clay
Ag	<1	<1	<1	<1	<1	<1	<1	<1
Al	19200	19800	19400	18800	19100	23600	19000	161000
Ba	169	171	120	162	199	160	153	245
Be	1.1	1.1	1.1	1.1	1.1	1.1	1.1	1.0
Ca	20300	19100	19100	16100	17100	19100	15900	24600
Cd	<0.5	<0.5	<0.5	<0.5	<0.5	<0.5	<0.5	<0.5
Co	13	13	13	12	13	14	14	11
Cr	40	40	40	38	40	45	39	33
Cu	56	40	40	44	36	37	33	30
Fe	30300	30700	30400	29100	30200	32600	31500	25900
K	3900	4000	3970	3600	3710	4670	3840	3240
Mg	12200	12100	11800	10500	11200	13600	11900	14100
Mn	367	366	351	339	349	369	329	360
Mo	<3	<3	<3	<3	<3	<3	<3	<3
Na	291	280	270	12000	184	455	525	1080
Ni	39	39	39	39	37	44	39	34
P	487	482	481	463	481	537	546	439
Pb	18	18	18	17	18	17	18	16
Sr	61.8	61.3	58.2	49.5	56.5	66.9	64.0	73.6
Ti	131	139	135	140	135	164	139	129
V	59	62	60	59	59	68	56	53
Zn	98	89	95	88	89	94	91	76
F^-	4	3	11	5	5	5	5	4
Cl^-	16.0	12.0	<5.0	13000	31.0	8.0	40.0	462.0
Br^-	<5.0	<5.0	<5.0	<5.0	<5.0	<5.0	<5.0	<5.0
NO_2-N	<2.0	<2.0	<2.0	<20.0	<2.0	<2.0	<2.0	<2.0
NO_3-N	<2.0	<2.0	<2.0	<2.0	<2.0	<2.0	<2.0	<2.0
PO_4^{-3}	<10	<10	<10	<10	<10	<10	<10	<10
SO_4^{-2}	10600	7970	19700	7440	980	7910	998	1220
pH	7.68	7.63	7.29	7.69	7.90	7.72	7.64	7.90
SAR	0.46	0.42	0.38	33.0	0.26	0.56	1.82	4.25
CEC (cmol/kg)	25.0	42.0	40.0	36.0	41.0	50.0	48.0	39.0

Notes:
- Values in mg/dry kg unless otherwise noted.
- SAR = sodium adsorption ratio.
- CEC = cation exchange capacity.
- SS BKG = Seven Sisters background section foundation clay from El. 266.5 to 266.0 m.
- SS Unstable = Seven Sisters unstable section foundation clay from El 265.9 to 265.3 m.
- Winnipeg Clay from University of Manitoba, southwest of the Frank Kennedy Centre at a depth of 6.1 m below grade.

Table 4.3. Pore fluid chemistry results.

	Reconstituted Clay						Seven Sisters Site		
Parameter	Gypsum Rich	DI Water	H_2SO_4	NaCl	Washed 1PV	Washed 6PV	Natural BKG	Natural Unstable	Forebay Water
Ca	552	548	581	2490	543	96	680	172	13.2
Cu	0.057	<0.050	0.107	2.650	0.200	0.193	--	--	<0.005
Fe	0.15	0.15	0.16	<1	0.01	<0.10	0.10	0.10	0.30
K	43	46	60	159	34	9	--	--	<1
Mg	330	312	534	1260	274	31	505	131	3.54
Mn	2.27	1.03	13.30	6.25	3.69	0.62	--	--	0.012
Na	94.1	89.6	99.0	17900	58.6	8.5	116	116	2.5
Zn	1.00	1.40	2.29	2.96	1.47	1.70	--	--	0.02
Cl-	1.3	3.1	3.6	33400	2.8	18.3	6.2	10.0	1.2
NO_2-N	<0.2	<0.2	<0.2	<20.0	<0.2	<0.2	--	--	<0.2
NO_3-N	<0.2	<0.2	<0.2	<2.0	<0.2	<0.2	--	--	<0.2
NH_3-N	0.08	<0.03	<0.03	1.58	0.16	0.12	--	--	0.04
PO_4^{-3}	<1	<1	<1	<10	<1	<1	--	--	<0.3
SO_4^{-2}	2810	2690	3380	3610	2240	224	3660	972	3.6
CO_3^{-2}	1	1	1	1	1	1	<1	<1	<1
HCO_3^-	226	184	656	171	348	167	61	88	43
pH	8.28	8.20	8.36	7.61	7.90	7.94	8.61	7.94	7.63
Alkalinity	187	153	540	142	287	139	100	145	43
DOC	35.2	35.9	34.0	52.9	22.7	11.8	--	--	9.1
TDS	3953	--	4987	58990	3328	470	--	--	54
Hardness	2741	2657	3654	11430	2489	367	--	--	47.5
Colour	110	92	92	84	60	18	--	--	50
EC	3890	3800	4590	90000	3530	685	4150	1650	96
Turbidity	1.1	1.2	1.3	3.3	0.6	0.6	--	--	7.5
Na/Ca	0.15	0.14	0.15	6.25	0.09	0.08	0.15	0.59	0.16
I	7.4×10^{-2}	7.1×10^{-2}	9.5×10^{-2}	1.2	6.6×10^{-2}	1.2×10^{-2}	9.6×10^{-2}	3.3×10^{-2}	1.5×10^{-3}
% Error	-4.5	-3.0	-4.0	-0.8	-0.4	-0.3	2.2	2.7	5.8

Notes:
- Values in mg/L unless otherwise noted.
- Alkalinity and hardness expressed as mg of $CaCO_3$/L
- Colour in TCU
- DOC = dissolved organic carbon
- TDS = total dissolved solids
- EC = electrical conductivity in µS/cm
- Turbidity in NTU
- I = Ionic strength in mol/kg
- SS Background = Seven Sisters background section foundation clay from El. 266.2 m.
- SS Unstable = Seven Sisters unstable section foundation clay from El. 266.0 m.
- Na/Ca = meq/L Na/meq/L Ca
- Percent Error = (cations-lanionsl)/(cations+lanionsl)x100%

Table 4.4. Saturation indices (SI) of common cementing minerals from PHREEQ equilibrium calculations in various pore fluids.

	Anhydrite $CaSO_4$	Gypsum $CaSO_4{:}2H_2O$	Calcite $CaCO_3$	Aragonite $CaCO_3$	Dolomite $CaMg(CO_3)_2$
Reconstituted Clay					
Gypsum Rich	-0.21	0.02	1.31	1.16	2.67
DI Water	-0.22	0.02	1.16	1.01	2.35
H_2SO_4	-0.19	0.05	1.74	1.59	3.67
NaCl	-0.05	0.14	1.32	1.18	2.77
Washed 1PV	-0.26	-0.01	1.11	0.96	2.14
Washed 6PV	-1.45	-1.23	0.58	0.44	1.02
Seven Sisters Natural Clay					
Background	-0.10	0.15	1.27	1.12	2.64
Unstable	-0.86	-0.61	0.52	0.37	1.13
Forebay Water	-3.76	-3.51	-1.03	-1.18	-2.36

Notes:
- SS Background = Seven Sisters background section foundation clay from El. 266.2 m.
- SS Unstable = Seven Sisters unstable section foundation clay from El. 266.0 m.
- Negative SI values indicate mineral dissolution
- Positive SI values indicate mineral precipitation
- SI values at zero indicate equilibrium conditions

Table 4.5. Example of yielding interpreted from multiple plots (CID test AMR1-T10).

	Interpreted Yield Point					
Plot Type	ε_{1y} (%)	σ_{1y}' (kPa)	q_y (kPa)	p_y' (kPa)	ε_v (%)	σ_1'/σ_{3y}'
σ_1' versus ε_1	4.0	237	136	146	2.3	2.4
p' versus ε_v	3.5	233	131	145	2.1	2.3
q versus ε_1	4.3	238	138	145	2.5	2.4
σ_1'/σ_3' versus ε_1	4.4	239	139	147	2.5	2.4
ε_v versus ε_1	3.5	233	131	145	2.1	2.3
Average	3.9	236	135	146	2.3	2.3

Table 4.6. Summary of oedometer results.

Clay Type	σ_{zc}' (kPa)	C_c	C_r	C_c/C_r
Gypsum Rich	180	0.75	0.10	7.5
DI Water	185	0.73	0.11	9.8
H_2SO_4	190	0.69	0.12	5.9
NaCl	195	0.75	0.11	7.0
Washed 1PV	190	0.73	0.12	6.2
Washed 6PV	180	0.80	0.11	7.1
Natural Background	266	0.36	0.12	3.1
Natural Unstable	383	0.52	0.12	4.3

Table 4.7. Yielding data (kPa).

Specimen	Test Type/Pressure (kPa)	Yield Point (Inner, Outer) p'	q	V	Normalizing Parameters p'_e	p'_c	σ'_{zc}
AMR1,2 Gypsum Rich							
AMR1-T7	CIU @ 100	106, 101	121, 138	2.577, 2.577	134	131	180
AMR1-T8	CIU @ 100	111, 93	134, 134	2.556, 2.556	145	131	180
AMR1-T10	CID @ 100	132, 145	98, 138	2.646, 2.589	128	131	180
AMR1-T11	Iso Con 325, CIU @ 325	130, 135	0, 0	2.625, 2.618	114	131	180
AMR1-T47	CIU @ 100	101, 108	116, 132	2.641, 2.624	111	131	180
AMR2-T12	CIU @ 100	91, 98	109, 121	--	--	131	180
AMR2-T13	CIU @ 100	99, 101	113, 133	--	--	131	180
AMR2-T14	CID @ 100	122, 136	80, 115	2.637, 2.603	121	131	180
AMR2-T15	Iso Con to 3363	125, 127	0, 0	2.585, 2.558	144	131	180
AMR2-T16	Iso Con 350, CIU @ 350	125, 130	0, 0	2.676, 2.600	122	131	180
AMR2-T23	Constant p' = 100	96, 100	103, 115	--	--	131	180
AMR2-T29	Constant p' = 100	96, 100	108, 125	2.603, 2.603	121	131	180
AMR2-T30	Ko to 350, CAU @350	155, 175	40, 46	2.611, 2.596	124	131	180
AMR2-T37	Lateral Expansion from 100	67, 56	55, 77	2.653, 2.683	88	131	180
AMR2-T39	Lateral Expansion from 100	60, 53	58, 69	2.640, 2.685	88	131	180
AMR2-T42	q/p' = 1.25 from 100	165, 170	82, 88	2.579, 2.579	133	131	180
AMR1-O4	Oedometer	153	39	2.534	158	131	180
AMR1-O5	Oedometer	152	39	--	--	131	180
AMR2-O7	Oedometer	137, 154	35, 41	2.541, 2.541	154	131	180
AMR1-O14	Oedometer	141, 153	36, 40	2.594, 2.594	125	131	180
AMR1 Freeze/Thaw							
AMR1-T48	CIU @ 100	83, 78	55, 78	2.433, 2.433	--	110	--
AMR1-T49	CID @ 100	128, 131	78, 99	2.272, 2.253	--	110	--
AMR1-T50	Iso Con 350, CIU @ 350	90, 110	0, 0	2.369, 2.330	--	110	--
AMR3 DI Water							
AMR3-T17	Iso Con 350, CIU @ 350	125, 130	0, 0	2.629, 2.629	109	130	180
AMR3-T27	CIU @ 100	103, 103	115, 124	2.622, 2.605	120	130	180
AMR3-T35	CID @ 100	127, 141	85, 127	2.559, 2.537	156	130	180
AMR3-T56	Constant p'=100	95, 100	114, 127	2.612, 2.612	117	130	180
AMR3-O8	Oedometer	145, 149	37, 39	2.498, 2.498	182	130	180
AMR3-O13	Oedometer	142, 153	37, 40	2.518, 2.518	168	130	180
AMR4 H2SO4							
AMR4-T22	CID @ 100	125, 140	74, 120	2.574, 2.560	165	135	190
AMR4-T24	Iso Con 350, CIU @ 350	130, 135	0, 0	2.597, 2.597	147	135	190
AMR4-T25	CIU @ 100	109, 109	104, 126	2.614, 2.560	165	135	190
AMR4-T26	Constant p' = 100	96, 100	108, 120	2.566, 2.571	159	135	190
AMR4-O11	Oedometer	158, 162	41, 42	2.563, 2.563	164	135	190

Table 4.7. Yielding data (kPa), continued.

Specimen	Test Type/Pressure (kPa)	Yield Point (Inner, Outer) p'	q	V	Normalizing Parameters p'_e	p'_c	σ'_{zc}
AMR6 NaCl							
AMR6-T40	Constant p'=100	96, 100	112, 127	2.574, 2.574	90	135	195
AMR6-T41	CID @ 100	125, 136	70, 115	2.551, 2.519	117	135	195
AMR6-T43	Iso Con 350, CIU @ 350	125, 135	0, 0	2.495, 2.495	131	135	195
AMR6-T45	CIU @ 100	104, 105	126, 137	2.551, 2.551	100	135	195
AMR6-O15	Oedometer	153, 171	40, 44	2.494, 2.494	131	135	195
AMR5, 7 Washed							
AMR5-T38 (1.1PV)	CID @ 100	133, 141	94, 123	2.552, 2.531	--	--	--
AMR5-O12 (1.1PV)	Oedometer	138, 162	35, 42	2.495, 2.474	--	--	--
AMR7-T51	CIU @ 100	93, 94	58, 91	2.792, 2.755	135	120	180
AMR7-T52	CID @ 100	119, 137	60, 100	2.761, 2.739	143	120	180
AMR7-T53	Constant p'=100	96, 100	88, 100	2.764, 2.764	131	120	180
AMR7-T54	Iso Con 350, CIU @ 350	110, 120	0, 0	2.775, 2.775	127	120	180
AMR7-T55	CID @ 100	115, 131	50, 96	2.758, 2.758	134	120	180
AMR7-O16	Oedometer	137, 145	35, 37	2.709, 2.709	158	120	180
Seven Sisters Background							
SS2.9A-T1	CIU @ 100	92, 96	67, 82	--	--	180	266
SS3.8D-T18	Iso Con 670, CIU @ 670	160, 170	0, 0	2.599, 2.586	191	180	266
SS3.6D-T19	CID @ 100	136, 140	108, 119	2.544, 2.544	237	180	266
SS3.5D-T32	Constant p' = 100	96, 100	96, 117	2.603, 2.603	176	180	266
SS3.9E-T33	Iso Con 3363, CIU @ 500	175, 190	0, 0	2.563, 2.563	215	180	266
SS3.9D-T36	Ko to 350, CAU @ 350	155, 165	40, 42	2.509, 2.509	283	180	266
SS3.5E-T46	q/p' = 1.25 from 100	164, 169	82, 87	2.490, 2.490	311	180	266
SS3.5A-O2	Oedometer	171, 178	44, 46	2.575, 2.575	202	180	266
SS3.7D-O9	Oedometer	138, 197	36, 51	2.513, 2.513	277	180	266
Seven Sisters Unstable							
Garinger, 2002	CIU @ 200	142, 142	113, 137	2.402, 2.402	214	280	383
Garinger, 2002	CIU @ 100	76, 76	42, 42	2.509, 2.509	112	280	383
SS10.7U-T20	CID @ 100	127, 167	85, 187	2.376, 2.376	251	280	383
SS11.9U-T31	Iso Con 350, CIU @ 350	175, 200	0, 0	2.330, 2.330	332	280	383
SS10.7U-T34	Constant p' = 100	96, 100	68, 85	2.588, 2.422	190	280	383
SS10.7U-T44	Iso Con ICL, CIU @ 500	250, 280	0, 0	2.369, 2.356	283	280	383
SS10.7U-O10	Oedometer	234, 299	60, 77	2.403, 2.277	458	280	383
Garinger, 2002	Oedometer	271, 271	70, 70	2.270, 2.270	478	280	383

Table 4.8. Isotropic elastic parameters.

	Reconstituted Clay							Natural Clay		
Parameter	Gypsum Rich	Gypsum Rich F/T	DI Water	H_2SO_4	NaCl	Washed 1PV	Washed 6PV	SS BKG	SS Unstable	Winnipeg
E (kPa)	13200	14300	10400	9400	8200	7500	5500	12300	7700	--
G (kPa)	14500	13900	10400	10200	8200	7600	5700	8600	7800	1000
K (kPa)	1300	670	830	1300	1400	--	400	3900	1800	3400

Table 4.9. Anisotropic elastic parameters.

Clay Type	Number of Tests	K/p_c'	$3G/p_c'$	J/p_c'
Reconstituted:				
Gypsum Rich	5	19.2	44.8	1.2
DI Water	2	112.3	105.3	-7.7
H_2SO_4	2	80.6	30.7	0.6
NaCl	2	32.9	111.0	-2.8
Washed 6PV	2	16.5	108.9	-1.3
Natural:				
Seven Sisters Background	4	15.6	33.4	-7.3
Seven Sisters Unstable	2	21.8	35.3	0.6
Winnipeg Clay	4-5	18.2	32.1	-6.9

Table 4.10. Hardening law.

	Reconstituted Clay							Natural Clay		
Parameter	Gypsum Rich	Gypsum Rich F/T	DI Water	H_2SO_4	NaCl	Washed 1PV	Washed 6PV	SS BKG	SS Unstable	SS Stable
K	0.052	0.120	0.074	0.060	0.059	--	0.085	0.071	0.060	--
λ	0.32	0.21	0.30	0.27	0.27	--	0.30	0.18	0.16	--

Table 4.11. Failure criterion.

Parameter	Reconstituted Clay							Natural Clay		
	Gypsum Rich	Gypsum Rich F/T	DI Water	H_2SO_4	NaCl	Washed 1PV	Washed 6PV	SS BKG	SS Unstable	SS Stable
M_{cs}	0.51	0.52	0.51	0.51	0.57	--	0.50	0.50	0.50	0.53
Φ'_{cs}	13.6	13.9	13.6	13.6	15.1	--	13.3	13.3	13.3	14.1
Mr	0.47	0.51	0.46	0.50	0.57	--	0.50	0.39	0.38	0.39
Φ'_r	12.6	13.6	12.3	13.3	15.1	--	13.3	10.6	10.3	10.7

Table 6.1. Coupled processes in clay soils (after Mitchell, 1993).

Flux	Potential Gradient			
	Temperature	Hydraulic	Electrical	Chemical
Heat	Thermal conduction (Fourier's Law)	Isothermal heat transfer	Peltier effect	Dufour effect
Fluids	Thermo-osmosis	Hydraulic conduction (Darcy's Law)	Electro-osmosis	Normal osmosis
Current	Thermo-electricity	Streaming current	Electrical conduction (Ohm's Law)	Diffusion and membrane potentials
Ions	Soret effect	Streaming current	Electrophoresis	Diffusion (Fick's Law)

Table 6.2. Geochemical Modelling Input Parameters.

Parameter	Value/Range	Comments
Time Step	1.7×10^9 s,	From: $K = 2 \times 10^{-9}$ - 2×10^{-7} m/s,
(Residence time per 2m cell)	1.7×10^8 s,	n = 0.6,
	1.7×10^7 s	i = 3.5 m head drop/20 m
Diffusion Coefficient	2×10^{-10} m^2/s	Assumed (Fetter, 1999)
Dispersivity	2 m, 10 m, 20 m	Assumed (Walton, 1988)
Initial Pore Fluid Chemistry	Table 4.3	Natural background location
Permeating Fluid Chemistry	Table 4.3	Forebay water

Table 6.3. Seepage and Mass Transport Modelling Input Parameters.

Parameter	Value/Range
K_{sat} Dyke	$5 \times 10^{-11} - 5 \times 10^{-8}$ m/s
	(See Figure 6.3 for unsaturated K function)
K_{sat} Upper Foundation Clay	$2.2 \times 10^{-11} - 2.2 \times 10^{-8}$ m/s
K_{sat} Lower Foundation Clay/Till	$2.9 \times 10^{-11} - 2.9 \times 10^{-8}$ m/s
K_y/K_x Upper Foundation Clay	1, 0.1, 0.01
Dispersivity	10 m

Note: - First listed value was used for base case.

Table 6.4. Stress-Deformation Modelling Input Parameters.

	Riprap shell	Embankment		Upper Foundation Clay		Lower Foundation Clay	
	SS-036 SS-040	SS-036	SS-040	SS-036	SS-040	SS-036	SS-040
Model	Linear elastic	Elastic-Plastic		Strain-softening (top 1m), Modified Cam-Clay		Elastic-Plastic	
E (MPa)	300	15	17	5.5	5.5	15	17
ν	0.35	0.45	0.45	0.45	0.45	0.45	0.45
γ (kN/m^3)	18	19	20	17	18	19	20
c (kPa)	n/a	35	20	n/a	n/a	35	20
ϕ (degrees)	n/a	23	24	n/a	n/a	23	24
$s_{u\,peak}$ (kPa)	n/a	n/a	n/a	136	138	n/a	n/a
$s_{u\,residual}$ (kPa)	n/a	n/a	n/a	95	120	n/a	n/a
Strain-softening rate (kPa/unit strain)	n/a	n/a	n/a	2000	650	n/a	n/a
OCR	n/a	n/a	n/a	1, 2, 2.3, 2.5, 3	1, 2, 2.3, 2.5, 3	n/a	n/a
M	n/a	n/a	n/a	1.1, 1.33, 1.5	1.1, 1.33, 1.5	n/a	n/a
Γ	n/a	n/a	n/a	1.7	1.7	n/a	n/a
λ	n/a	n/a	n/a	0.16	0.16	n/a	n/a
κ	n/a	n/a	n/a	0.07	0.07	n/a	n/a

Note: - SS-036 = Unstable section
- SS-040 = Stable section
- Base case for Modified Cam-Clay used an OCR = 2.5 with an M = 1.5

Table 6.5. Slope Stability Modelling Input Parameters.

	Unstable Section				Stable Section			
	γ_{sat} (kN/m^3)	C' (kPa)	Φ' (post-peak)	Φ' (residual)	γ_{sat} (kN/m^3)	C' (kPa)	Φ' (post-peak)	Φ' (residual)
Rip-rap Shell	18	0	35	-	18	0	35	-
Dyke Fill	19	20	23	-	20	20	24	-
Upper Foundation	17	5	13	9	18	5	14	9
Lower Foundation	19	20	23	-	20	20	24	-

Table 6.6. Slope Stability Modelling Results.

Upper Foundation Model		FS for Stable Section			FS for Unstable Section		
		Φ'=14°	Φ'=9°	Φ'=14° & 9°	Φ'=13°	Φ'=9°	Φ'=14° & 9°
MCC							
OCR	M						
1.0	1.33	1.19	1.00	-	1.07	0.93	-
2.3	1.1	1.19	1.00	1.07	1.07	0.93	0.95
2.5	1.5	1.19	1.00	1.07	1.06	0.93	0.95
3.0	1.33	1.18	0.99	-	1.06	0.925	-
Strain-softening		1.24	1.04	-	1.17	1.01	-

Note: - MCC = Modified Cam-Clay
- Φ'=14° & 9° models were zoned with 9° specified for yielded areas of the upper foundation clay

Table 7.1. Slope Stability Modelling Results with Excess Pore Water Pressure ($\Delta u = m\Delta p'$) Using Post-Peak Strengths in the Upper Foundation Clay.

Factor of Safety	m = 1.0	m = 0.5	m = 0.25
Stable Section	0.85	1.02	1.11
Unstable Section	0.83	0.94	1.01

FIGURES

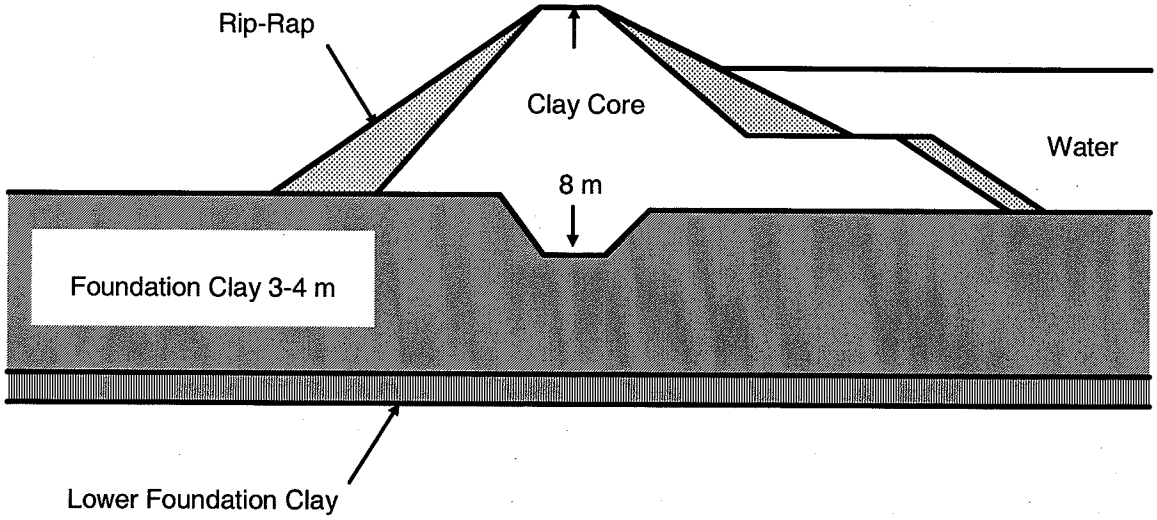

Figure 1.1. Cross-section of dyke.

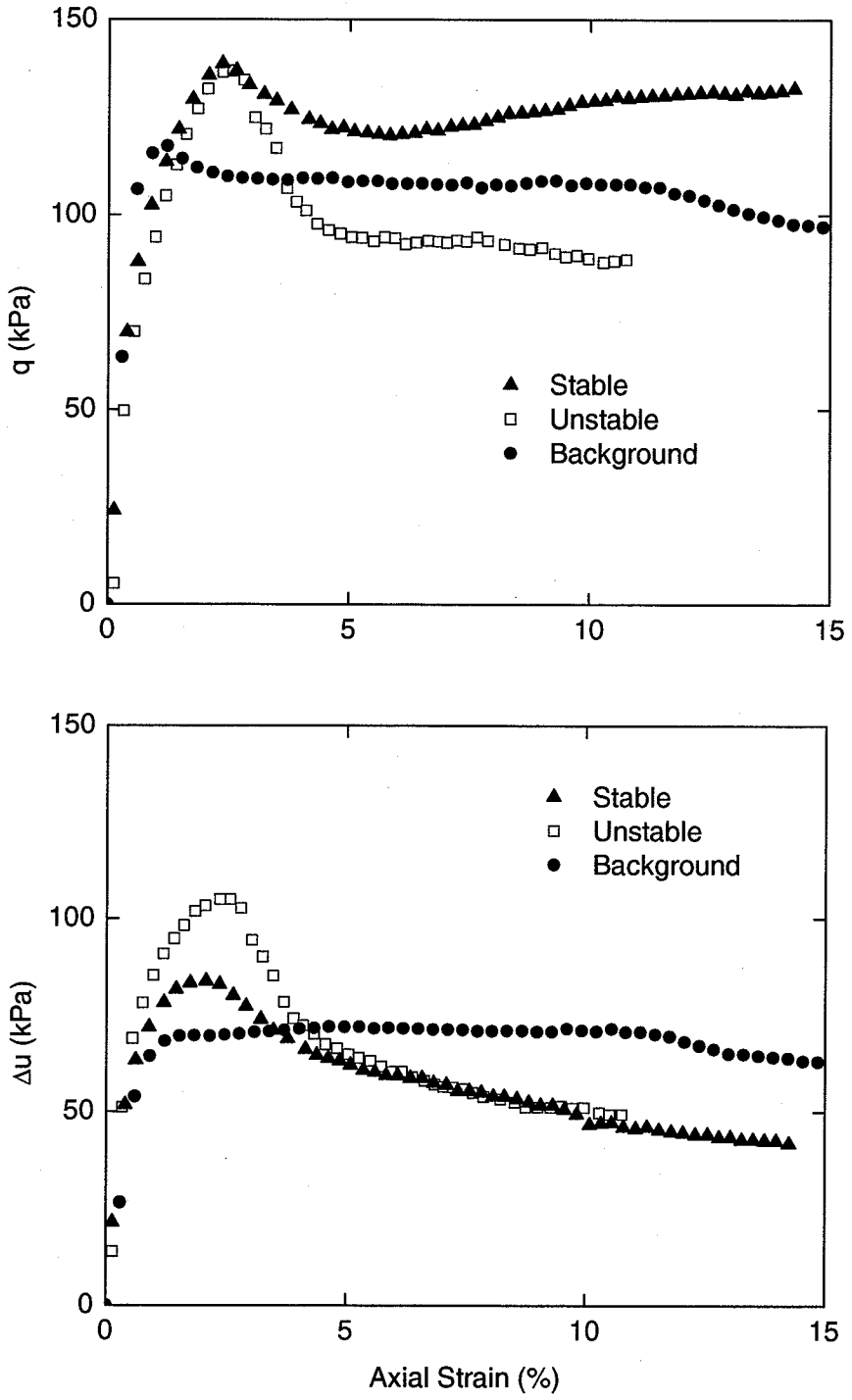

Figure 1.2. Deviator stress and change in pore water pressure versus axial strain for the stable, unstable and background sections.

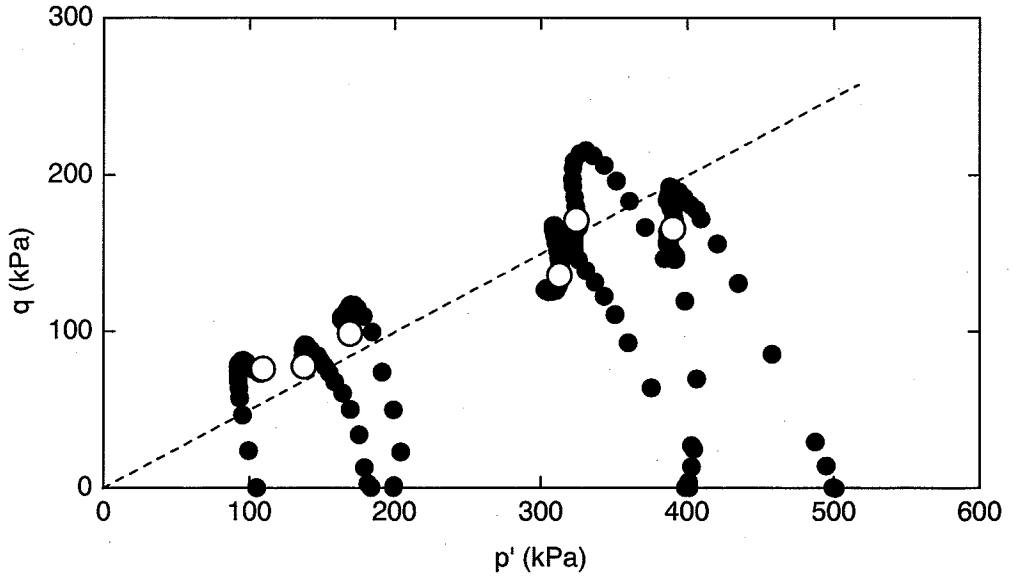

Figure 1.3. CIŪ triaxial test results for the background section.

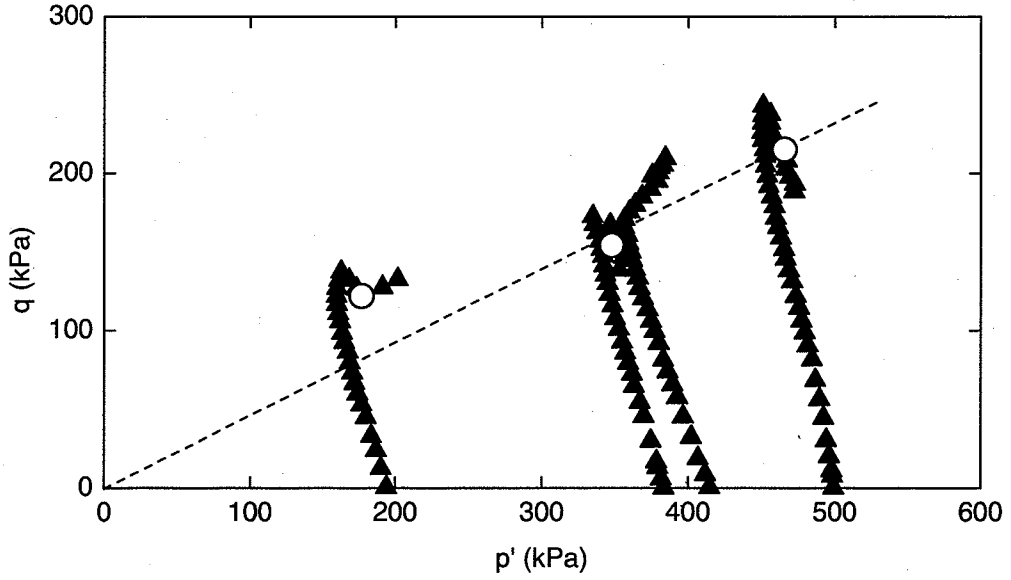

Figure 1.4. CIŪ triaxial test results for the stable section.

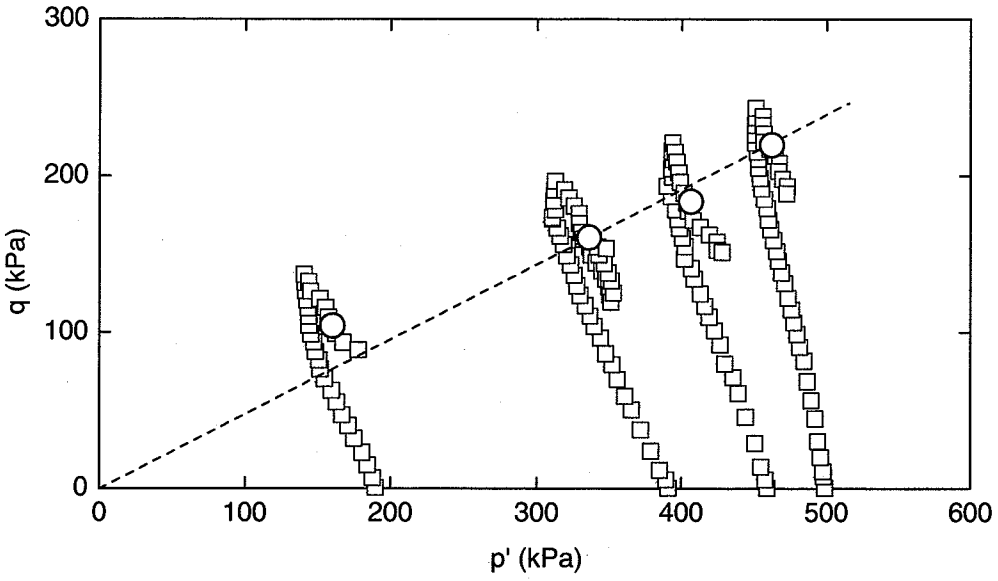

Figure 1.5. CIŪ triaxial test results for the unstable section.

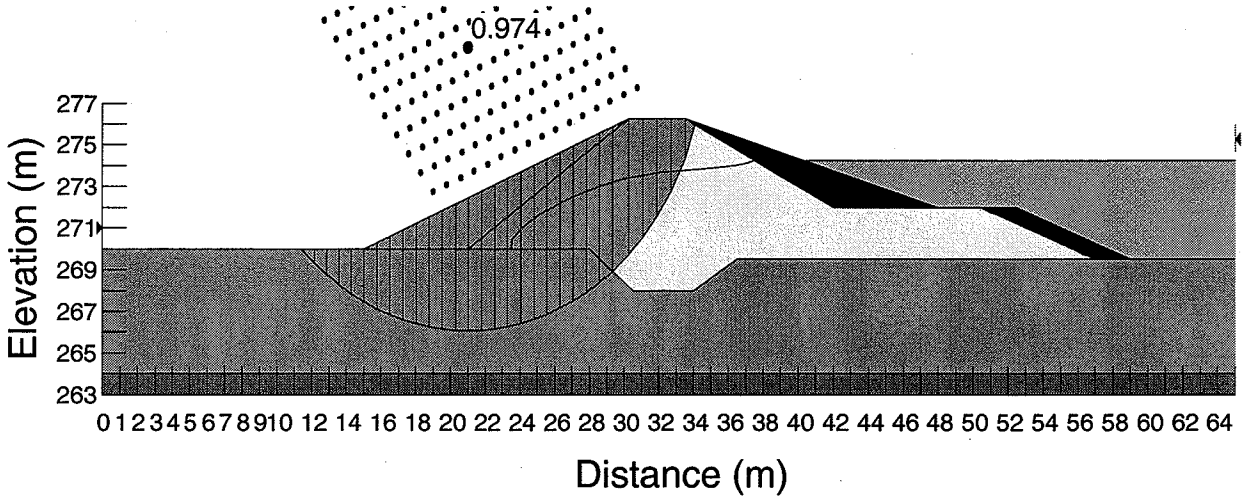

Figure 1.6. Slope stability analysis for the unstable section with input from stress-deformation analysis and residual strength parameters in the upper foundation clay (after Garinger, 2002).

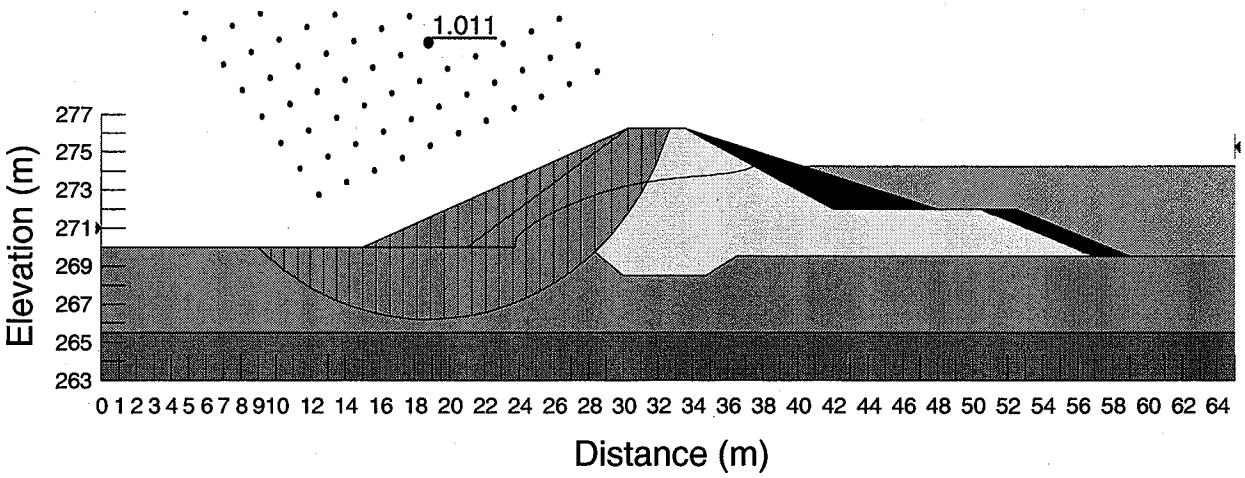

Figure 1.7. Slope stability analysis for the stable section with input from stress-deformation analysis and residual strength parameters in the upper foundation clay (after Garinger, 2002).

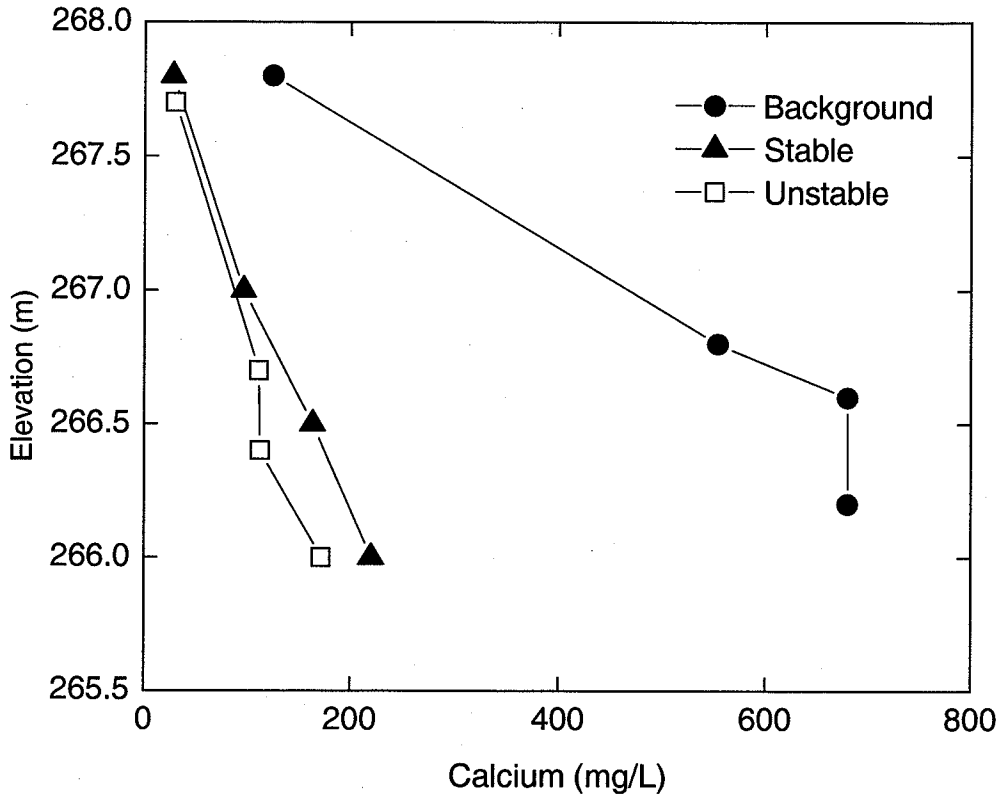

Figure 1.8. Calcium concentration versus elevation.

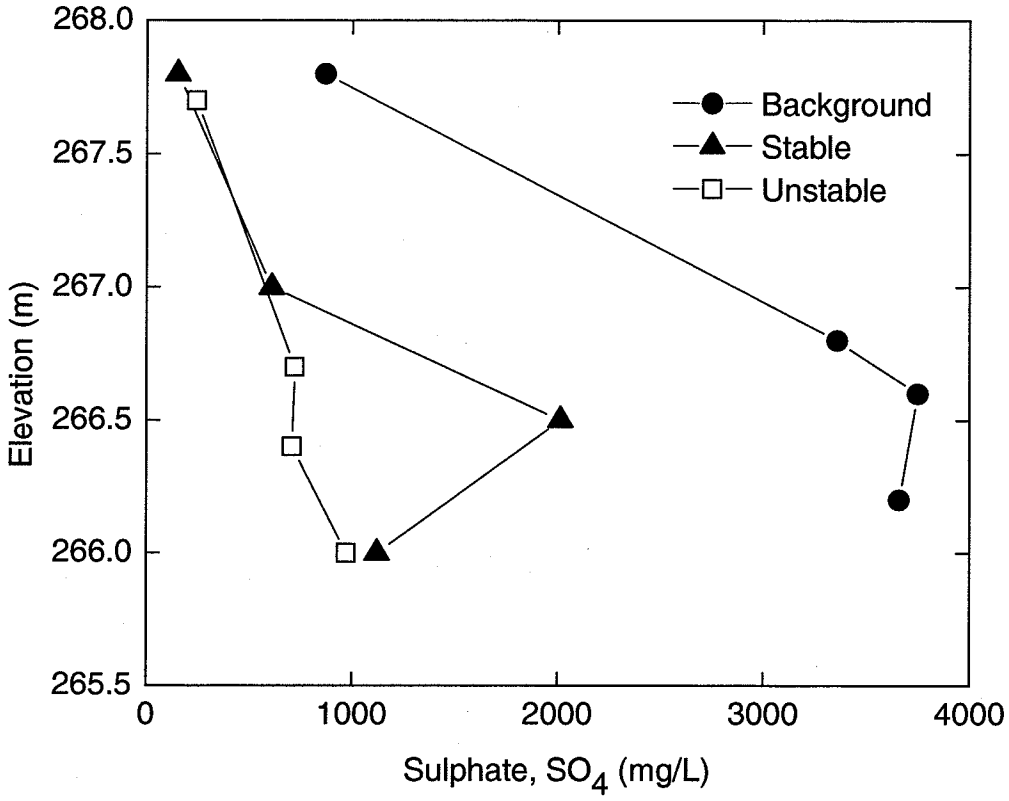

Figure 1.9. Sulphate concentration versus elevation.

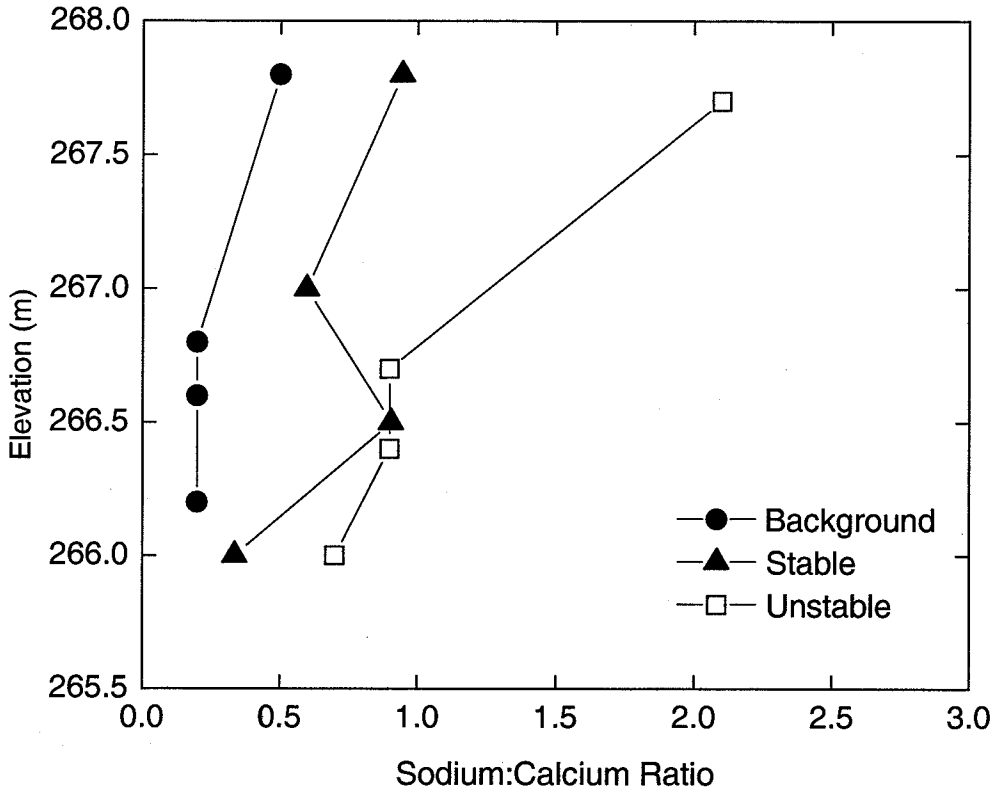

Figure 1.10. Sodium to calcium ratio versus elevation.

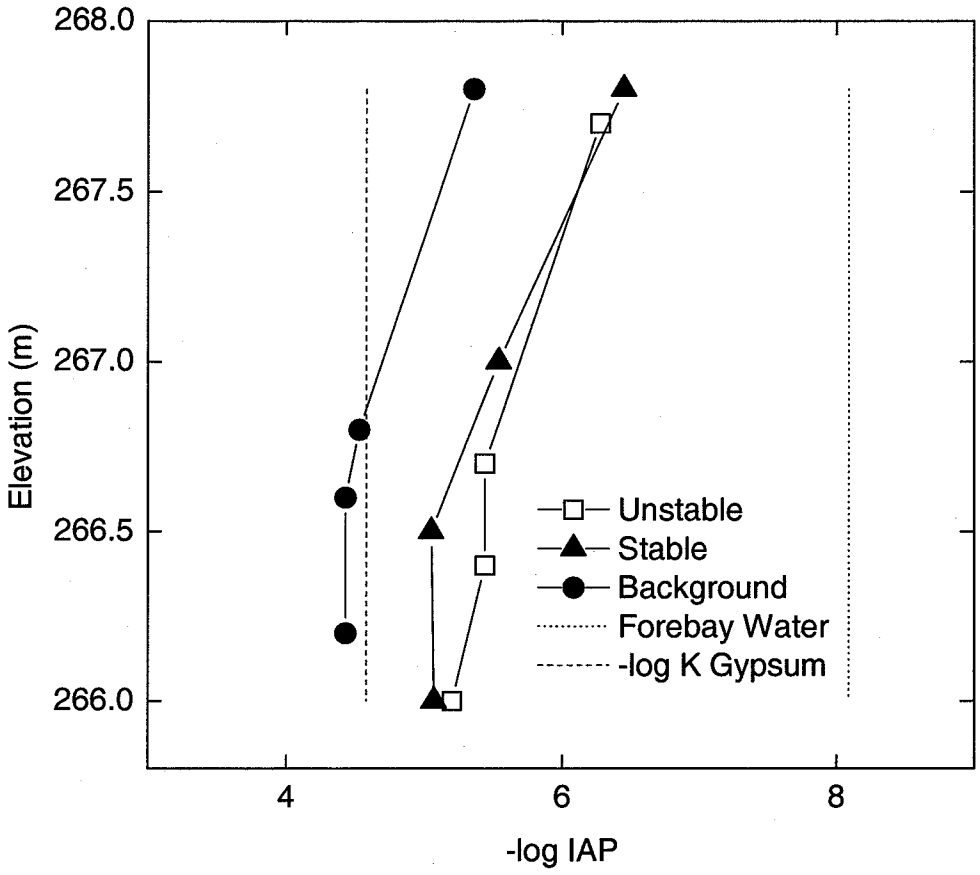

Figure 1.11. Ion activity product (IAP) for gypsum versus elevation.

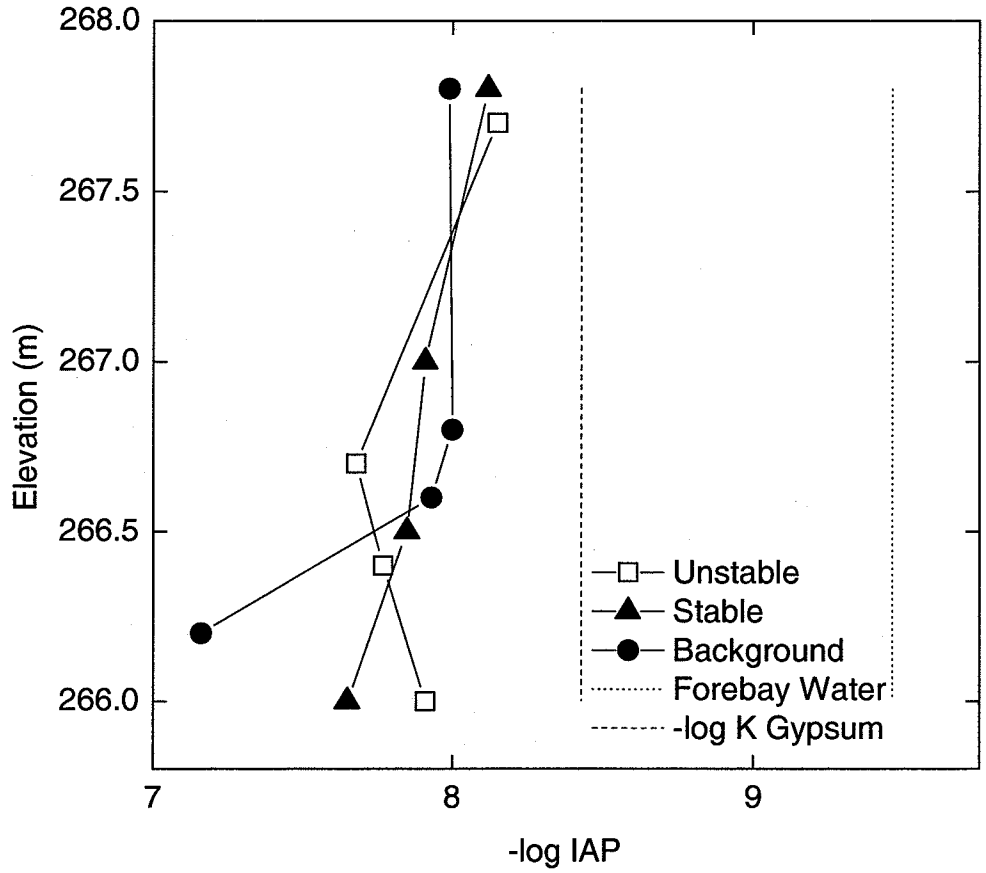

Figure 1.12. Ion activity product (IAP) for calcite versus elevation.

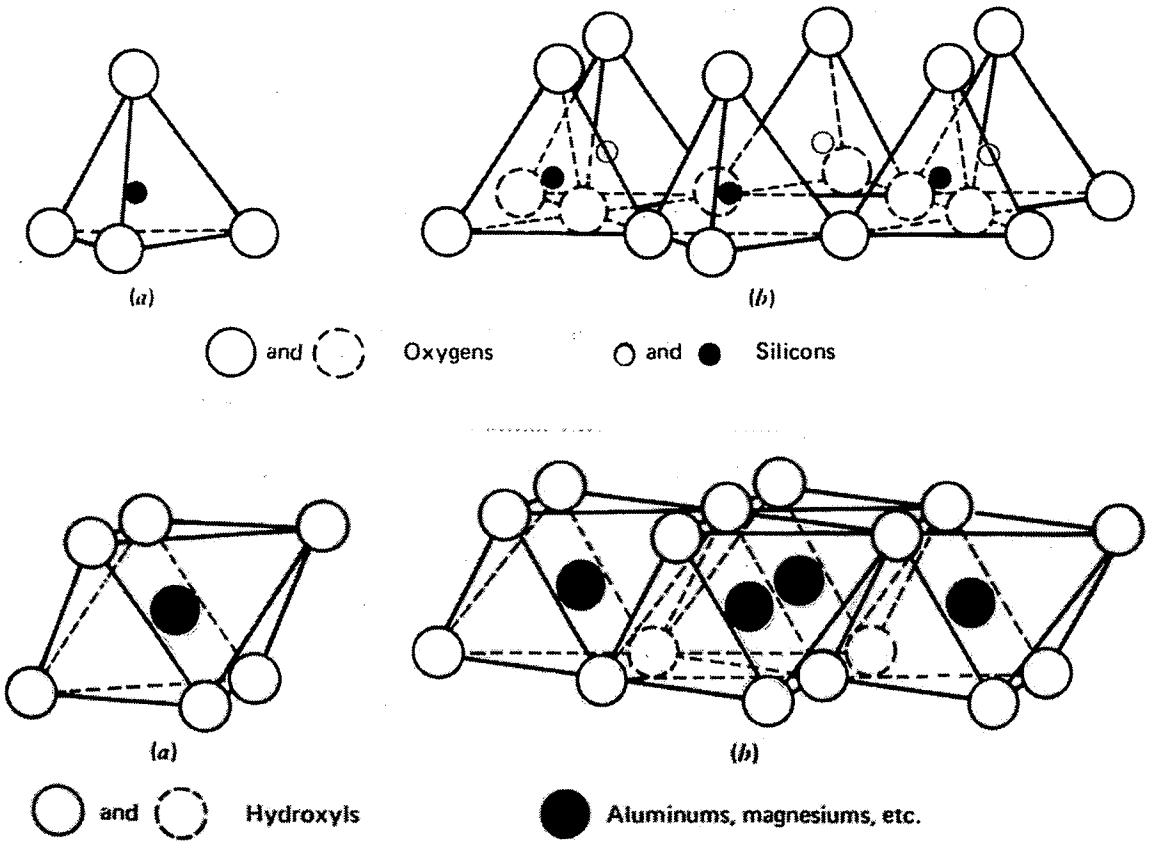

Figure 2.1. The basic silica tetrahedral and aluminum octahedral units (after Mitchell, 1993).

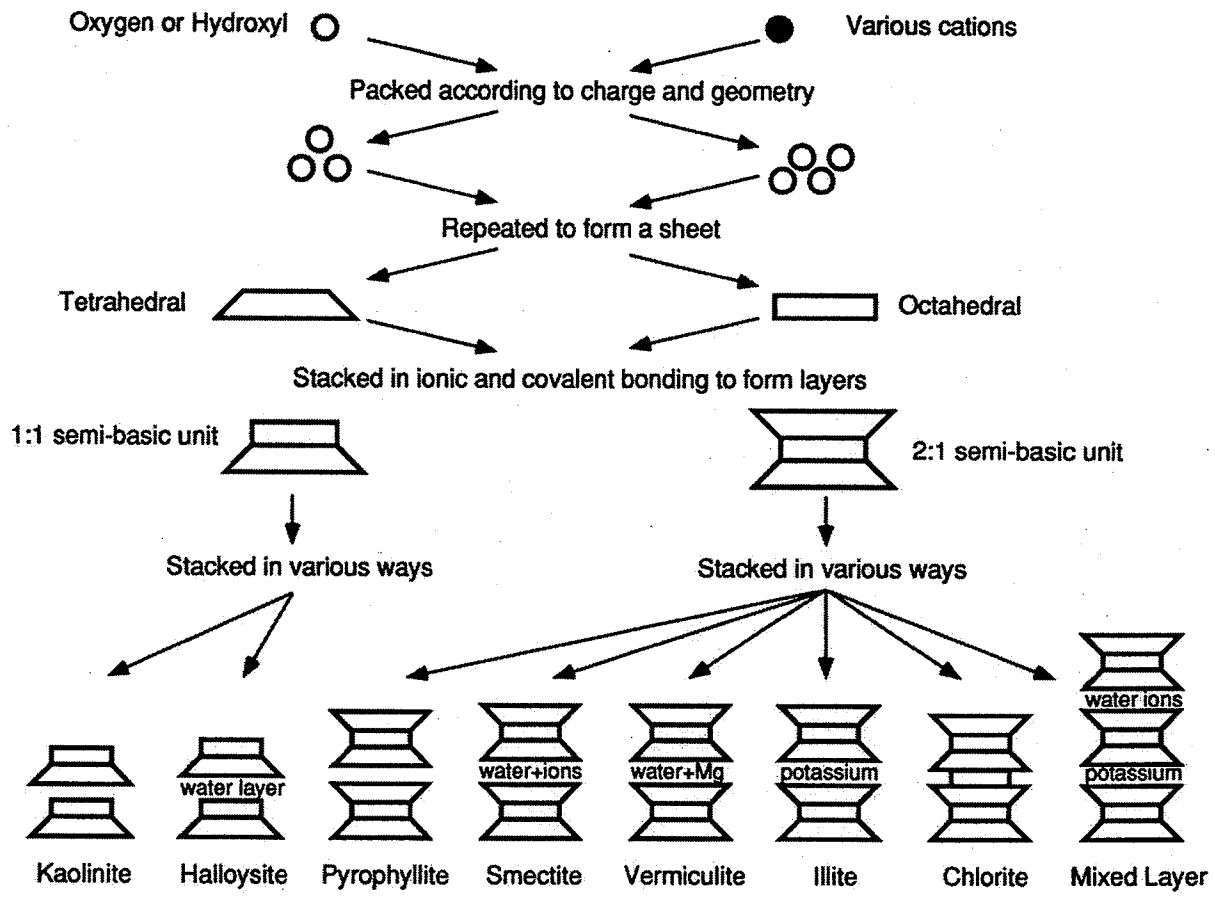

Figure 2.2. Clay minerals (after Mitchell, 1993).

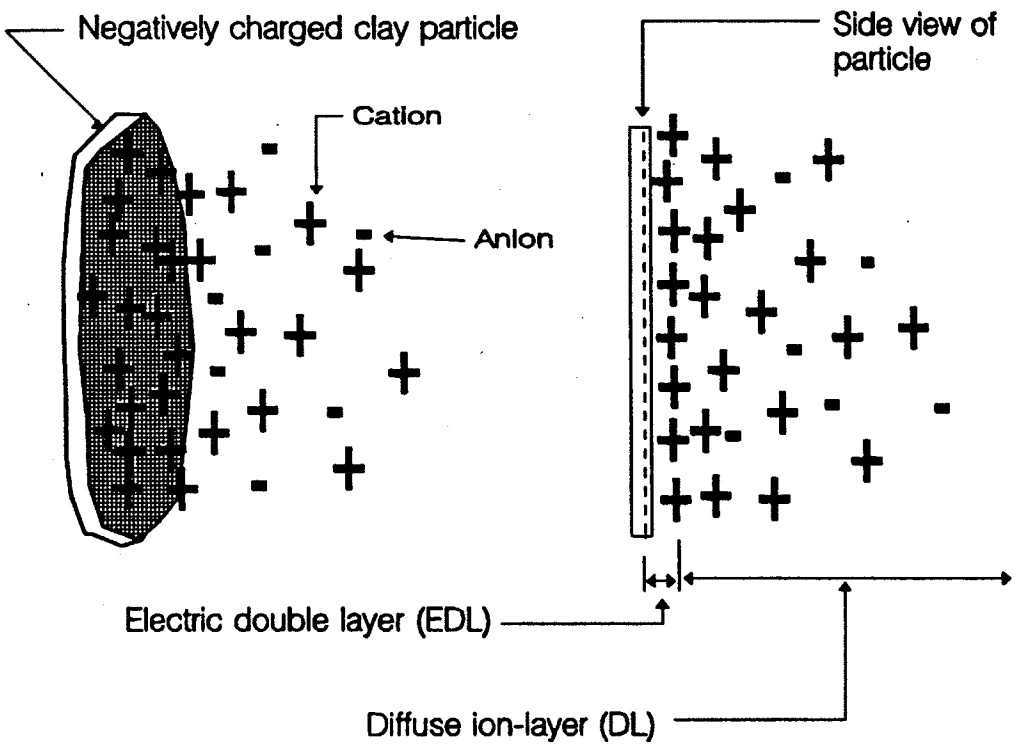

Figure 2.3. The DDL model showing a negatively charged clay particle interacting with ions in a clay-water-electrolyte system (after Yong et al, 1992).

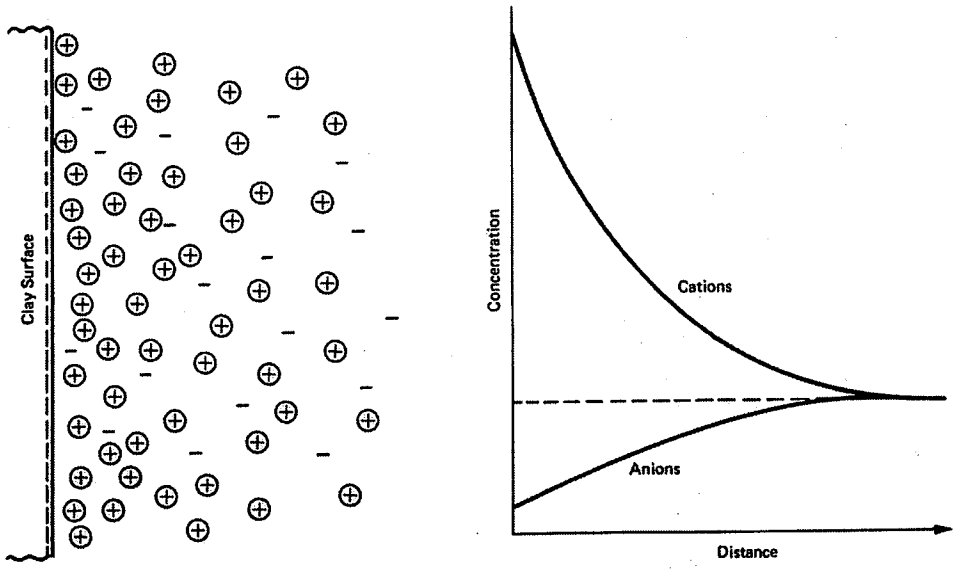

Figure 2.4. The distribution of ions in the DDL (after Mitchell, 1993).

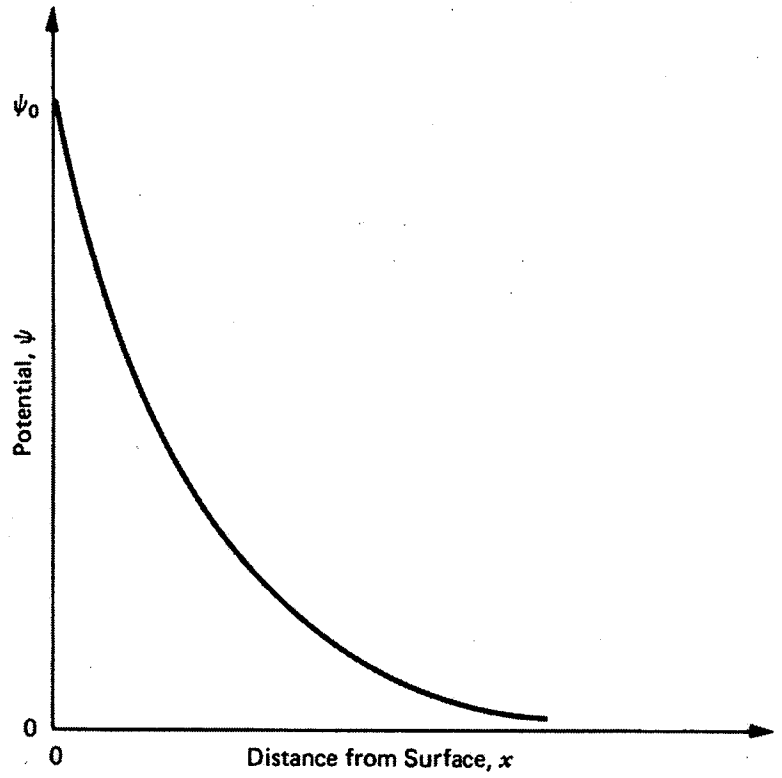

Figure 2.5. The variation of electrical potential with distance from the surface of a charged clay particle (after Mitchell, 1993).

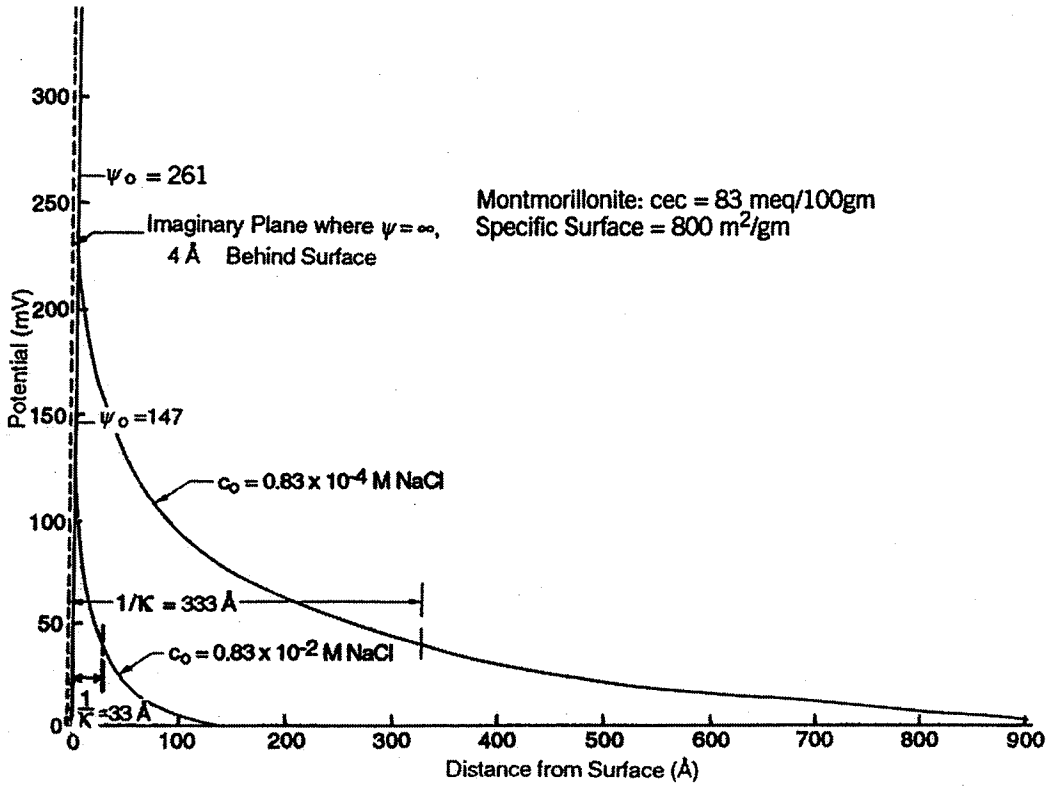

Figure 2.6. The influence of ion concentration on DDL thickness (after Mitchell, 1993).

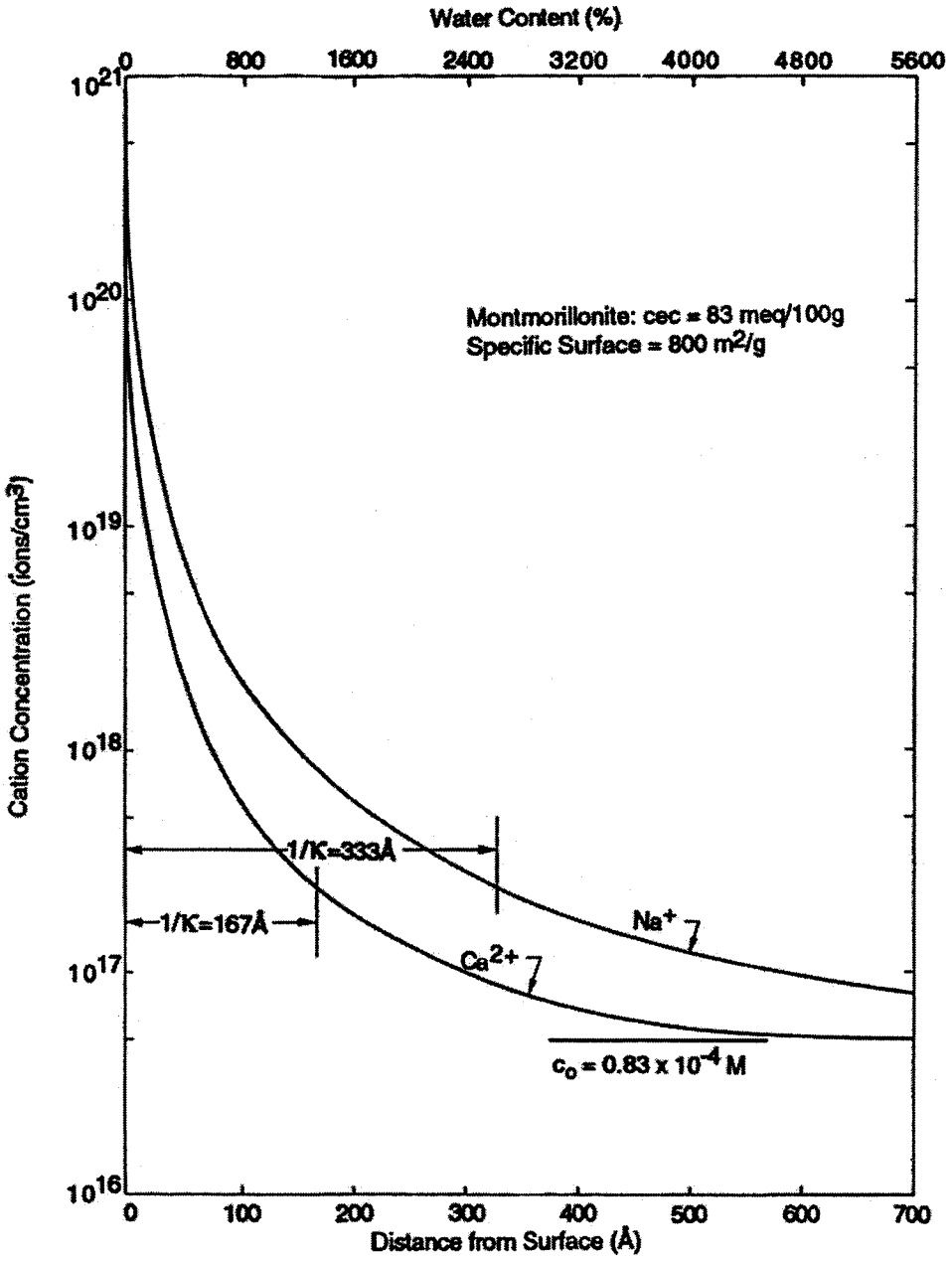

Figure 2.7. The influence of valence on DDL thickness (after Mitchell, 1993).

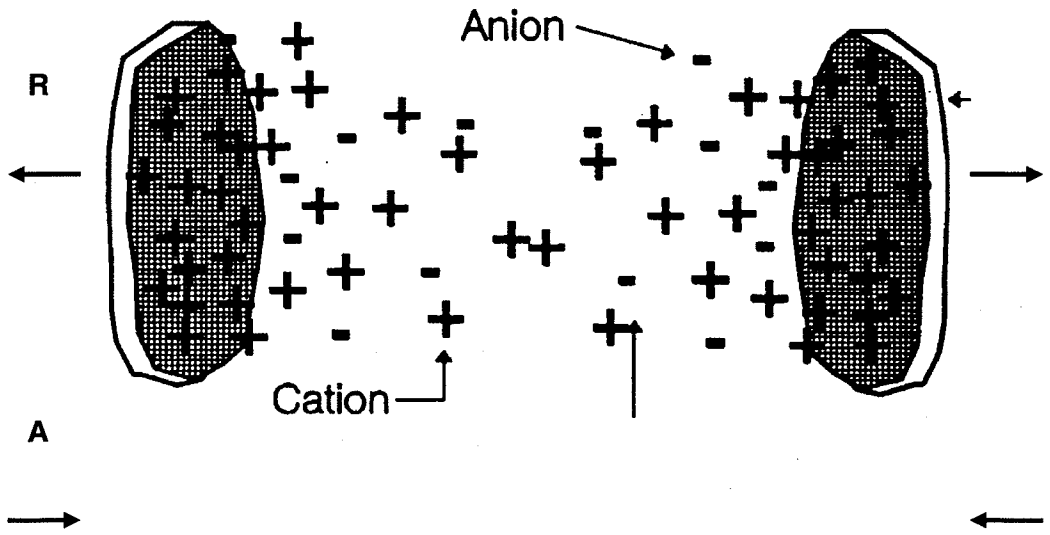

Figure 2.8. Stresses acting between two facing clay particles (after Yong et al, 1992).

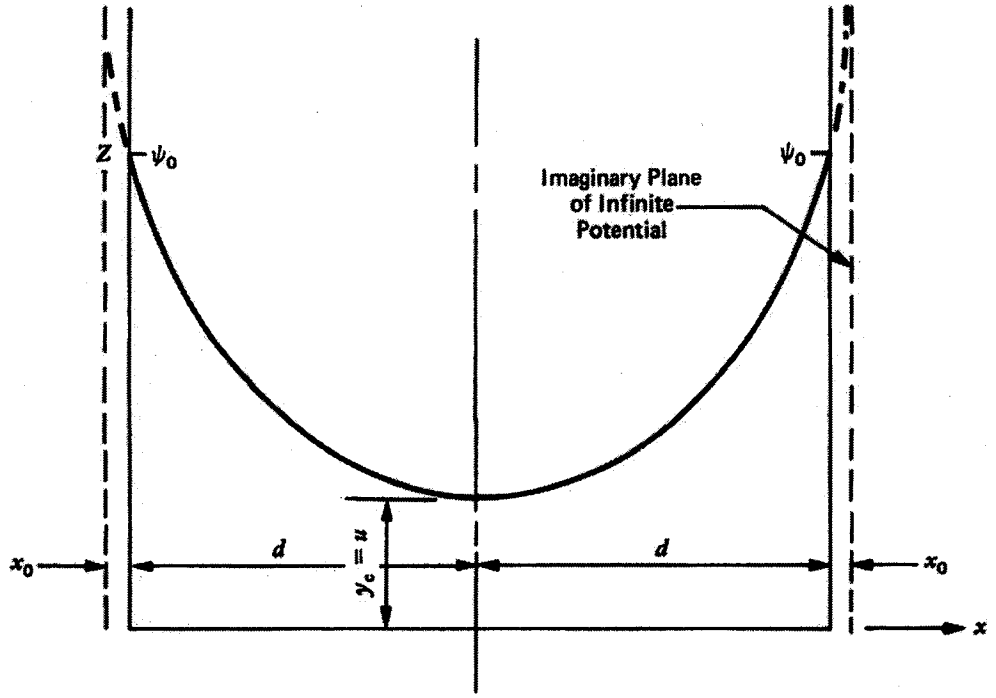

Figure 2.9. Overlap of potential fields between clay particles (after Mitchell, 1993).

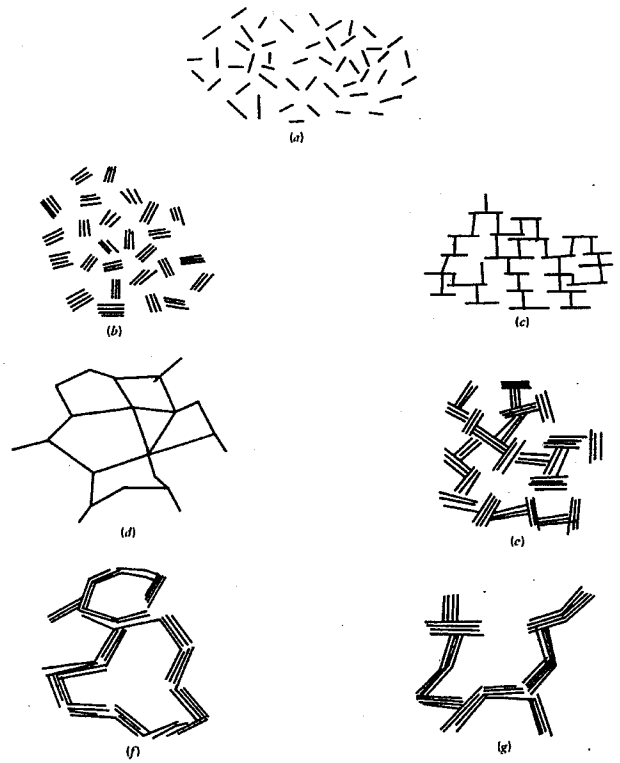

Figure 2.10. Particle arrangements in clay suspensions: (a) dispersed and deflocculated, (b) face to face aggregated but deflocculated, (c) edge to face flocculated but dispersed, (d) edge to edge flocculated but dispersed, (e) edge to face flocculated and aggregated, (f) edge to edge flocculated and aggregated, (g) edge to face and edge to edge flocculated and aggregated (after Mitchell, 1993).

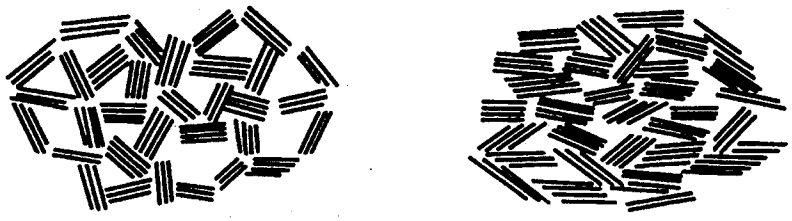

(c)

Figure 2.11. Particle arrangement within an aggregate of natural clay (after Mitchell, 1993).

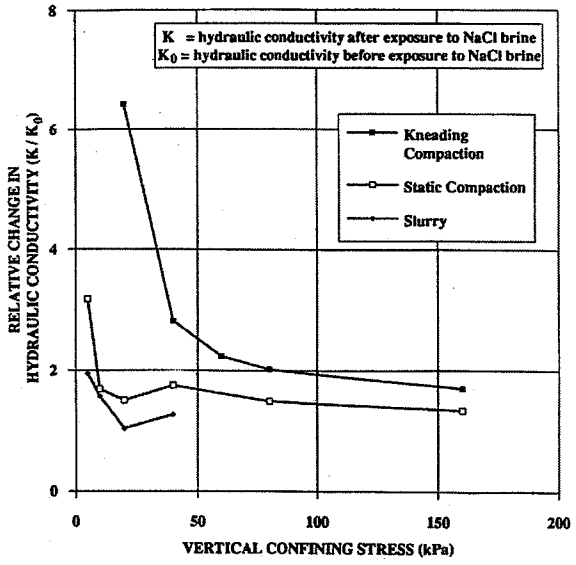

Figure 2.12. Variation in hydraulic conductivity versus. confining stress for compacted and slurry clay specimens (after Barbour and Yang, 1993).

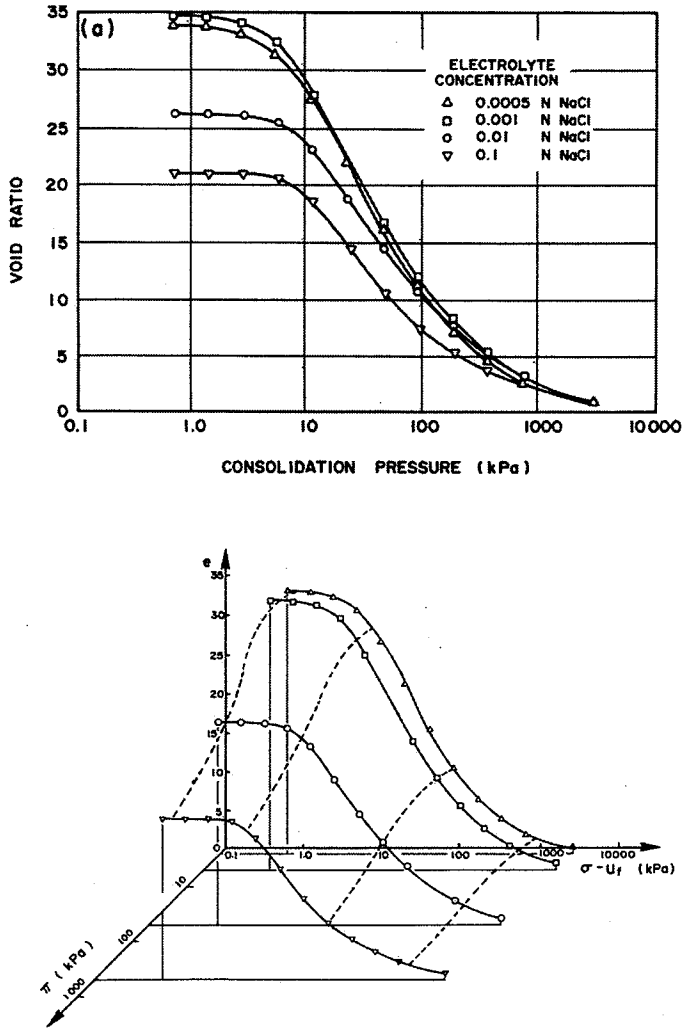

Figure 2.13. Consolidation curves for Na-montmorillonite containing a range of electrolyte concentrations (after Mesri and Olson, 1971; Barbour and Fredlund, 1989).

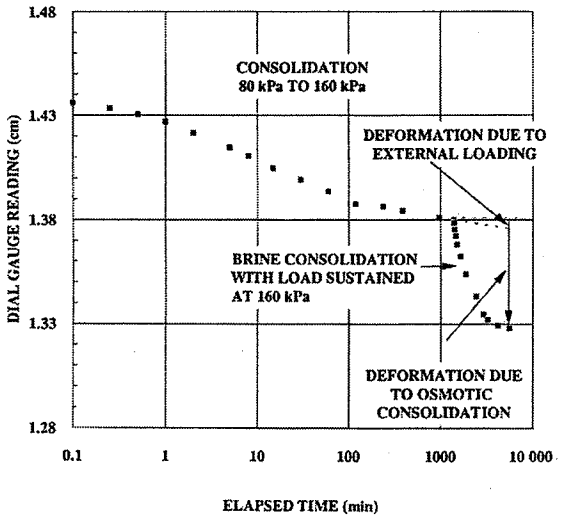

Figure 2.14. Consolidation curve for a specimen as it is permeated with brine (Barbour and Yang, 1993).

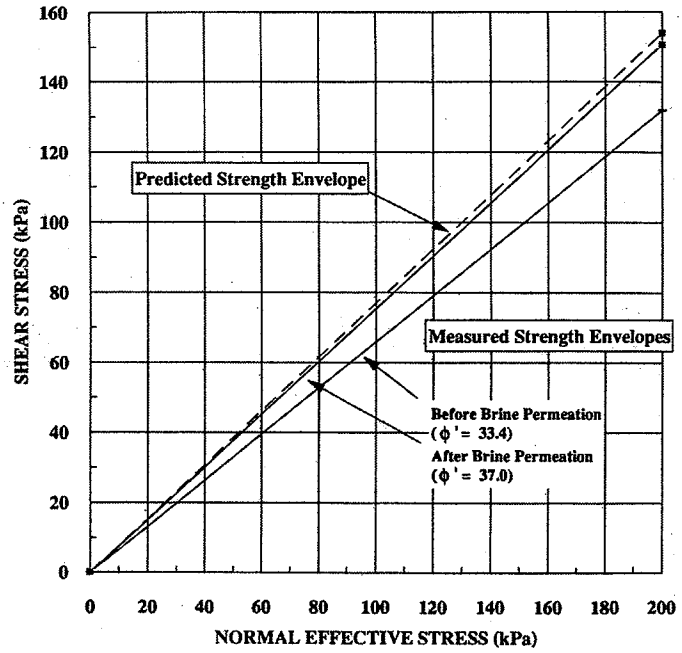

Figure 2.15. Change in ϕ' after brine permeation of Regina clay (after Barbour and Yang, 1993).

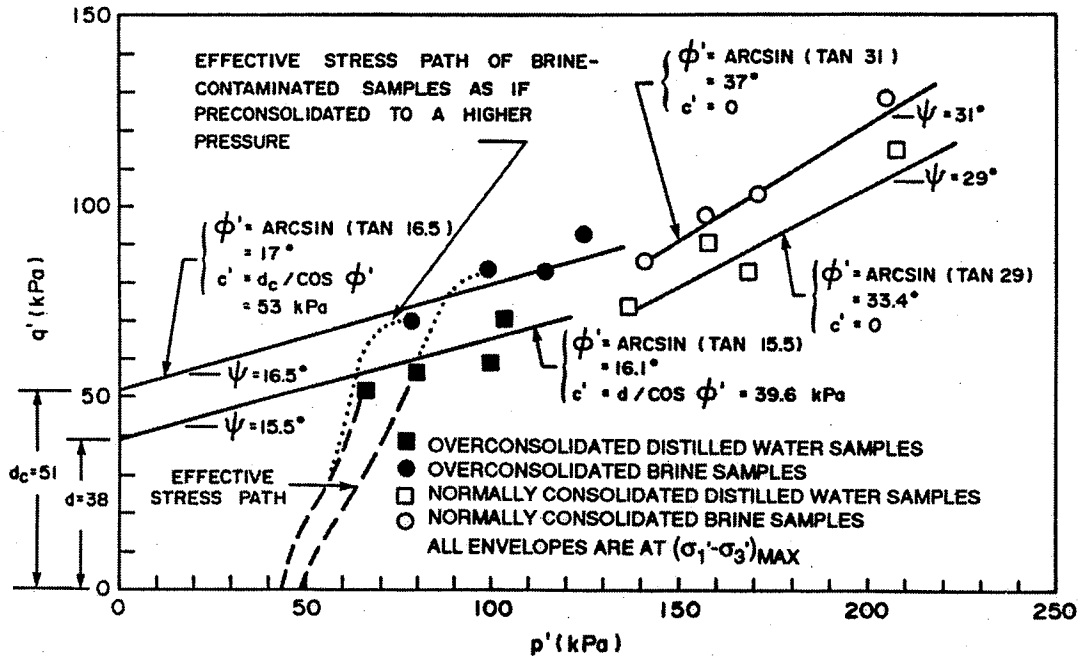

Figure 2.16. Change in strength envelope after brine permeation of Regina clay (after Ho, 1985).

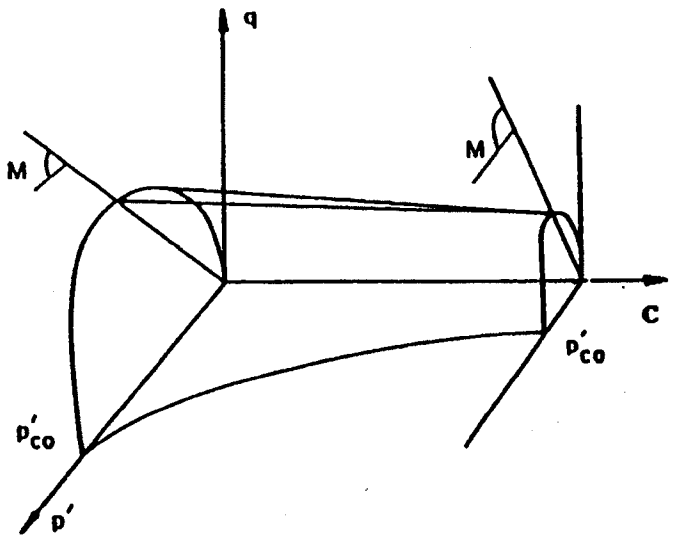

Figure 2.17. Chemical softening of the elastic domain for a Modified Cam-Clay model (after Hueckel, 2001).

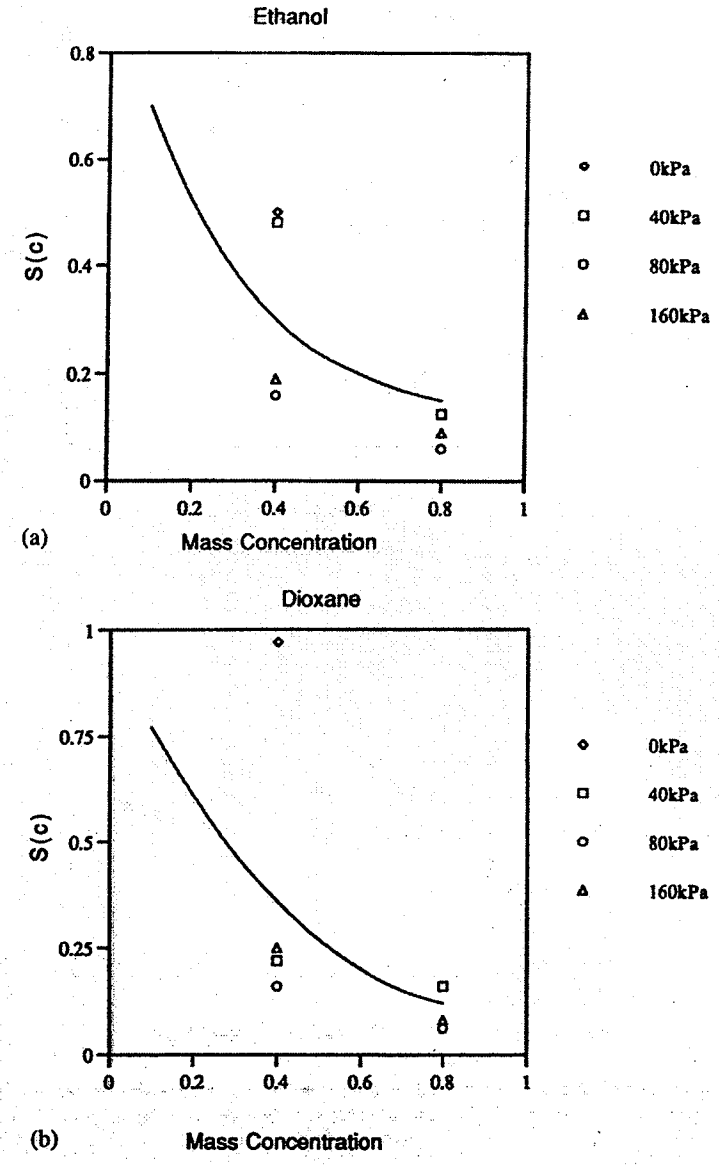

Figure 2.18. Modelled chemical softening functions S(c) versus concentration compared to measured results for various external loads (after Hueckel, 1997).

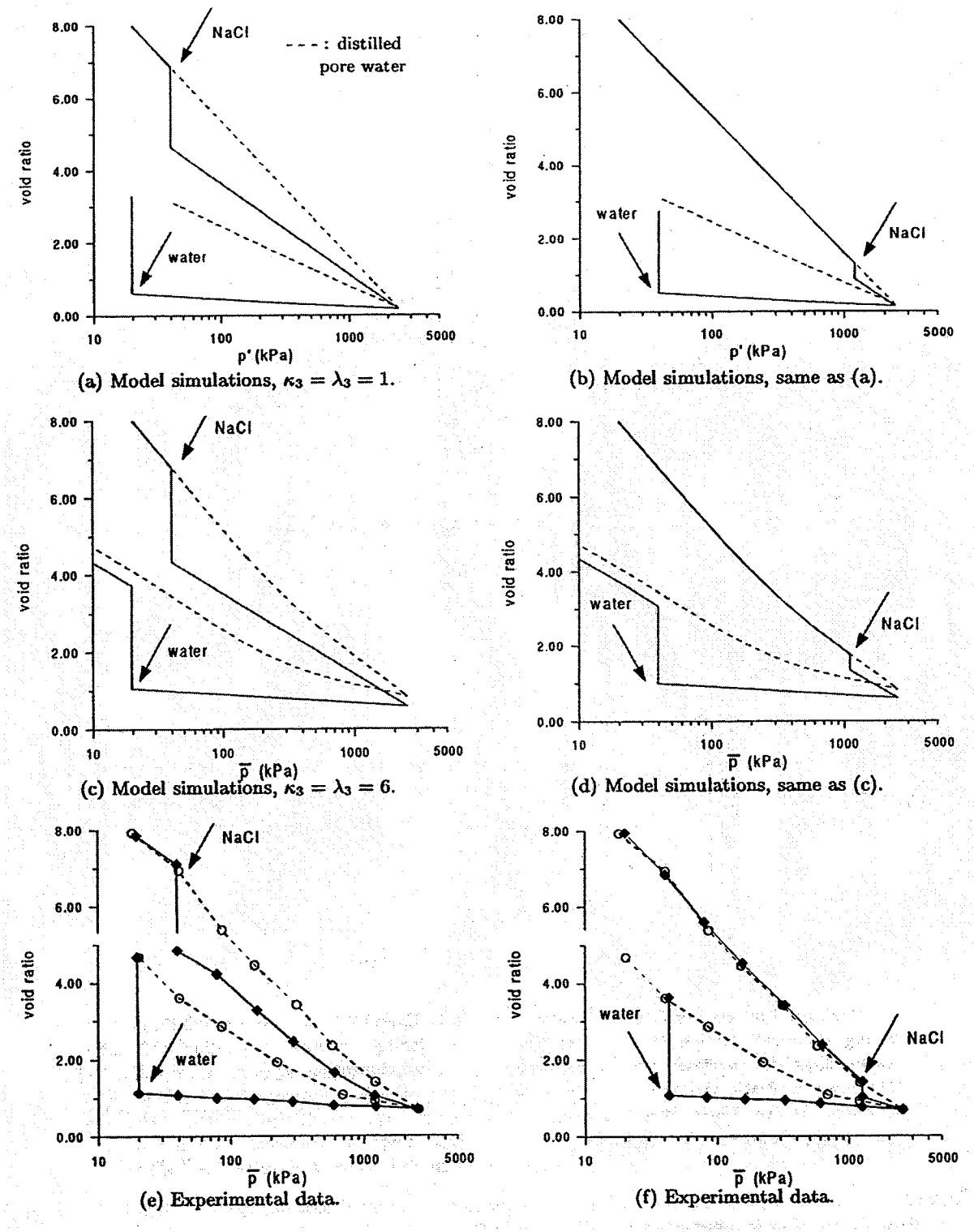

Figure 2.19. Model simulations and experimental data for Ponza bentonite permeated with NaCl brine compared to DI water (after Loret et al., 2001).

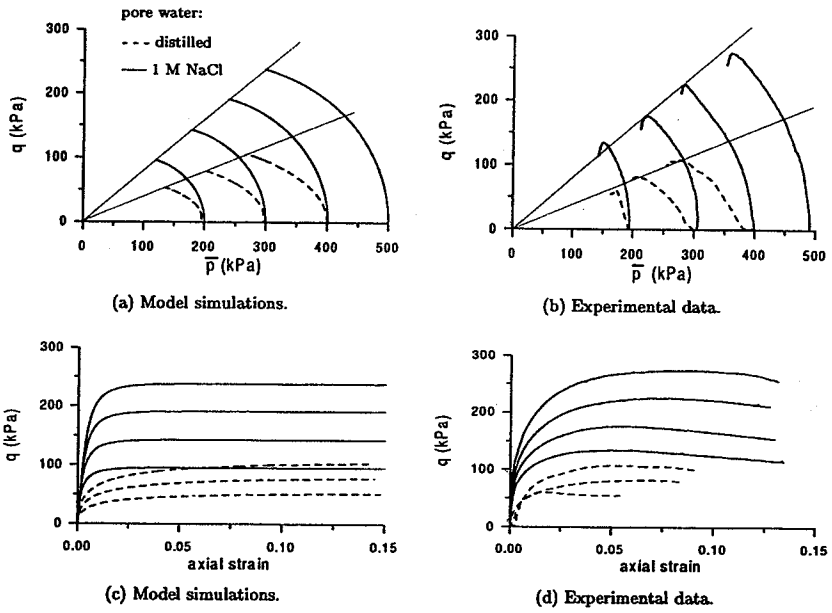

Figure 2.20. Model simulations and experimental data for triaxial tests conducted on Bisacia clay reconstituted with NaCl brine and distilled water (after Loret et al., 2001).

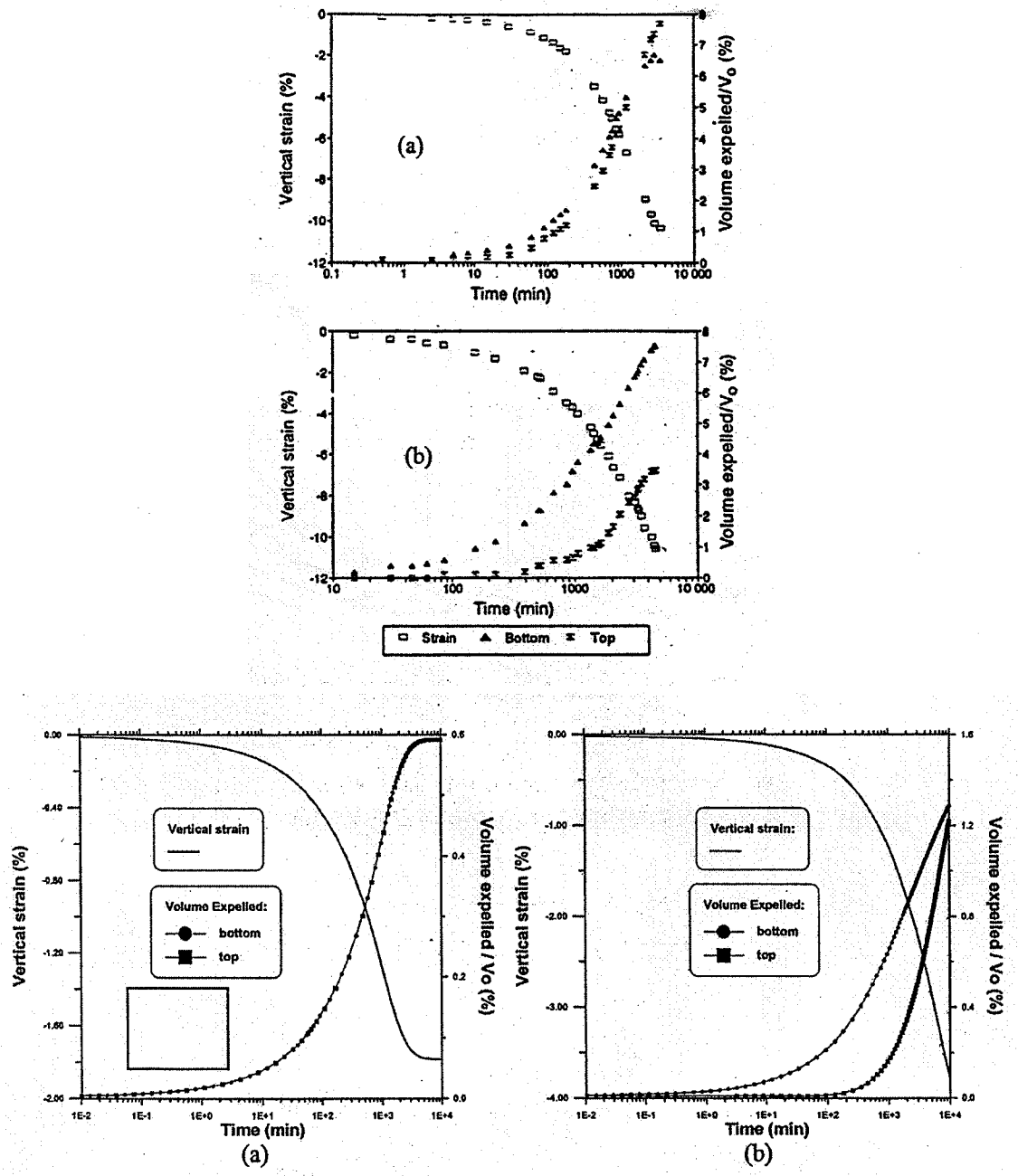

Figure 2.21. Observed (top) and modelled (bottom) strains for bentonite permeated with a saturated KCl solution (after Guimaraes et al., 2001).

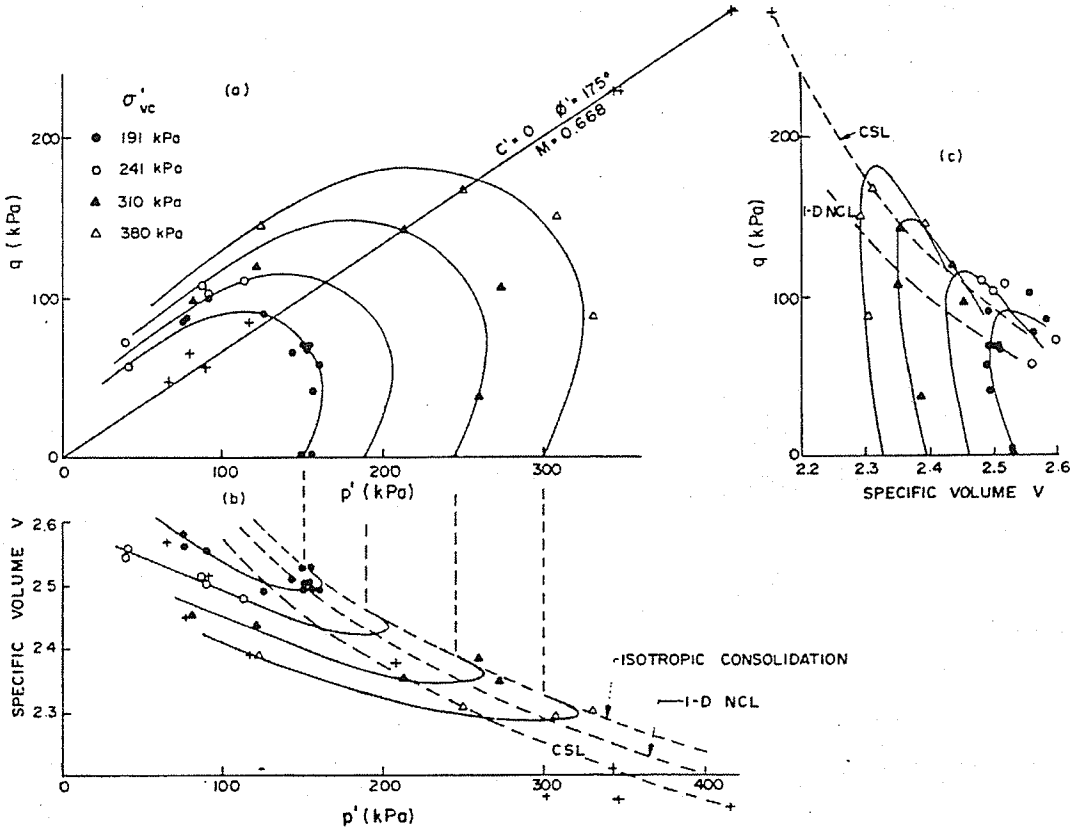

Figure 2.22. Yield loci for Winnipeg clay (after Graham et al., 1983).

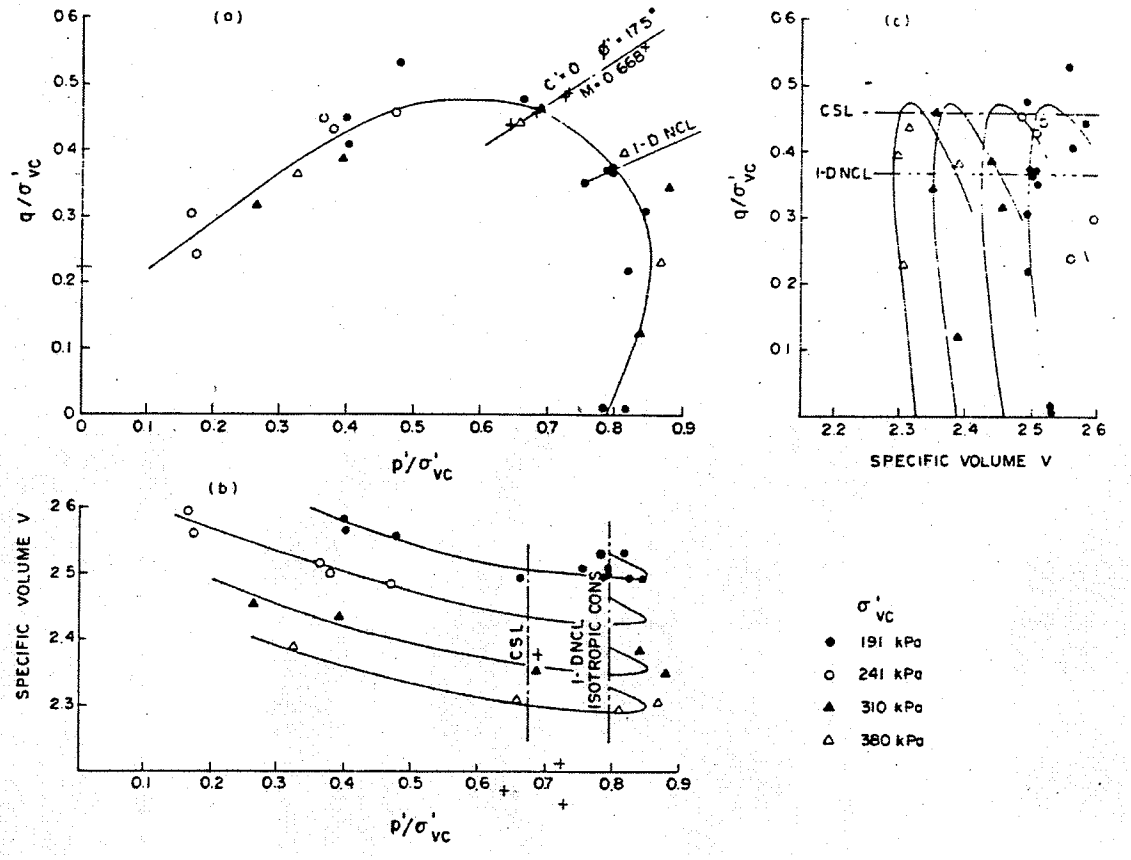

Figure 2.23. Normalized yield loci for Winnipeg clay (after Graham et al., 1983).

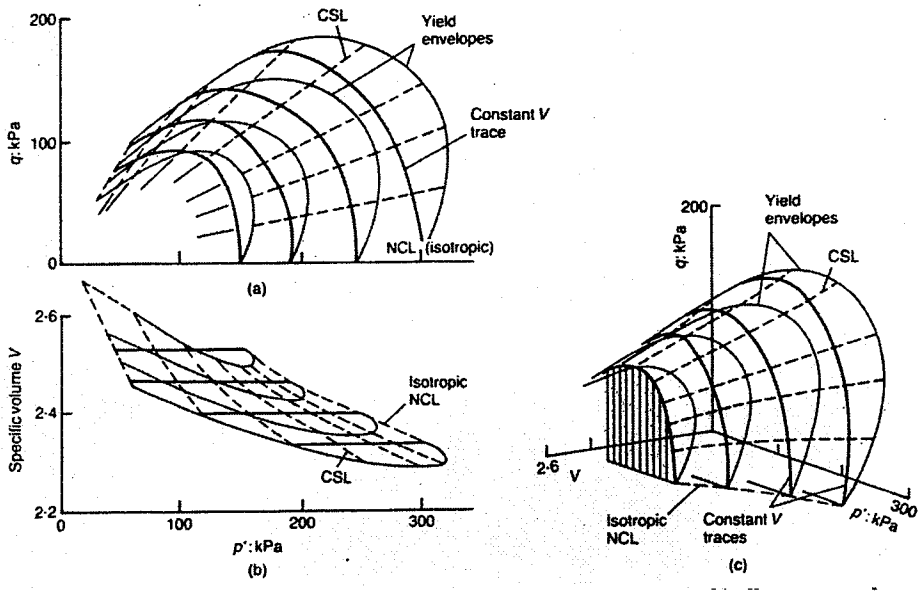

Figure 2.24. State boundary surface for Winnipeg clay (after Graham et al., 1988).

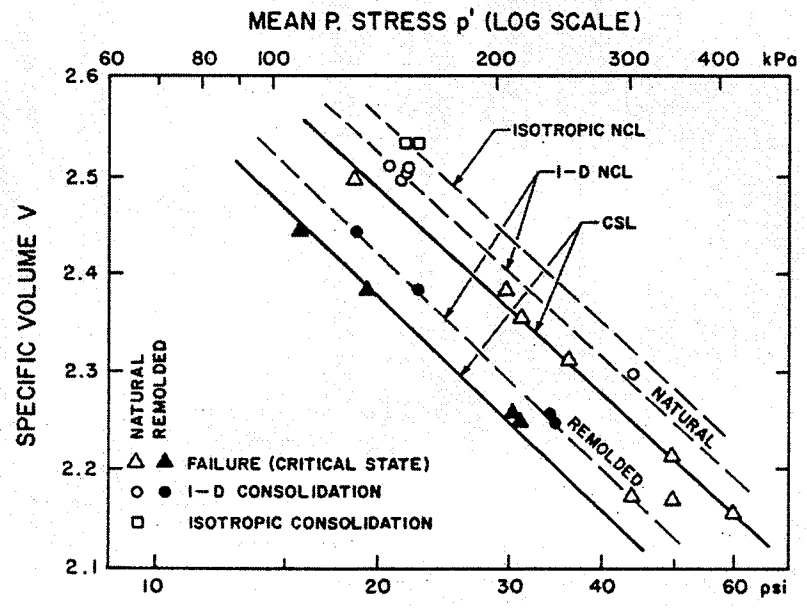

Figure 2.25. Normal consolidation and critical state lines for natural and reconstituted Winnipeg clay (Graham and Li, 1985).

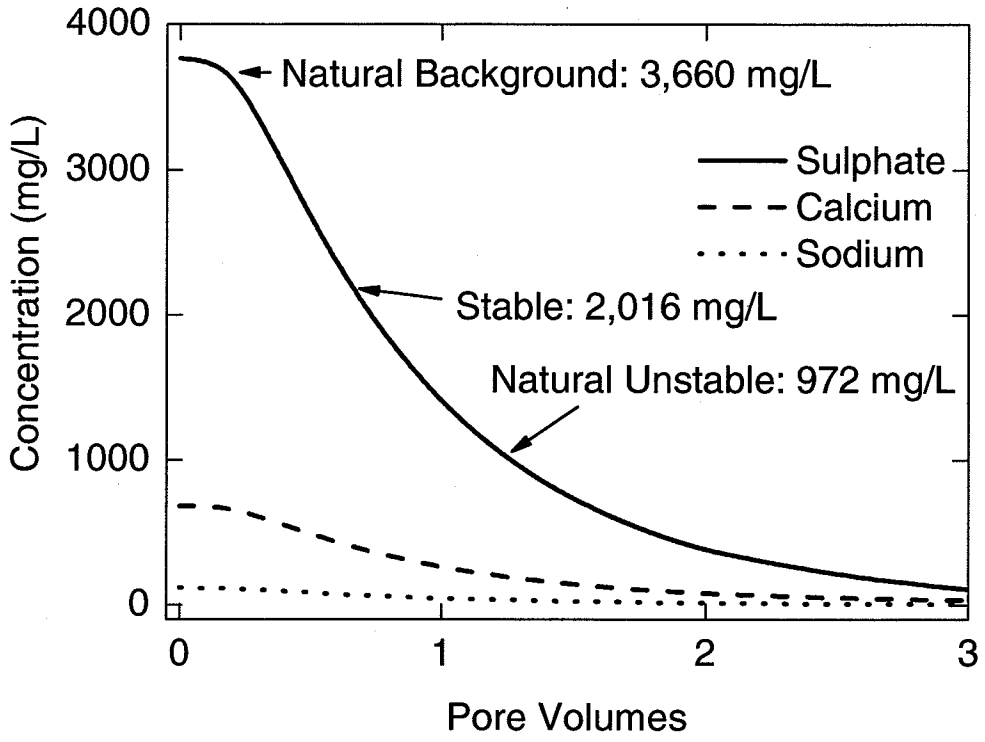

Figure 3.1. PHREEQ transport simulation of sulphate, calcium and sodium being leached from the Seven Sisters foundation clay by the flow of forebay water.

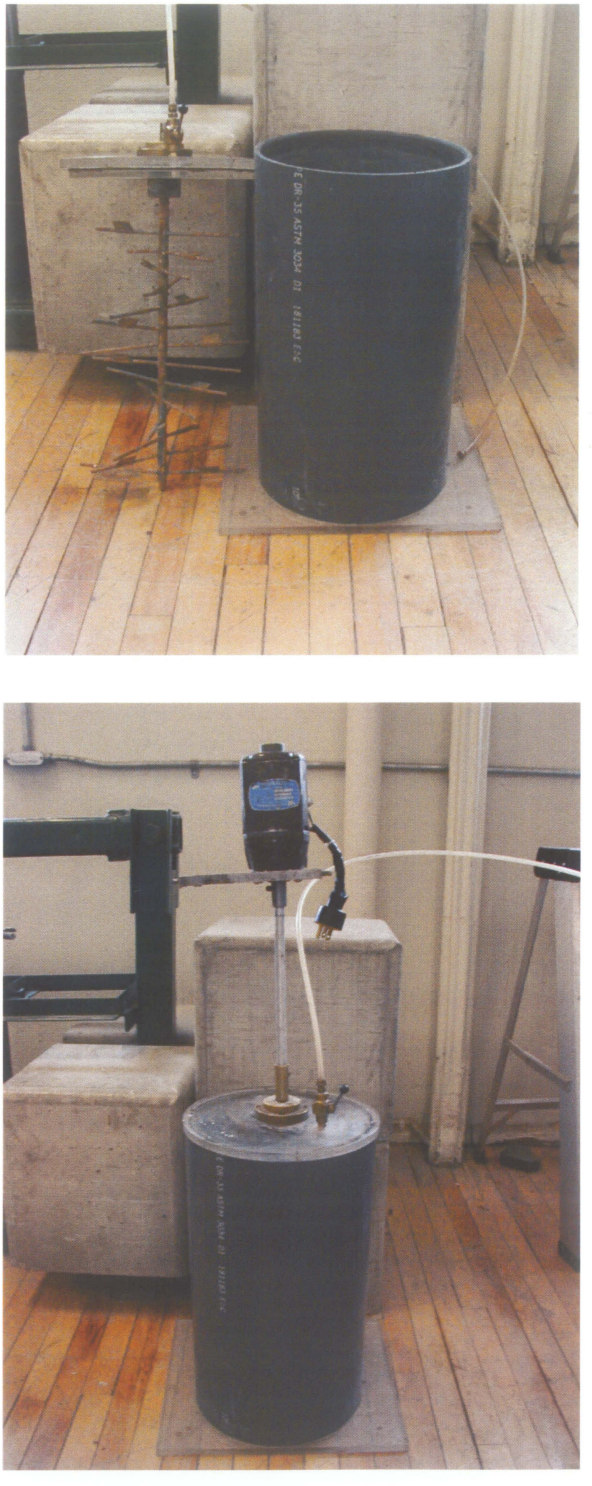

Figure 3.2 Mixing chamber used for the preparation of slurries.

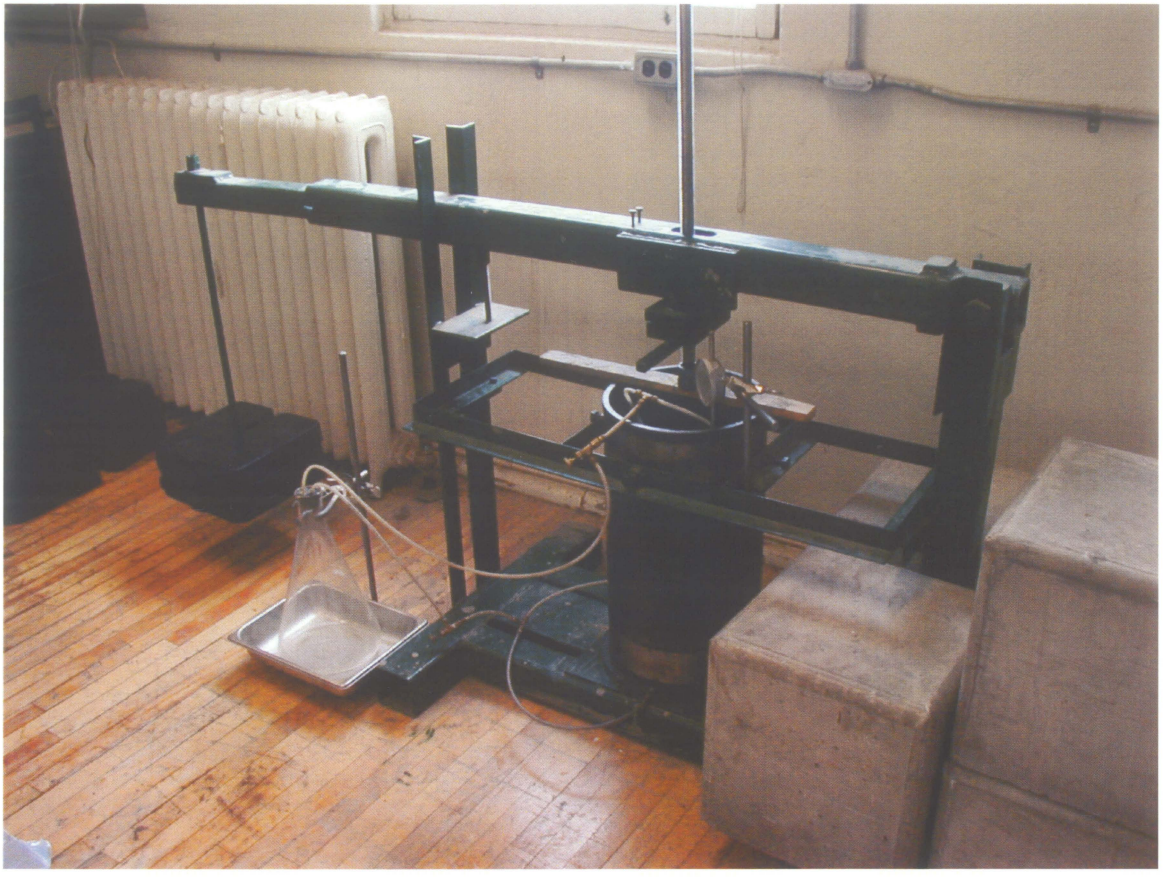

Figure 3.3. One-dimensional consolidation apparatus.

Figure 3.4. Extrusion of a block of clay from consolidation chamber.

Figure 3.5. Slow mixing chamber used to wash the clay.

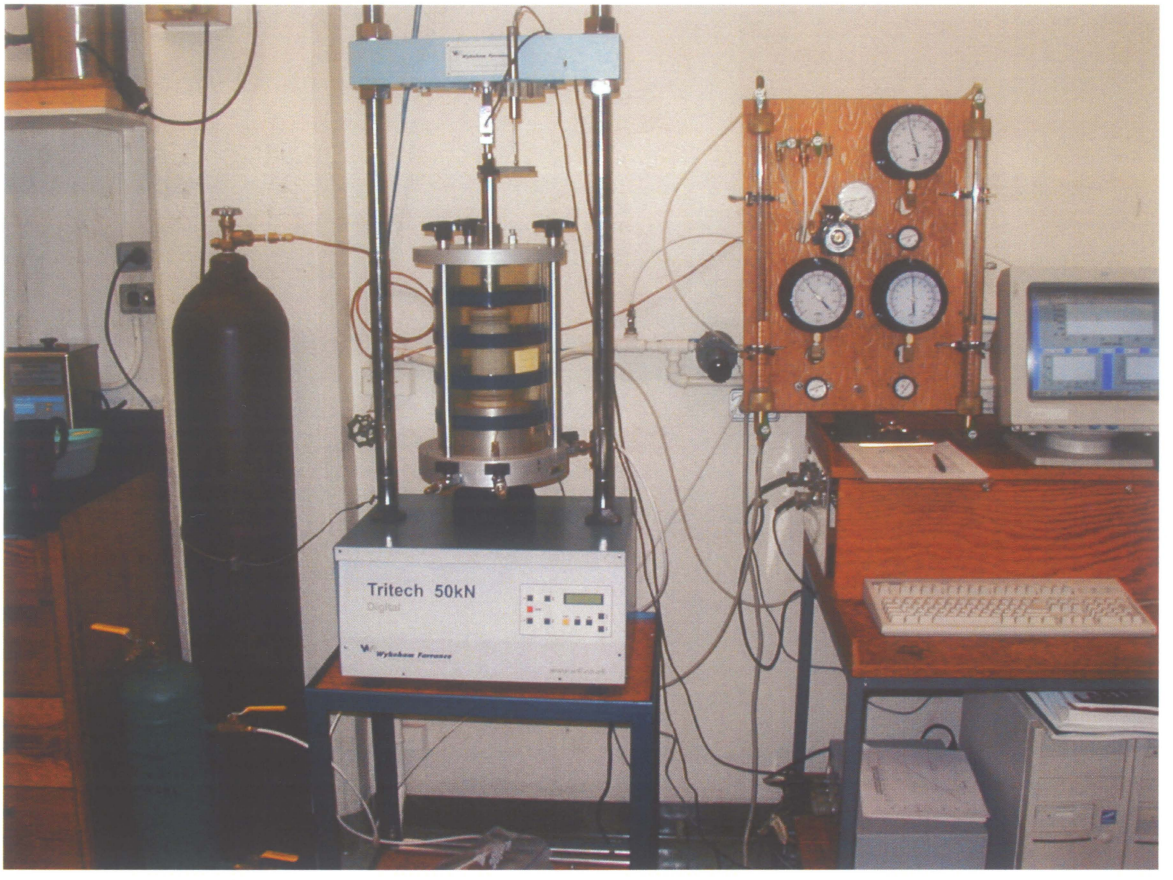

Figure 3.6. Triaxial testing equipment.

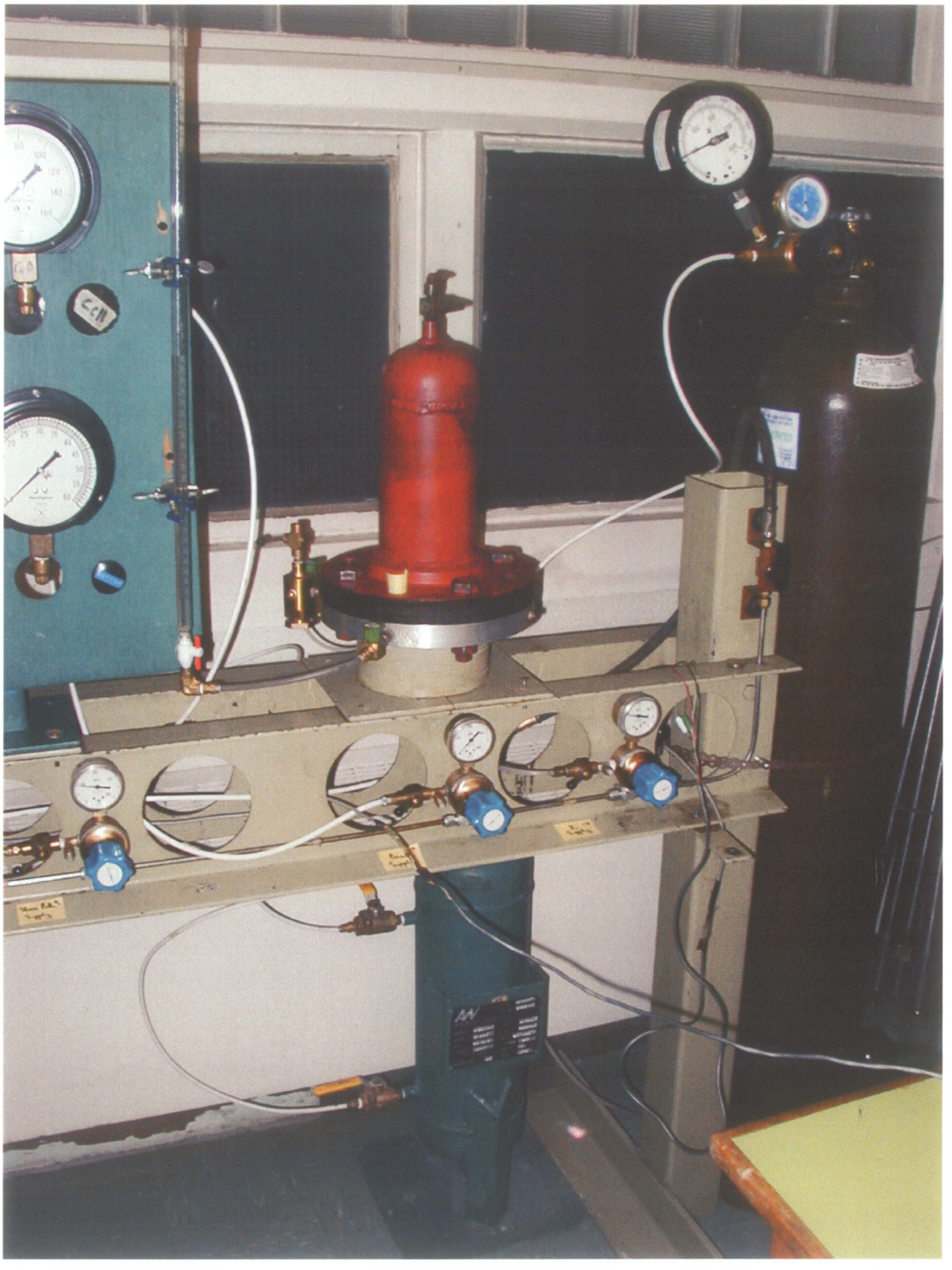

Figure 3.7. High pressure (4 MPa) isotropic consolidation cell.

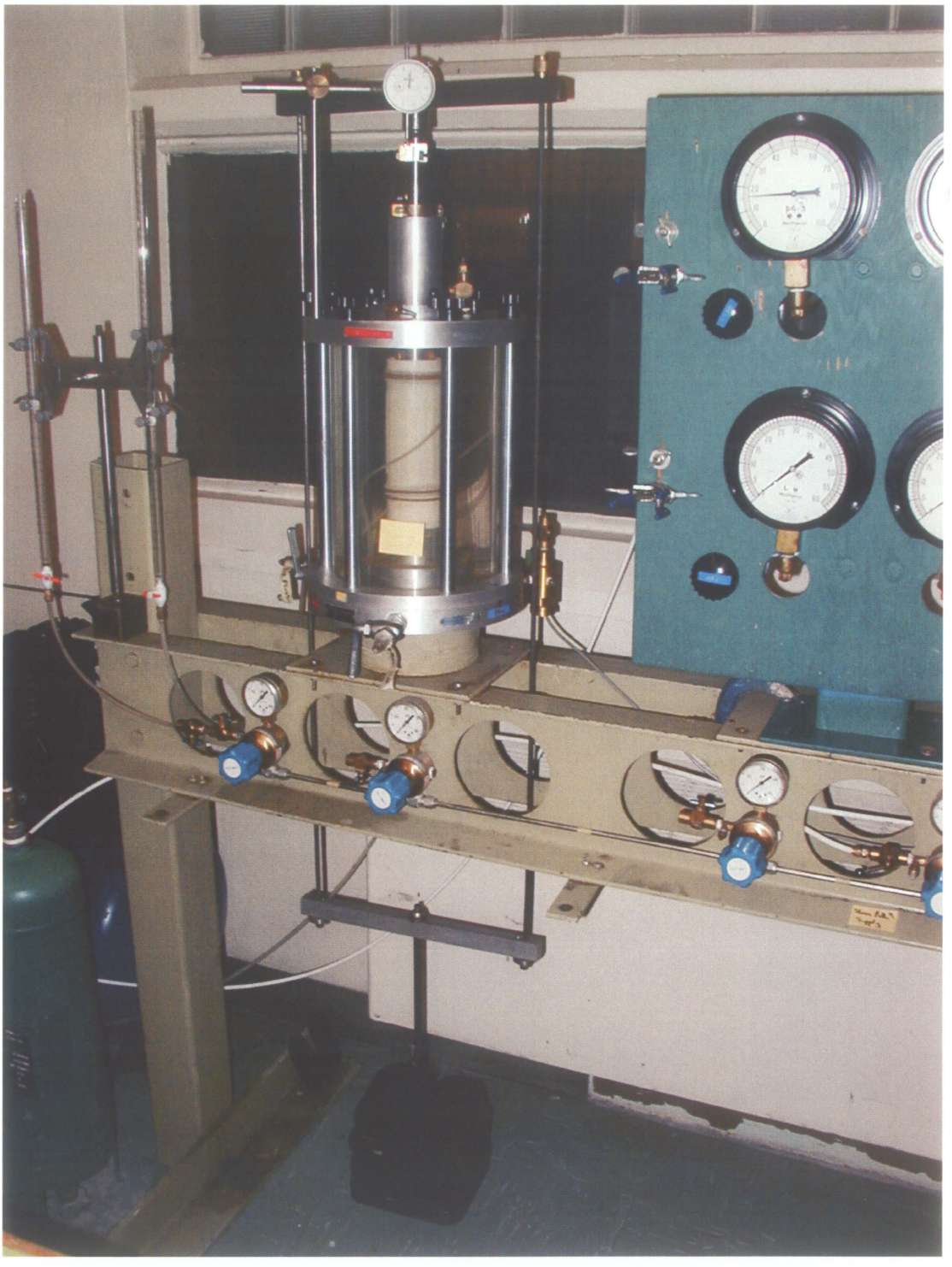

Figure 3.8. Triaxial apparatus used for stress-controlled tests.

Figure 4.1. Photograph of a clay sample from 3.5 to 4.0 m below grade (El. 266.5 to 266.0 m) at the Seven Sisters background section. Note the vertical fissure containing a white sulphate pocket near the centre of the specimen and the horizontal laminations.

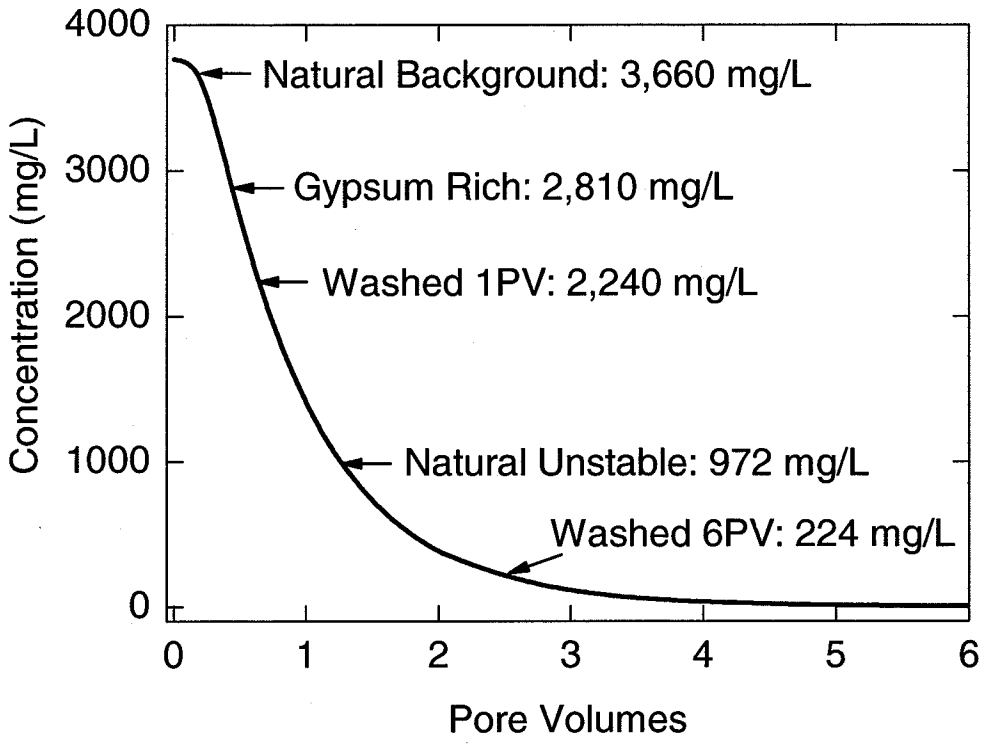

Figure 4.2. Tested soils compared to the leaching simulation results for sulphate.

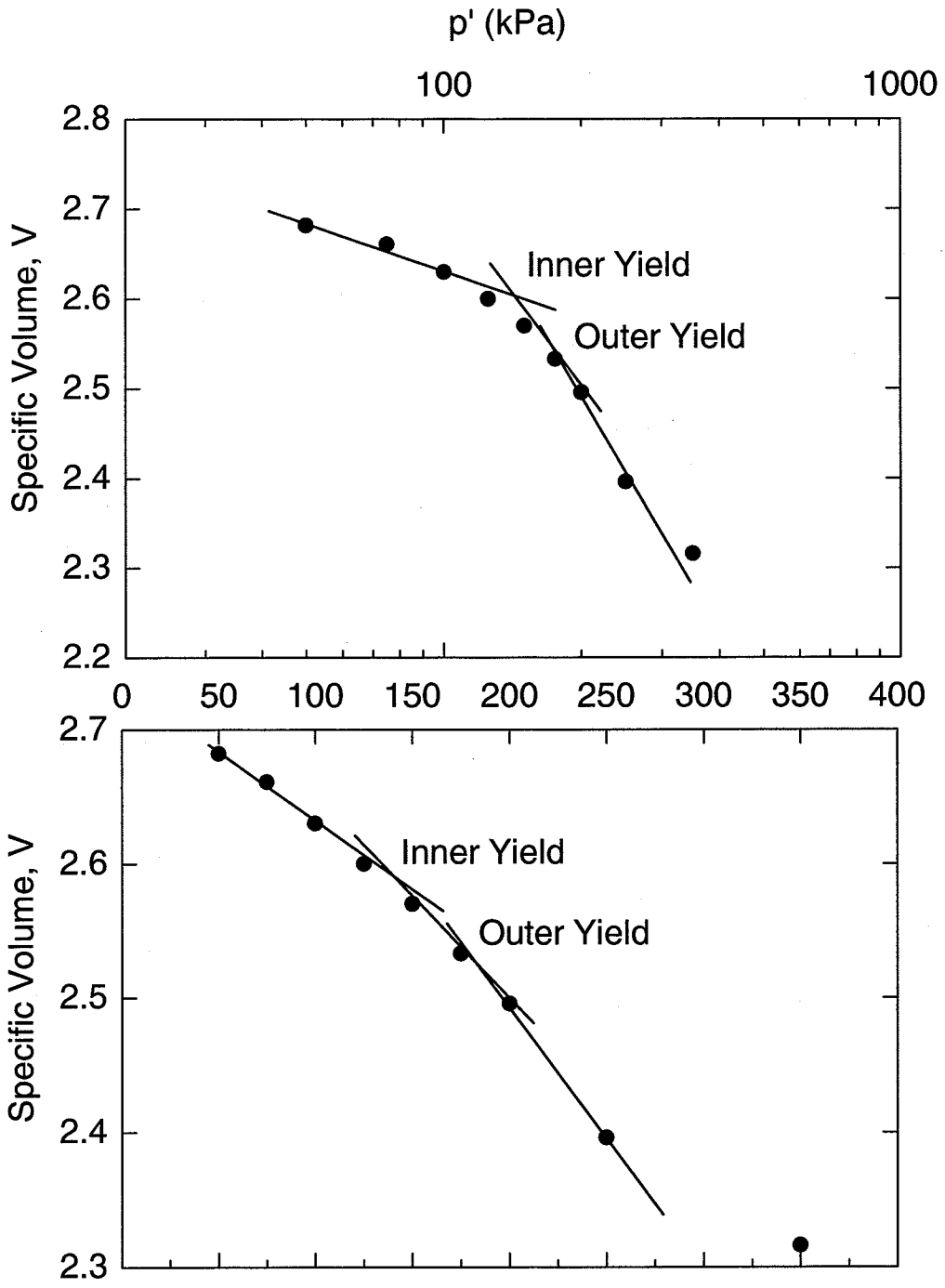

Figure 4.3. Isotropic consolidation of gypsum rich reconstituted clay (specimen AMR2-T16) in a standard triaxial cell. Data is presented on log (upper) and linear (lower) scales. Yield was interpreted as the intersections of the lines.

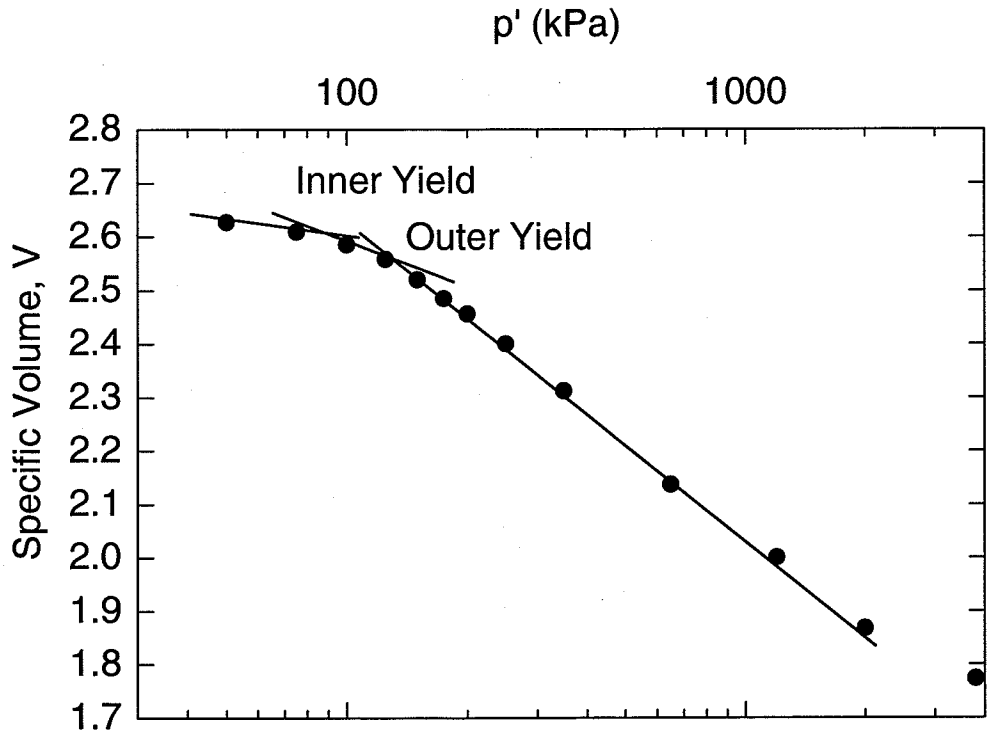

Figure 4.4. Isotropic consolidation of gypsum rich reconstituted clay (specimen AMR2-T15) in a high pressure triaxial cell.

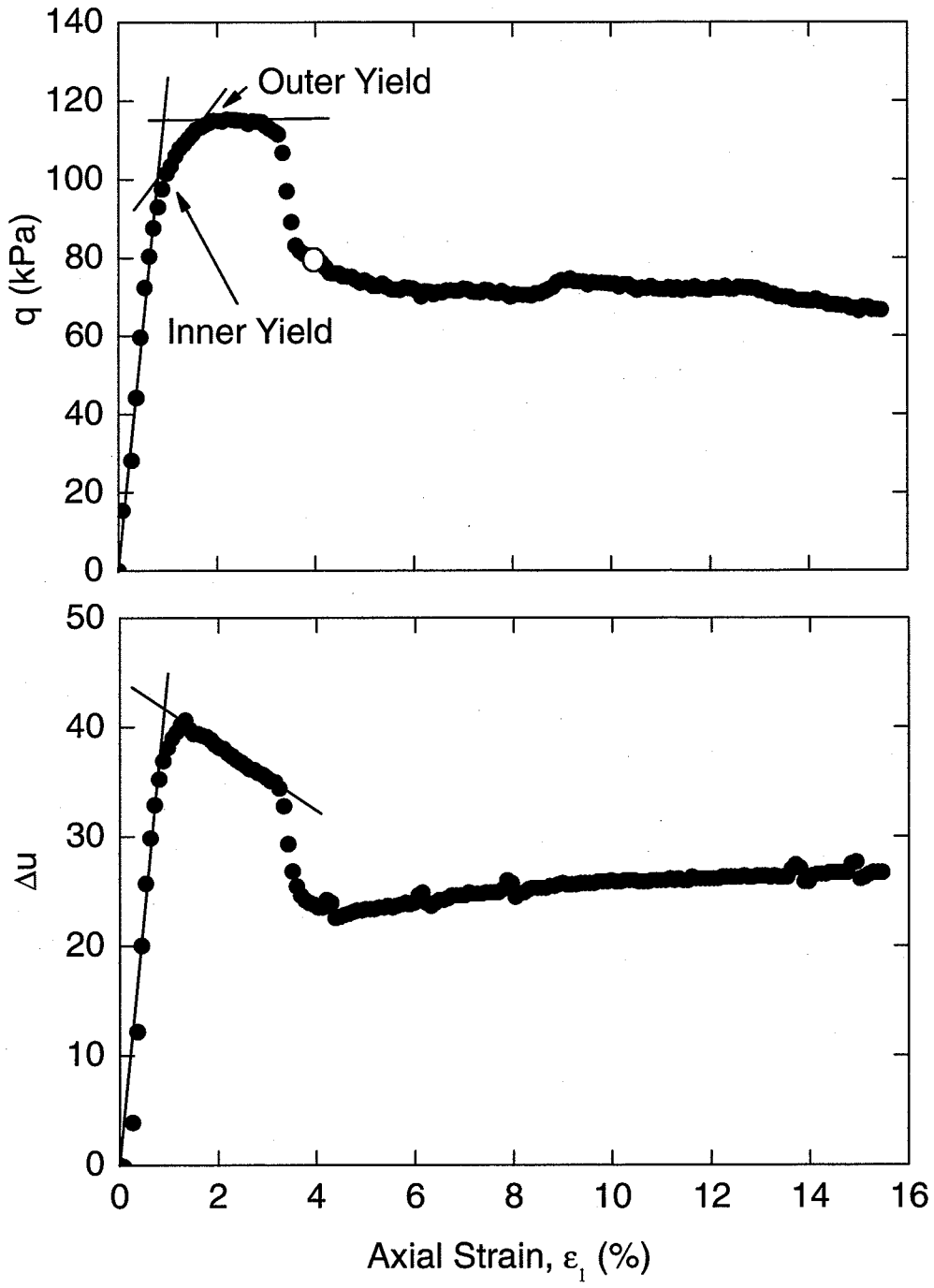

Figure 4.5. Example of deviator stress and change in pore water pressure versus axial strain data for a CIŪ test conducted on gypsum rich reconstituted clay (specimen AMR1-T47). Open circle is at interpreted post-peak/critical state.

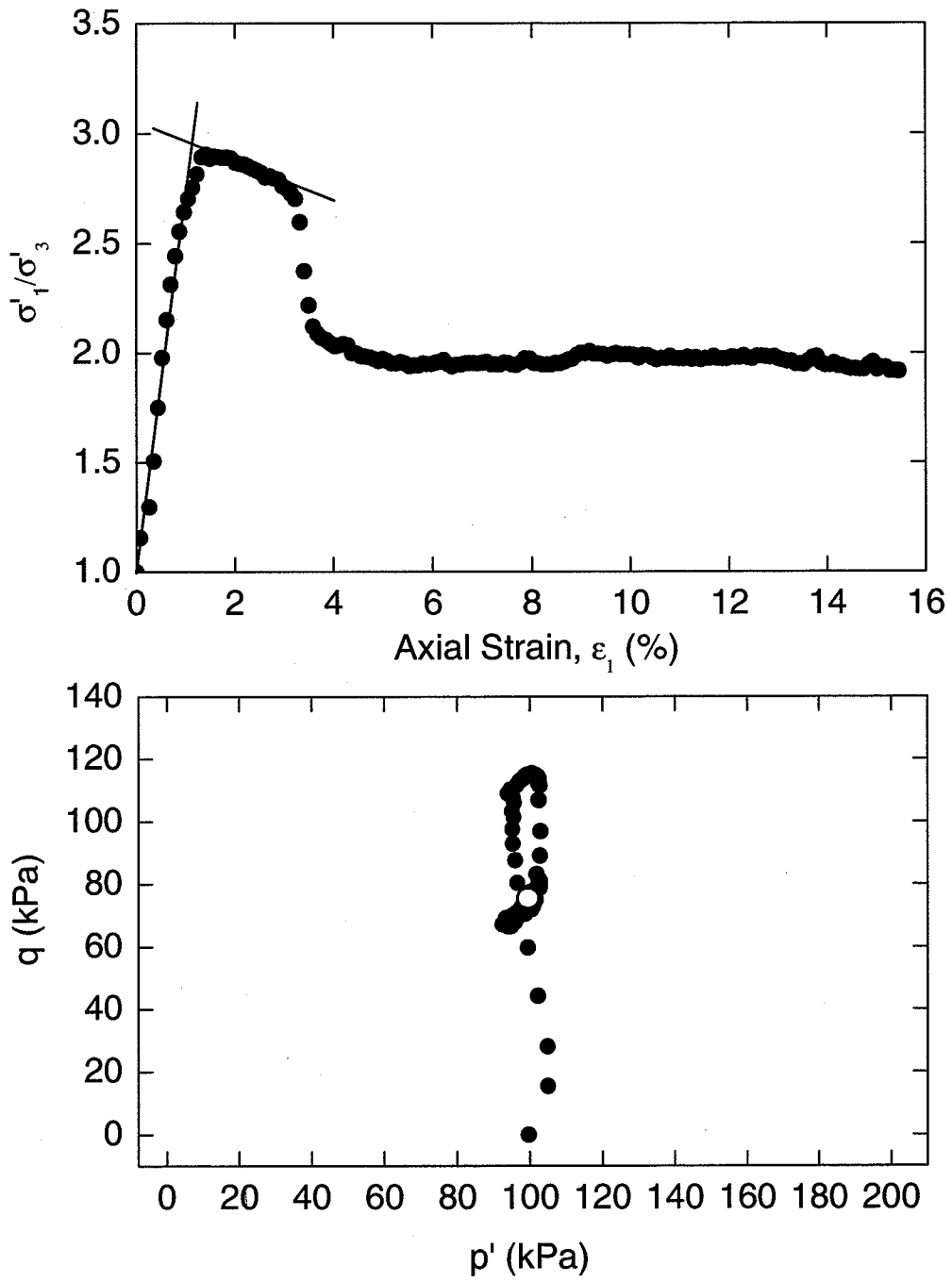

Figure 4.6. Example of principal effective stress ratio versus axial strain and deviator stress versus mean effective stress results for a CIŪ test conducted on gypsum rich reconstituted clay (specimen AMR1-T47). Open circle is at interpreted post-peak/critical state.

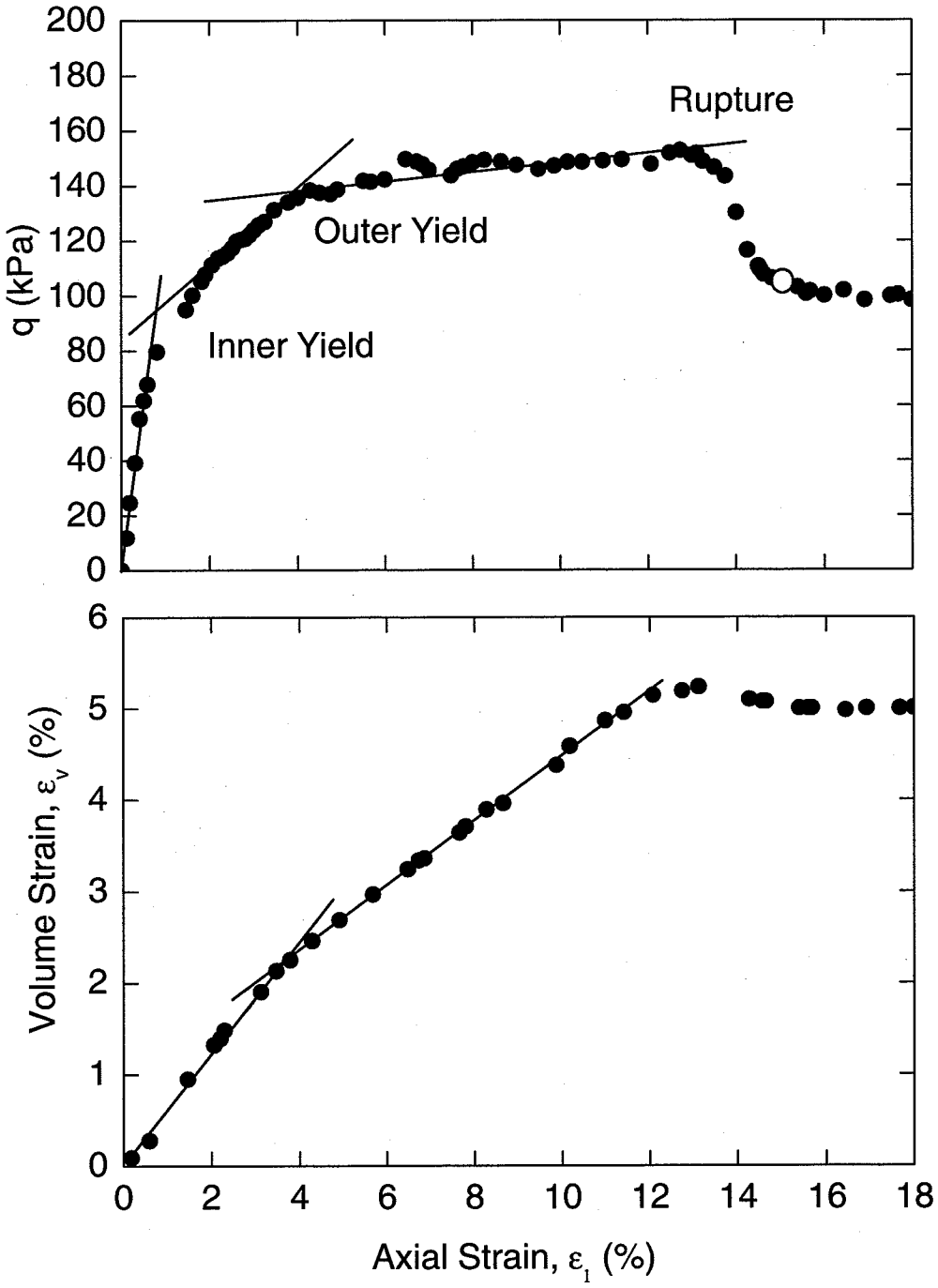

Figure 4.7. Example of deviator stress and volume strain versus axial strain results for a CID test conducted on gypsum rich reconstituted clay (specimen AMR1-T10). Open circle at interpreted post-peak/critical state.

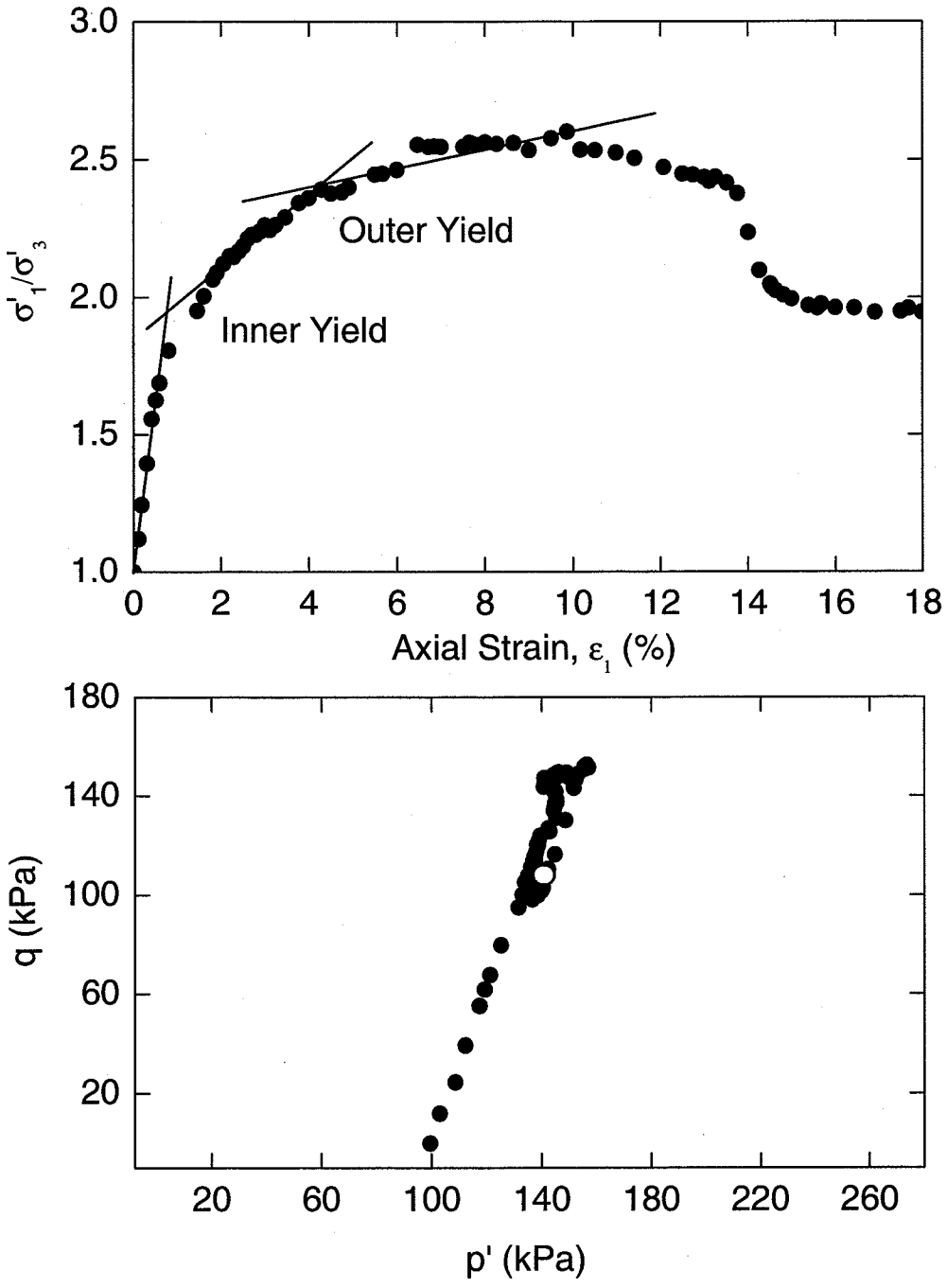

Figure 4.8. Example of principal effective stress ratio versus axial strain and deviator stress versus mean effective stress results for a CID test conducted on gypsum rich reconstituted clay (specimen AMR1-T10).

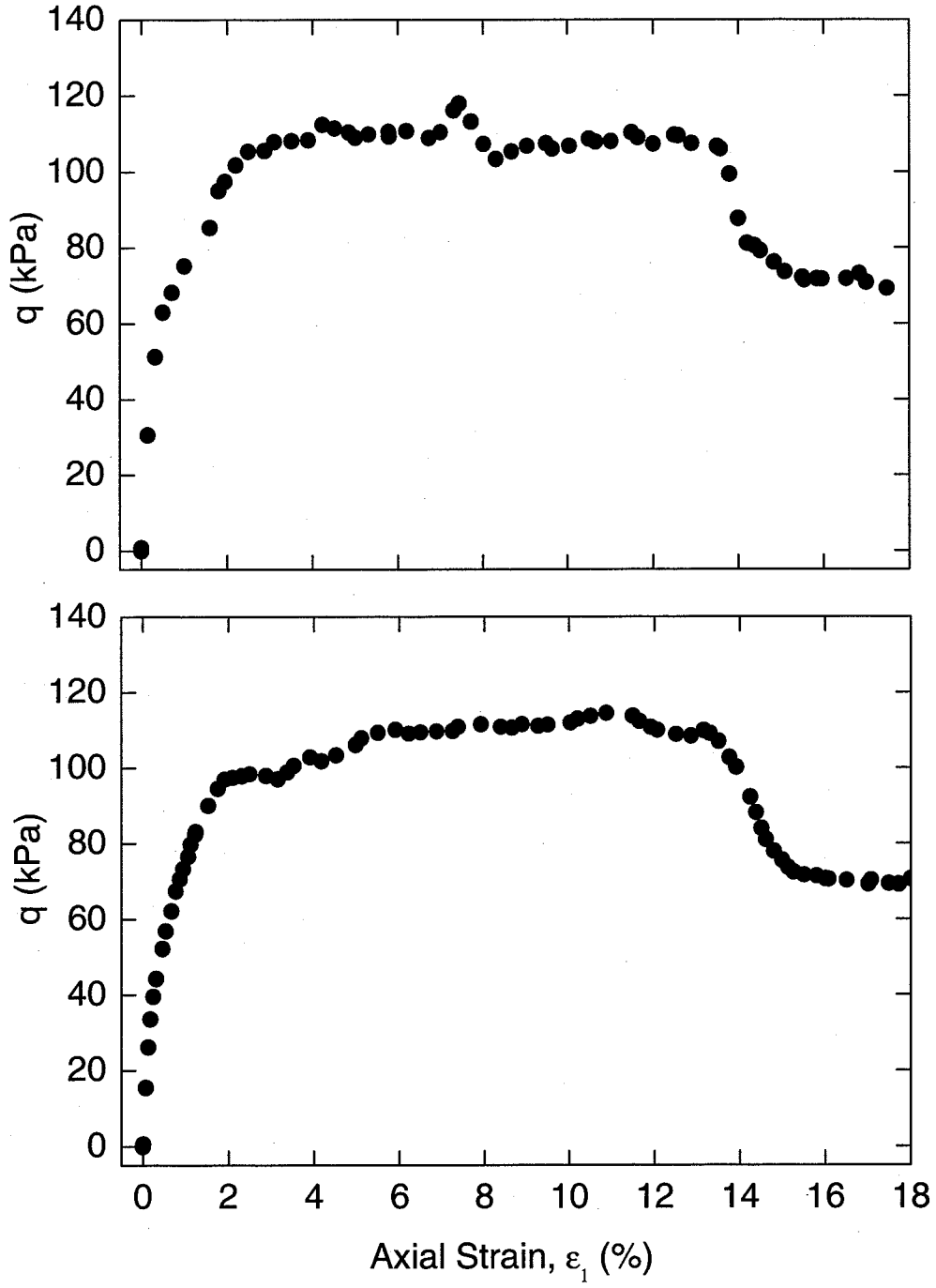

Figure 4.9. Comparison between CID results using two different triaxial cells and constant rate of strain presses. Both tests were conducted on washed (6PV) reconstituted clay (specimens AMR7-T52, upper plot and AMR7-T55, lower plot).

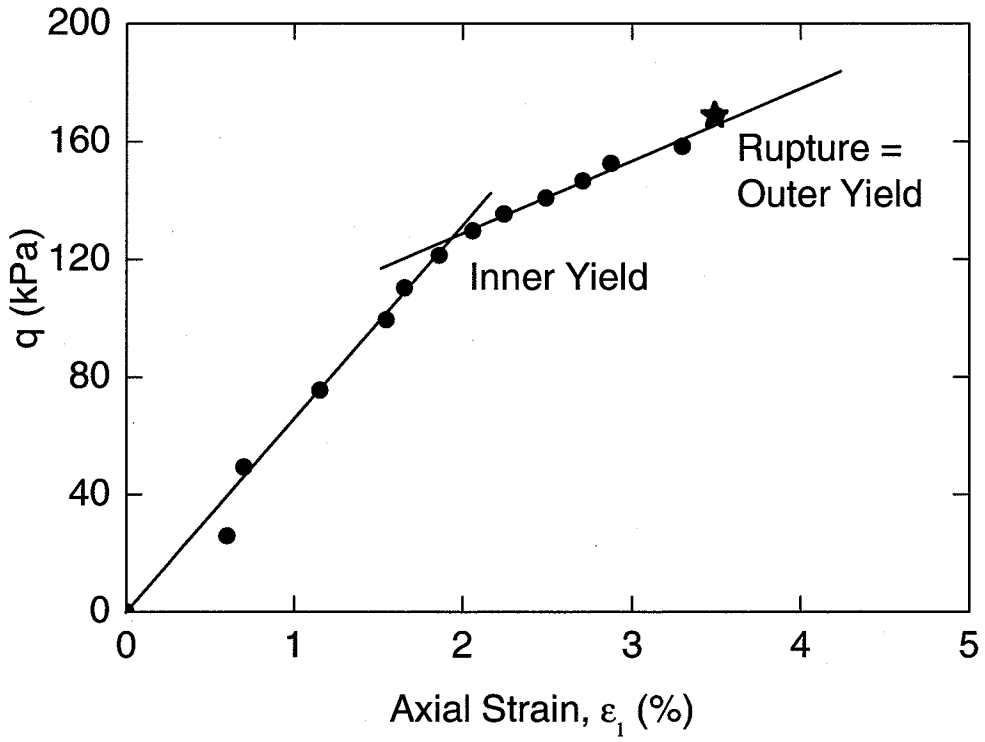

Figure 4.10. Example of deviator stress versus axial strain results for a constant p′ test conducted on gypsum rich reconstituted clay (specimen AMR2-T29). The constant p′ tests were all conducted under drained, stress-controlled conditions with p′ = 100 kPa.

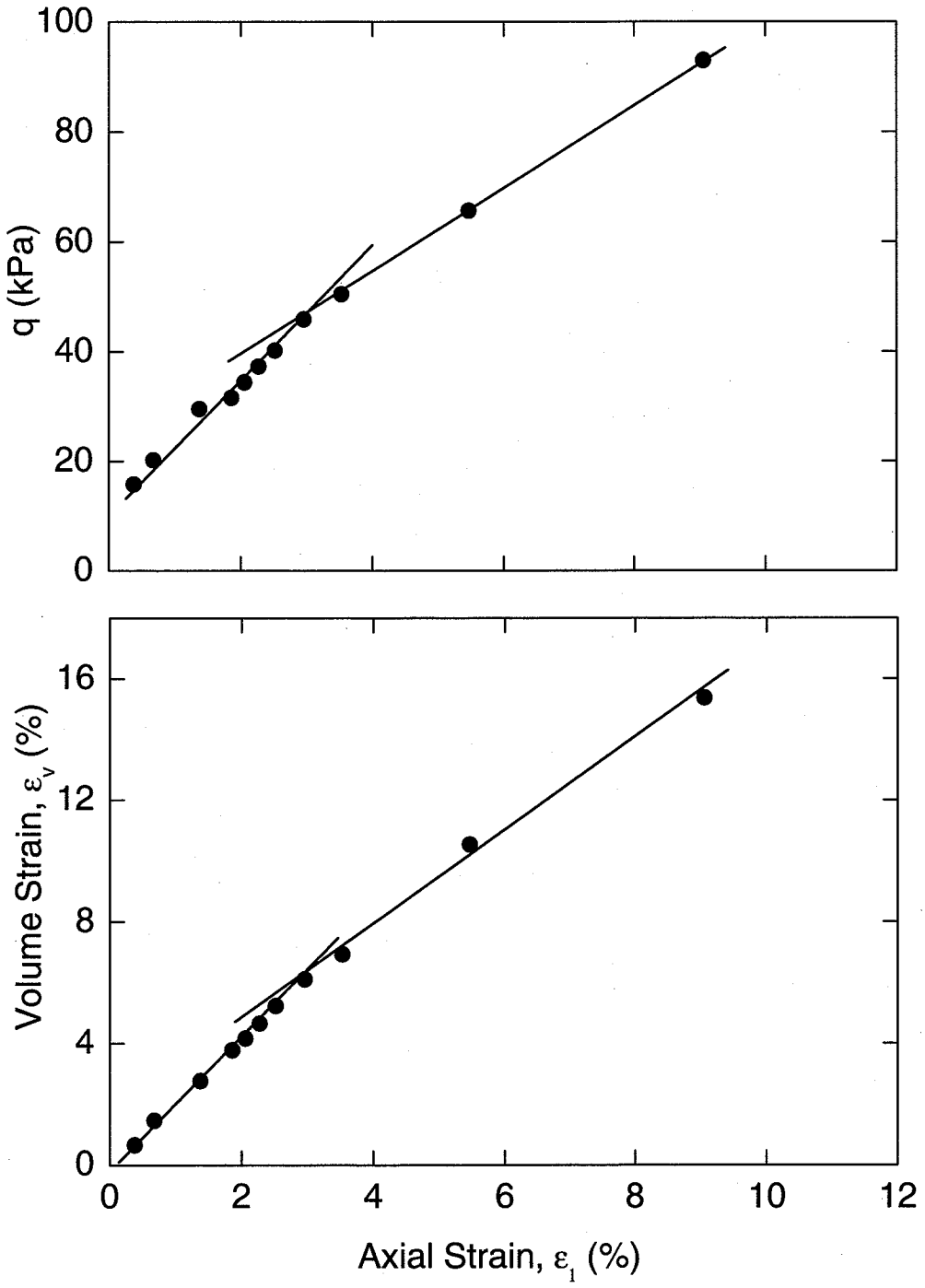

Figure 4.11. Example of deviator stress and volume strain versus axial strain results for a K_0 consolidation test conducted on gypsum rich reconstituted clay (specimen AMR2-T30). The K_0 consolidation tests were conducted following K_0 = 0.78 under drained, stress-controlled conditions followed by strain-controlled shearing at the final stress state.

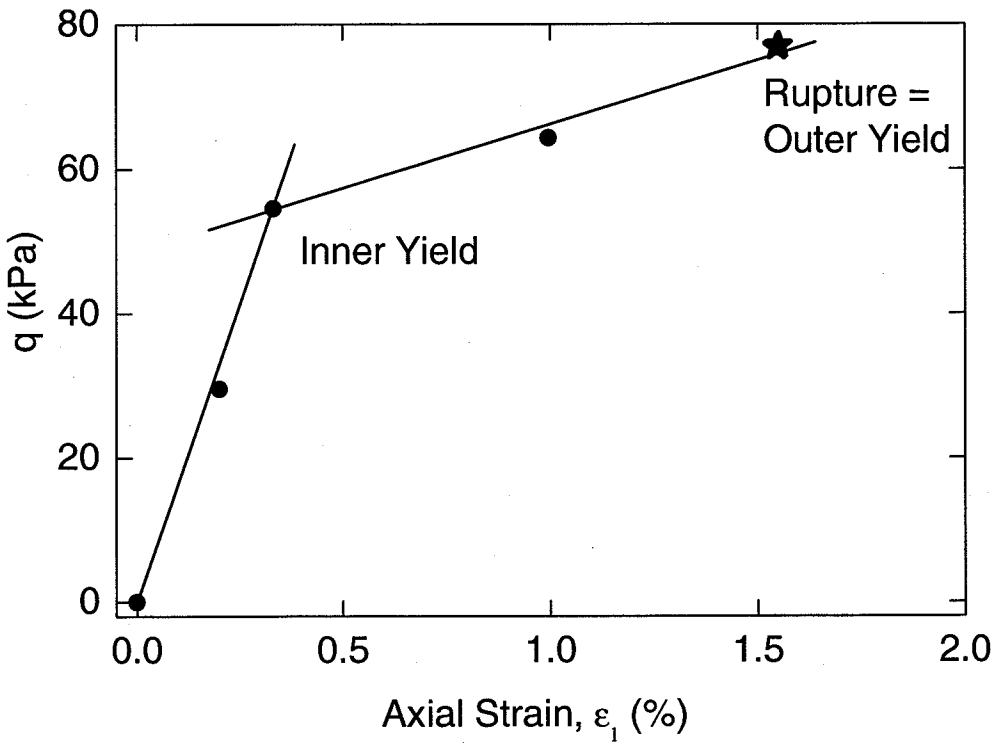

Figure 4.12. Example of deviator stress versus axial strain results for a defined stress path test following q/p' = -1.5 (-3/2), conducted on gypsum rich reconstituted clay (specimen AMR2-T37). The defined stress path tests were all conducted under drained, stress-controlled conditions.

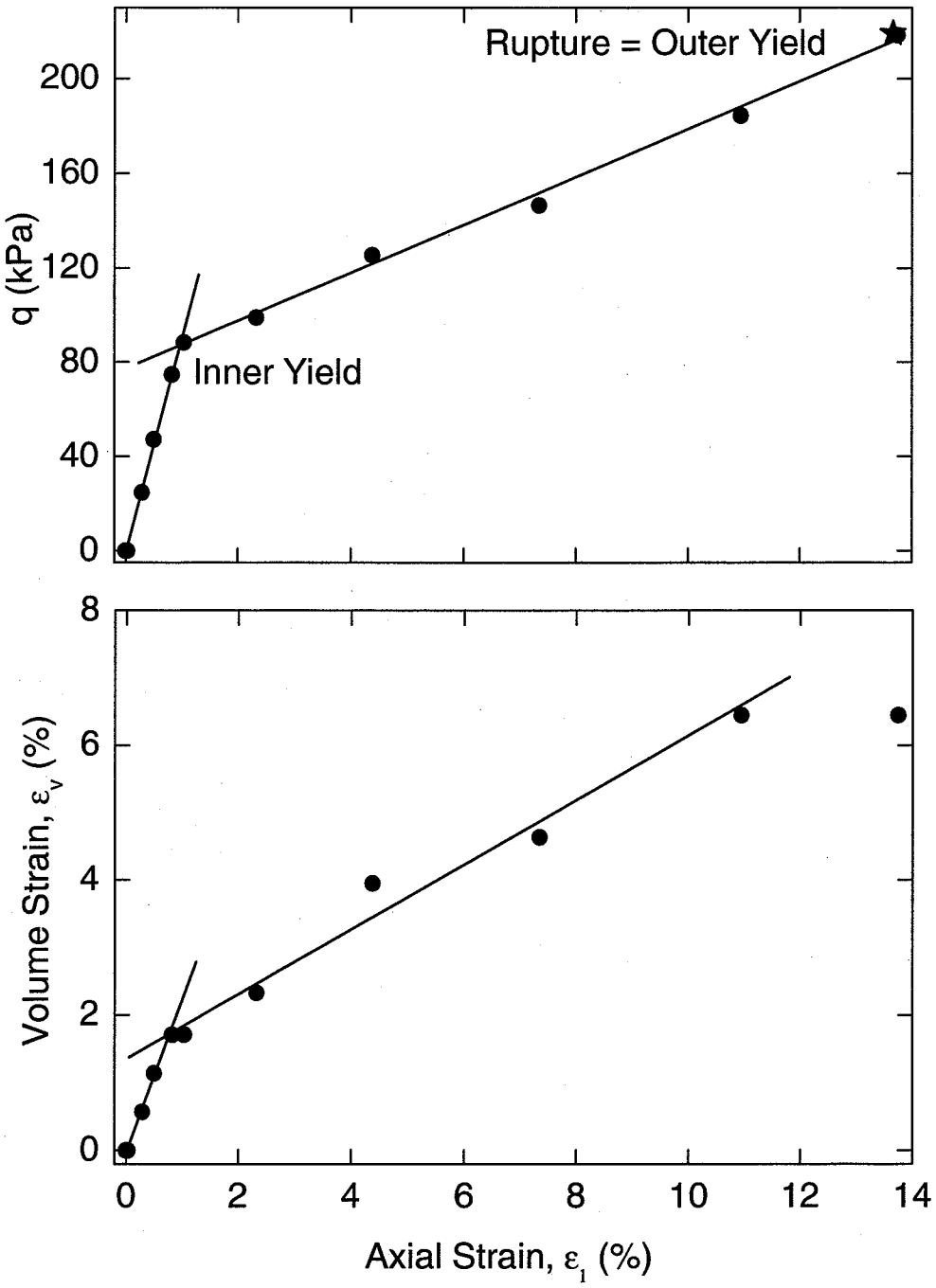

Figure 4.13. Example of deviator stress versus axial strain results for a defined stress path test following q/p' = 1.25, conducted on gypsum rich reconstituted clay (specimen AMR2-T42).

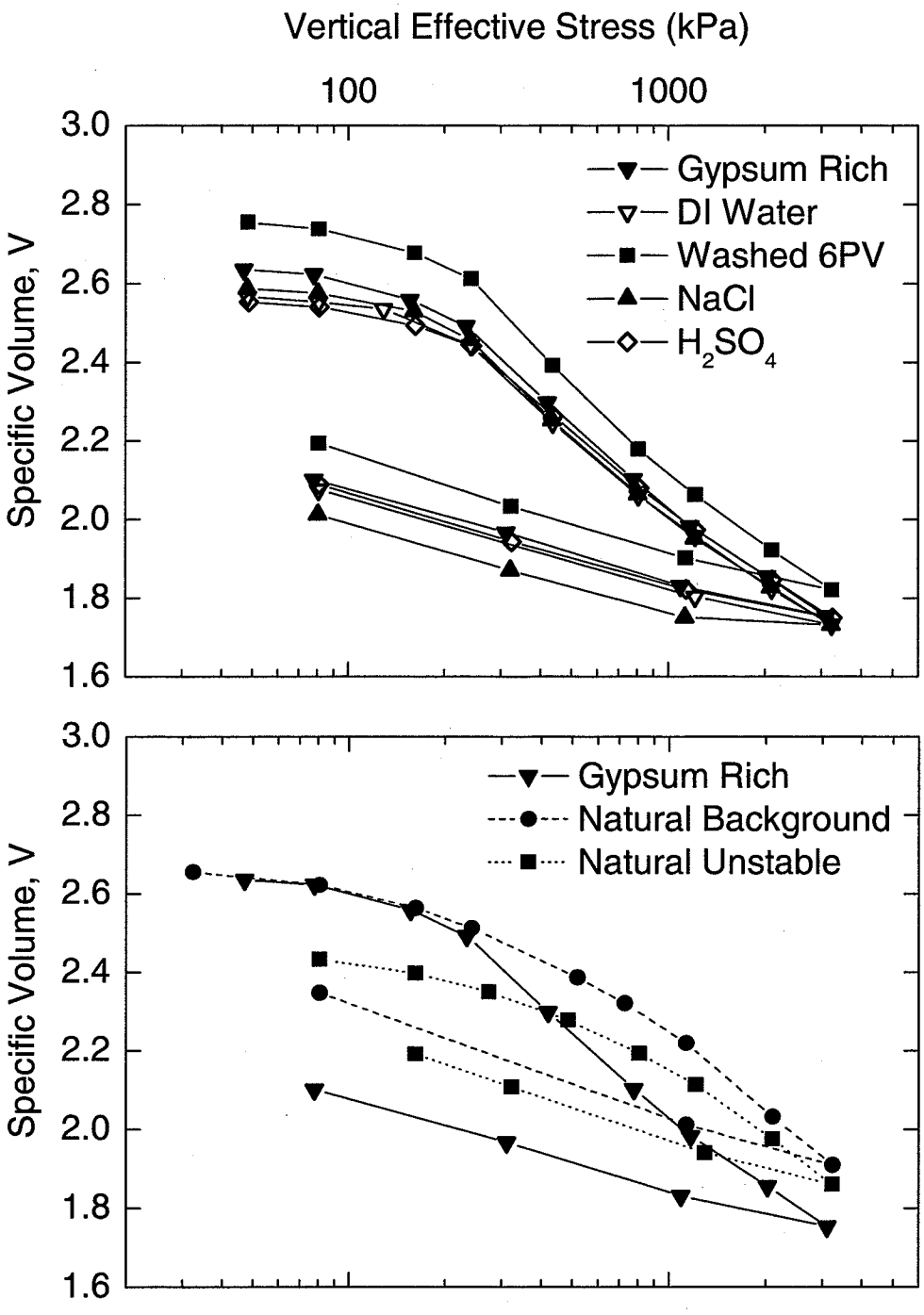

Figure 4.14. Oedometer test results for reconstituted (upper) and natural (lower) specimens.

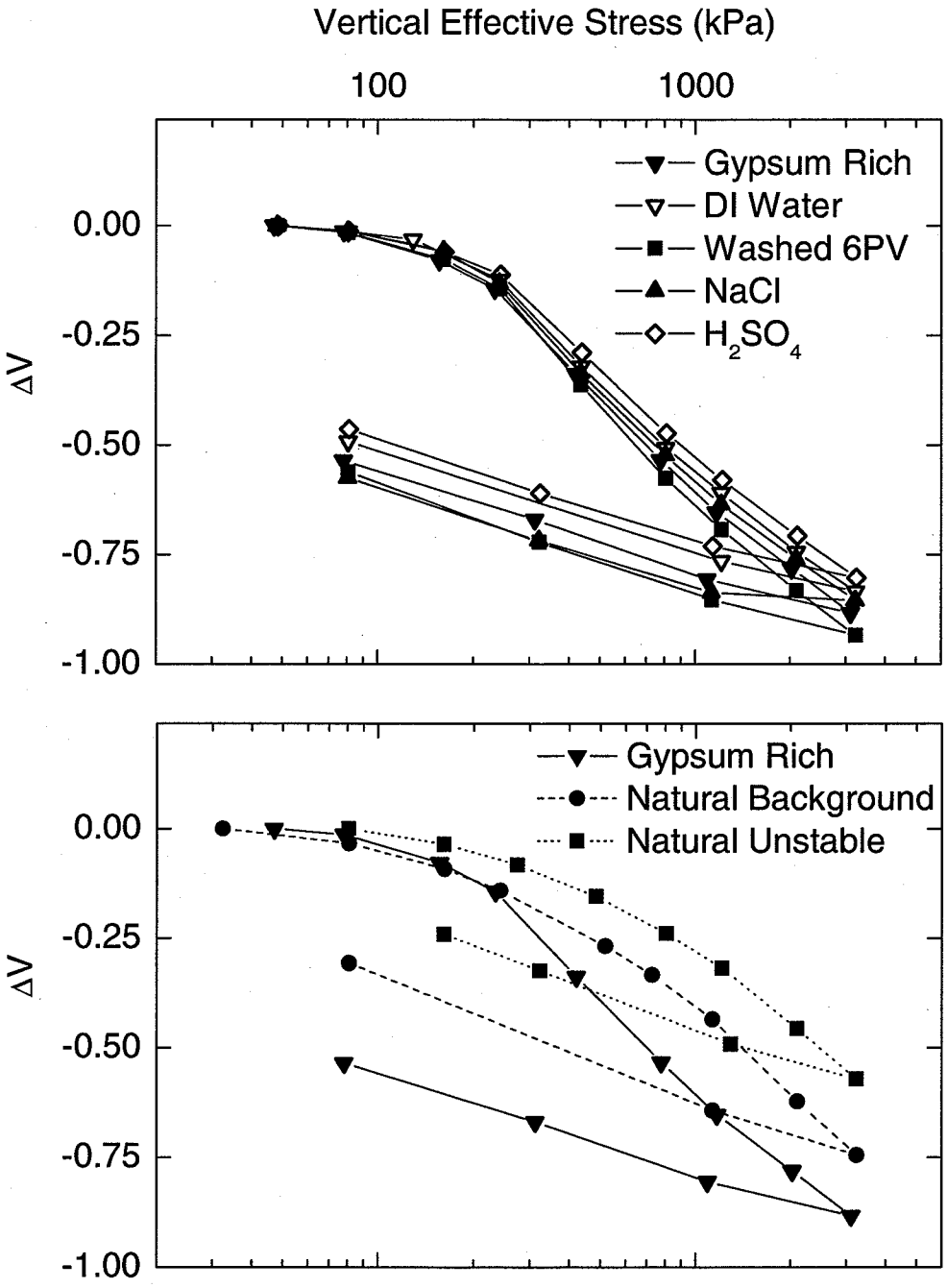

Figure 4.15. Oedometer test results for reconstituted (upper) and natural (lower) specimens plotted as change in specific volume.

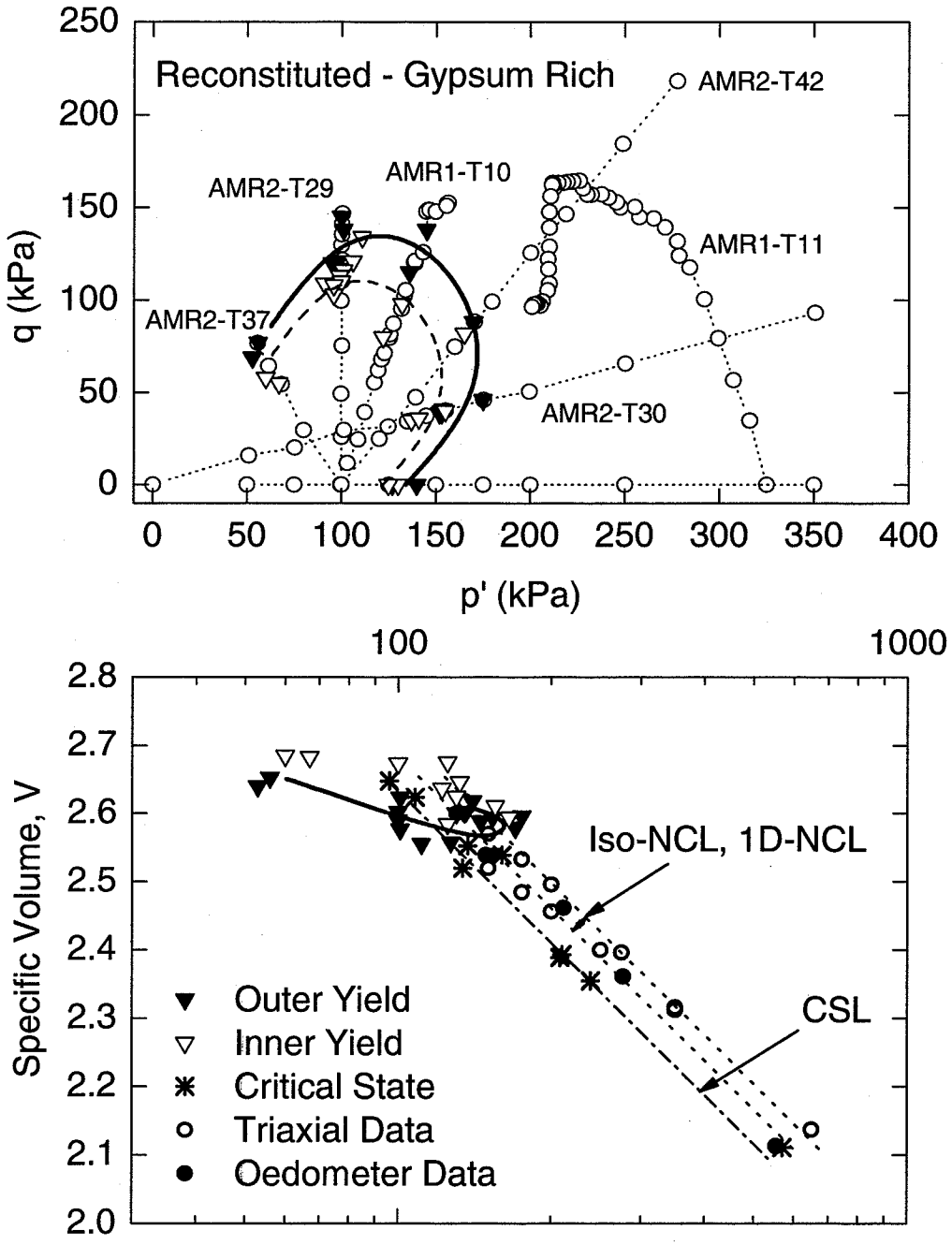

Figure 4.16. Yield locus for clay reconstituted with gypsum rich water (2,000 mg/L) in DI water.

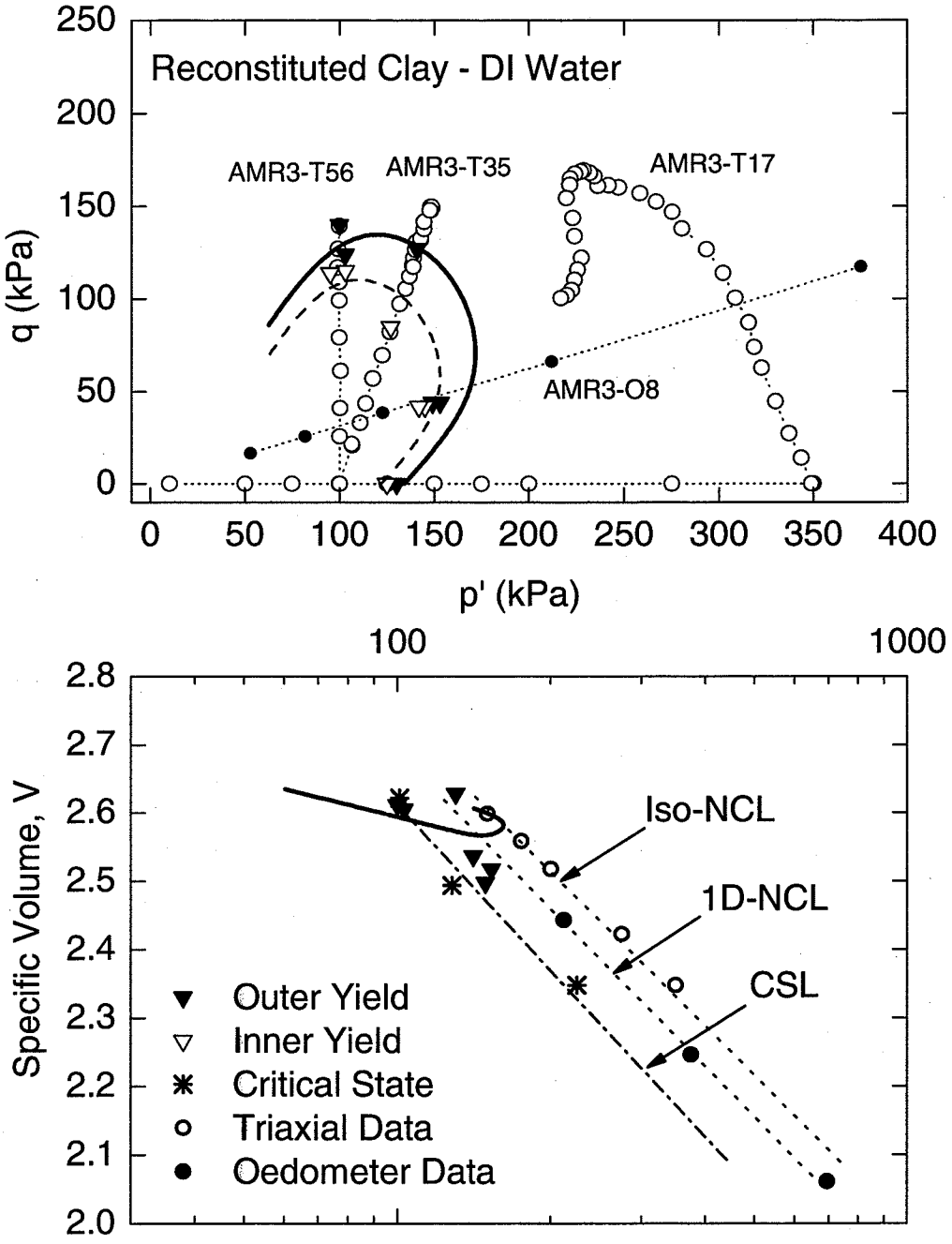

Figure 4.17. Yield locus for clay reconstituted with deionized water.

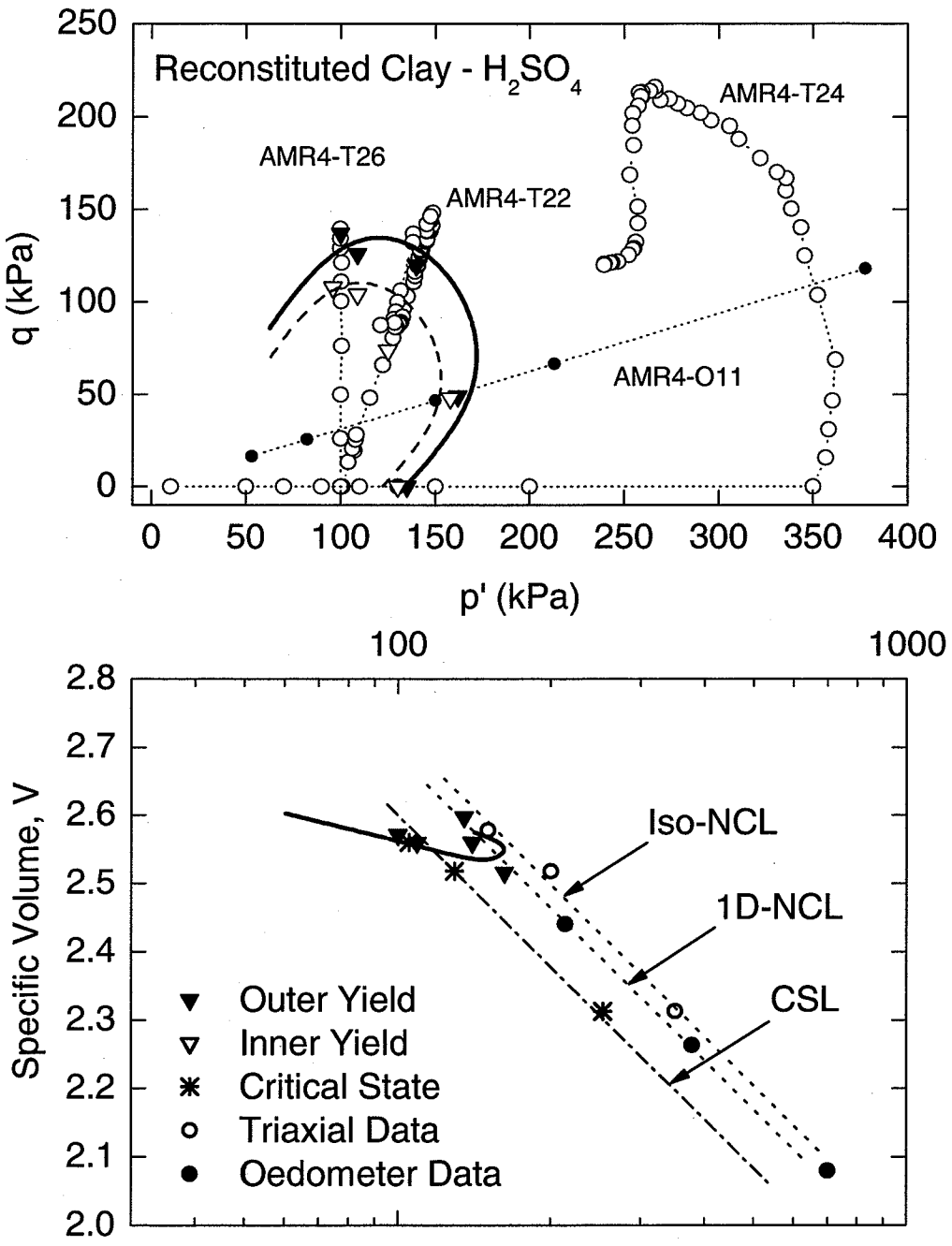

Figure 4.18. Yield locus for acidified (H_2SO_4) reconstituted clay.

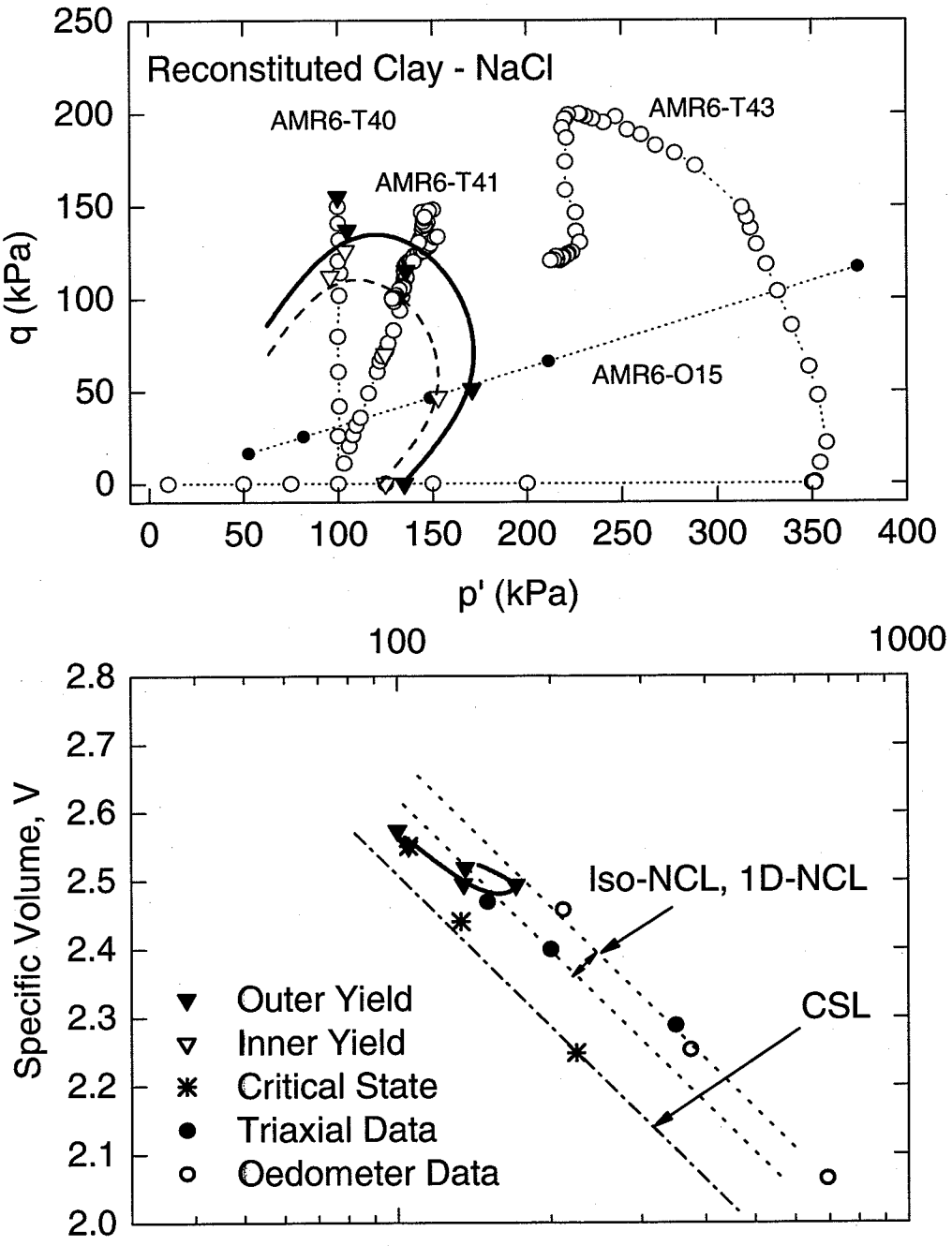

Figure 4.19. Yield locus for clay reconstituted with 50 g/L NaCl water.

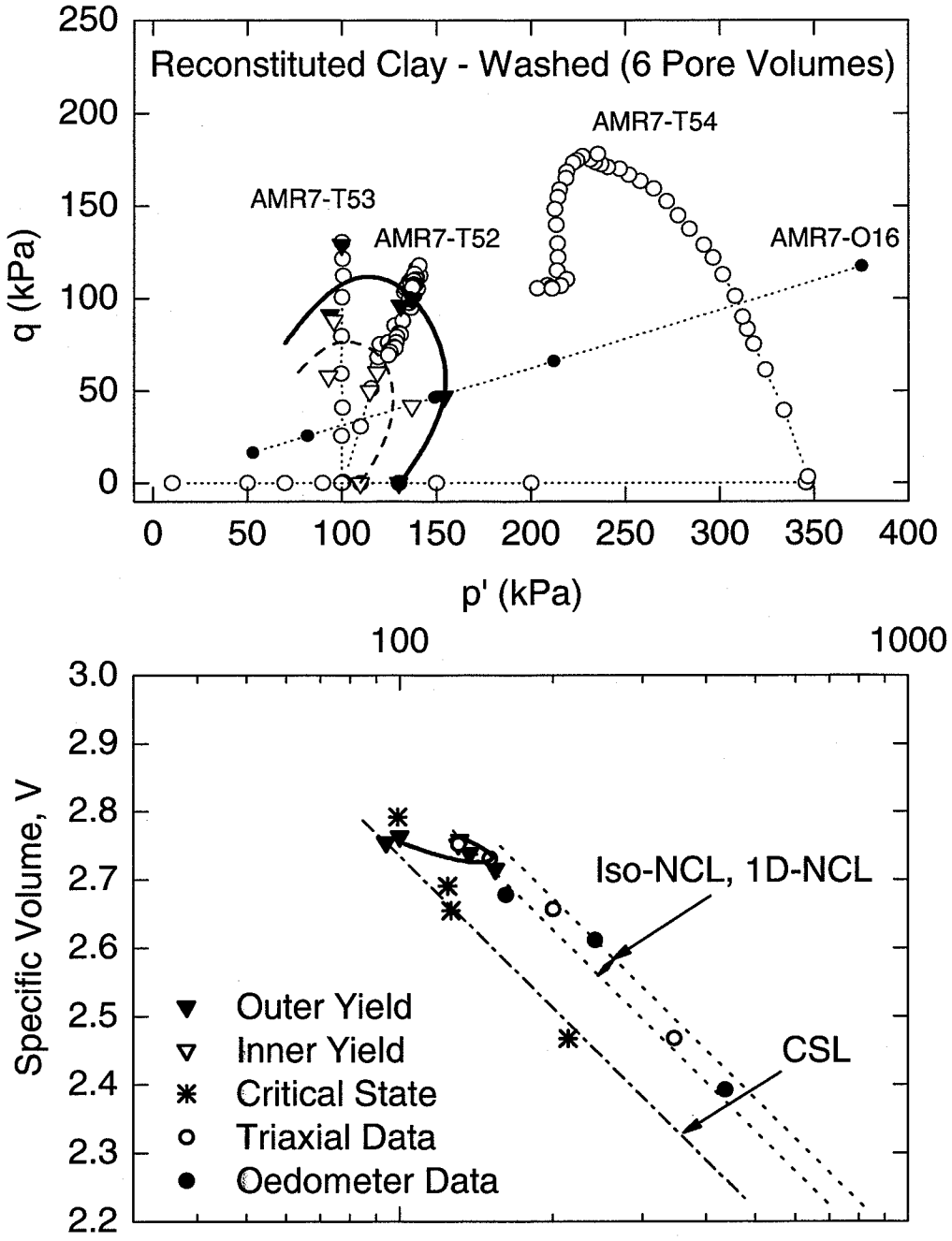

Figure 4.20. Yield locus for washed (6 pore volumes) reconstituted clay.

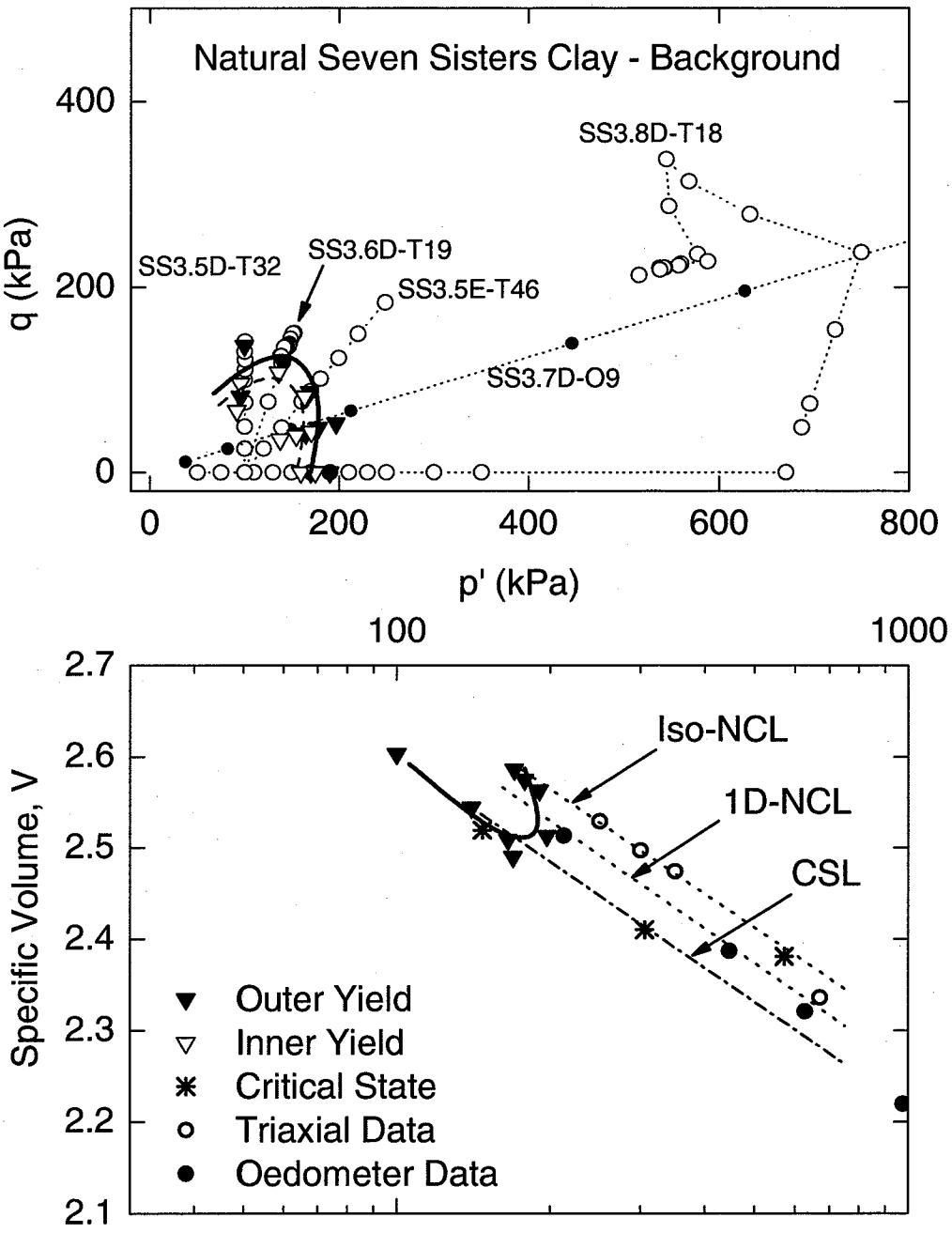

Figure 4.21. Yield locus for natural clay from the background location at Seven Sisters.

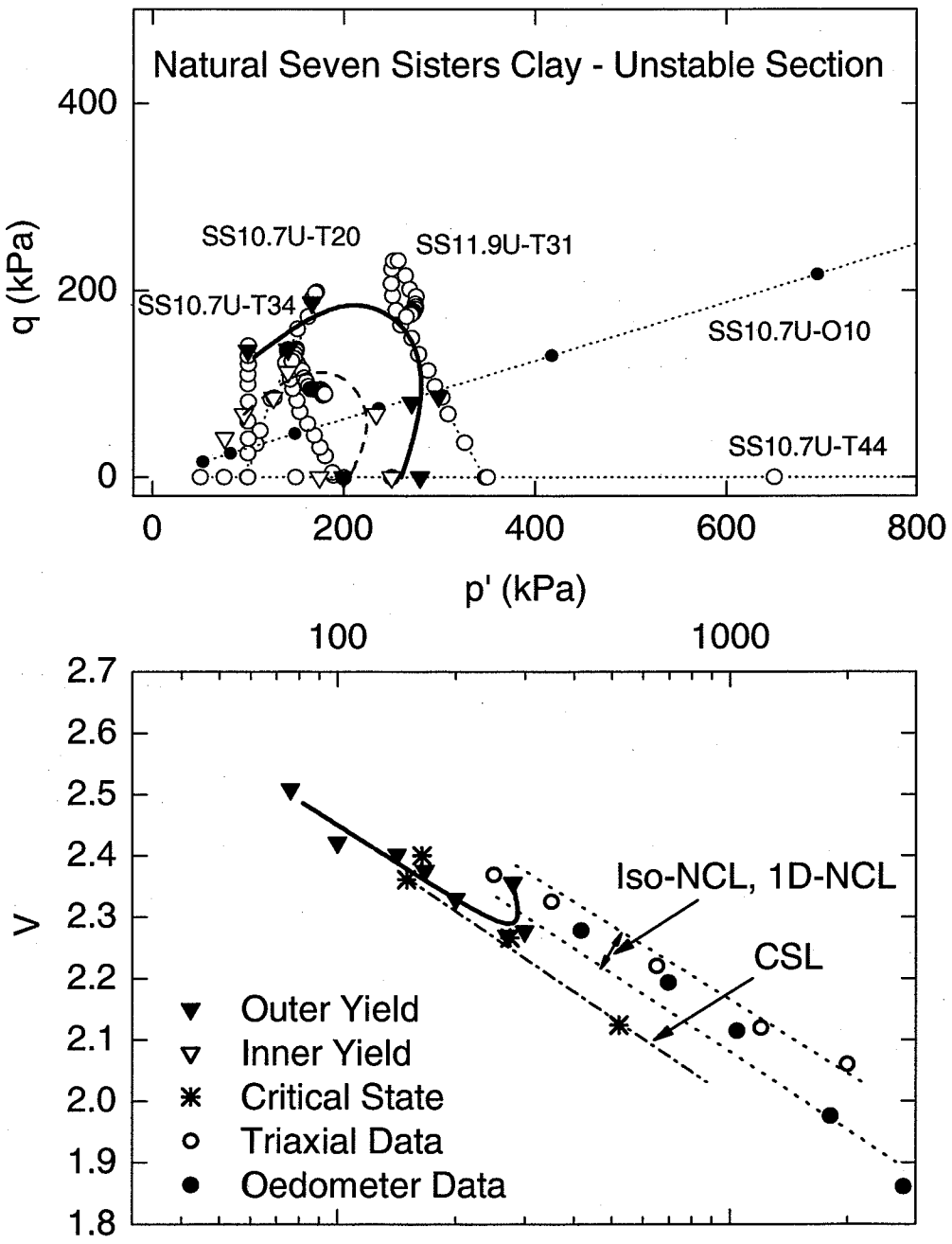

Figure 4.22. Yield locus for natural clay from the unstable section at Seven Sisters.

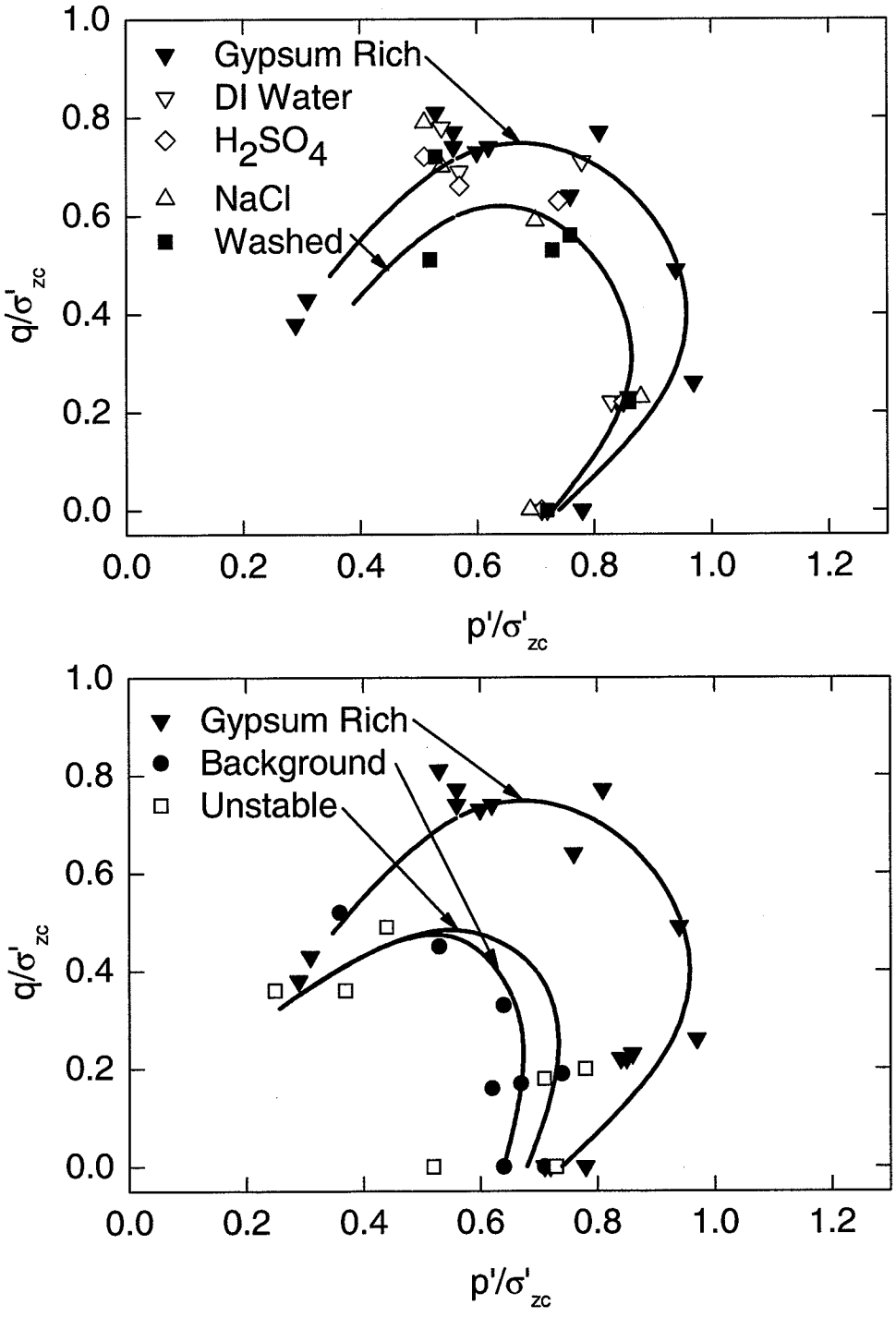

Figure 4.23. Outer yield points for reconstituted (top) and natural (bottom) Seven Sisters clay, normalized with respect to measured preconsolidation pressure. Reconstituted gypsum rich yield locus included in bottom plot for comparison.

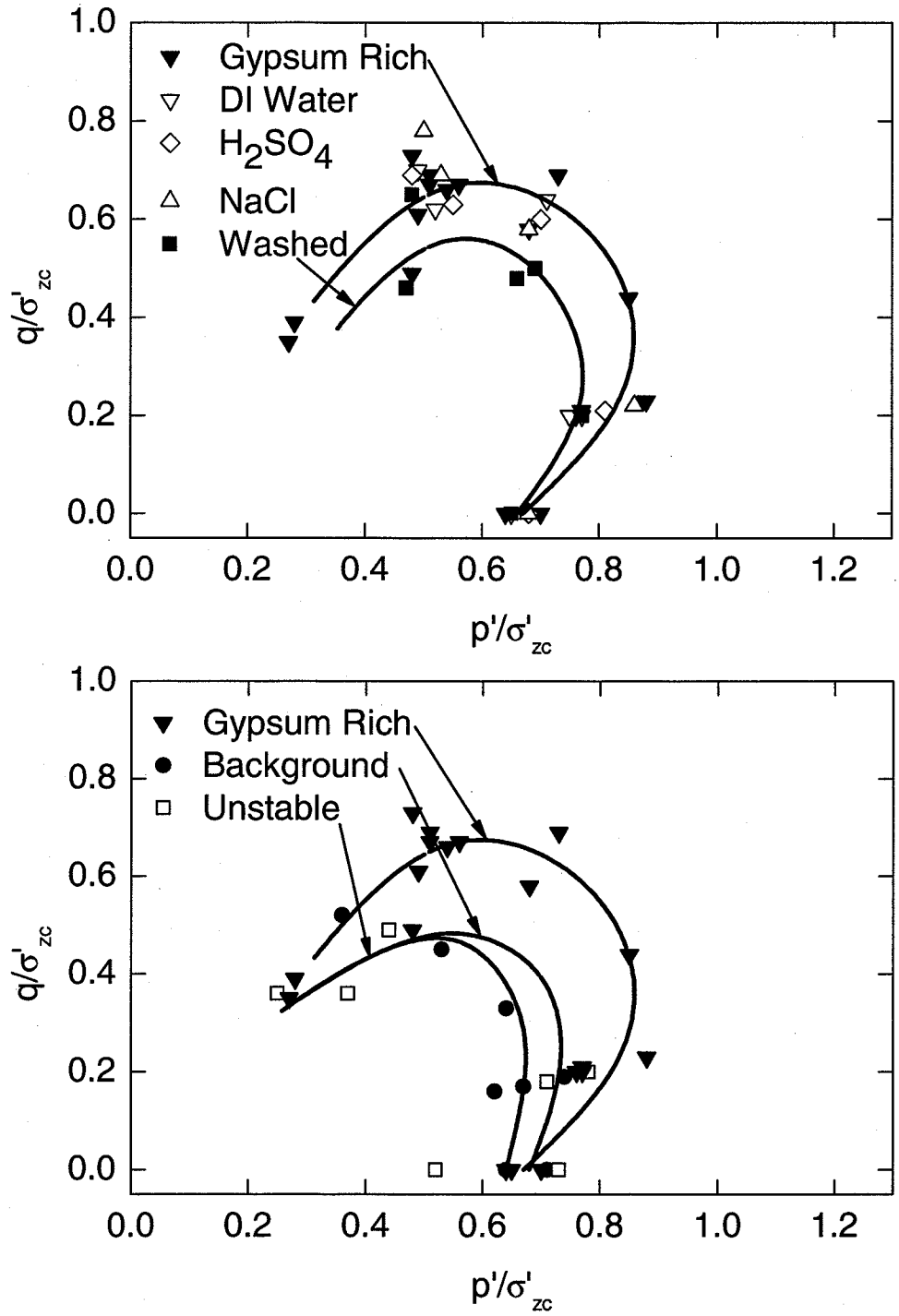

Figure 4.24. Outer yield points for reconstituted (top) Seven Sisters clay, normalized with respect to the applied (225 kPa – 25 kPa side wall friction) 1D pressure during consolidation. Natural specimens (bottom) were normalized with respect to the measured preconsolidation pressure. Reconstituted gypsum rich yield locus included in bottom plot for comparison.

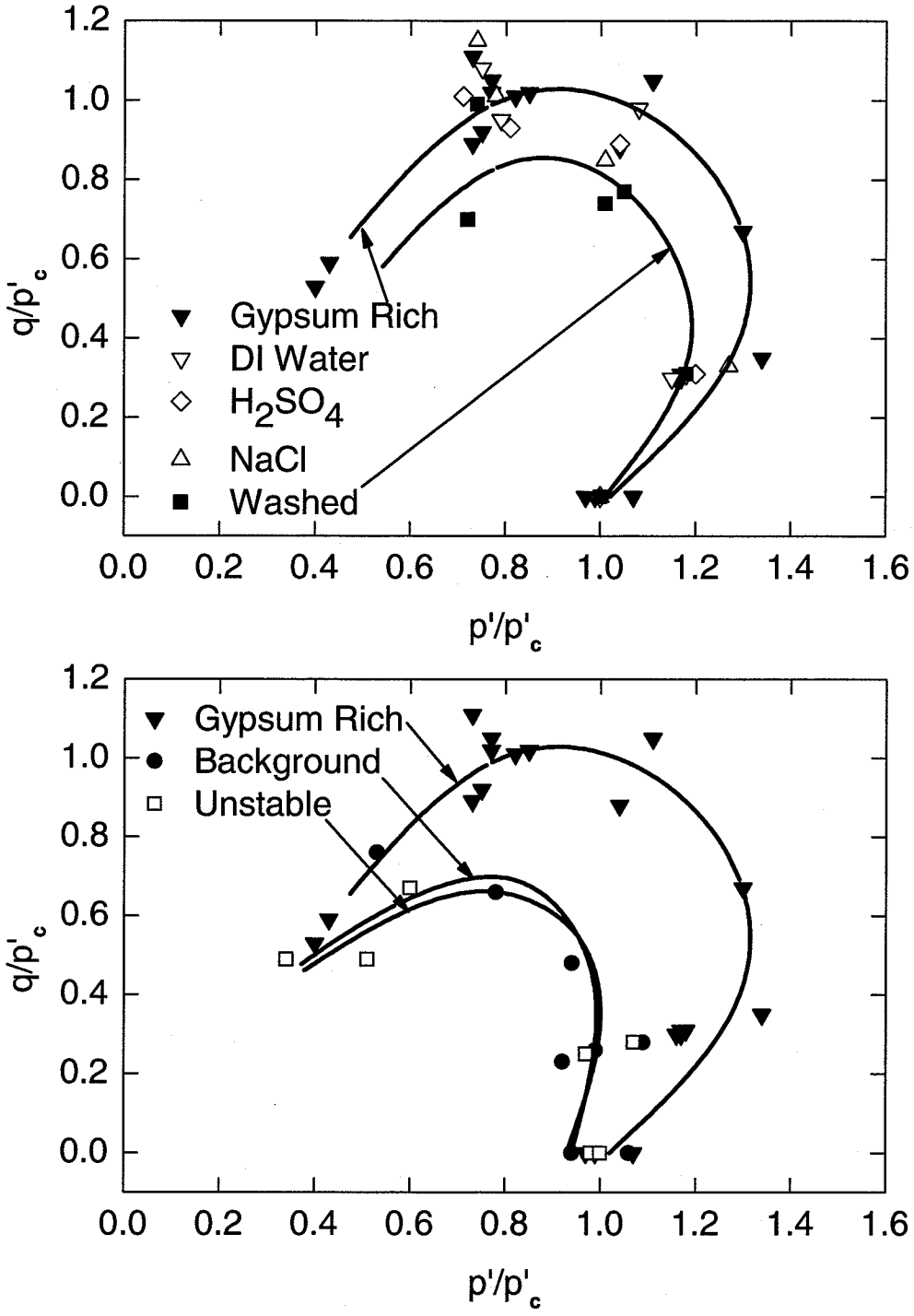

Figure 4.25. Outer yield points for reconstituted (top) and natural (bottom) Seven Sisters clay, normalized with respect to the measured isotropic p'_c. Reconstituted gypsum rich yield locus included in bottom plot for comparison.

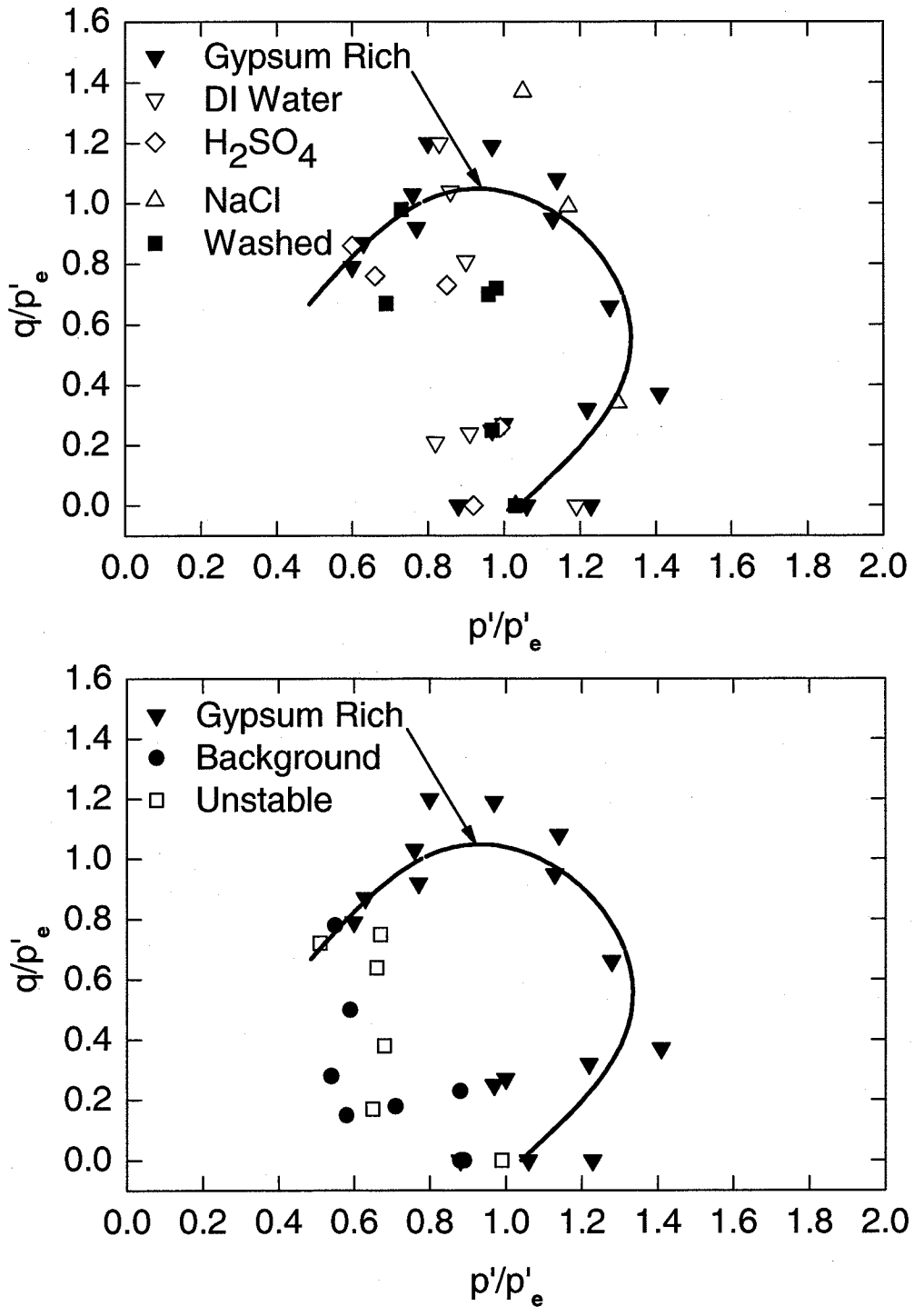

Figure 4.26. Outer yield points for reconstituted (top) and natural (bottom) Seven Sisters clay, normalized with respect to p'_e. Reconstituted gypsum rich yield locus included in bottom plot for comparison.

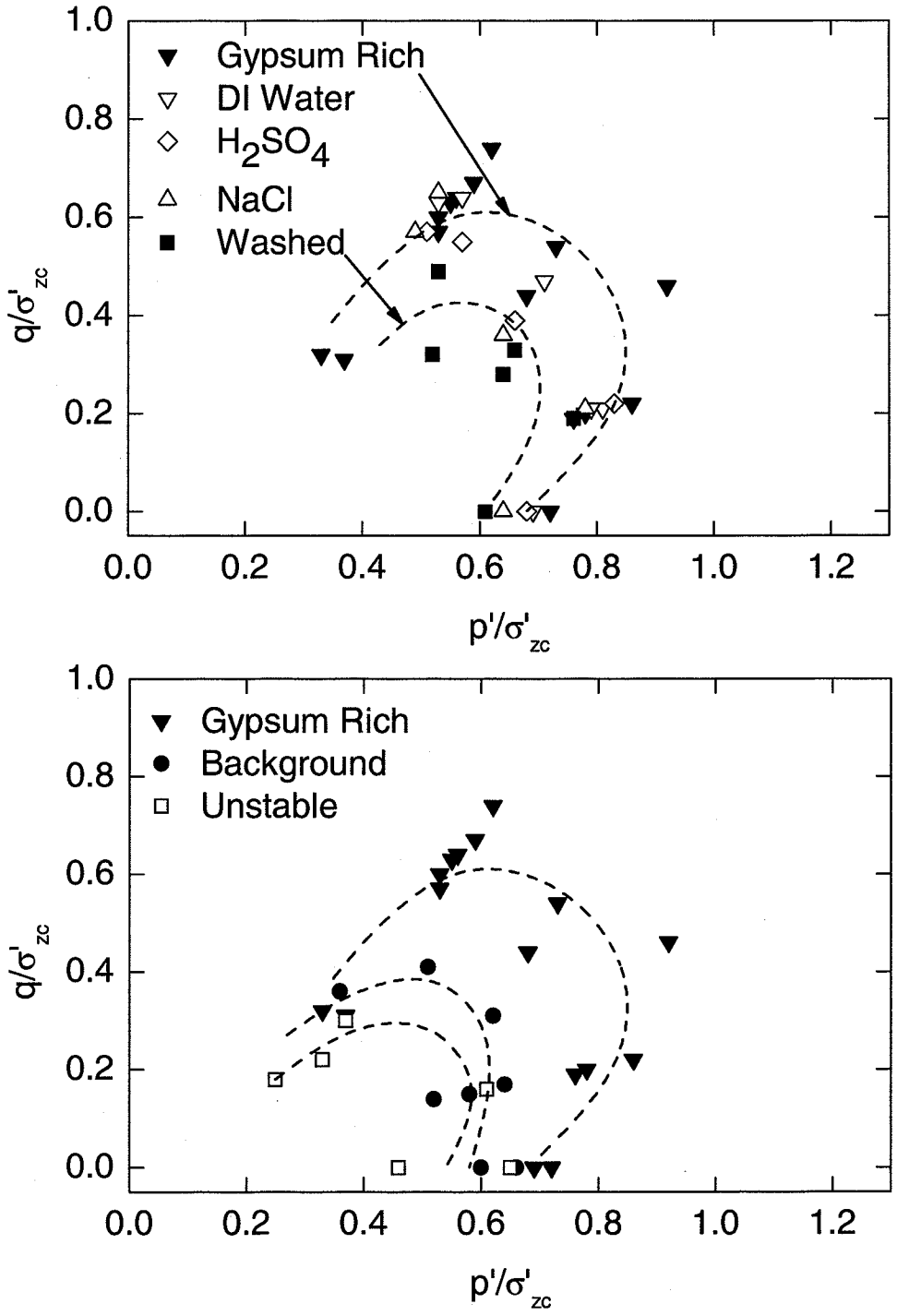

Figure 4.27. Inner yield points for reconstituted (top) and natural (bottom) Seven Sisters clay normalized with respect to measured preconsolidation pressure. Reconstituted gypsum rich yield locus included in bottom plot for comparison.

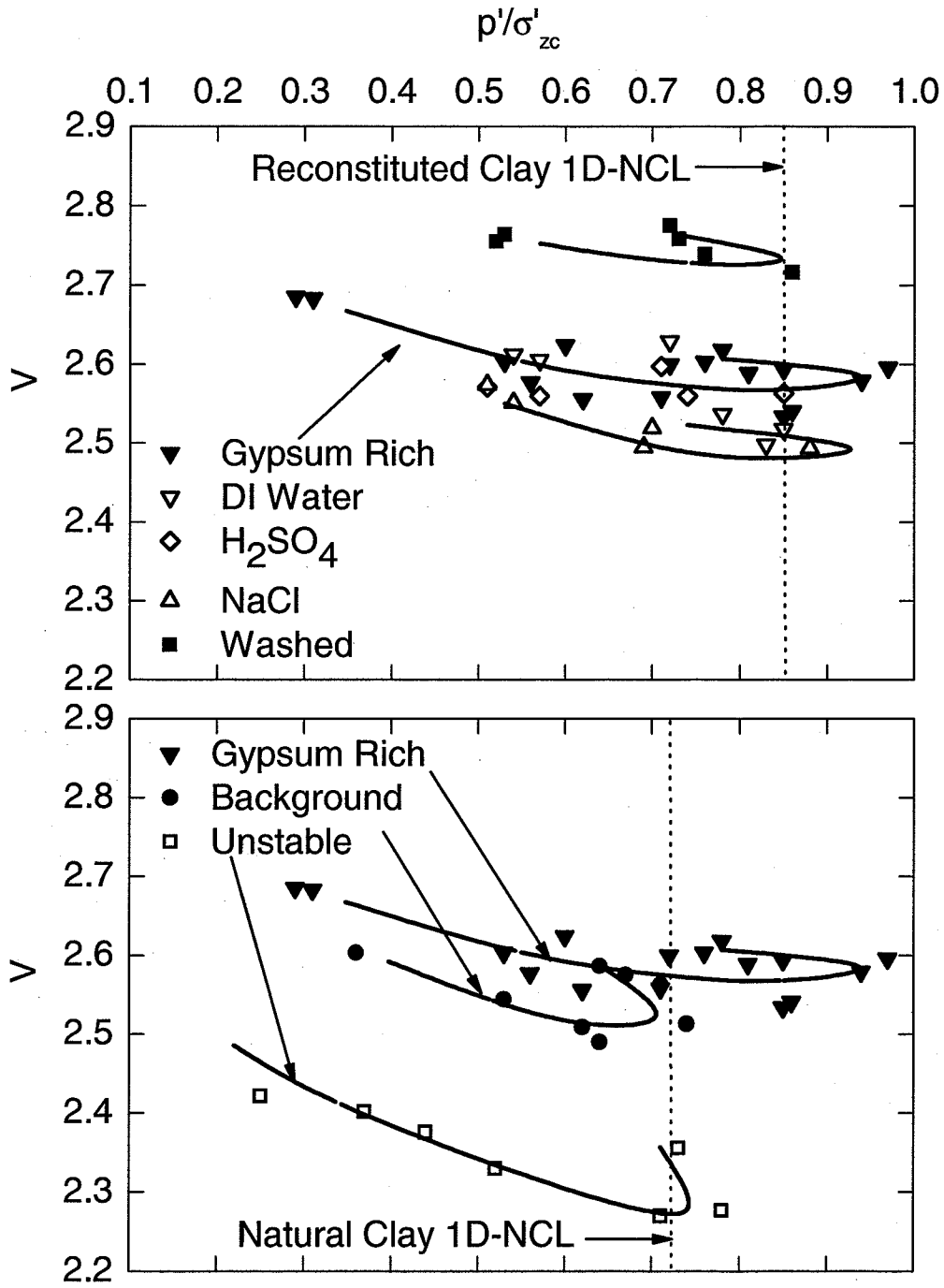

Figure 4.28. Yield loci in p'/σ'_{zc}, V-space for reconstituted (top) and natural (bottom) Seven Sisters clay normalized with respect to preconsolidation pressure. Reconstituted gypsum rich yield locus included in bottom plot for comparison.

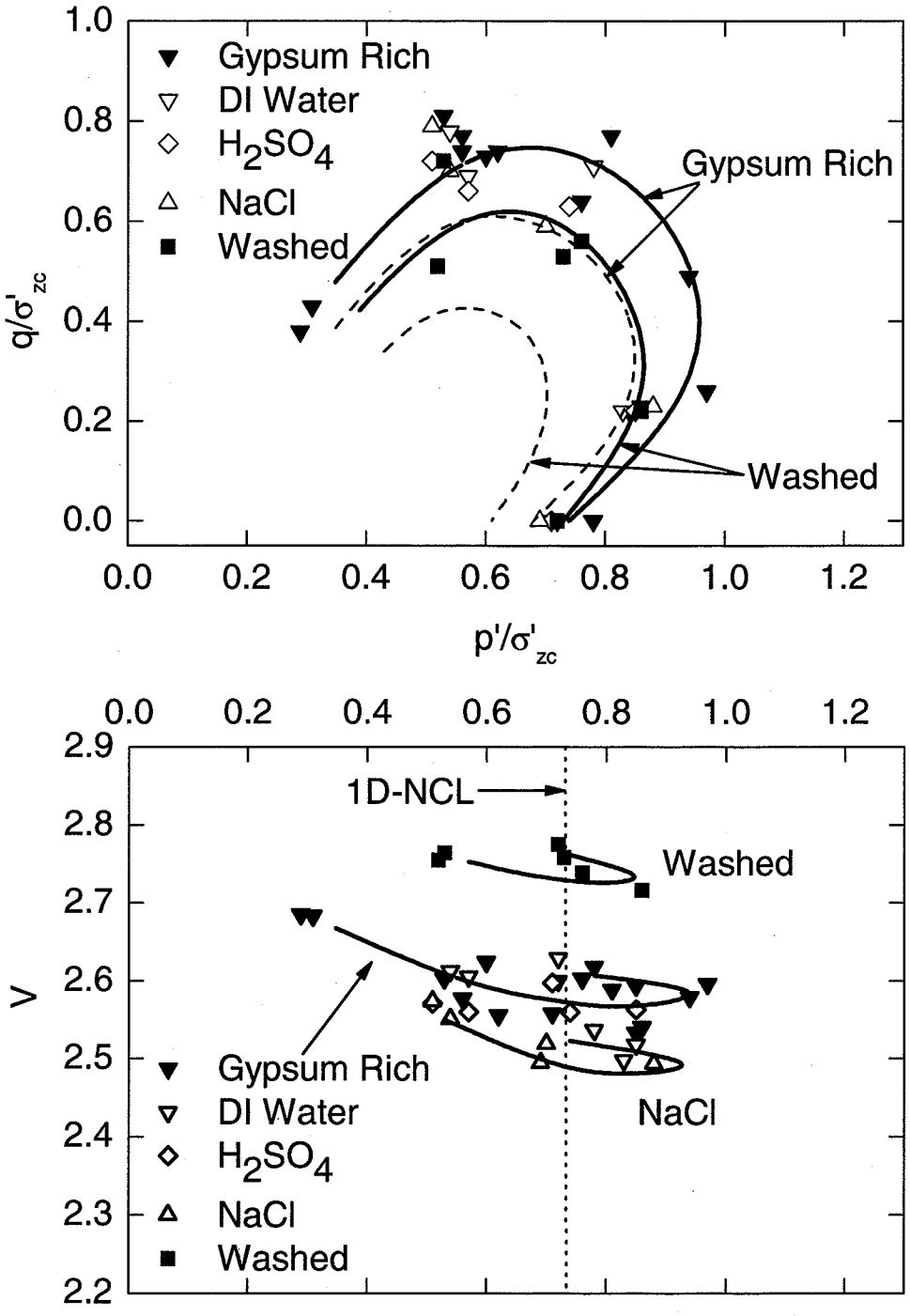

Figure 4.29. Yield loci in p'/σ'_{zc}, q/σ'_{zc}, V-space for reconstituted Seven Sisters clay normalized with respect to the measured preconsolidation pressure. The solid lines represent the outer yield loci and the dashed lines represent the inner yield loci. For clarity, only the outer yield points are shown.

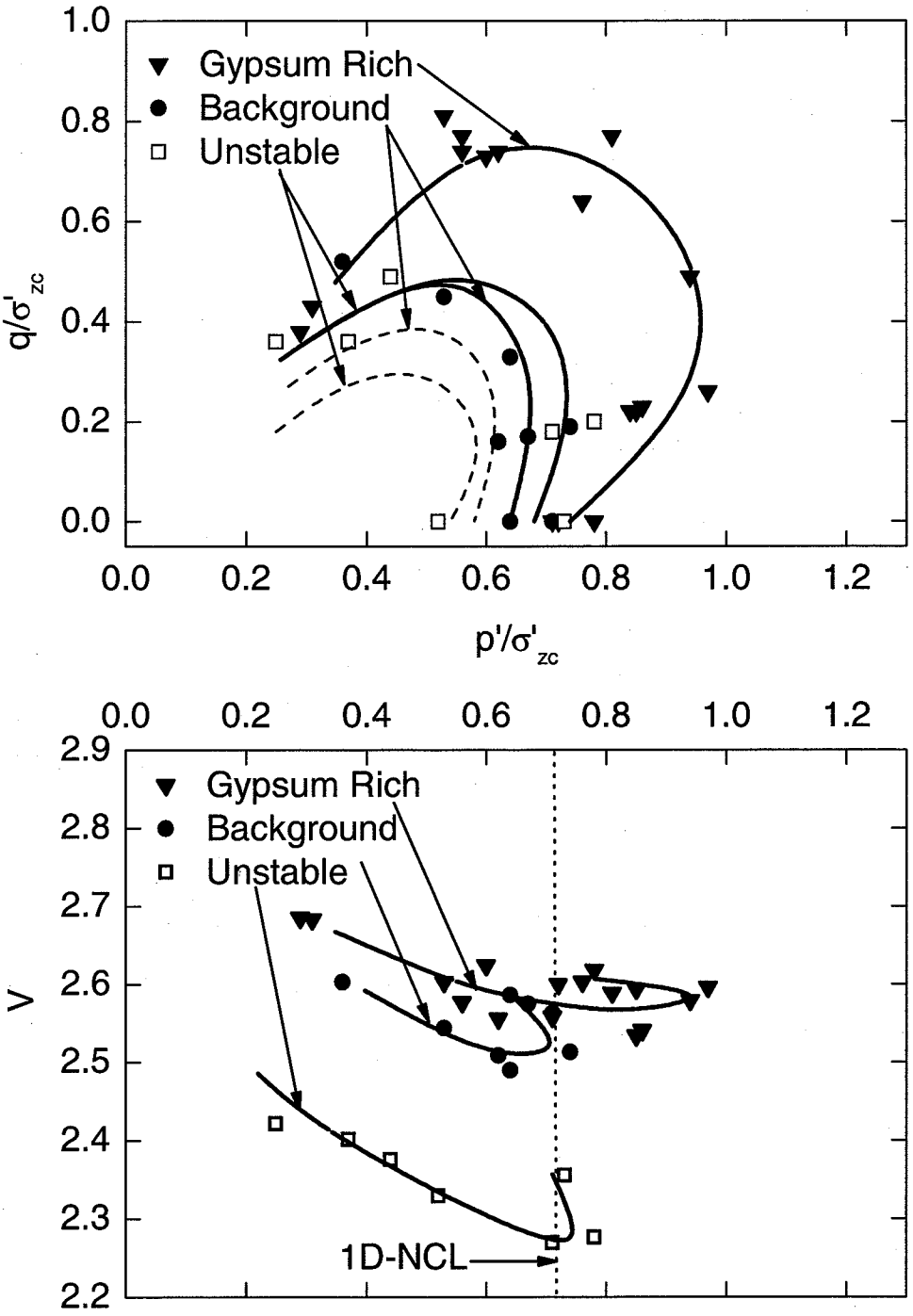

Figure 4.30. Yield loci in p'/σ'_{zc}, q/σ'_{zc}, V-space for natural Seven Sisters clay normalized with respect to the measured preconsolidation pressure. The solid lines represent the outer yield loci and the dashed lines represent the inner yield loci. For clarity, only the outer yield points are shown.

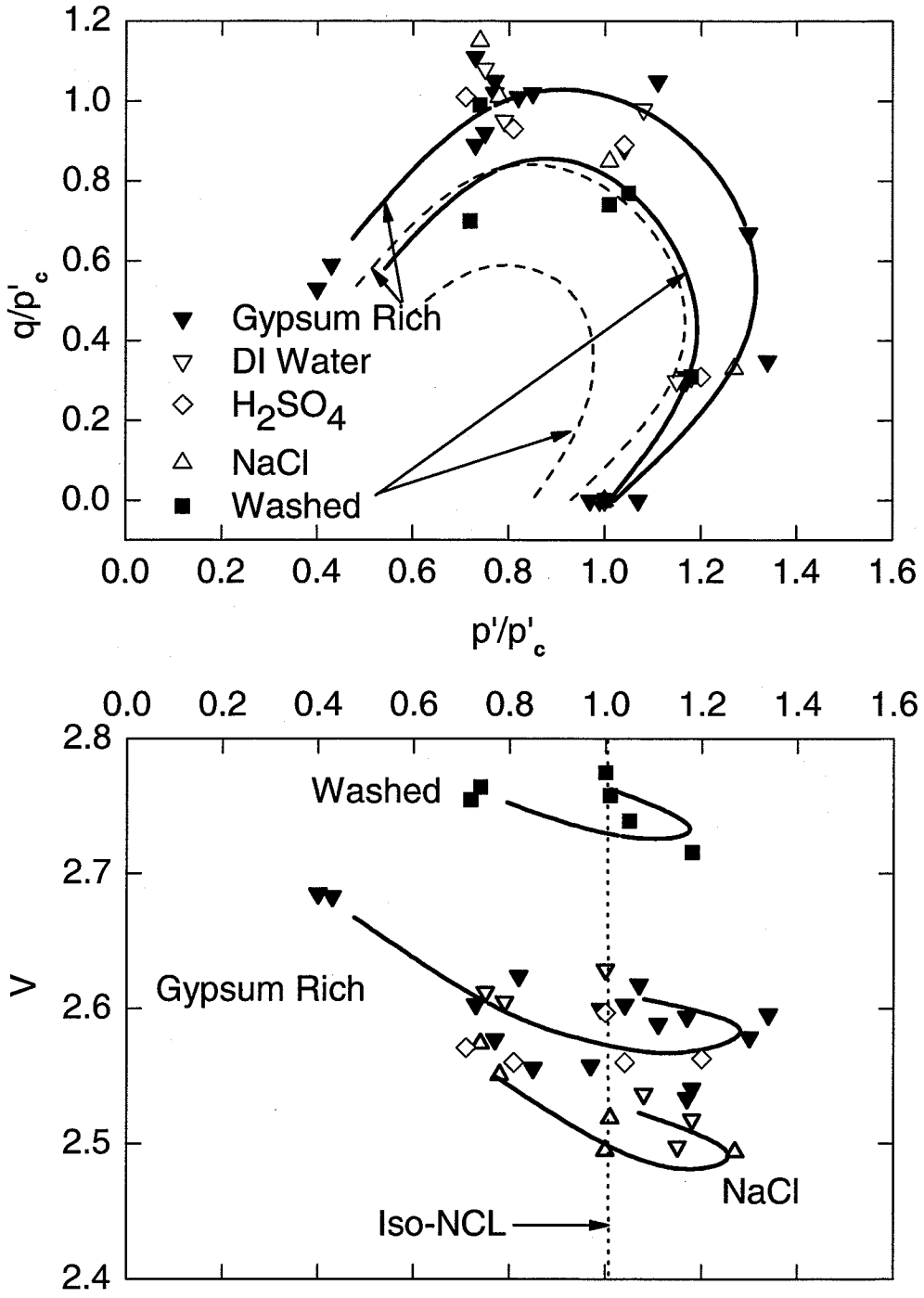

Figure 4.31. Yield loci in p'/p'_c, q/p'_c, V-space for reconstituted Seven Sisters clay normalized with respect to the measured isotropic preconsolidation pressure. The solid lines represent the outer yield loci and the dashed lines represent the inner yield loci. For clarity, only the outer yield points are shown.

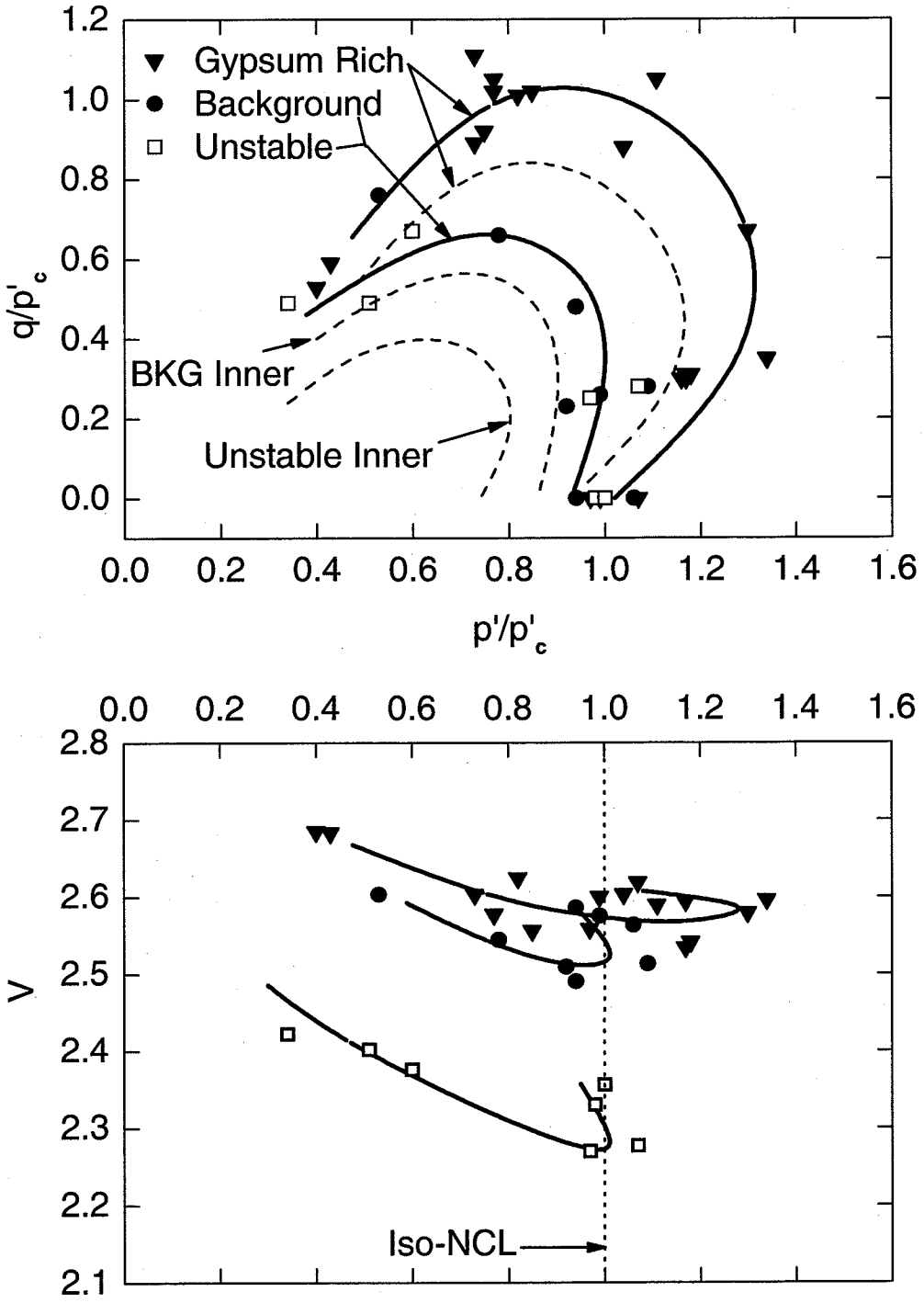

Figure 4.32. Yield loci in p'/p'_c, q/p'_c, V-space for natural Seven Sisters clay normalized with respect to the measured isotropic preconsolidation pressure. The solid lines represent the outer yield loci and the dashed lines represent the inner yield loci. For clarity, only the outer yield points are shown.

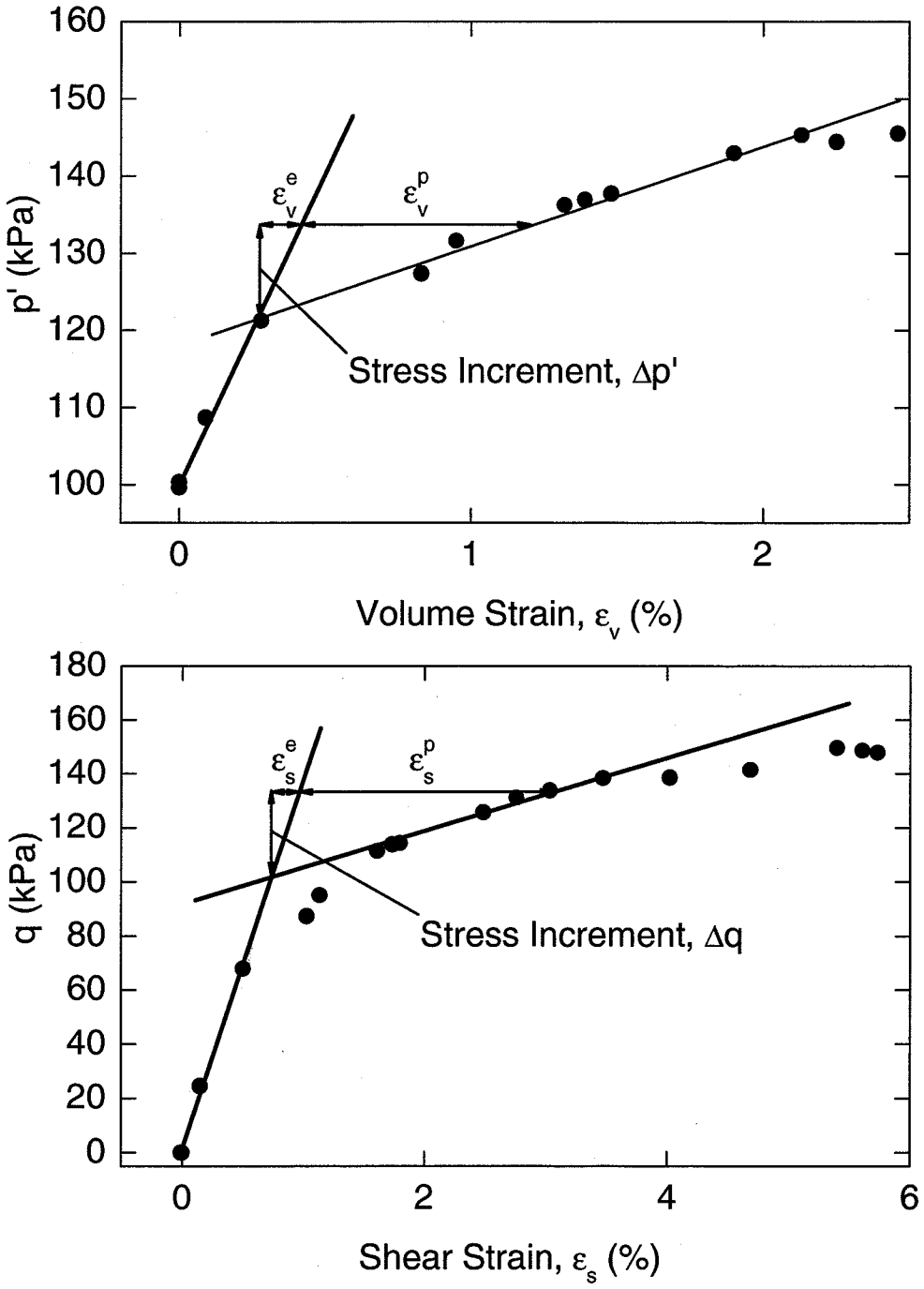

Figure 4.33. Graphical method of determining plastic strains by separation of elastic strains. Data from Specimen AMR1-T10.

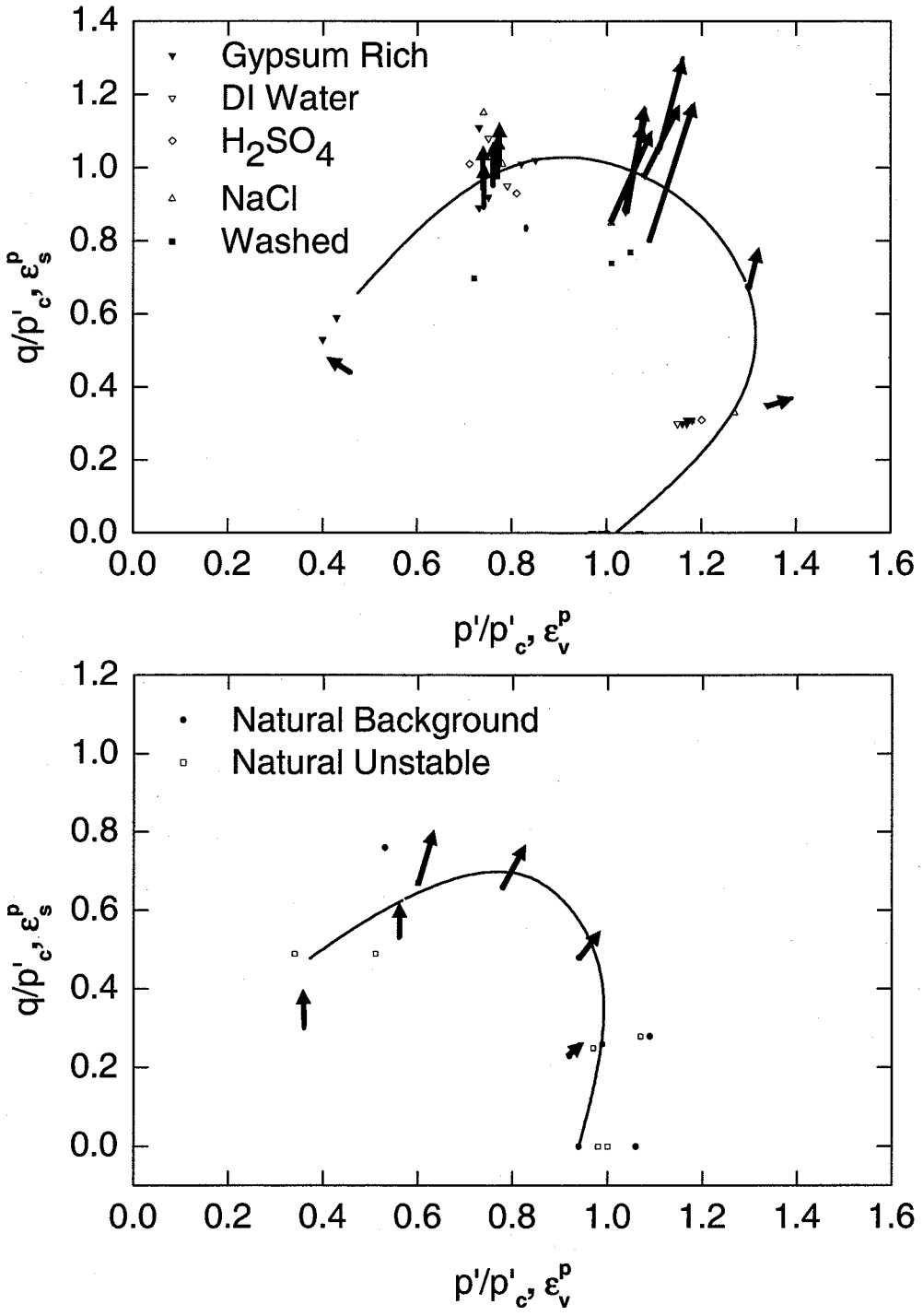

Figure 4.34. Plastic strain increment vectors.

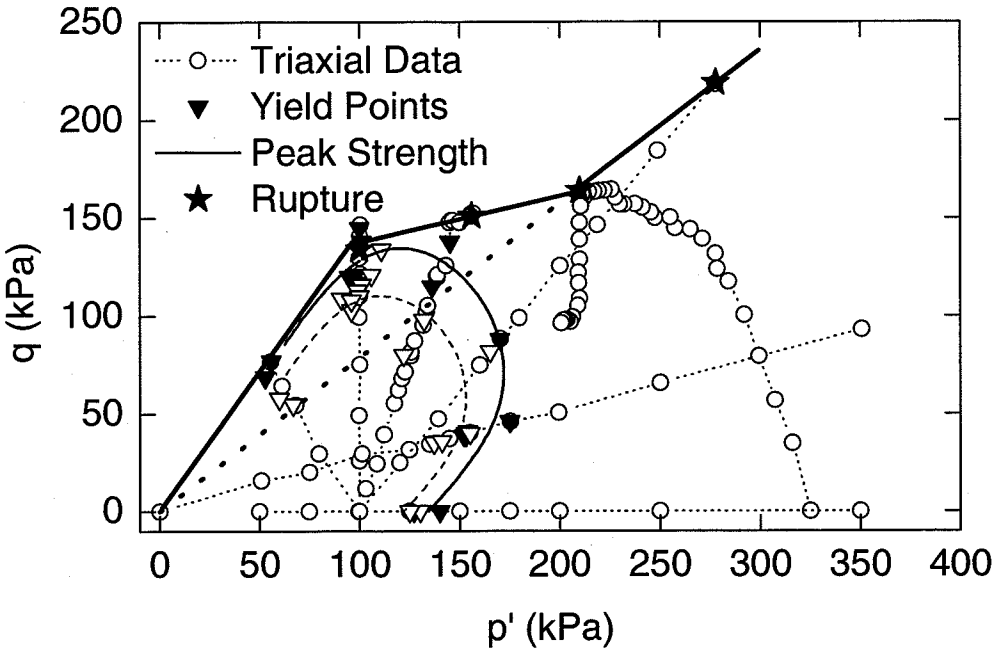

Figure 5.1. Peak strength envelope for the gypsum rich reconstituted clay.

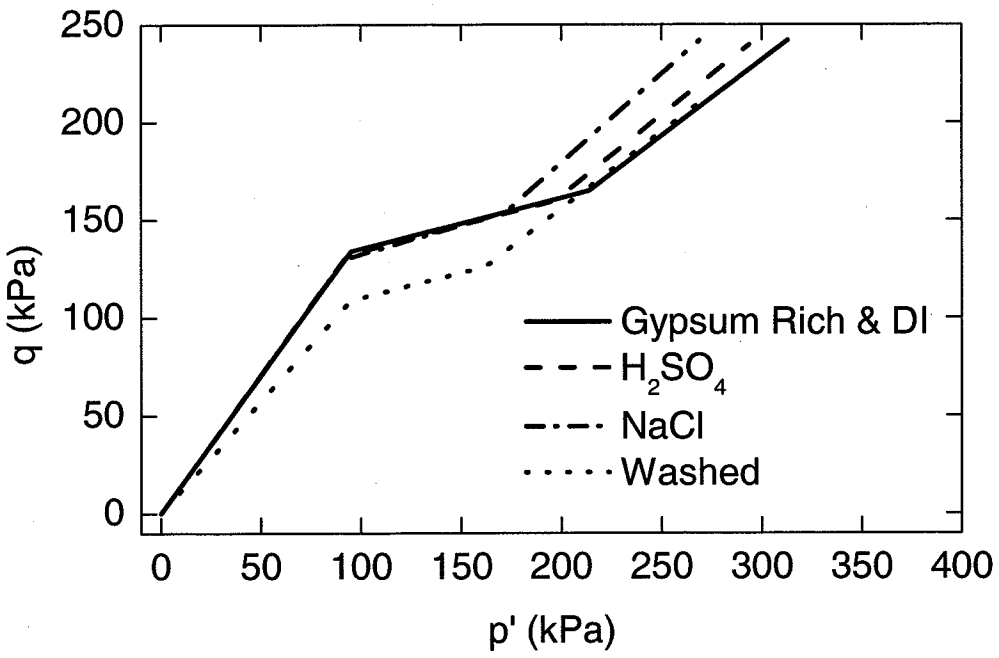

Figure 5.2. Peak strength envelopes for the reconstituted clays.

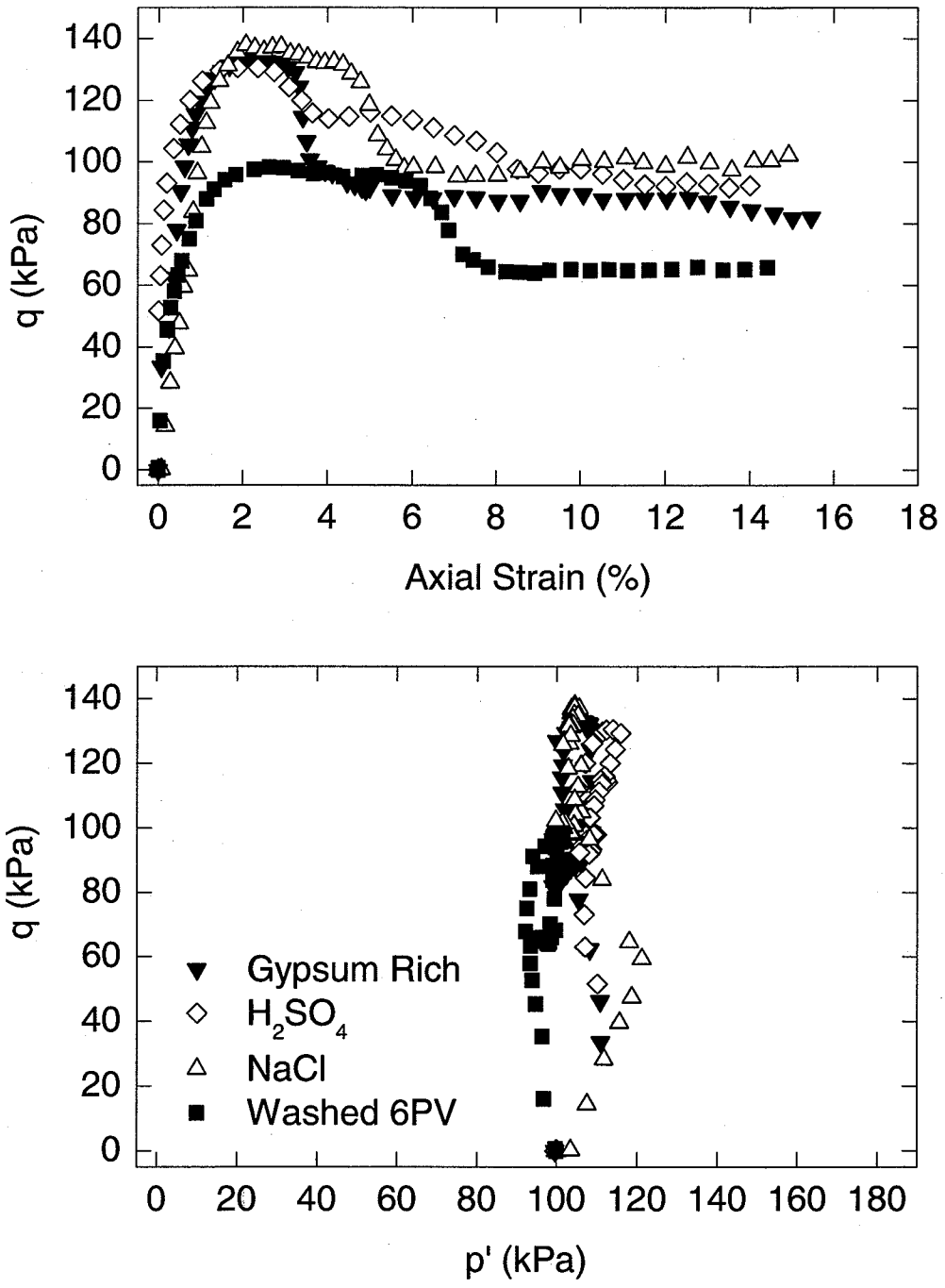

Figure 5.3. Comparison of CIŪ triaxial test results for reconstituted clays with different pore fluid chemistry.

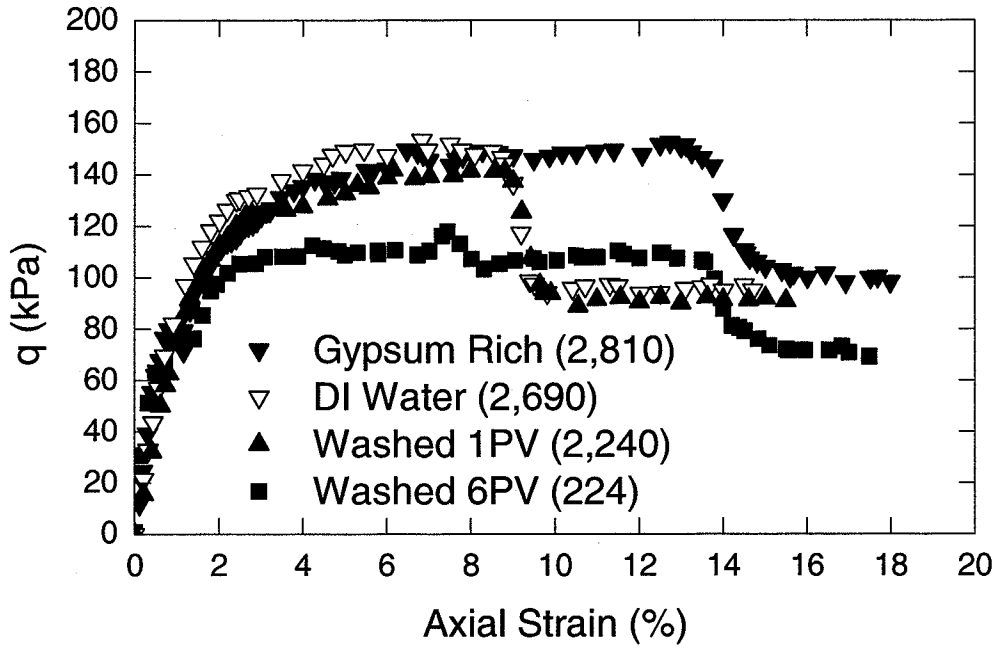

Figure 5.4. Comparison of CID triaxial test results for reconstituted clays with varying amounts of sulphate. Values in brackets are sulphate concentrations in mg/L.

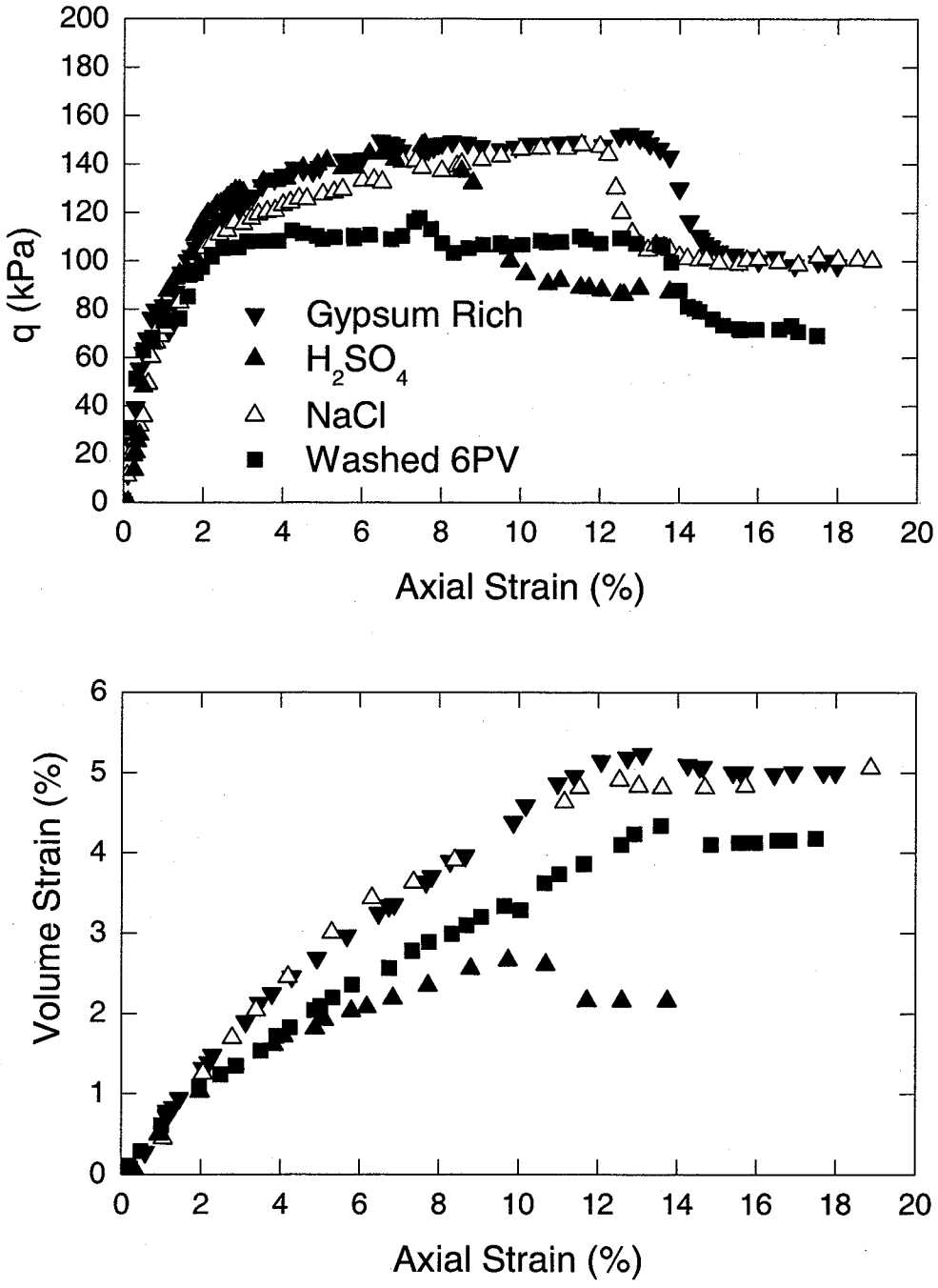

Figure 5.5. Comparison of CID triaxial test results for reconstituted clays with different pore fluid chemistry.

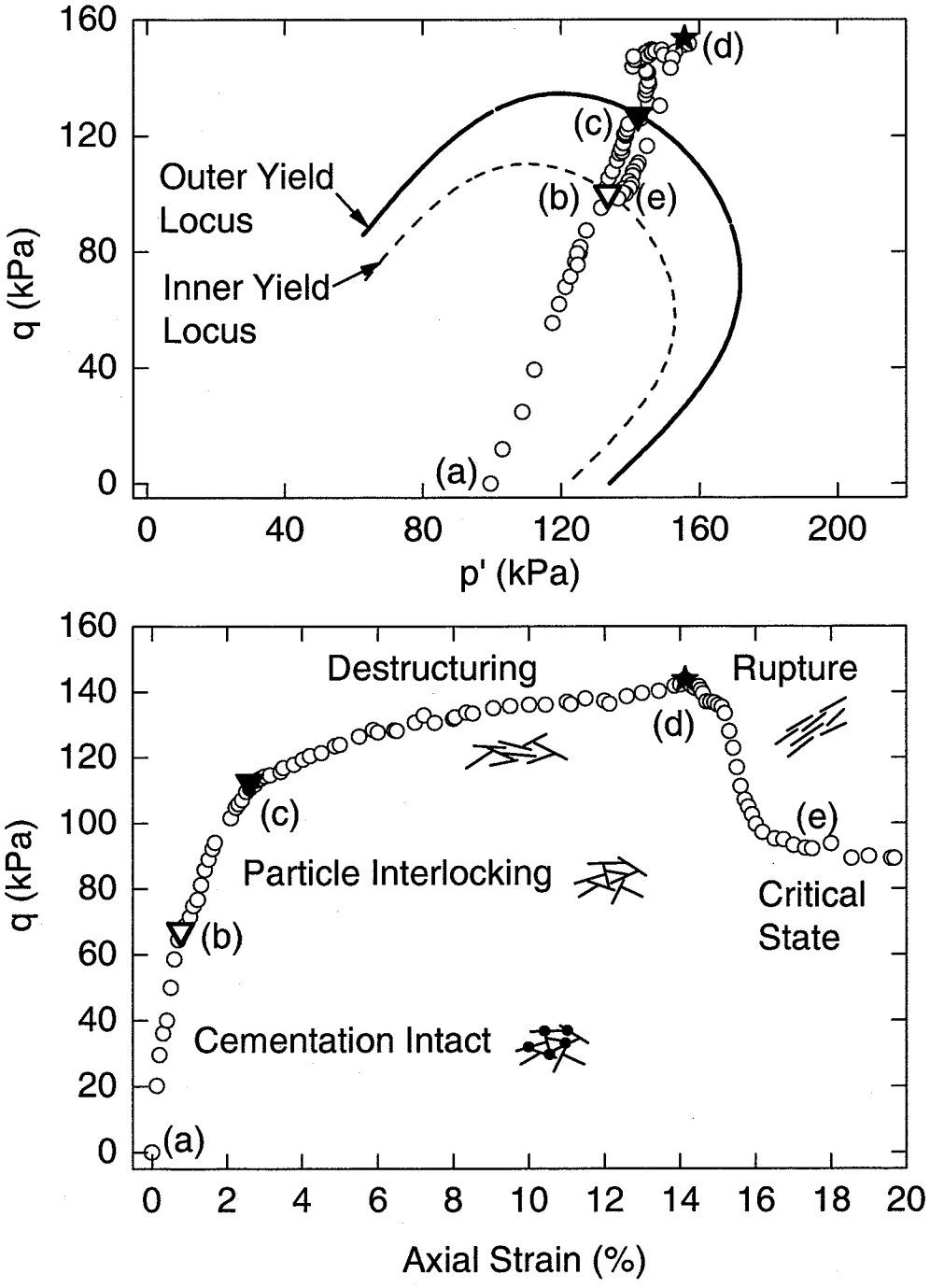

Figure 5.6. Tracking of a CID stress path with its corresponding stress-strain curve as if passes through the yield loci to critical state (gypsum rich specimen AMR1-T10).

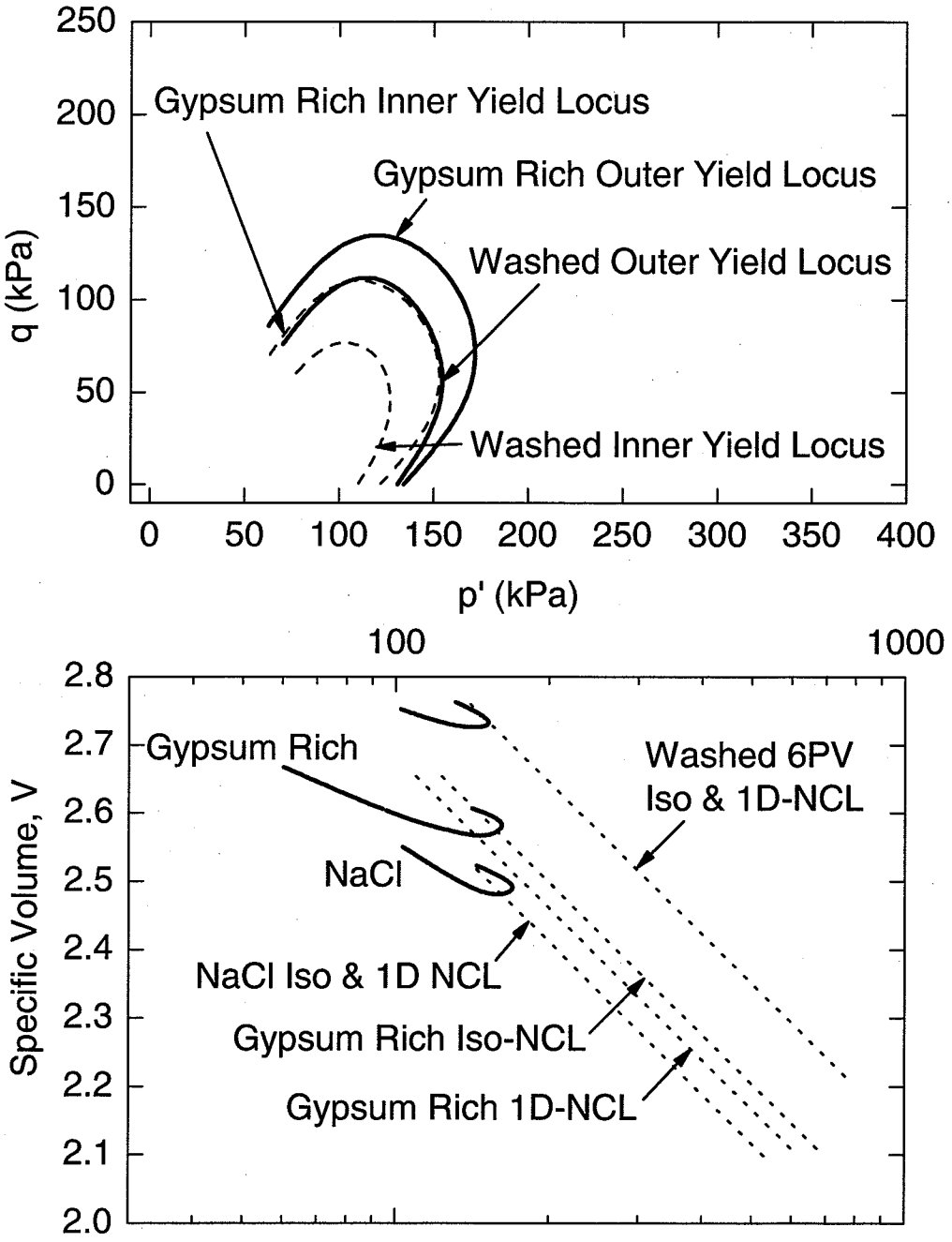

Figure 5.7. Yield loci for the gypsum rich, washed 6PV, and NaCl specimens compared in arithmetic space.

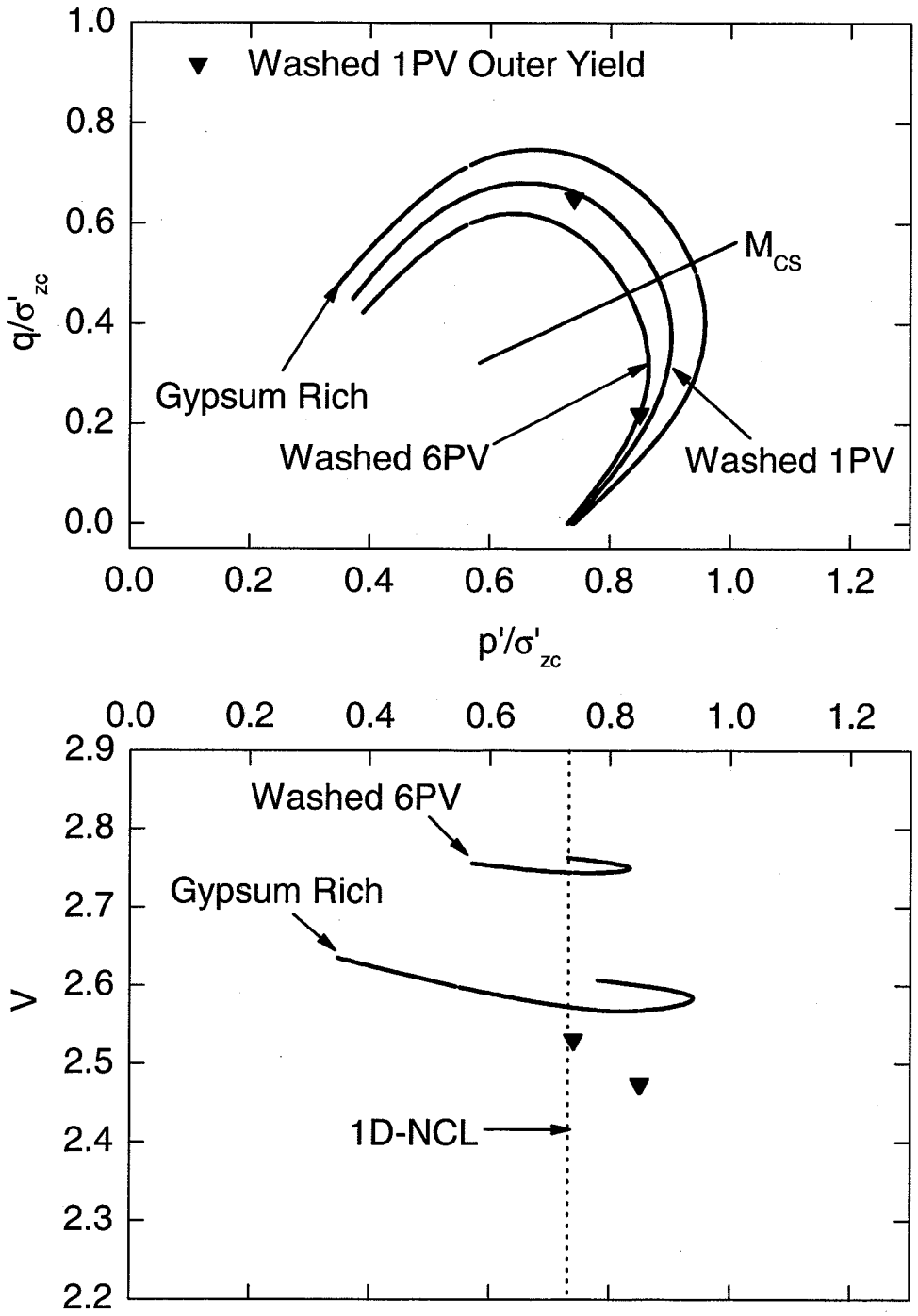

Figure 5.8. Outer yield points for the washed 1PV specimens compared to the gypsum rich and washed 6PV yield loci.

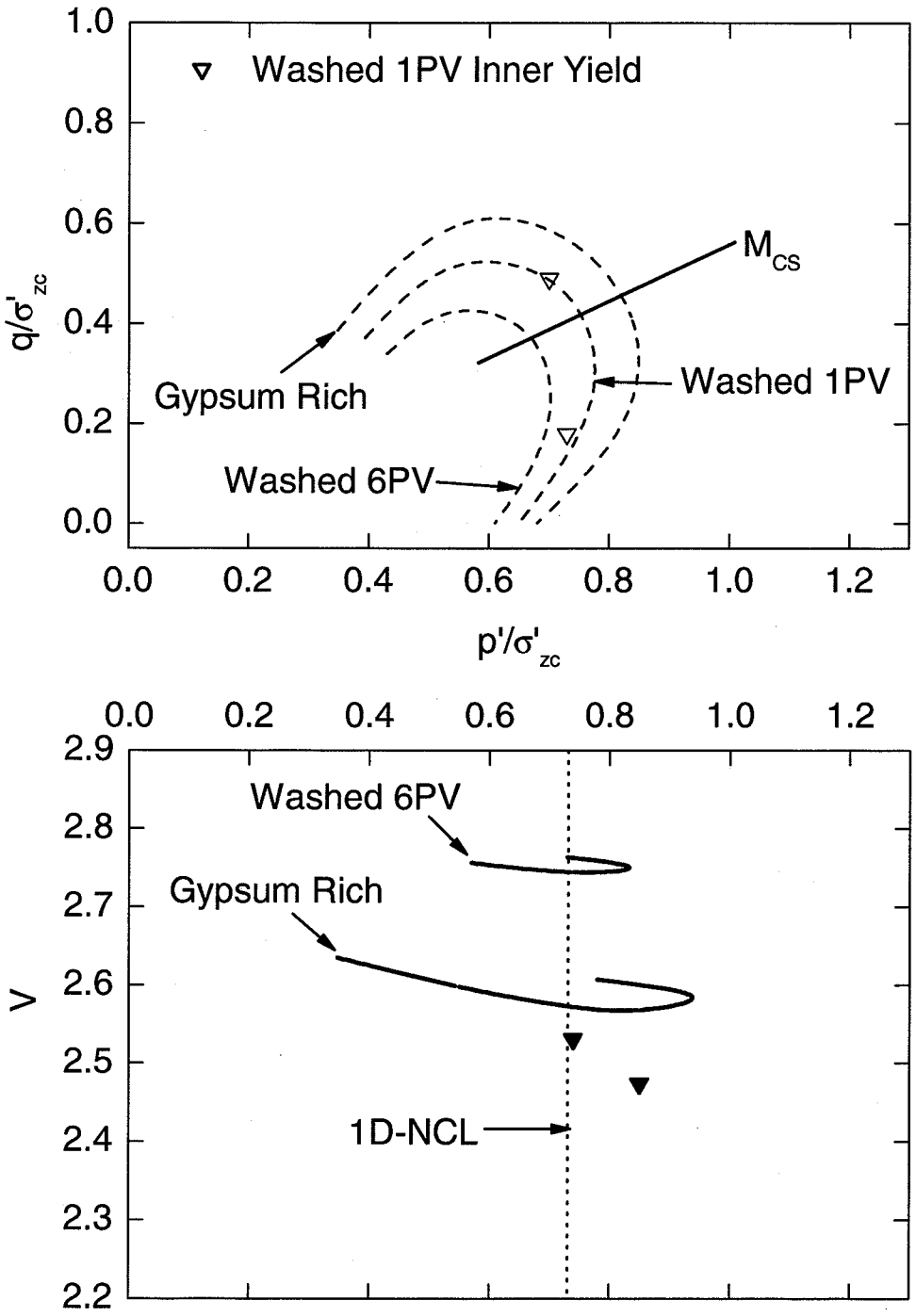

Figure 5.9. Inner yield points for the washed 1PV specimens compared to the gypsum rich and washed 6PV yield loci.

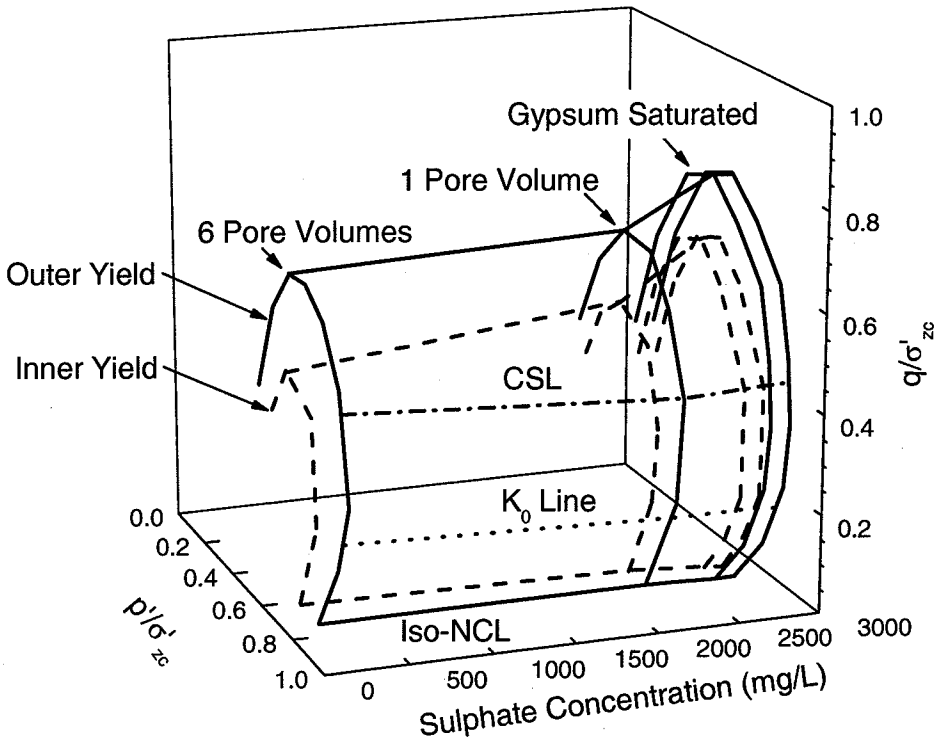

Figure 5.10. Yielding in p'/σ'_{zc}, q/σ'_{zc}-space as a function of sulphate concentration.

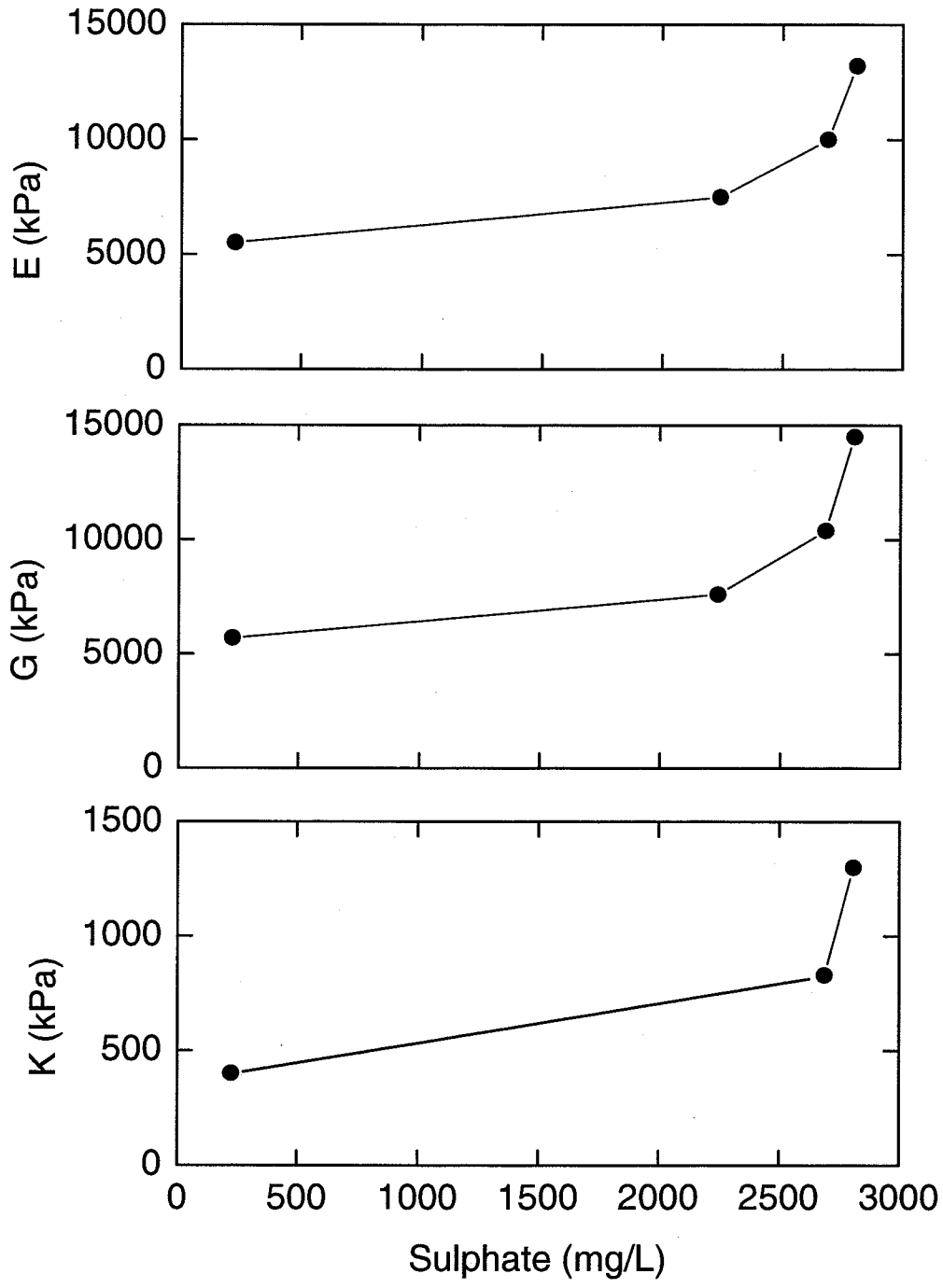

Figure 5.11. Isotropic elastic parameters as a function of sulphate concentration.

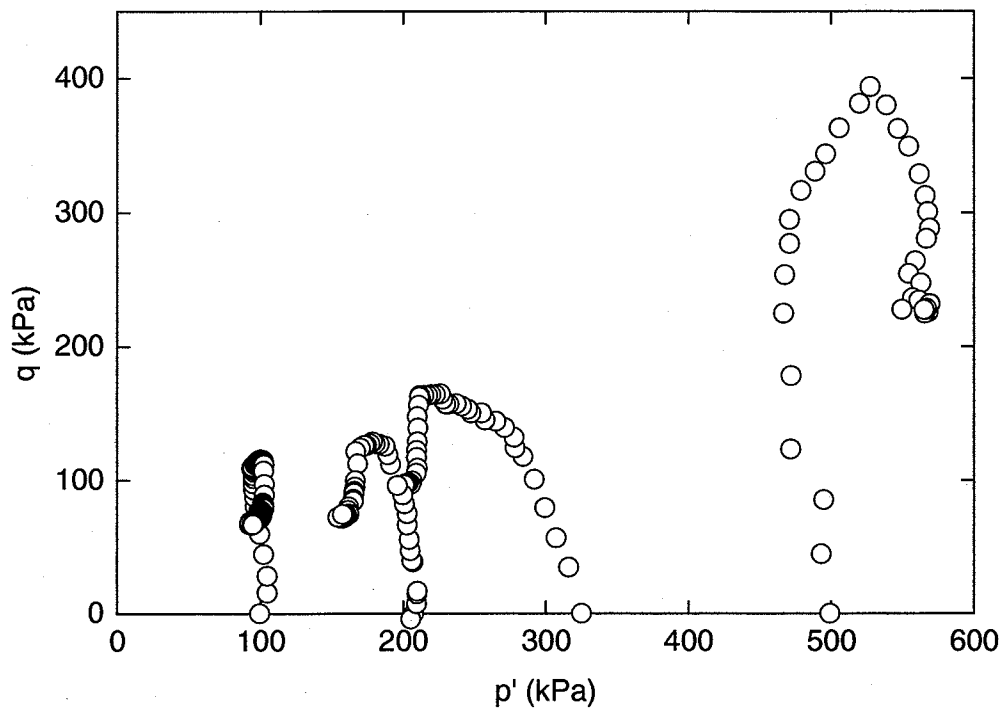

Figure 5.12. CIŪ triaxial test results for the clay reconstituted with gypsum-rich water.

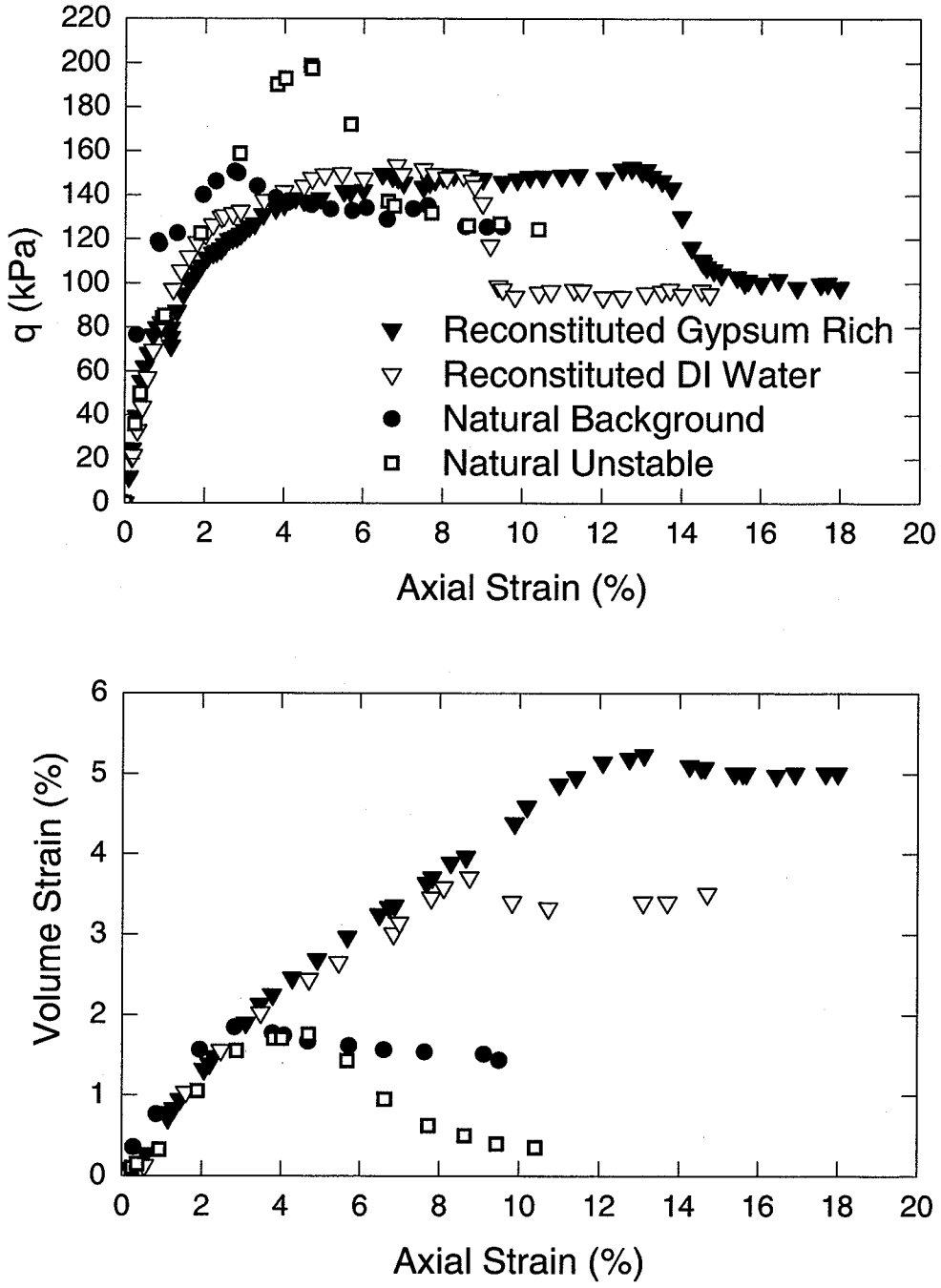

Figure 5.13. Comparison of CID triaxial test results for reconstituted and natural clays.

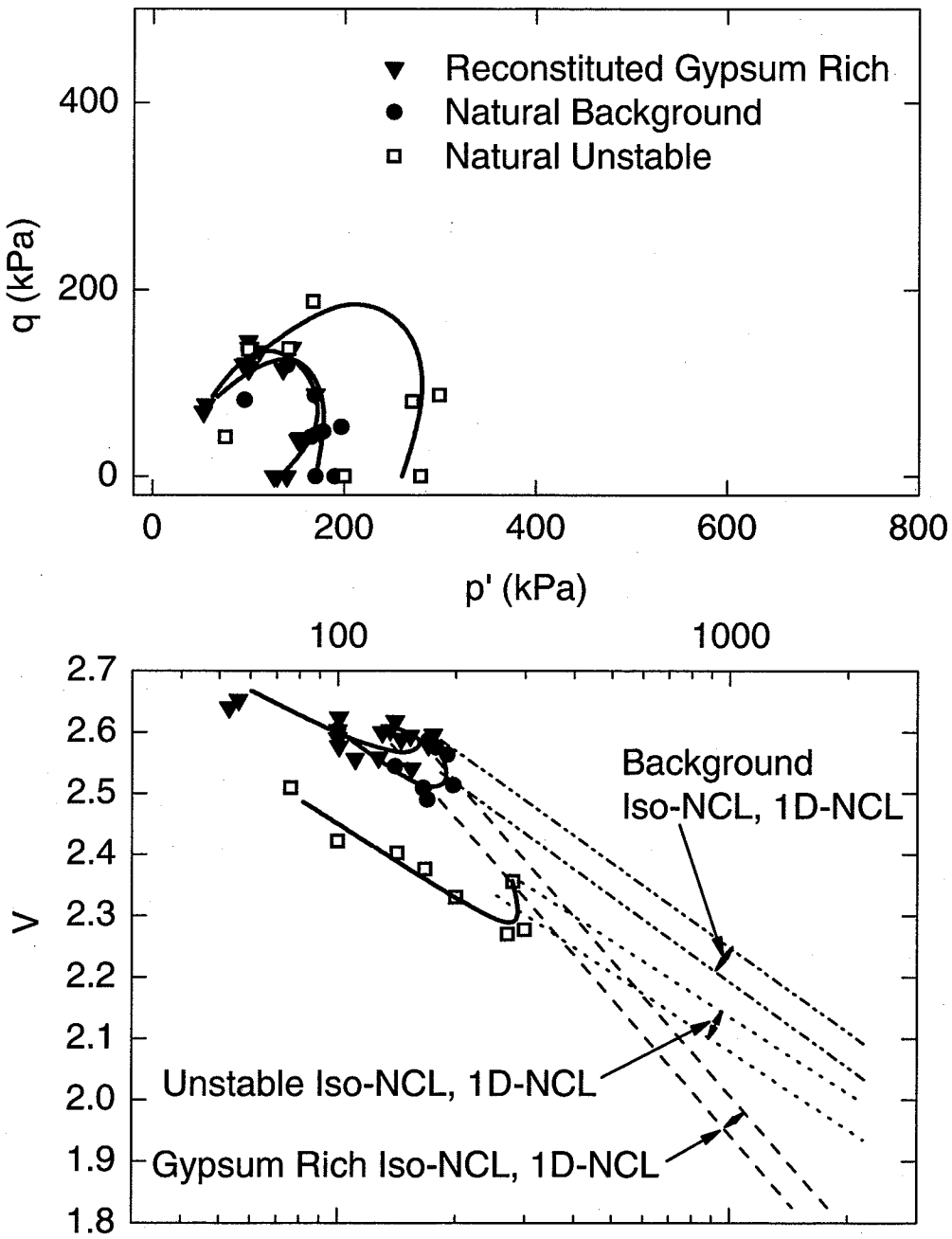

Figure 5.14. Yield loci for the natural Seven Sisters specimens compared to the reconstituted gypsum rich clay.

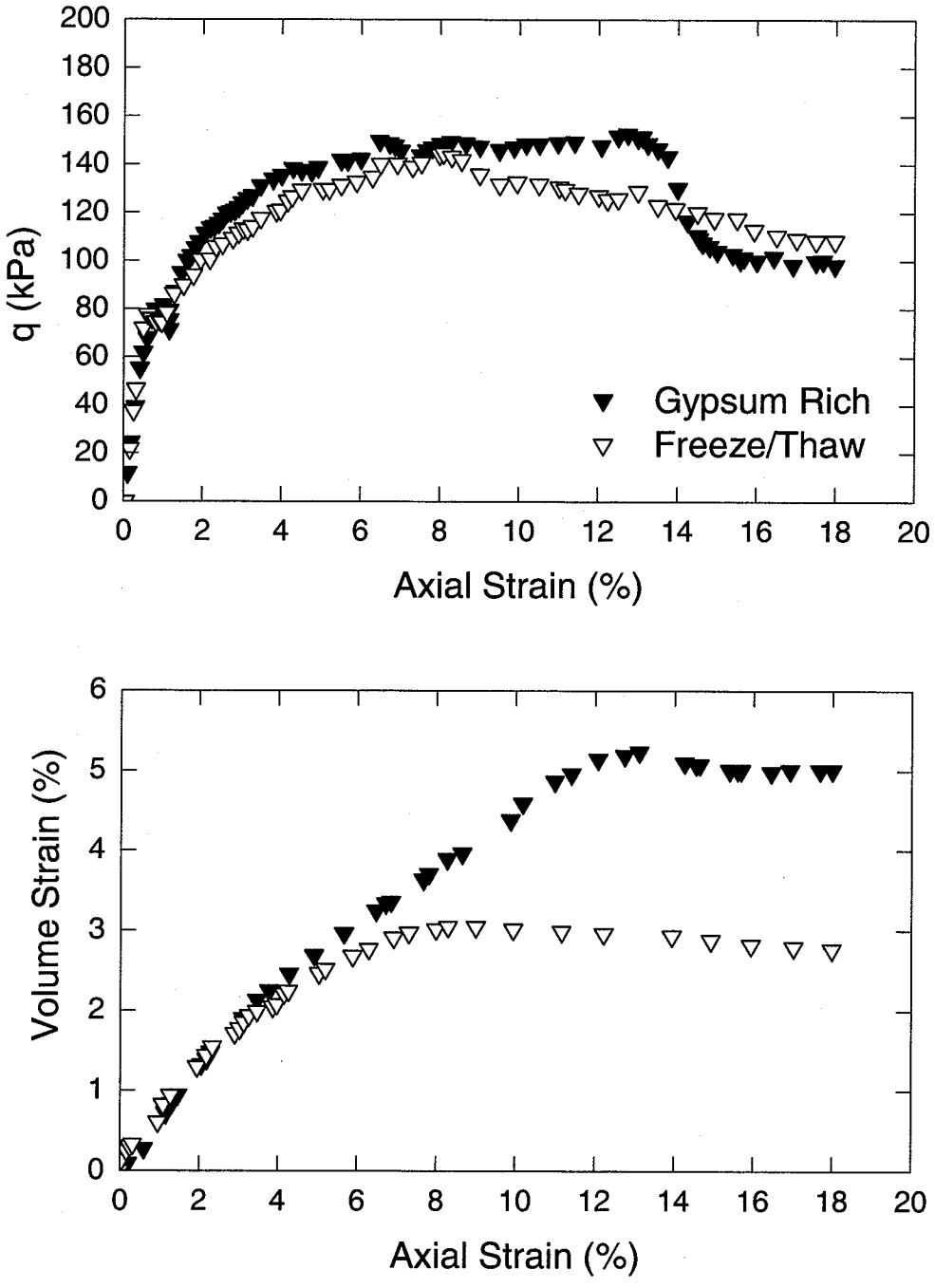

Figure 5.15. Comparison of CID results for frozen/thawed and unfrozen reconstituted clays.

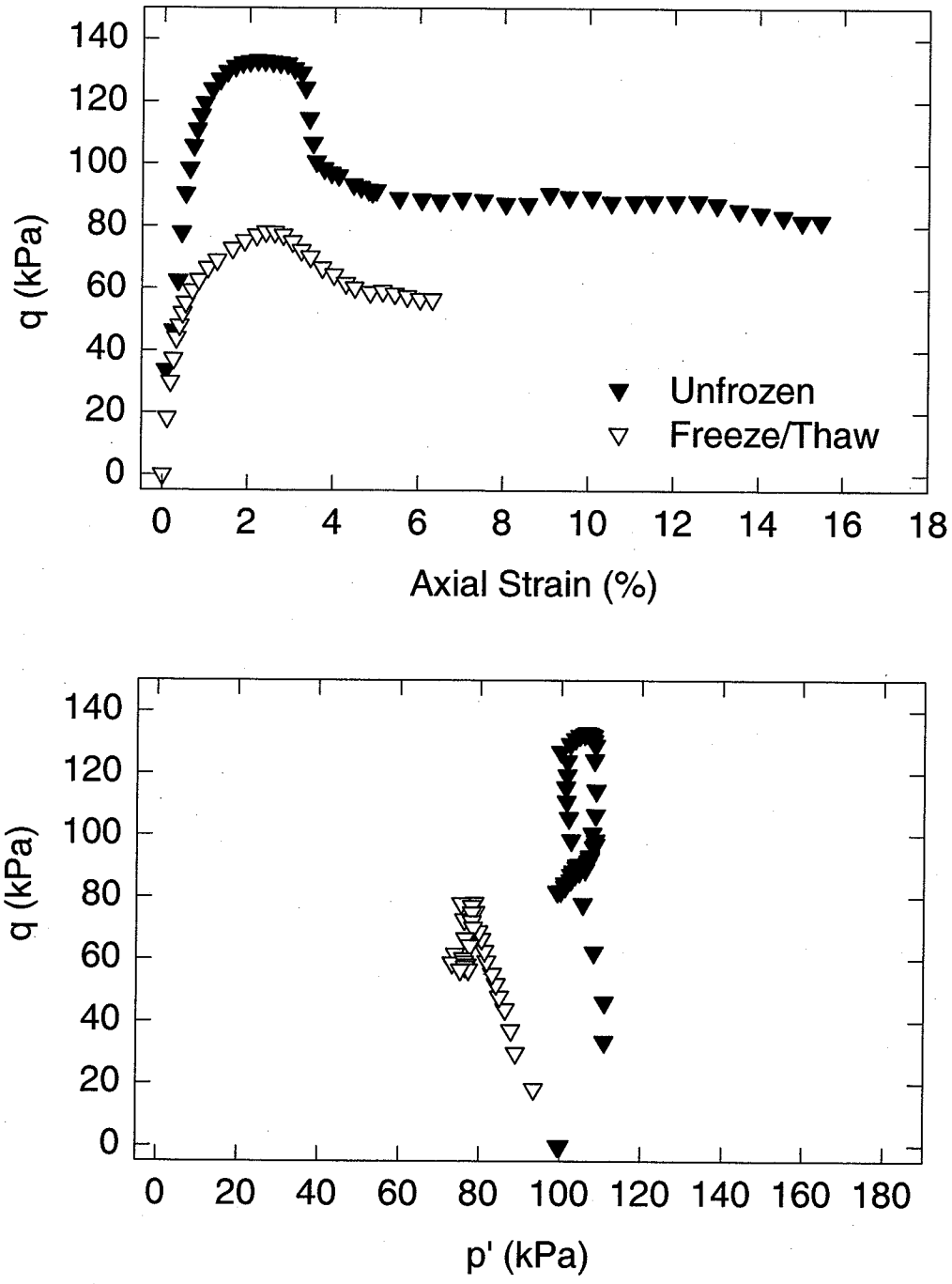

Figure 5.16. Comparison of CIŪ results for frozen/thawed and unfrozen reconstituted clays.

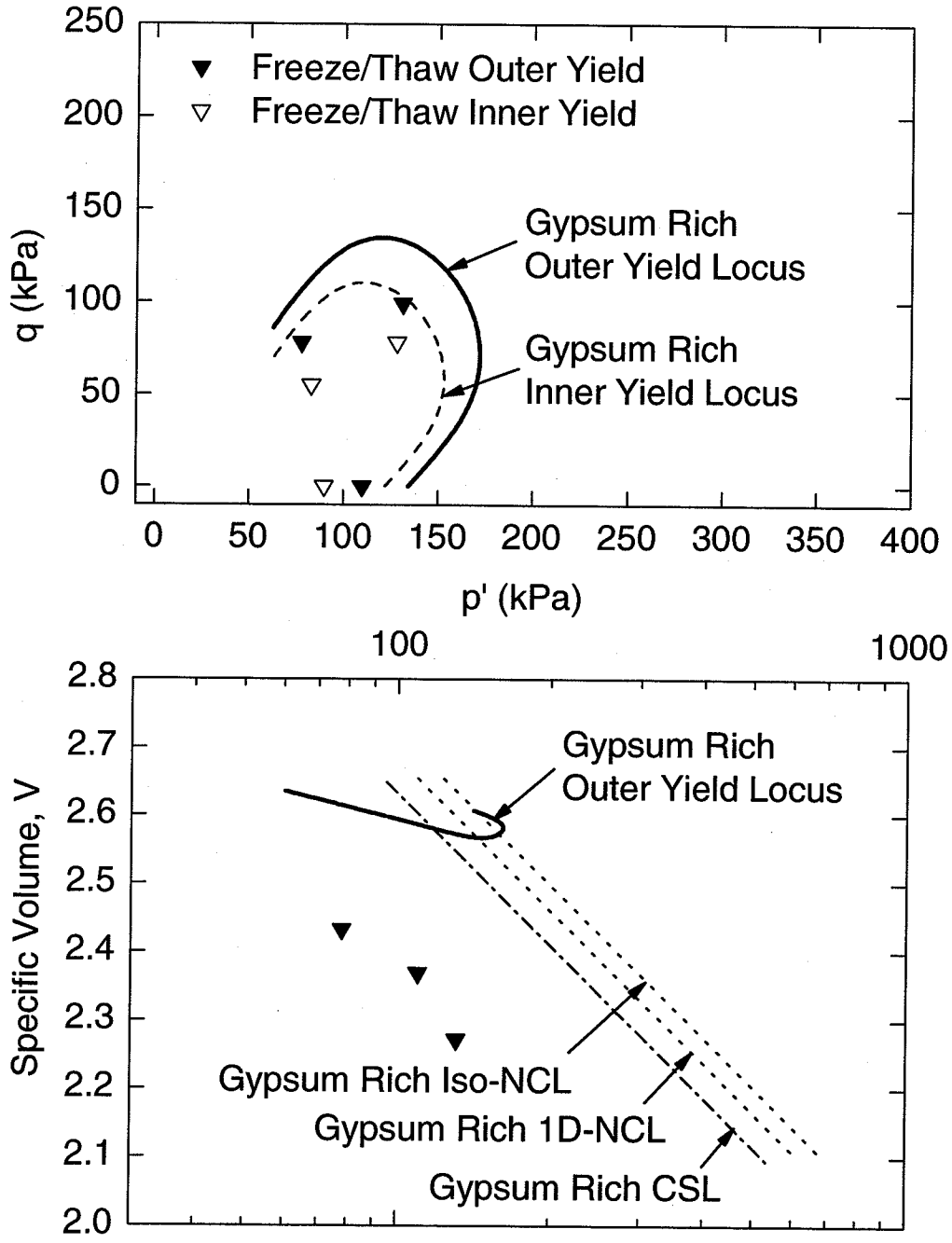

Figure 5.17. Yield points for the freeze/thaw specimens compared to the yield loci for the reconstituted gypsum rich specimens.

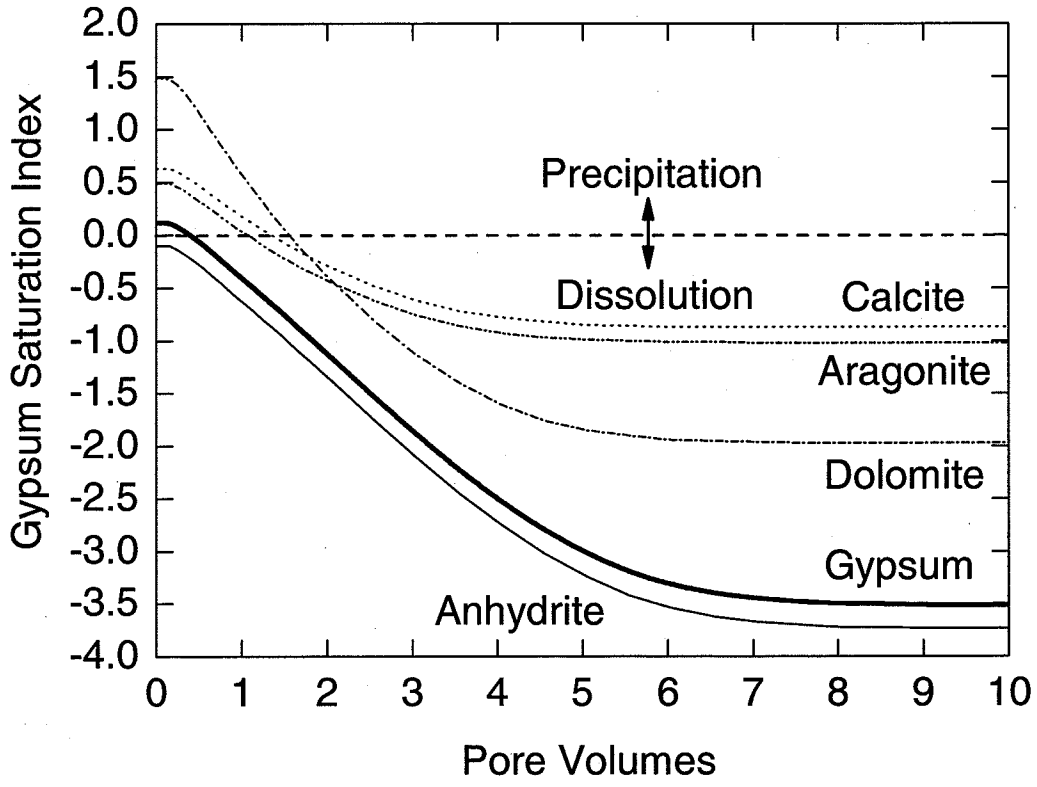

Figure 6.1. Geochemical model results for saturation indices of various potential cementing minerals as a function of number of pore volumes permeated through the column of foundation clay.

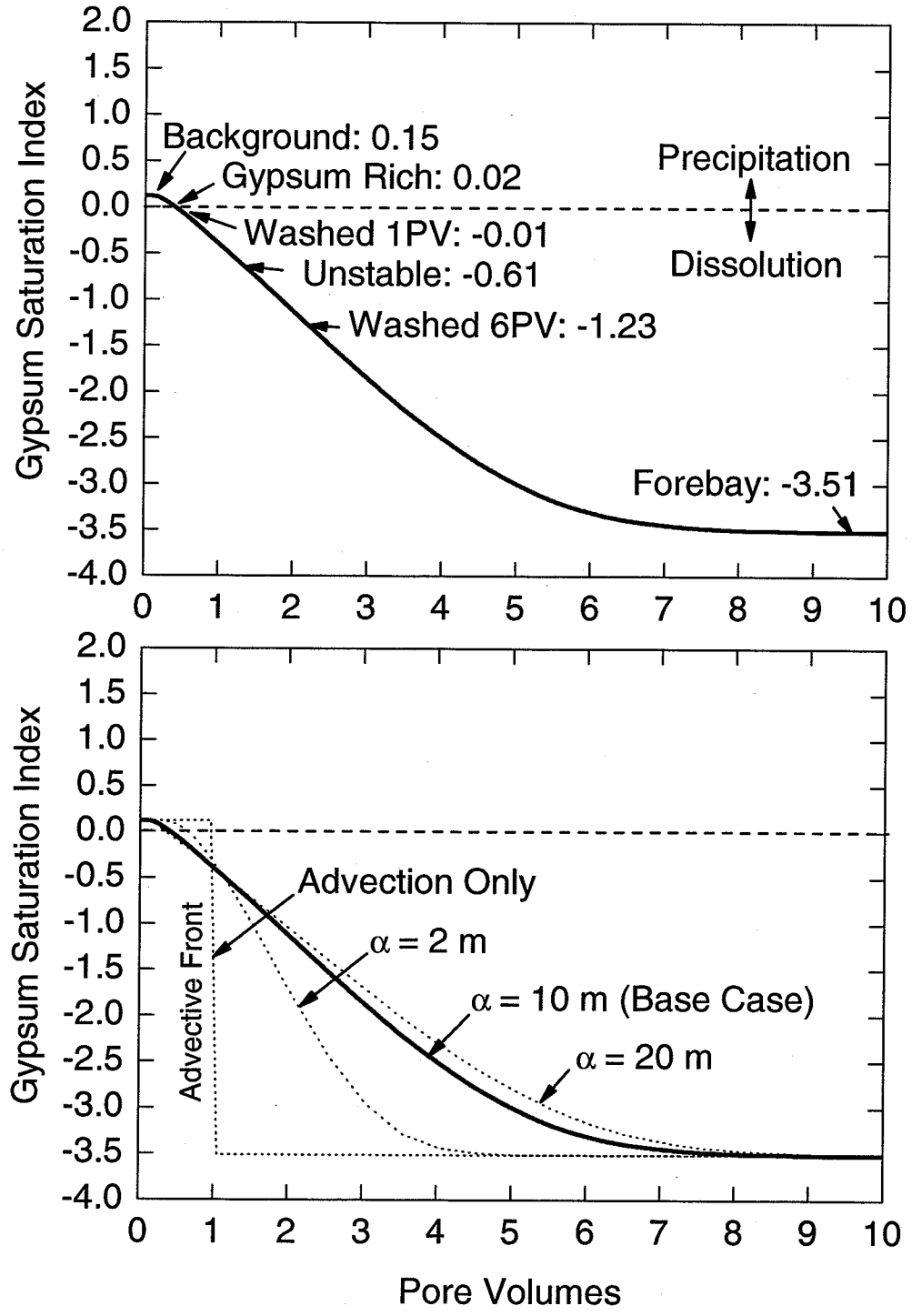

Figure 6.2. Geochemical model results for gypsum saturation index versus number of pore volumes compared to the measured values for selected natural and reconstituted clays. The lower diagram shows the sensitivity of the cross-over point (from gypsum precipitation to gypsum dissolution) to a range of dispersivity (α) values.

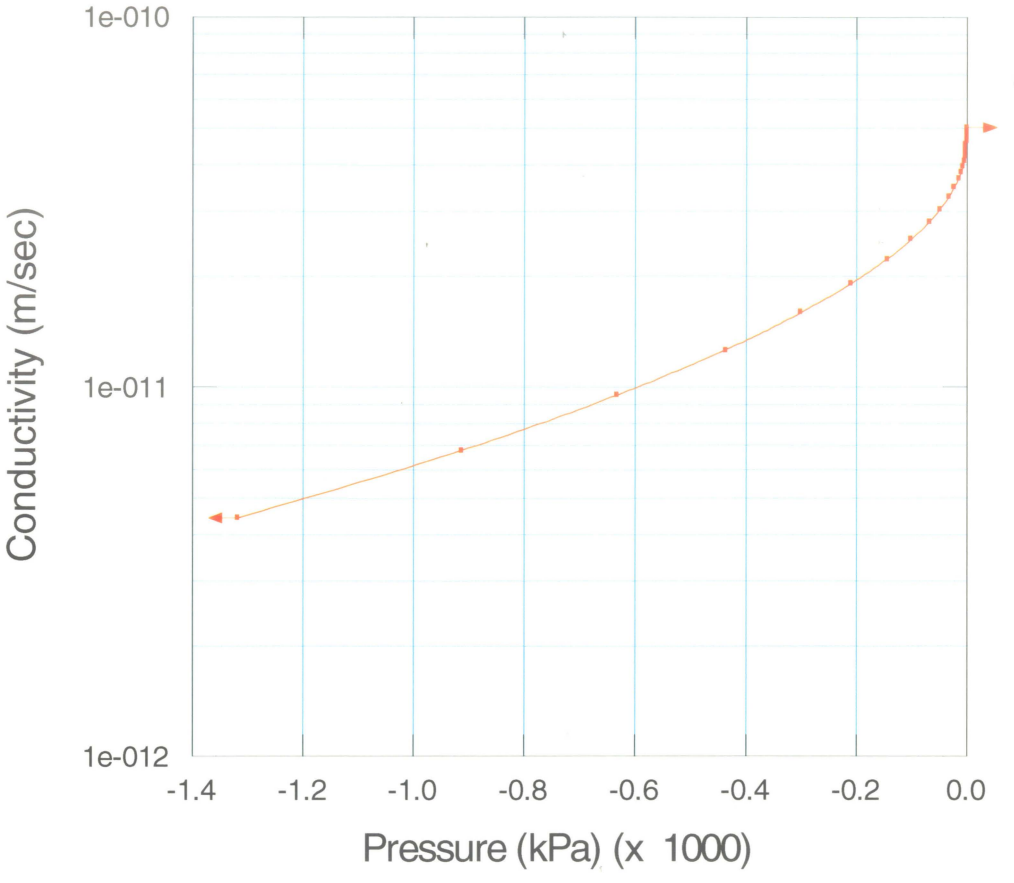

Figure 6.3. Unsaturated hydraulic conductivity function utilized for the clay core of the dyke.

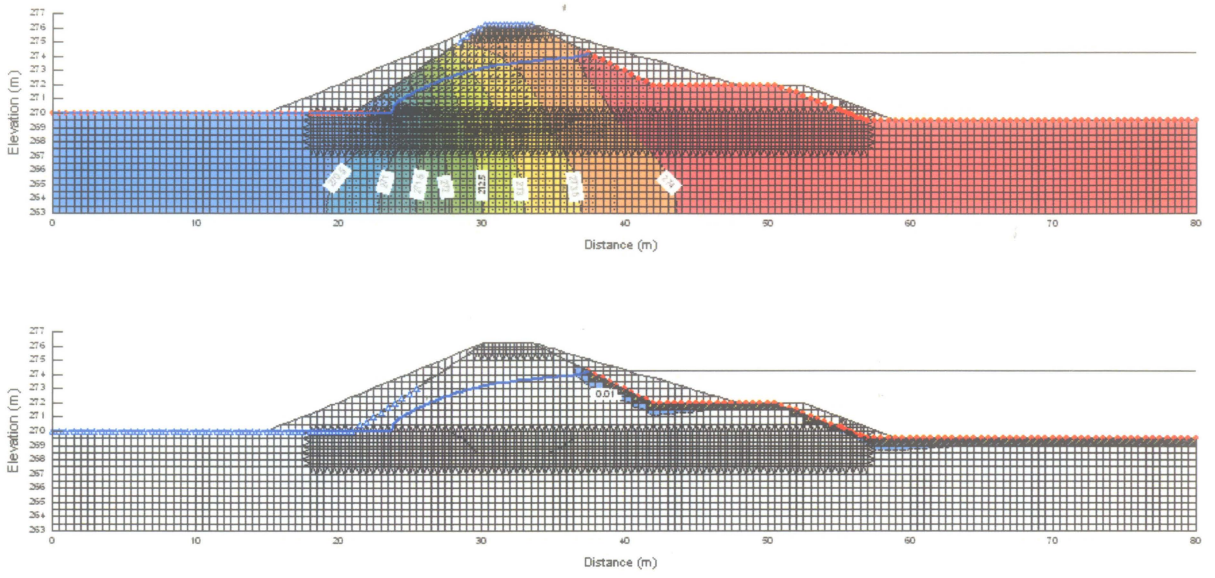

Figure 6.4. Seepage (top) and mass transport (bottom) modelling results using the base model parameters determined by Garinger (2002) ($K_{x,y\ dyke}$ = 5x10^{-11} m/s, $K_{x,y\ upper\ foundation}$ = 2.2x10^{-11}, $K_{x,y\ lower\ foundation}$ = 2.9x10^{-11}). Transport model units are C/C_0 x 100% relative to the forebay water chemistry.

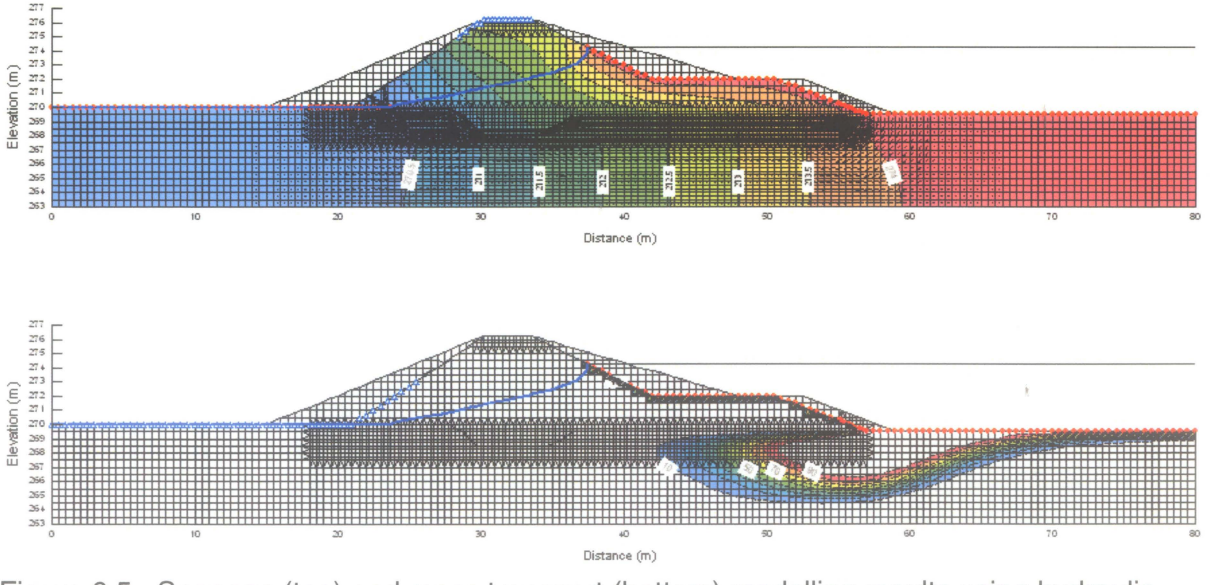

Figure 6.5. Seepage (top) and mass transport (bottom) modelling results using hydraulic conductivity values for the foundation clay three orders of magnitude higher than the base model ($K_{x,y\ dyke}$ = 5x10^{-11} m/s, $K_{x,y\ upper\ foundation}$ = 2.2x10^{-8}, $K_{x,y\ lower\ foundation}$ = 2.9x10^{-8}). Transport model units are C/C_0 x 100% relative to the forebay water chemistry.

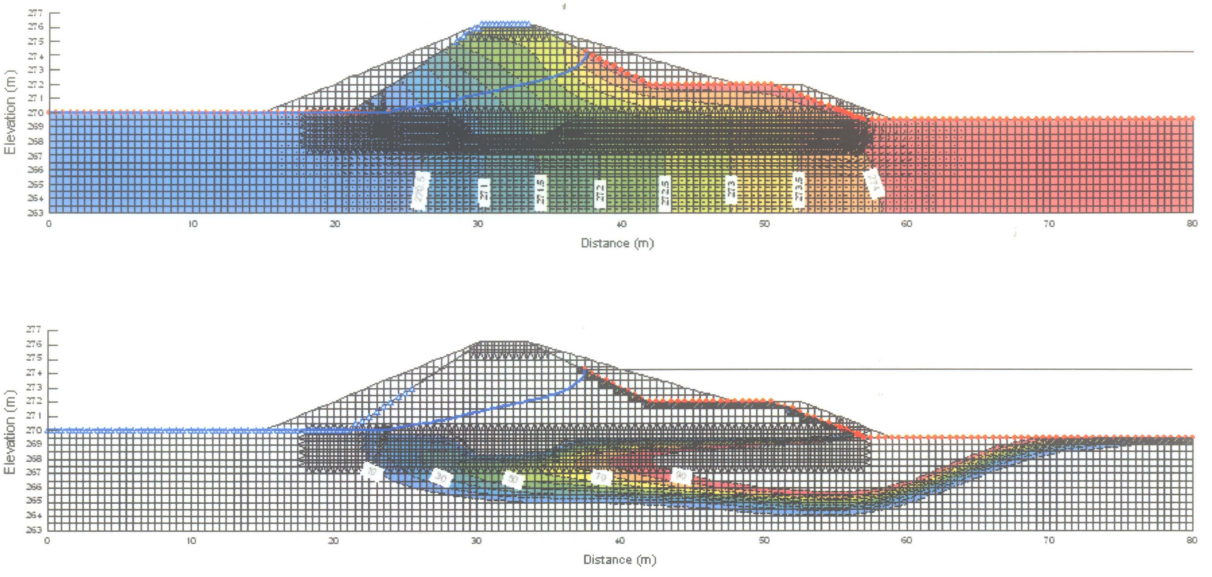

Figure 6.6. Seepage (top) and mass transport (bottom) modelling results using hydraulic conductivity values for the upper foundation clay three orders of magnitude higher than the base model ($K_{x,y\ dyke}$ = 5x10^{-11} m/s, $K_{x,y\ upper\ foundation}$ = 6x10^{-8}, $K_{x,y\ lower\ foundation}$ = 2.9x10^{-8}). Transport model units are C/C_0 x 100% relative to the forebay water chemistry.

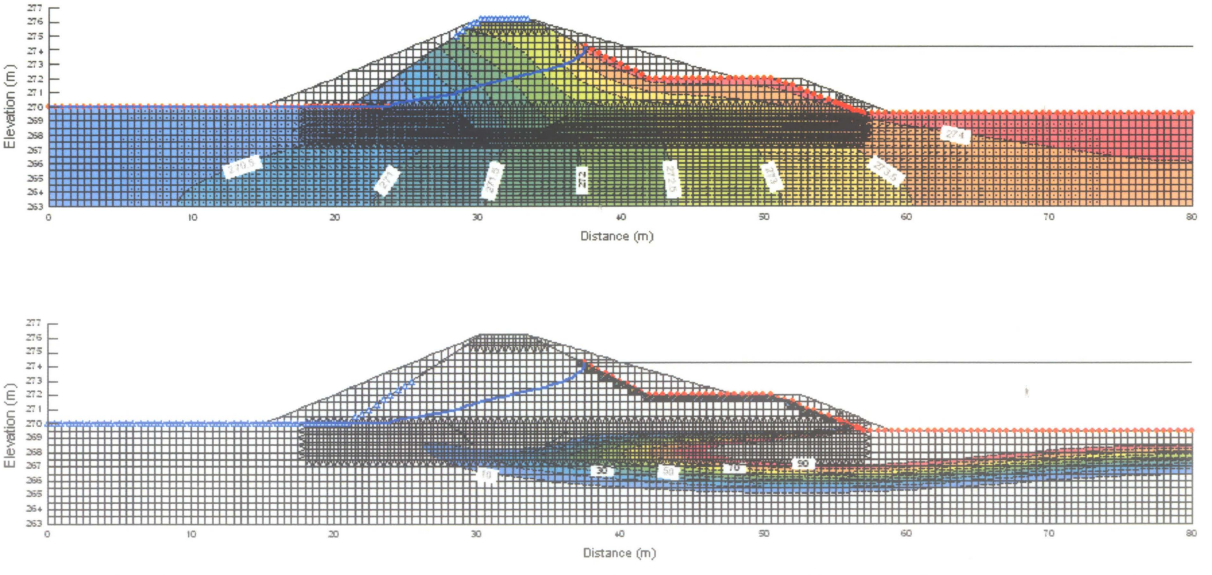

Figure 6.7. Seepage (top) and mass transport (bottom) modelling results using hydraulic conductivity values for the upper and lower foundation clays 3.5 orders of magnitude higher than the base model with a K_y/K_x ratio of 0.1 ($K_{x,y\ dyke}$ = 5x10^{-11} m/s, $K_{x\ foundation}$ = 6x10^{-8}, $K_{y\ foundation}$ = 6x10^{-9}). Transport model units are C/C_0 x 100% relative to the forebay water chemistry.

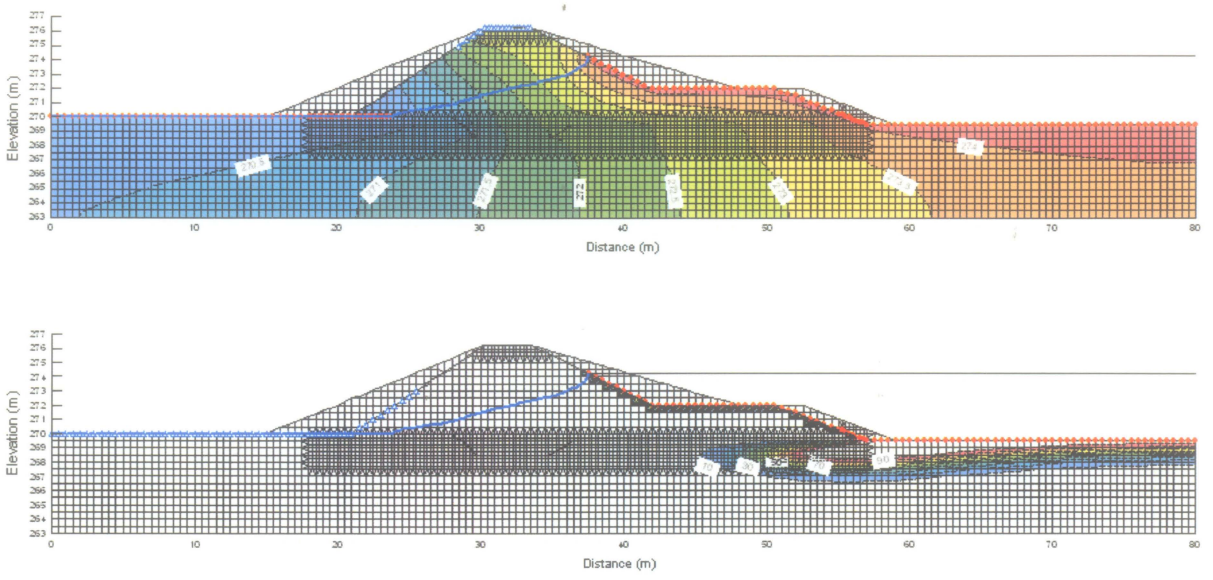

Figure 6.8. Seepage (top) and mass transport (bottom) modelling results using hydraulic conductivity values for the upper and lower foundation clays three orders of magnitude higher than the base model with a K_y/K_x ratio of 0.1 ($K_{x,y\ dyke}$ = $5x10^{-11}$ m/s, $K_{x\ foundation}$ = $2.2x10^{-8}$, $K_{y\ foundation}$ = $2.2x10^{-9}$). Transport model units are C/C_0 x 100% relative to the forebay water chemistry.

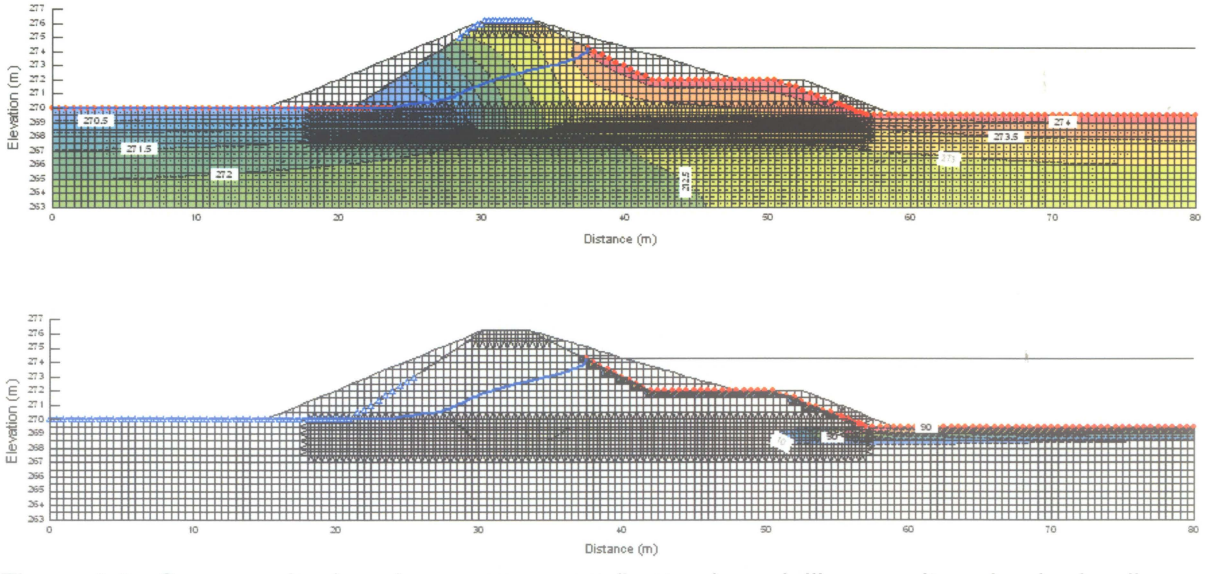

Figure 6.9. Seepage (top) and mass transport (bottom) modelling results using hydraulic conductivity values for the upper and lower foundation clays three orders of magnitude higher than the base model with a K_y/K_x ratio of 0.1 ($K_{x,y\ dyke}$ = $5x10^{-11}$ m/s, $K_{x\ foundation}$ = $2.2x10^{-8}$, $K_{y\ foundation}$ = $2.2x10^{-10}$). Transport model units are C/C_0 x 100% relative to the forebay water chemistry.

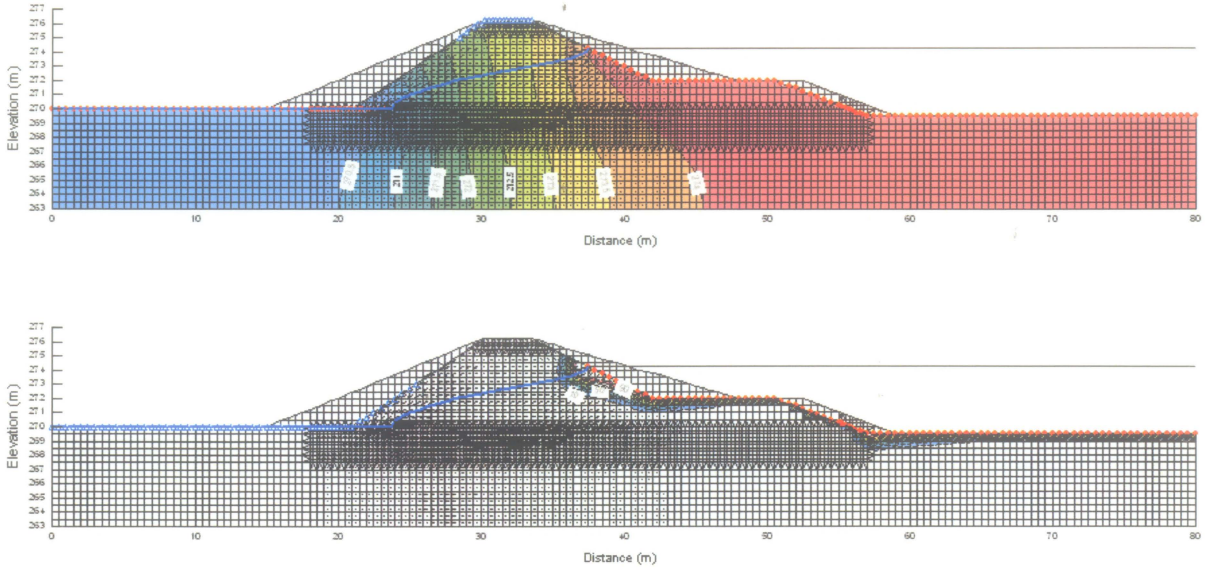

Figure 6.10. Seepage (top) and mass transport (bottom) modelling results using hydraulic conductivity values for the dyke, upper and lower foundation clays three orders of magnitude higher than the base model with no anisotropy ($K_{x,y\ dyke}$ = 5x10^{-8} m/s, $K_{x,y\ foundation}$ = 6x10^{-8}). Transport model units are C/C_0 x 100% relative to the forebay water chemistry.

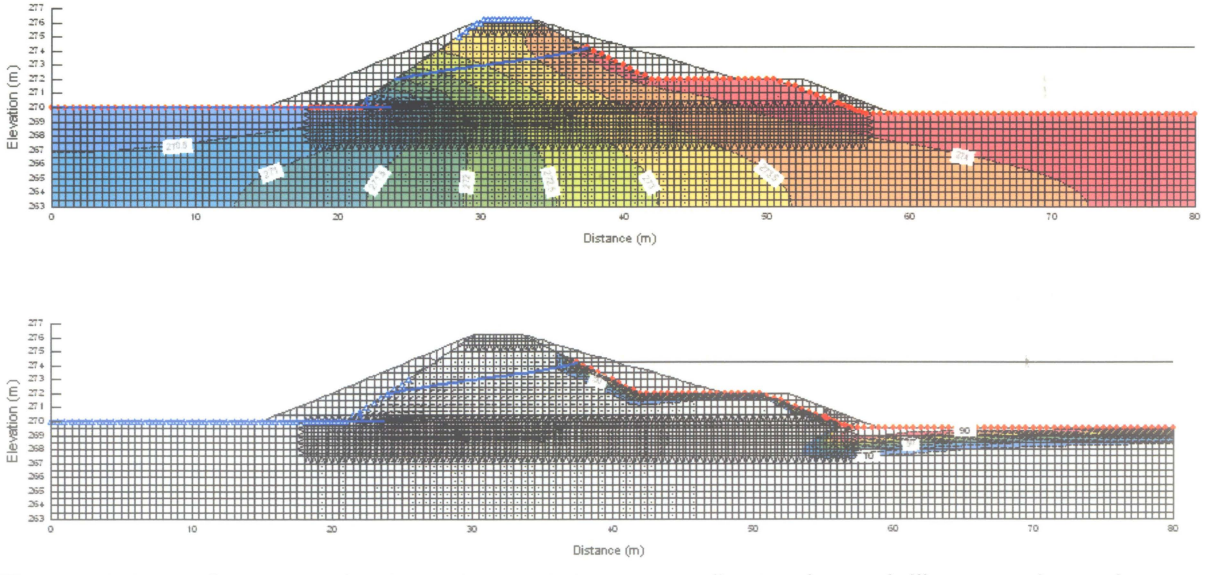

Figure 6.11. Seepage (top) and mass transport (bottom) modelling results using hydraulic conductivity values for the dyke, upper and lower foundation clays three orders of magnitude higher than the base model with a K_y/K_x ratio of 0.1 ($K_{x\ dyke}$ = 5x10^{-8} m/s, $K_{y\ dyke}$ = 5x10^{-9} m/s, $K_{x\ foundation}$ = 6x10^{-8}, $K_{y\ foundation}$ = 6x10^{-9}). Transport model units are C/C_0 x 100% relative to the forebay water chemistry.

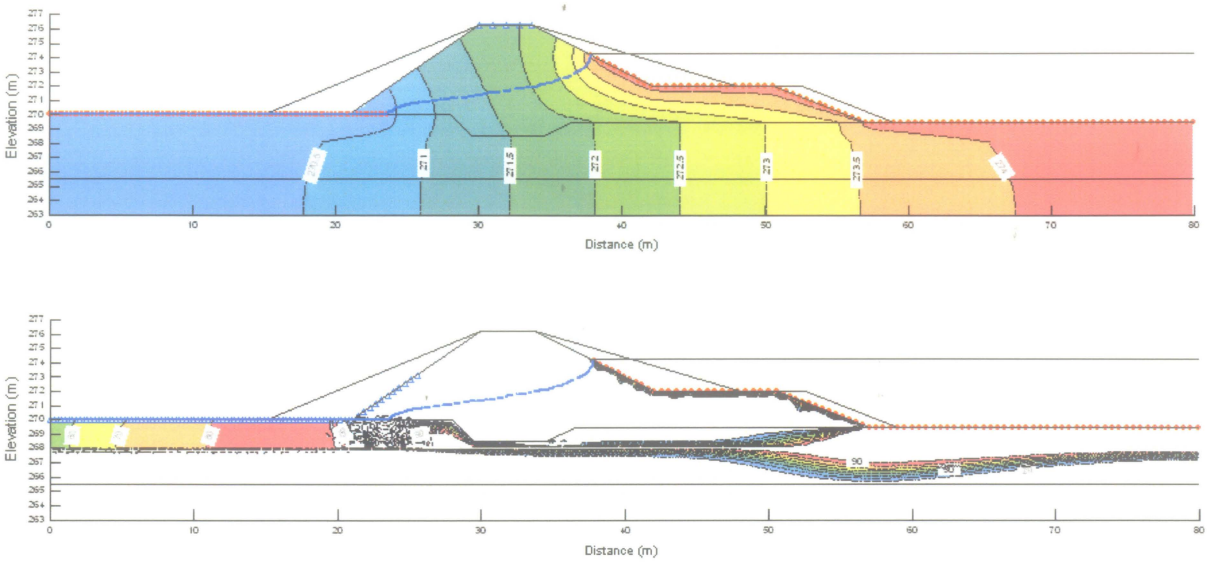

Figure 6.12. Seepage (top) and mass transport (bottom) modelling results using the base model parameters with a 0.1 m fine sand seam ($K_{x,y\ dyke}$ = $5x10^{-11}$ m/s, $K_{x,y\ upper\ foundation}$ = $2.2x10^{-11}$, $K_{x,y\ lower\ foundation}$ = $2.9x10^{-11}$, $K_{sand\ seam}$ = $1x10^{-5}$). Transport model units are C/C_0 x 100% relative to the forebay water chemistry.

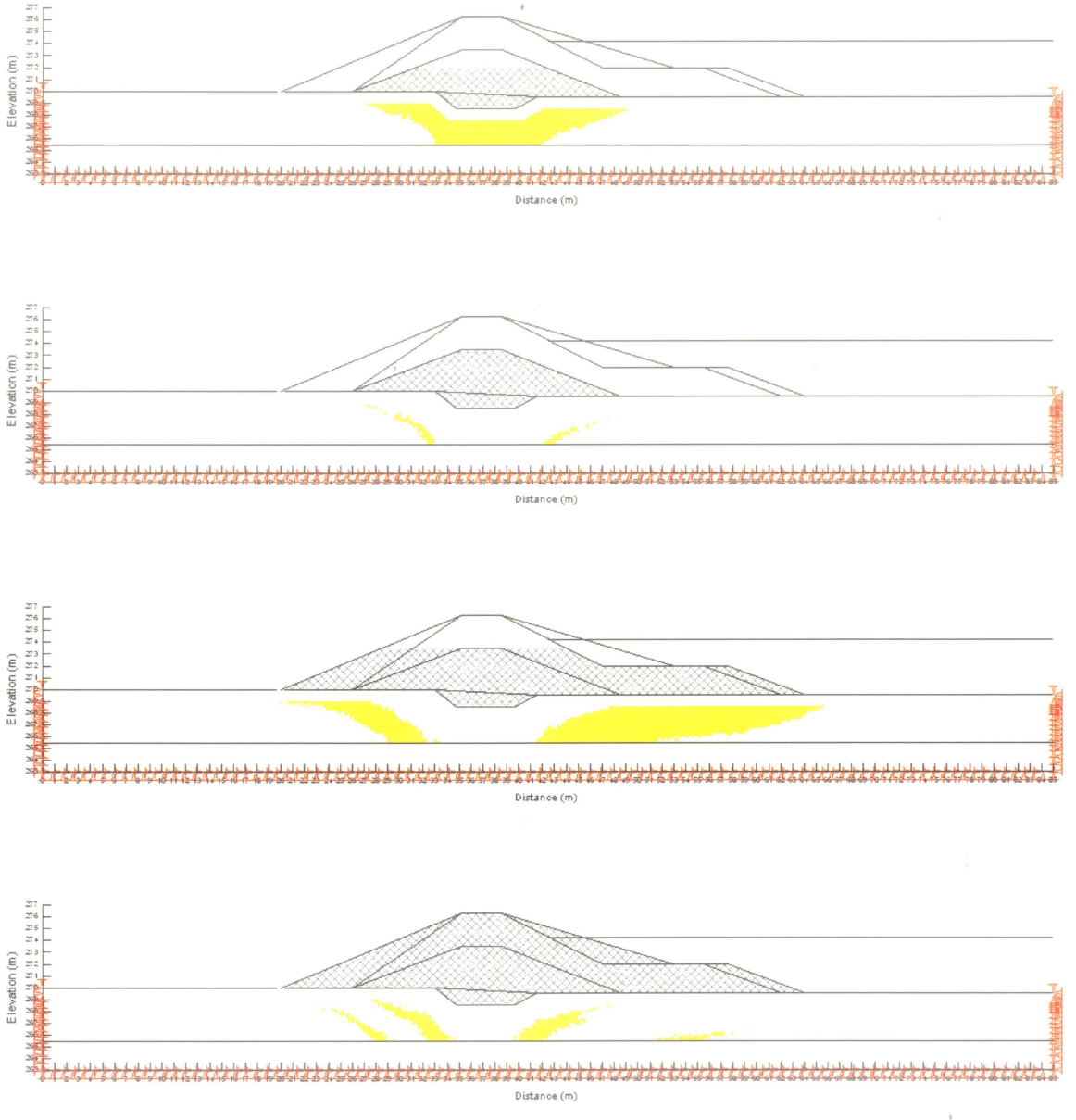

Figure 6.13. Base case (OCR = 2.5, M = 1.5) deformed meshes and yielded zones for the stable section.

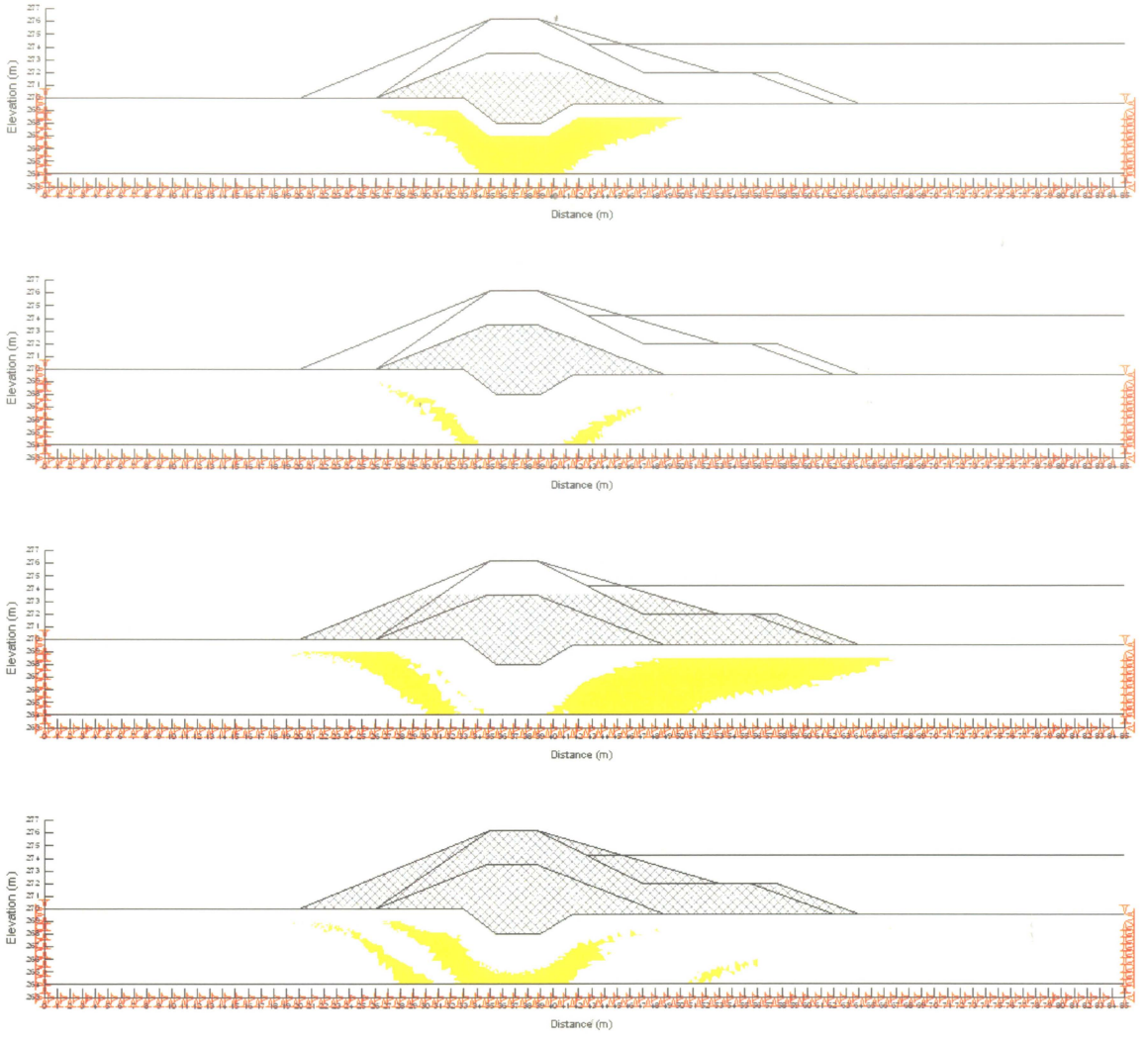

Figure 6.14. Base case (OCR = 2.5, M = 1.5) deformed meshes and yielded zones for the unstable section.

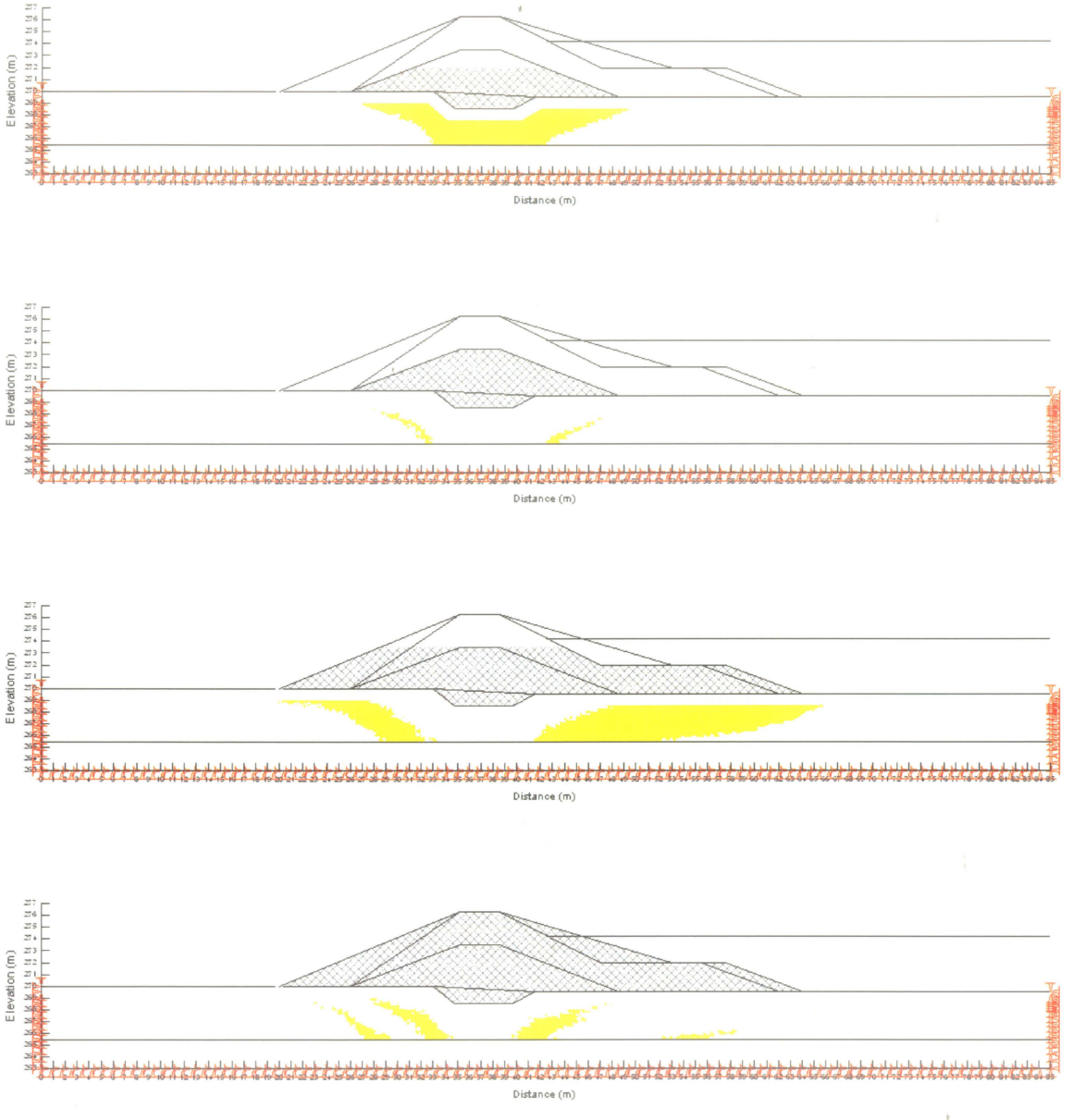

Figure 6.15. Deformed meshes and yielded zones for the stable section using a reduced yield locus (OCR = 2.3, M = 1.1).

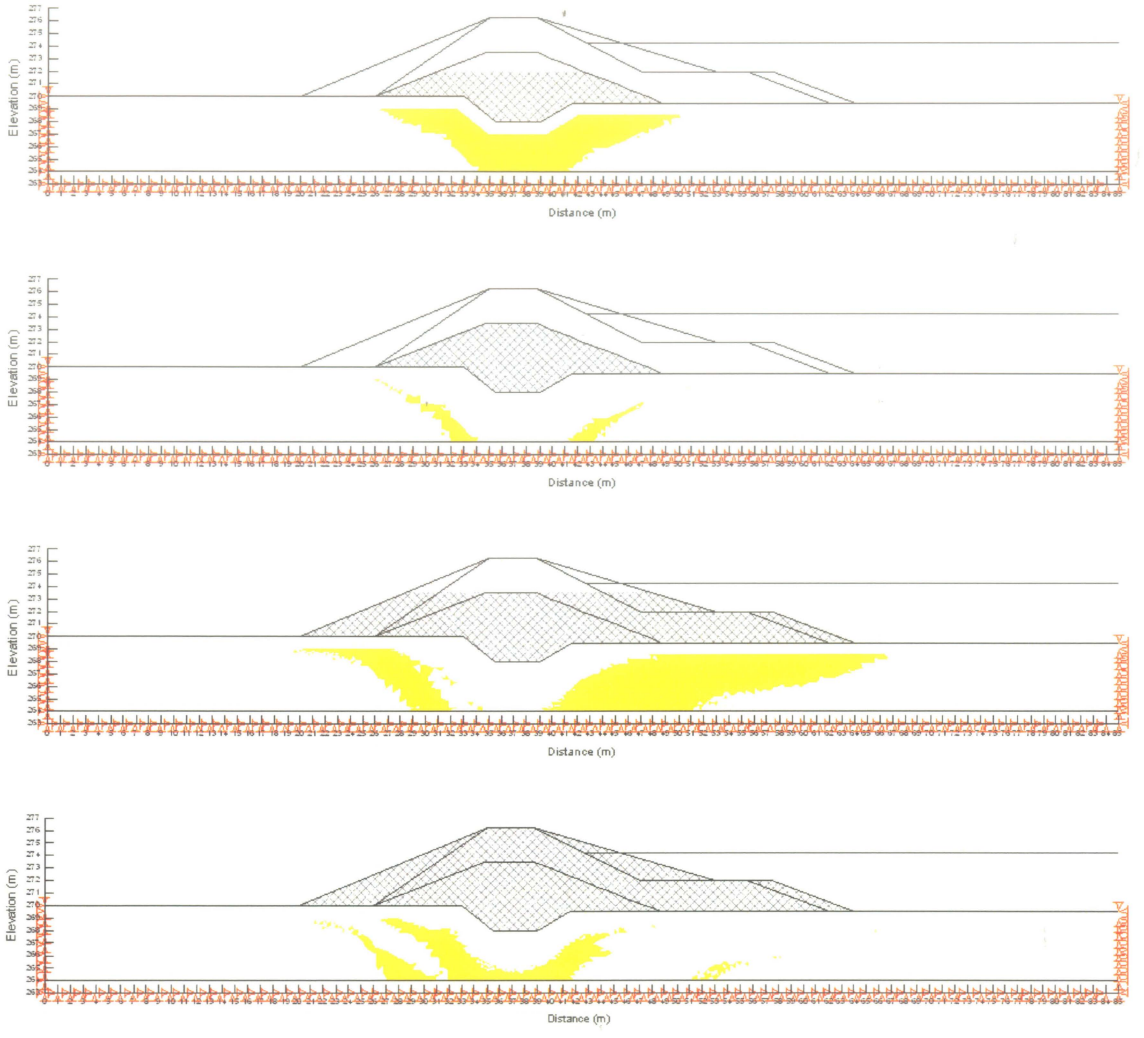

Figure 6.16. Deformed meshes and yielded zones for the unstable section using a reduced yield locus (OCR = 2.3, M = 1.1).

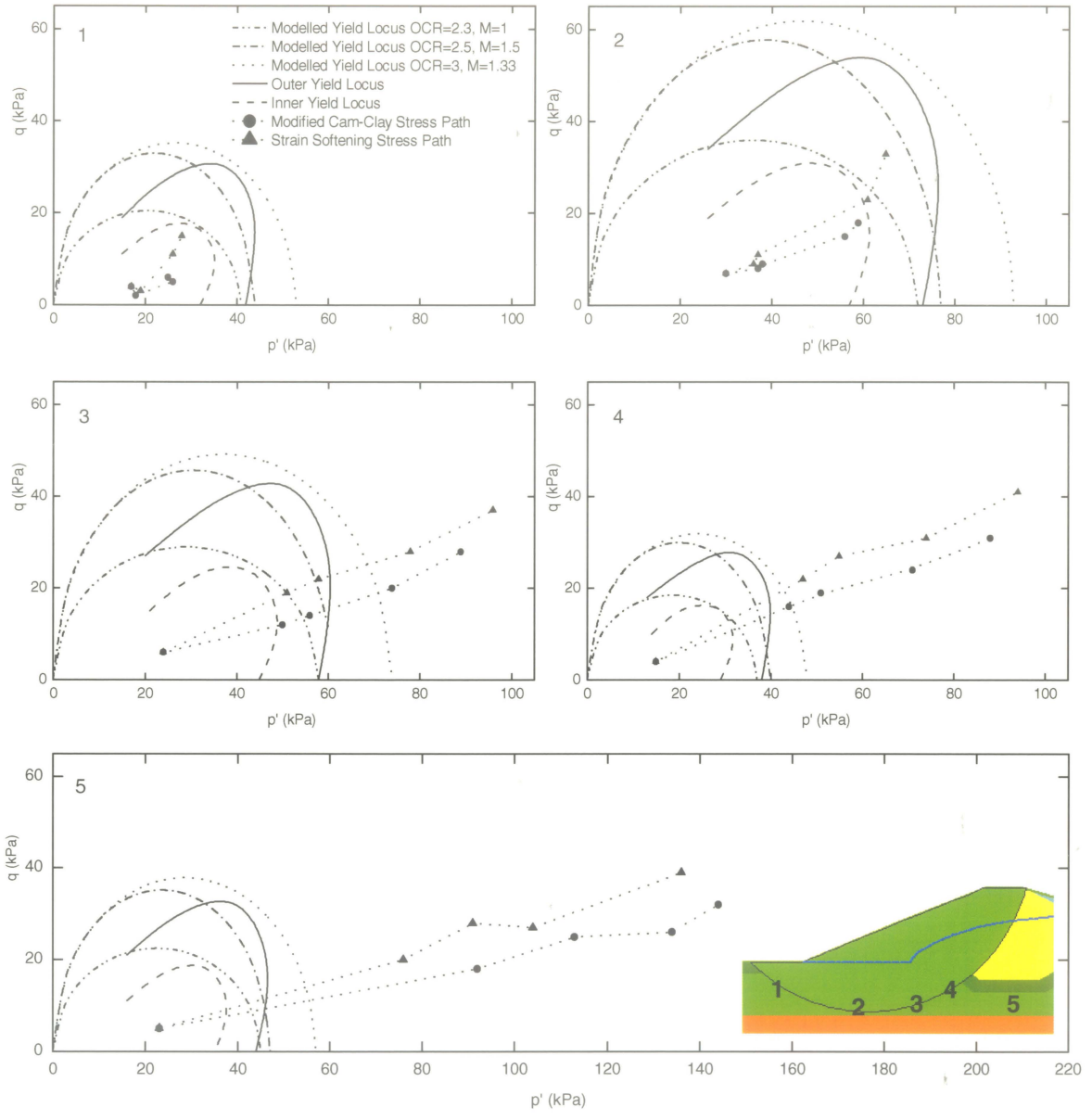

Figure 6.17. Comparison of the modelled Cam-Clay yield loci to the anisotropic yield loci determined from the laboratory testing program for four points along the failure surface (1 to 4) and one point beneath the centre line of the dyke (5) for the stable section. Stress paths shown are for construction of the dyke using the strain-softening and Modified Cam-Clay constitutive models for the upper foundation clay.

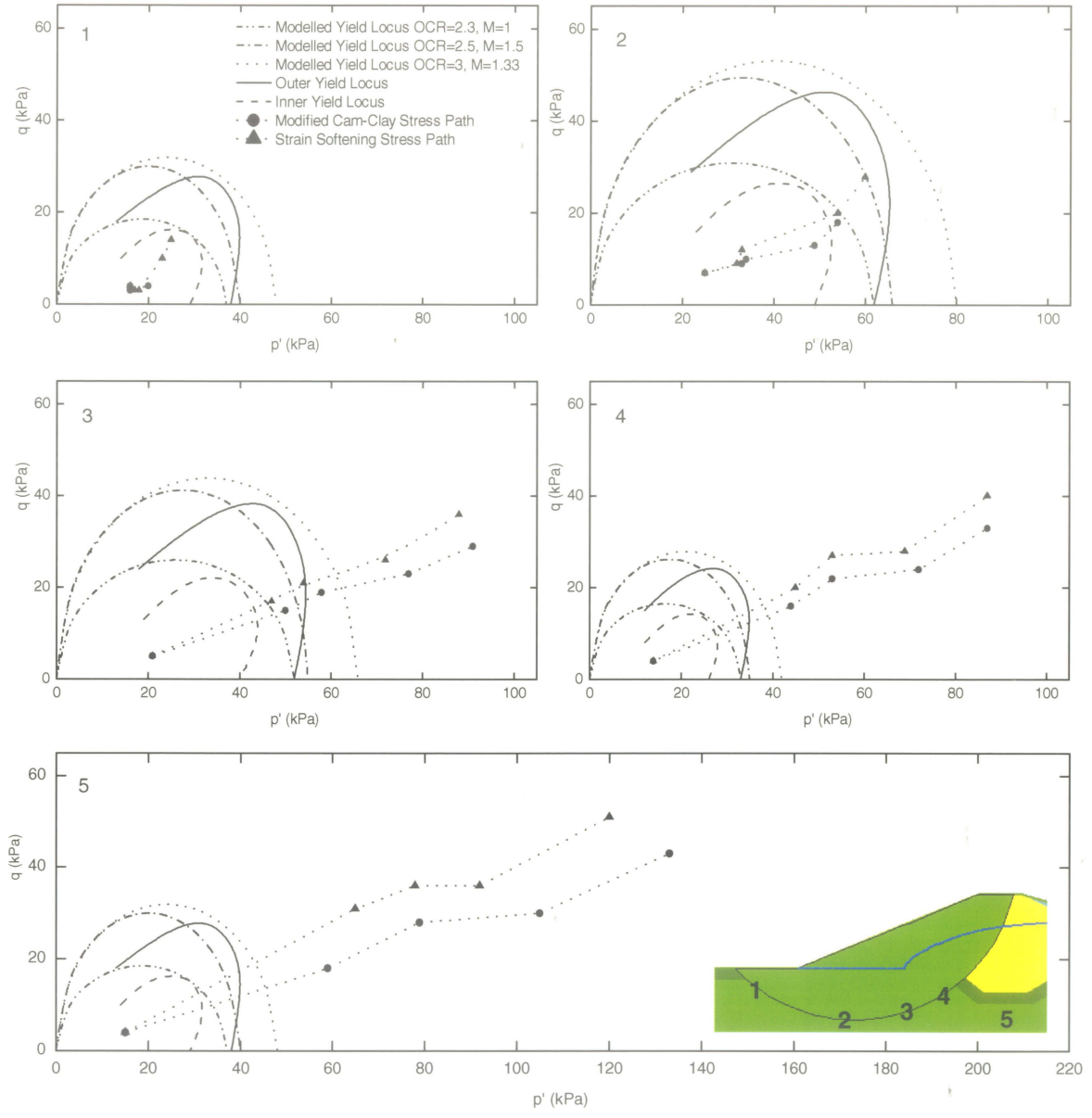

Figure 6.18. Comparison of the modelled Cam-Clay yield loci to the anisotropic yield loci determined from the laboratory testing program for four points along the failure surface (1 to 4) and one point beneath the centre line of the dyke (5) for the unstable section. Stress paths shown are for construction of the dyke using the strain-softening and Modified Cam-Clay constitutive models for the upper foundation clay.

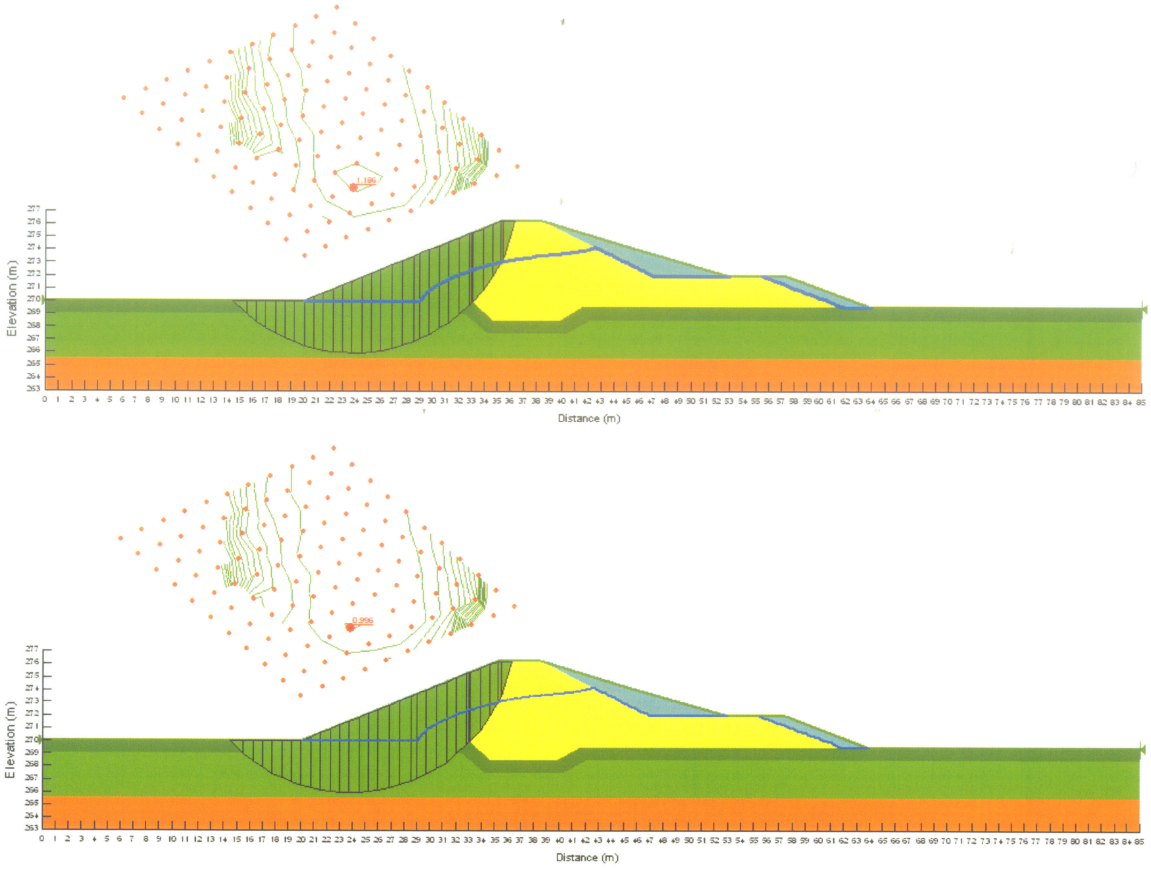

Figure 6.19. Slope stability modelling results for the stable section using the base case Modified Cam-Clay yield locus in the upper foundation clay (OCR = 2.5, M = 1.5). The slope was determined to be stable if post-peak strength ($\Phi' = 14^{o}$) was operative (upper diagram) and unstable if residual strength ($\Phi' = 9^{o}$) was operative (lower diagram).

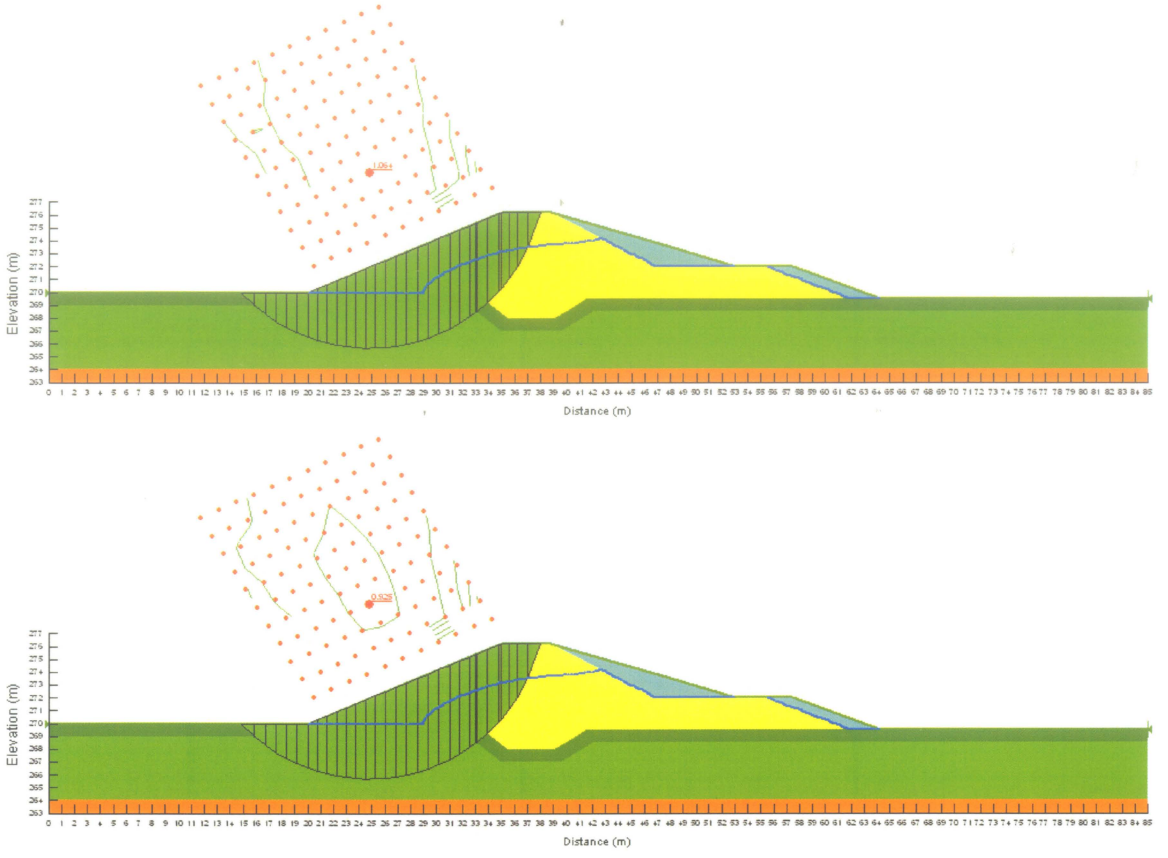

Figure 6.20. Slope stability modelling results for the unstable section using the base case Modified Cam-Clay yield locus in the upper foundation clay (OCR = 2.5, M = 1.5). The slope was determined to be unstable if either post-peak strength ($\Phi' = 13^{o}$, upper diagram) or residual strength ($\Phi' = 9^{o}$, lower diagram) are operative.

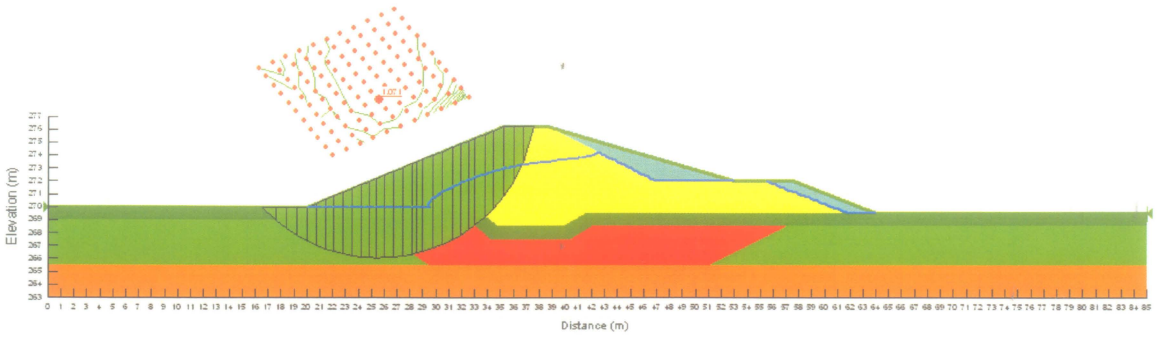

Figure 6.21. Slope stability modelling results for the stable section with the strength of the upper foundation zoned based on the results of the stress-deformation analysis. Yielded areas were assigned a lower strength ($\Phi' = 9^{o}$). The same results were obtained for both the base case yield locus (OCR = 2.5, M = 1.5) and the reduced yield locus (OCR = 2.3, M = 1.1).

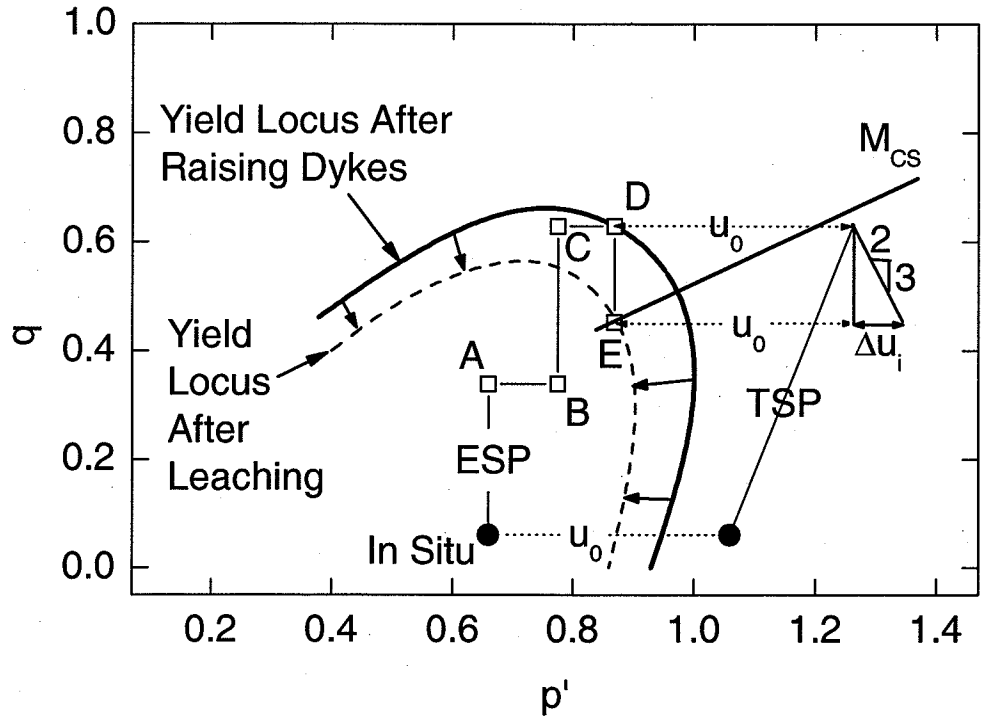

Figure 7.1. Strain-softening induced excess pore water pressure triggered by a reduction in the yield locus due to leaching.

APPENDIX A:

Guide to CD Contents

Specimen/Folder Name	Clay Type	Test Type
SS2.9A-T1	Seven Sisters Background Section	CIU @ 100 kPa
SS2.9B-T2	Seven Sisters Background Section	CIU @ 400 kPa
SS3.5A-T3	Seven Sisters Background Section	CIU @ 200 kPa
SS3.5A-T4	Seven Sisters Background Section	CIU @ 500 kPa
SS2.9B-T5	Seven Sisters Background Section	CIU @ 200 kPa
SS3.5A-T6	Seven Sisters Background Section	CIU @ 400 kPa
AMR1-T7	Gypsum Rich	CIU @ 100 kPa
AMR1-T8	Gypsum Rich	CIU @ 100 kPa
AMR1-T9	Gypsum Rich	CIU @ 200 kPa
AMR1-T10	Gypsum Rich	CID @ 100 kPa
AMR1-T11	Gypsum Rich	Isotropic Consolidation to 327 kPa, CIU @ 327 kPa
AMR2-T12	Gypsum Rich	CIU @ 100 kPa
AMR2-T13	Gypsum Rich	CIU @ 100 kPa
AMR2-T14	Gypsum Rich	CID @ 100 kPa
AMR2-T15	Gypsum Rich	Isotropic Consolidation to 3363 kPa, CIU @ 500 kPa
AMR2-T16	Gypsum Rich	Isotropic Consolidation to 350 kPa, CIU @ 350 kPa
AMR3-T17	Deionized Water	Isotropic Consolidation to 350 kPa, CIU @ 350 kPa
SS3.8D-T18	Seven Sisters Background Section	Isotropic Consolidation to 670 kPa, CIU @ 670 kPa
SS3.6D-T19	Seven Sisters Background Section	CID @ 100 kPa
SS10.7U-T20	Seven Sisters Unstable Section	CID @ 100 kPa
AMR2-T21	Gypsum Rich	Constant p' = 100 kPa
AMR4-T22	H2SO4	CID @ 100 kPa
AMR2-T23	Gypsum Rich	Constant p' = 100 kPa
AMR4-T24	H2SO4	Isotropic Consolidation to 350 kPa, CIU @ 350 kPa
AMR4-T25	H2SO4	CIU @ 100 kPa
AMR4-T26	H2SO4	Constant p' = 100 kPa
AMR3-T27	Deionized Water	CIU @ 100 kPa
AMR3-T28	Deionized Water	CAU @ p' = 100 kPa, q = 26 kPa
AMR2-T29	Gypsum Rich	Constant p' = 100 kPa
AMR2-T30	Gypsum Rich	Ko to 350, CAU @ p' = 350 kPa, q = 93 kPa
SS11.9U-T31	Seven Sisters Unstable Section	Isotropic Consolidation to 350 kPa, CIU @ 350 kPa
SS3.5D-T32	Seven Sisters Background Section	Constant p' = 100 kPa
SS3.9E-T33	Seven Sisters Background Section	Isotropic Consolidation to 3363 kPa, CIU @ 500 kPa
SS10.7U-T34	Seven Sisters Unstable Section	Constant p' = 100 kPa
AMR3-T35	Deionized Water	CID @ 100 kPa
SS3.9D-T36	Seven Sisters Background Section	Ko to 350, CAU @ p' = 350 kPa, q = 93 kPa
AMR2-T37	Gypsum Rich	Lateral Expansion from p' = 100 kPa
AMR5-T38	Washed 1 Pore Volume	CID @ 100 kPa
AMR2-T39	Gypsum Rich	Lateral Expansion from p' = 100 kPa
AMR6-T40	NaCl	Constant p' = 100 kPa
AMR6-T41	NaCl	CID @ 100 kPa
AMR2-T42	Gypsum Rich	q/p' = 1.25/1 from p' =100 kPa
AMR6-T43	NaCl	Isotropic Consolidation to 350 kPa, CIU @ 350 kPa
SS10.7U-T44	Seven Sisters Unstable Section	Isotropic Consolidation to 3400 kPa, CIU @ 500 kPa
AMR6-T45	NaCl	CIU @100 kPa
SS3.5E-T46	Seven Sisters Background Section	q/p' = 1.25/1 from p' =100 kPa

Specimen/Folder Name	Clay Type	Test Type
AMR1-T47	Gypsum Rich	CIU @100 kPa
AMR1-T48	Gypsum Rich, Freeze/Thaw	CIU @ 100 kPa
AMR1-T49	Gypsum Rich, Freeze/Thaw	CID @ 100 kPa
AMR1-T50	Gypsum Rich, Freeze/Thaw	Isotropic Consolidation to 350 kPa, CIU @ 350 kPa
AMR7-T51	Washed 6 Pore Volumes	CIU @ 100 kPa
AMR7-T52	Washed 6 Pore Volumes	CID @ 100 kPa
AMR7-T53	Washed 6 Pore Volumes	Constant p' = 100 kPa
AMR7-T54	Washed 6 Pore Volumes	Isotropic Consolidation to 350 kPa, CIU @ 350 kPa
AMR7-T55	Washed 6 Pore Volumes	CID @ 100 kPa
AMR3-T56	Deionized Water	Constant p' = 100 kPa
SS2.9A-O1	Seven Sisters Background Section	Oedometer
SS3.5A-O2	Seven Sisters Background Section	Oedometer
SS2.9B-O3	Seven Sisters Background Section	Oedometer
AMR1-O4	Gypsum Rich	Oedometer
AMR1-O5	Gypsum Rich	Oedometer
AMR1-O6	Gypsum Rich	Oedometer
AMR2-O7	Gypsum Rich	Oedometer
AMR3-O8	Deionized Water	Oedometer
SS3.7D-O9	Seven Sisters Background Section	Oedometer
SS10.7U-O10	Seven Sisters Unstable Section	Oedometer
AMR4-O11	H2SO4	Oedometer
AMR5-O12	Washed 1 Pore Volume	Oedometer
AMR3-O13	Deionized Water	Oedometer
AMR1-O14	Gypsum Rich	Oedometer
AMR6-O15	NaCl	Oedometer
AMR7-O16	Washed 6 Ppore Volumes	Oedometer